Skeletal malformations in the Fuzzy mutant mouse

Yannakoudakis, Basil

Awarding institution:
King's College London

Department of Craniofacial Development and Stem Cell Biology,
King's College London, London, UK.

Skeletal malformations in the *Fuzzy* mutant mouse

by

Basil Z. Yannakoudakis

A thesis submitted to King's College London for the degree of Doctor of Philosophy.

October 2014

Supervised firstly by:

Dr. Karen J. Liu

Department of Craniofacial Development and Stem Cell Biology,
King's College London, London, UK.

and secondly by:

Dr. Abigail S. Tucker

Department of Craniofacial Development and Stem Cell Biology,
King's College London, London, UK.

Examined by: Prof. Dr. Malcolm Logan

and by: Dr. Erwin Pauws

Statement of originality

I declare that all the work presented in this thesis, unless otherwise acknowledged, is my own.
This project provides an original contribution to the knowledge of this subject.

Signed …… Date……

Acknowledgements

Financial support was provided by the medical research council.

There are a number of people who I would like to thank for providing me with continuous support over the last four years.

First and foremost I would like to thank my primary supervisor, Dr. Karen Liu. Without her expertise, guidance and belief, none of this would have been possible.

I would also like to thank my second supervisor, Dr. Abigail Tucker, for giving me advise throughout the course of this project.

If it weren't for my immediate team, none of this would have been possible. All past and present members of the Liu group are massively appreciated. This includes Tree and Jacqui for showing me the ropes; Sandra for always making time for me, and Wills for his insight from day one. In addition, I would like to thank all of the newest lab members, Hadeel, Daniel and Anna, for making my final year so enjoyable.

A big thank you also goes to Angela Gates and Rebecca Wiltshire for always knowing how to help. In addition, I would like to thank my friends who have always been there for advice whenever I needed them, particularly Adil, Johnny, Ben, Andy, Mark, Finn and Guillerme.

Furthermore, I would like to thank my girlfriend, Jenny, for being so understanding and always being there for me. Last but not least I would like to thank my family. Larry and Stephanie for always encouraging me. Finally, my parents, Marina and Zachary, for always believing me and supporting me more then I ever could have asked for.

Abstract

The skeleton is an important structural framework for vertebrates that consists of bone and cartilage. Generally, the vertebrate skeletal system can be categorized into the appendicular, trunk and craniofacial skeletons. Each of these have different cellular origins and form through two distinct mechanisms: endochondral ossification, in which a cartilaginous template is first formed and then replaced by bone; or intramembranous ossification, in which cellular precursors are directly differentiated into bone. Some skeletal structures, such as the mandible, are unique and form via combinations of both processes. Skeletal dysplasias can affect both types ossification. Patients with ciliopathies manifest with multiple defects that affect most skeletal systems. In addition, two other classes of disease, the craniosynostosis syndromes and the chondrodysplasias, have several skeletal phenotypes also seen in ciliopathies, such as short limbs and craniosynostosis. In this project I focus on a ciliopathic mouse model, *Fuzzy*, in which both endochondral and intramembranous bones are affected. Cilia are cellular organelles that have multiple functions from fluid flow to signal transduction. They are associated with signalling perturbations in different pathways such as Hedgehog and Wnt. Specifically, I investigate molecular mechanisms, which cause micrognathia, mandibular hyperossification and short long bones. Furthermore, this project aims to compare and contrast some overlapping phenotypes between ciliopathies, chondrodysplasias and craniosynostosis syndromes, such as vertebral and sternal defects. Results obtained indicate that many craniofacial defects in the *Fuzzy* mutant, including micrognathia, mandibular hyperossification and craniosynostosis, can be rescued with genetic reduction of *Fgf8*. Defects affecting other skeletal elements are not rescued. These data suggest that loss of *Fuzzy* converges on *Fgf8* regulation during craniofacial development, but effects on other skeletal systems are probably due to other signalling perturbations, notably Hedgehog signalling.

List of abbreviations

BMP4:	Bone morphogenetic protein 4
CKI:	Casein Kinase I
CLAMP:	CaLponin Homology and Microtubule-associated protein
COL1:	Type 1 Collagen
COL2:	Type 2 Collagen
COLX:	Type 10 Collagen
DHH:	Desert Hedgehog
DVL:	Dishevelled
FGF:	Fibroblast Growth Factor
FGFR:	Fibroblast Growth Factor Receptor
FUZ:	Fuzzy
GliA:	Gli activator
GliR:	Gli repressor
GSK3:	Glycogen synthase kinase 3
Hh:	Hedgehog
IFT-A:	Intra-flagellar transport protein A
IFT-B:	Intra-flagellar transport protein B
IFT:	Intra-flagellar transport
IHH:	Indian Hedgehog
MC:	Meckel's cartilage
NC:	Neural Crest
OFD:	Oro-Facial Digital Syndrome
PCP:	Plana cell polarity
PKA:	Protein Kinase A
Ptc:	Patched
PTHrP:	Parathyroid hormone-related protein
RUNX2:	Runt-related transcription factor 2
SHH:	Sonic Hedgehog
SMO:	Smoothened
SUFU:	Suppressor Of Fused

Table of Contents

Table of Figures

Chapter 1 General Introduction

1.1 The skeleton

The skeleton consists of bone and cartilage and is the structural framework for all vertebrates. Broadly speaking it can be classified into the axial and the appendicular skeleton. These portions of the skeleton form through different mechanisms and from different cellular origins (Reviewed by (Olsen et al., 2000). Generally, ossification can occur in two different methods: endochondral ossification, in which a cartilage template is first formed and then replaced by bone; and intramembranous ossification, in which bone is formed in the absence of cartilage. These two processes are described in detail in section 1.3. This project aims to compare the two types of ossification in a ciliopathic model: the *Fuzzy* mutant mouse (Gray et al., 2009).

The axial skeleton consists of the trunk and craniofacial skeleton. The former consists of the vertebrae, ribs and pelvis, whilst the latter gives rise to the head and face. The appendicular skeleton gives rise to the long bones and the sternum. Embryonically, these different skeletal regions develop from different cellular origins.

1.1.1 Embryonic origins of the skeleton

In vertebrates, the skeleton is derived from three different embryonic cell types. The lateral plate mesoderm gives rise to the appendicular skeleton, the paraxial mesoderm gives rise to the trunk skeleton, and the cranial neural crest (NC) contributes to most of the craniofacial skeleton (Hall and Miyake, 1992, Cohn and Tickle, 1996, Tam and Trainor, 1994). These precursors all arise from discrete regions in and around the neural tube on the dorsal region of vertebrates (schematized in fig 1.1). Initially, the ectoderm is differentiated into the neural plate and a non-neural epithelium. As the edges of the neural plate come together and fuse to form the neural tube, NC cells are induced (Gallera, 1971, Gilbert, 2006).

Once formed, the NC cells delaminate, undergoing an epithelial to mesenchymal transition as they leave the neural tube, and migrate to the periphery of the embryo (Duband et al., 1995). Subsequently, depending on their position along the rostral-caudal axis of the embryo, NC cells differentiate into a variety of cell types. The cranial neural crest cells give rise to the majority of the facial skeleton. Vagal, sacral and trunk NC are the more caudal cells. Trunk NC give rise to structures such as the adrenal gland and pigment cells while vagal and sacral NC give rise to the enteric nervous system and the parasympathetic ganglia, respectively (Trainor, 2005, Murdoch et al., 2012, Simkin et al., 2013, Gilbert, 2006).

Embryonic origins of the craniofacial skeleton

Cranial neural crest cells give rise to many craniofacial structures including but not limited to craniofacial neurons, teeth, cartilage, bone and connective tissue of the head and face. There are distinct populations of NC cells arising from the forebrain, midbrain and hindbrain, which migrate to populate the head and face (LaBonne and Bronner-Fraser, 1998, Knecht and Bronner-Fraser, 2002). Cells from the midbrain, or presumptive posterior mesencephalon, populate the first branchial arch (Osumi-Yamashita et al., 1997). This is schematized in Fig 1.2.

The branchial arches (BA) consist of a series of paired protrusions. They are lined up on either side of the midline along the ventral region of the embryo (Fig 1.2 shows a lateral view). BAs are formed by NC cells surrounding a mesodermal core. Both cell populations give rise to different skeletal structures of the head and face. NC cells give rise to the upper and lower jaw, and the frontal bone of the calvaria, whilst mesodermal cells give rise to the parietal bone of the calvaria and posterior parts of the cranium (Noden, 1983, Noden, 1988). The majority of craniofacial cartilage and bone is derived from BA1. Cranial NC populates this arch by migrating from the first and second rhombomeres, the hindbrain and the midbrain. Cells that populate BA1 ultimately go on to form craniofacial structures including, but not limited to the upper and lower jaws and the palate (Gilbert, 2006). Formation of these bones is by both endochondral and intramembranous ossification (See chapter 5).

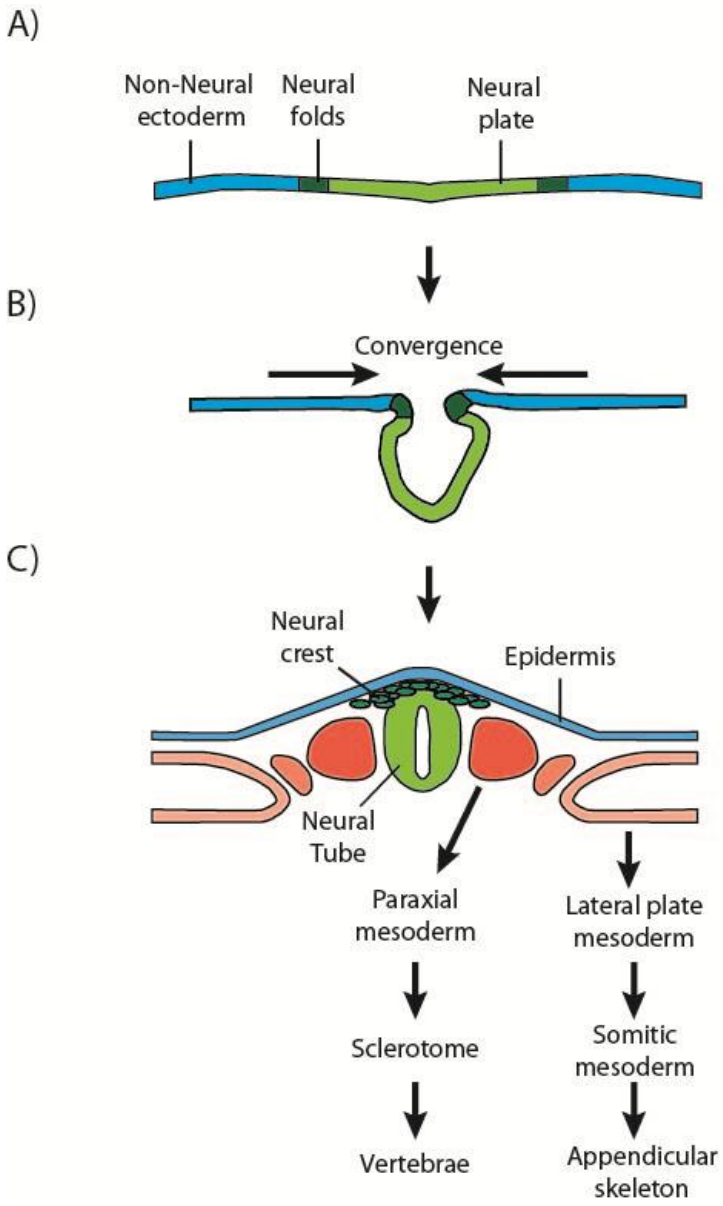

Figure 1.1 Cellular origins of the skeleton

A) Dorsal tissue is separated into neural and non-neural ectoderm, which flank the neural folds. Neural folds specify the neural crest.

B) Neurulation occurs as the non-neural ectoderm converges to form the neural tube.

C) Neural crest cells arise from the neural folds and the non-neural ectoderm forms a continuous epidermis. Paraxial mesoderm is formed adjacent to the neural tube and is subsequently specified into sclerotome, which gives rise to the vertebra. The lateral plate mesoderm is formed more laterally and gives rise to the somatic mesoderm, subsequently giving rise to the appendicular skeleton.

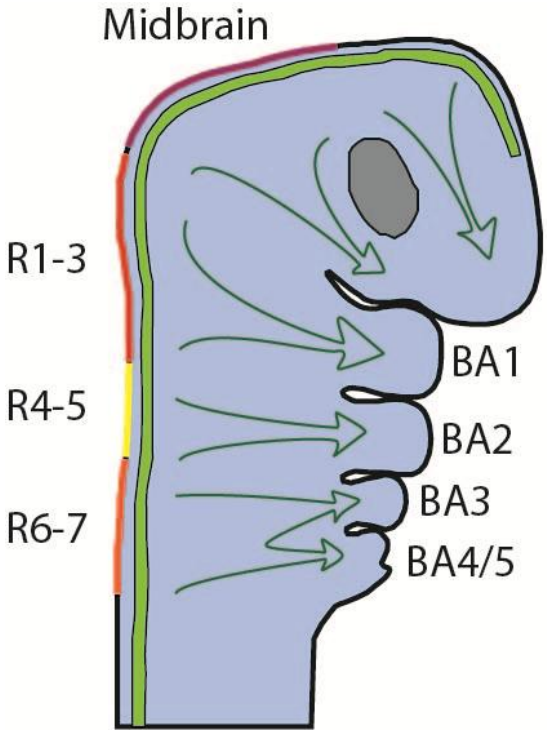

Figure 1.2 Schematic of a lateral view of the mammalian branchial arches.

Dorsally the embryo can be segmented into rhombomeres (R1-R7) and the midbrain. Streams of neural crest cells originate from these regions and migrate into the branchial arches. Neural crest derived mesenchyme that populates Branchial arch 1 predominantly gives rise to the craniofacial skeleton.

Embryonic origins of the appendicular skeleton

The appendicular skeleton is derived from the lateral plate mesoderm. This consists of two mesodermal sheets, the splanchnic mesoderm and the somatic mesoderm, which are specified during neurulation (schematized in Fig 1.1 C). The former covers the dorsal endoderm and forms a mesothelium that covers visceral organs. The latter covers the ventral ectoderm and gives rise to connective tissue of the limb bud and appendicular skeleton. This skeletal derivative is thought to form entirely via endochondral ossification.

Embryonic origins of the trunk skeleton

The trunk skeleton, made up of the vertebra and ribs, is derived from the paraxial mesoderm, which flanks the neural tube on the dorsal region of the embryo (Schematized in Fig 1.1 C). This mesoderm is ultimately segmented into somites, which subsequently give rise to sclerotomal cells (Christ and Ordahl, 1995). The sclerotome migrates away from the somites and gives rise to different tissue types including the dorsal dermis and skeletal muscles as well as the trunk skeleton (Brand-Saberi and Christ, 2000). This comprises the vertebra, ribs and pelvis, all of which form through endochondral ossification. Development of the spine will be discussed in more detail in chapter 6.

Apart from the embryonic origins from which different skeletal elements form, the key difference between them is in the method through which they ossify. Endochondral ossification is preceded by the formation of a cartilaginous template, whilst intramembranous ossification does not.

1.1.2 Cartilage

Cartilage is a flexible, avascular connective tissue, consisting of chondrocyte cells contained in a rich extracellular matrix (ECM). This tissue is hugely important throughout animals ranging from fish to amphibian to mammal, and for this reason it is highly evolutionarily conserved (Hall, 2005). The ECM in which the chondrocytes sit is composed of different types of collagens, most commonly collagen type II (COL2), as well as glycosaminoglycans (GAGs), such as proteoglycans, and various other

connective tissue fibers, such as elastin (Hall, 2005). Differences in cartilaginous composition contribute to different functions and define three main types of vertebrate cartilage: hyaline, elastic and fibrocartilage.

Elastic cartilage consists of col2 and many elastic fibers, such as elastin and fibronectin. These fibers are densely packed enabling support of structures such as the pinna (the external ear.) Fibrocartilage consists mostly of type 1 collagen fibers (COL1) arranged in parallel groups. In this way, dense COL1 fibers provide a high degree of tensile strength and provide support during fracture healing and in structures such as the vertebral disks (Hall, 2005).

Hyaline cartilage predominantly consists of GAGs and COL2. It is found at the articular tips of bones, the tips of ribs as well as the trachea and bronchi (Hall, 2005). High COL2 presence accounts for the high tensile strength found in this cartilage, and the high GAG content provides resistance to pressure. Due to its flexible yet supportive nature, hyaline cartilage acts as a template for bone formation during the process of endochondral ossification.

1.1.3 Bone development

Bone is extremely dense connective tissue, which has important roles in support, protection of internal organ and production bone marrow, which is needed for differentiation of lymphocytes and erythrocytes (Zhu et al., 2007, Morrison and Scadden, 2014, Hall, 2005). Structurally, it consists mainly of mineralized osseous tissue, of which there are two main types; cortical bone and cancellous bone. Cortical bone is very dense and typically makes up outer-bone mass. They have many small hollow passages running through them, called lacunae, which house bone forming cells known as osteocytes, and allow transport of ions such as calcium and phosphate (Talmage, 1970, Hall, 2005, Enlow, 1962). Cortical bone typically surrounds cancellous bone. Cancellous bone is less dense and highly vascular due to the presence of spicules of calcified fiber which are called trebeculae, (Odgaard, 1997). These fibers have space between them to house bone marrow and allow metabolic activity, such as hematopoiesis and calcium ion exchange (Morrison and Scadden, 2014, Hall, 2005).

On a cellular level, bone is formed from osteoblasts, which mature into osteocytes. The former produces a matrix, consisting of unmineralized osteoid. Osteoid is a metabolic bone matrix, which predominantly consists of type 1 collagen (COL1). Once this matrix forms, osteoblasts can mature into osteocytes to form mature bone. Osteocytes synthesize COL1 as well as other proteins, such as osteopontin (Hall, 2005). They are ultimately permeated with mineralized hydroxyapatite, which is a natural mineral consisting of calcium, phosphate and hydroxide (Clarke, 2008). Bone formation is a dynamic process in which osseous tissue is constantly being formed by osteoblasts and osteocytes as well as reabsorbed by osteoclasts. This is needed for maintenance of integrity and bone repair (Hall, 2005).

As mentioned above, bone formation occurs through two key processes: a cartilage-dependent process called endochondral ossification, and cartilage-independent intramembranous ossification.

Endochondral Ossification

Endochondral ossification, seen in the majority of skeletal elements in the body, is a well-characterised event in which cartilage is deposited and undergoes maturation, which is required for subsequent bone formation (reviewed by (Olsen et al., 2000). This occurs in a structure known as the growth plate and is schematized in Fig 1.7 .

The initial cartilage template is formed from precursor cells, which aggregate at the site of cartilage formation, adhere to each other and become more tightly packed in a process called cellular condensation. This is done under the control of the transcription factor SOX9. In the presence of SOX5 and SOX6, SOX9 homodimerizes and directly binds to the first intronic enhancer of *Col2a.* (Lefebvre et al., 1998)(Bernard et al., 2003, Ng et al., 1997, Bell et al., 1997) The importance of this is seen in *Sox9* null mice, in which conditional inactivation in the limb bud results in an absence of long bone skeleton (Akiyama et al., 2002).

These precursors are then differentiated into a specialized cell type known as chondrocytes. They deposit an extracellular matrix rich in collagens:

COL2, Collagen 9 and Collagen 11, as well as extracellular matrix components such as aggrecans, and GAGs (Hall, 2005, Han and Lefebvre, 2008). This happens within a structure called the perichondrium, which is a layer of connective tissues surrounding the developing cartilage. In the growth plate these are referred to as resting chondrocytes. Under signaling cues, such as Fgf and Hh signaling (expanded upon in section 1.3), they are induced to proliferate in columns running parallel to the orientation of the developing skeletal element.

Proliferating chondrocytes then differentiate into pre-hypertrophic and hypertrophic chondrocytes. During this process, morphological changes occur and cells become enlarged in size. These hypertrophic chondrocytes alter their collagen secretion from COL2 to a more 'mature' COLX, which is specific to hypertrophic chondrocytes (Shen, 2005). It is the formation of proliferative and hypertrophic chondrocytes, which is believed to drive longitudinal growth of the endochondral skeleton.

Onset of hypertrophy is associated with the transcription factor RUNX2, which then upregulates factors necessary for osteoblast differentiation, including *Osterix* (Nakashima et al., 2002). Angiogenesis and vascularization of the mature cartilage enables delivery of hematocytes, osteoblasts and osteoclasts, which degrade the cartilage and synthesize bone in discrete regions known as primary ossification centers. These different stages of chondrocyte differentiation and bone deposition take place in a spatially organized structure known as the growth plate. Key signaling pathways relevant to this project that are involved in endochondral ossification will be described in section 1.3.

Intramembranous ossification

A variety of craniofacial bones, such as the cranial vault and sutures; as well as the lateral part of the clavicles, which are part of the appendicular skeleton, form via an alternative strategy without a cartilaginous template. This is called intramembranous ossification (Noden, 1992, Garzon-Alvarado et al., 2014). During this process, precursor cells, typically mesoderm or neural crest derived, undergo condensations similar to those described in

endochondral ossification. As in endochondral ossification, RUNX2 activity commits these cells to the osteoblast lineage and haploinsufficiency of *Runx2* results in reduced ossificion of intramembranous bones (Nakashima et al., 2002, Komori et al., 1997, Lee et al., 1997).

1.2 Signaling pathways relevant to this project

Multiple signaling pathways are involved in development of the skeleton. These pathways include Wnt, Hedgehog (Hh), fibroblast growth factor signaling (Fgf) and bone-morphogenetic protein (BMP) signaling, to name a few. In this section I will describe the Wnt, Hh and FGF signaling, as they are particularly relevant to this project.

1.2.1 Wnt signaling

Wnt signaling is comprised of multiple intracellular signaling pathways: Wnt/b-catenin (or canonical Wnt), planar cell polarity (PCP) and the Wnt/calcium pathways. All of these pathways are initiated by binding of an extracellular Wnt ligand to the transmembrane Frizzled (Fz) receptor. The two most relevant to this thesis are the canonical and PCP pathways.

Wnt ligands are secreted glycoproteins that are heavily modified prior to extracellular release. They can signal to the cell from which they were synthesized (autocrine signaling) or to neighboring cells (paracrine signaling). Post-translational modifications include lipid additions such as glycosylation and palmitoylation, which serve multiple roles from targeting ligands to different cellular domains and assistance in receptor binding (Smolich et al., 1993, Willert et al., 2003, Cong et al., 2004, Tanaka et al., 2002). Classically it was believed that different Wnts conferred differential pathway activation. Recently however, it has been shown that 'non-canonical Wnts' can activate the canonical pathway in certain contexts (He et al., 1997, Mikels and Nusse, 2006, Tao et al., 2005). This suggests that pathway specification is determined by the cellular context in which ligands bind to FZ and its co-receptors.

Binding of the Wnts to FZ activates the intracellular protein Dishevelled (DVL). It is through this protein that signaling of both canonical and PCP pathways are mediated.

Canonical Wnt signaling

Canonical Wnt signaling is mediated through β-catenin, which is a transcriptional co-activator. On binding of canonical Wnt ligands to FZ, DVL inhibits the formation of a β-catenin destruction complex. This complex consists of multiple proteins including adenomatosis polyposis coli (APC), Axin and glycogen synthase kinase-3 (GSK-3).

In the absence of canonical Wnt ligand, the destruction complex phosphorylates β-catenin, which leads to ubiquitination and targeting of b-catenin to the proteosome for degradation. On ligand binding, the destruction complex is disrupted, leaving β-catenin is free to translocate into the nucleus and bind to TCF/LEF1 factors facilitating downstream transcription. These transcription factors control functions ranging from progenitor cell expansion, cell migration and cell fate decisions (well reviewed by (Grigoryan et al., 2008). Canonical Wnt signaling is schematized in Fig 1.3.

Non-canonical Wnt PCP signaling

PCP signaling does not involve β-catenin. It refers to the coordinated orientation of cells and structures along the plane of an epithelial surface. The pathway gives polarity to cells, thereby enabling them to perform complex and coordinated movements. As such, in mice, PCP is needed for cell orientation and migration that drives processes such as neural tube closure, and orientation of stereocilia in the cochlea (Montcouquiol et al., 2003, Wang et al., 2005a, Kibar et al., 2001, Murdoch et al., 2001)

Like the canonical pathway, PCP is dependent on Wnt binding to FZ and subsequent signaling via DVL. Outcomes of this pathway stem from a variety of different intracellular signaling cascades. For example, the establishment of polarity has been best described in *Drosophila*. Asymmetric localization of Dsh (the invertebrate homologue of DVL) and another core PCP transmembrane protein, Van Gogh (Vang) distinguishes “proximal” versus

"distal" sides of the cell (Figure X). During this process, Vang is localized asymmetrically and recruits an accessory protein Prickle (Pk). Pk subsequently binds to Dvl and inhibits the formation of local Dsh and Fz complexes. In this way, Vang/Pk complexes are activated in different cellular regions to one another, thus inducing polarity (schematized in fig 1.4). Although this has been best described in controlling hair cell orientation in *Drosophila*, loss of core PCP components, such as DVL and VANGL2 in mice results in non-uniform cell orientation in the cochlea and a loss of PCP dependent digit extension (Wang et al., 2005a, Gao et al., 2011). With regards to cell motility, PCP signaling induces a cascade resulting in actin rearrangement. In this situation, FZ activation of DVL initiates a signaling cascade of the Rho GTPase family, such as RhoA, Cdc42 and Rac, which are involved in cytoskeletal remodeling (Schlessinger et al., 2009).

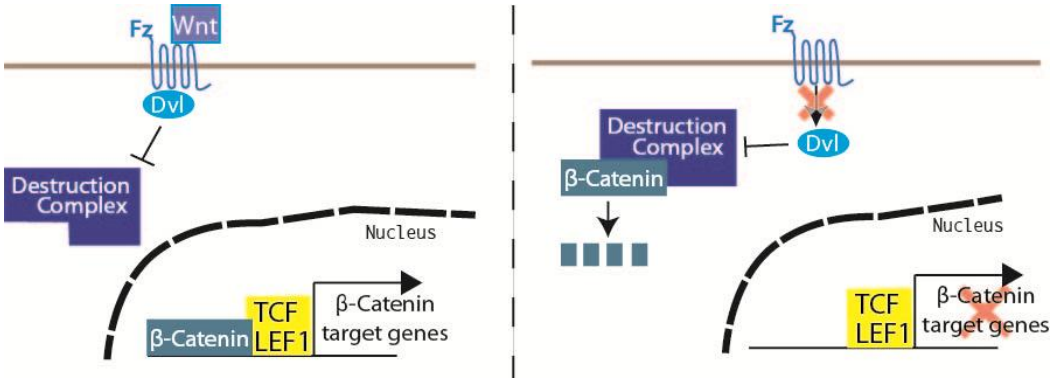

Figure 1.3 Schematic of canonical wnt signaling

The Wnt ligand binds to the transmembrane Frizzled (Fz) receptor. Subsequently, Dischevelled (Dvl) inhibits a β-catenin destruction complex, enabling β-catenin mediated transcription of TVC and LEF1 target genes.

In the anbsence of the Wnt ligand, Dvl does not inhibit the destruction complex. Accordingly β-catenin is targeted for proteosomal degradation and there is no transcription of down stream targets.

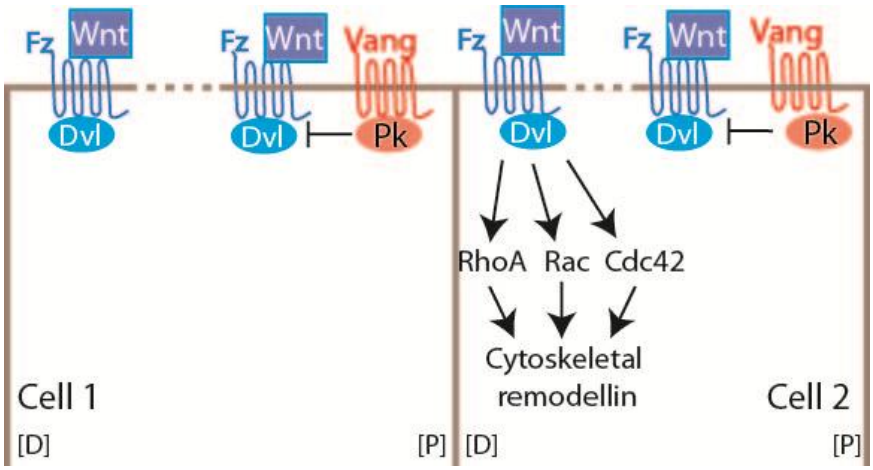

Figure 1.4 Schematic of non-canonical Wnt PCP signaling

Differential accumulation of Frizzled (Fz) and Dishevelled (Dvl) on the 'dorsal' side of the cell, compared to Van-Gogh (Vang) and Prickle (Pk) on the 'proximal' side, induces polarity. This is established by feedback signaling from Vang/Pk to Fz/Dvl in the 'proximal' region.

Fz and Dvl can also influence the actin cytoskeleton by signaling through the Rho-GTPase signaling cascade.

1.2.2 Hedgehog signaling

Hedgehog (Hh) signaling is a key developmental pathway during embryogenesis. Like Wnt signaling, its main function is in transduction of extracellular signals into intracellular responses. This is done via Hh ligand binding to the extracellular Patched (PTC) receptor. Subsequent downstream events are mediated by Gli transcription factors.

In mammals there are three Hh ligands: Desert Hedgehog (DHH), Indian Hedgehog (IHH) and Sonic Hedgehog (SHH). The former is important for spermatogenesis whilst the latter two are more involved throughout development (Clark et al., 2000). Like the Wnts, Hh ligands are proteins that undergo multiple post-translational lipidation modifications prior to secretion (Pepinsky et al., 1998, Chamoun et al., 2001). Lipid modification, as well as oligomerisations is reported to contribute to long range signaling, whilst membrane tethering influences short range events (Vyas et al., 2008, Zeng et al., 2001, Gallet et al., 2006, Pathi et al., 2001). As such HHs are known to travel short and relatively long distances to bind to PTC. As such they have been seen to 300μm in vertebrate limb buds (Briscoe and Therond, 2013).

Structurally all three ligands are similar and can all bind to and activate Ptc and its co-receptors (Kavran et al., 2010). In addition, the amino terminal of HHs is sufficient to induce downstream signaling events (Porter et al., 1996, Bumcrot et al., 1995, Lee et al., 1994) Comparative analysis, in cell and organ culture, has been carried out to determine whether there are differences between each ligand to mediate downstream events. This, revealed that in most contexts, such as limb bud explant manipulation of digit patterning, and Hh regulation of hypertrophy, there is differential potency between them such that SHH>IHH>DHH (Pathi et al., 2001). In neural plate explants, however, they were equipotent in inducing *Islet-1,* which is typically induced by *Shh* during neurogenesis. PTC exists in two homologues with PTC1 thought to be the major receptor during embryogenesis (Adolphe et al., 2014). In the absence of Hh ligands, PTC inhibits transmembrane protein

smoothened (SMO). Hh binding to PTC stops this inhibition and allows SMO to mediate downstream Hh events (Wang et al., 2009).

Gli proteins mediate transcriptional responses to Hh signaling. In mammals, there are three different Gli proteins which all have similar DNA binding properties. They all contain a C-terminal activation domain whilst only Gli2 and Gli3 contain an N-terminal repressor domain (Pan and Wang, 2007, Briscoe and Therond, 2013). When at full length, Gli2 and Gli3 can be processed into either activators or repressors however Gli2 mostly provides activator activity whilst Gli3 usually provides repressor activity (Matise et al., 1998, Litingtung et al., 2002, Pan and Wang, 2007). Gli1 has not been shown to have essential roles in mammals, but excessive Gli1 activity is associated with tumorigenicity (Park et al., 2000, Clement et al., 2007, Stecca et al., 2007).

In general terms, in the absence of the Hh ligand, PTC inhibits activity of SMO. This enables full length Gli2 and Gli3 to be phosphorylated by protein kinase A (PKA), Casein kinase I (CKI) and GSK3β. Phosphorylation causes proteolytic cleavage of full length Glis into their repressor forms (Liu et al., 2005b, Tuson et al., 2011, Sillibourne et al., 2002, Barzi et al., 2010). Conversely, binding of Hh ligands to PTC relieves inhibition of SMO. Active SMO enables Glis to avoid post-translational processing and in this way they are maintained in their long-form activator forms. Therefore, as a result of Hh ligand binding, there is an increase in the amount of Gli activator (GliA) compared to Gli repressor (GliR). This is schematized in Fig 1.5.

Adding further complexity to the Hh signaling pathway, different Glis act individually or in combination to regulate tissue specific processes (Ruiz i Altaba, 1999, Pan and Wang, 2007). Hence, proper Hh signal transduction is dependent on the ratios of Gli activators to Gli repressors and different target genes respond differentially to these ratios. For example, in mouse neural tube formation, ventral neuronal differentiation is dependent on inhibition of Gli repressors whilst in floor plate induction; Gli2 activators are crucial (Matise et al., 1998, Ruiz i Altaba, 1999). In recent years, proper Hh

signaling has been seen to be dependent on proper formation of the cilia. This will be expanded upon in section 1.4.

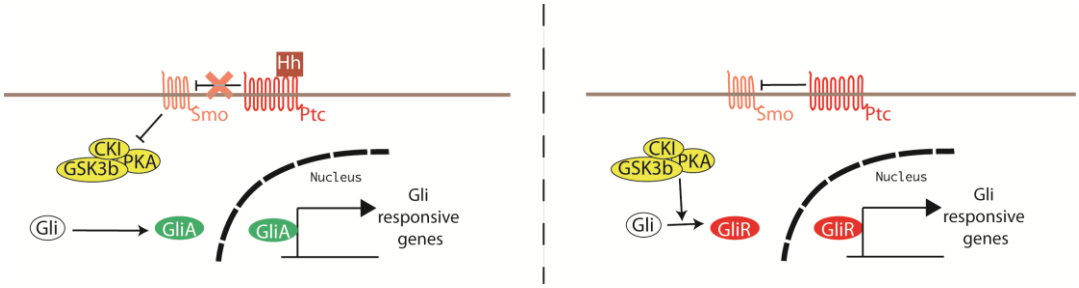

Figure 1.5 Basic schematic of Hedgehog signaling

On binding of the Hedgehog (Hh) ligand, Patched (Ptc) no longer inhibits Smoothened (Smo). Smo inhibits multiple phosphorylation proteins, which enables full length Gli to act as a transcriptional activator (GliA).

In the absence of the Hh ligand, Ptc inhibits Smo. As a result, phosphorylation proteins target full length Gli for proteosomal degradation into its repressor form (GliR).

1.2.3 FGF signaling

FGF signaling is an important mechanism through which a variety of biological processes are controlled. These range from early developmental programs of the embryo, regulation of cellular behaviors such as cell survival, proliferation and differentiation; and control of tissue behavior such as patterning, morphogenesis and organogenesis (Niswander et al., 1993, Bellusci et al., 1997, Peters et al., 1993). As a result of the diverse roles of FGF signaling, it is no surprise that aberrant FGF signaling has been associated with a plethora of human diseases ranging from deafness to skeletal malformations (Mohammadi et al., 2005).

The diverse roles of FGF signaling have evolved through the presence of a large number of FGF ligands, coupled with multiple forms of FGF Receptors (FGFRs) and co-receptors, which are expressed in a tissue specific context. In mammals, there are 18 secreted FGF glycoprotein ligands numbered FGF 1-10 and FGF 16-23. FGFs 11-14 are intracellular proteins that function in a receptor-independent manner. FGFs 15, -19, -21 and -23 circulate in the blood stream to exert their functions in a hormone-like manner; whilst FGFs 1-10, 16-18, -20 and -22 act as local growth factors (Goldfarb, 2005, Itoh and Ornitz, 2008). All FGFs have a homologous central region flanked by highly divergent amino and carboxy termini (Goetz et al., 2010, Kalinina et al., 2009).,The different activities of the ligands can be partially attributed to these varying regions (Mohammadi et al., 2005). In addition, alternative splicing, as seen in FGF8 in the brain, and FGF10, in part confers ligand-receptor specificity (Olsen et al., 2006, Yeh et al., 2003).

Ligands act through transmembrane FGFRs, of which there are 5.
Structurally, the FGFR1-4 are similar and consist of an extracellular immunoglobulin (Ig)-like domain, a transmembrane domain and an intracellular tyrosine kinase domain. FGFR5 lacks the tyrosine kinase domain. The extracellular portions of FGFRs consist of 3 Ig-like motifs (IgI-IgIII). It is the IgII and IgIII regions that are essential for ligand binding. Extracellular portions of FGFRs also have an ‘acid box’, which is a serine-

threonine rich domain that sits in the linker region between IgI and IgII, and is thought to be important for auto-inhibition.

During signal transduction, ligands must bind specifically to FGFRs. Receptor diversity is established by exon skipping, which removes the acid box, and alternative splicing in the IgIII domain. Through these mechanisms, FGFR1-4 are diversified into 7 main FGFRs as a means to generate different ligand affinity (Beenken and Mohammadi, 2009). Receptor diversity is tissue specific, for example with regards to FGFR2, the –b isoforms are typically expressed in epithelia, whilst –c isoforms are usually expressed in mesenchyme (Orr-Urtreger et al., 1993).

A functioning ligand-receptor interaction consists of ligand binding to IgII and –III and associated heperan sulphate proteoglycans. This leads to dimerization of the receptors and is essential for signal transduction to occur (Schlessinger et al., 2000). Receptor dimerization causes a change in conformation of the FGFRs. This subsequently activates the intracellular tyrosine kinase domains to trans-phosphorylate each other. Consequently there is recruitment of adapter proteins and activation of different intracellular signaling cascades. Three key pathways regulate cell proliferation, survival and motility. In each case, a variety of accessory proteins are required to bind to the FGFR in order to mediate these responses.

FGFR substrate 2 (FRS2), son of sevenless (SOS), growth factor-receptor bound 2 (GRB2), Phospholipase Cγ (PLCγ) and GRB2-associated binding protein 1 (GAB1) are key accessory proteins. FRS2, GRB2 and SOS initiate a MAPK cascade. This primarily promotes genes required for cell proliferation; however, it can also lead to cell differentiation and migration. On the other hand, FRS2, GRB2 and GAB1 stimulate AKT kinase to inhibit apoptotic factors, thus promoting cell survival. Thirdly, PLCγ initiates a complex cascade involving diacyglycerol (DAG) and protein kinase C (PKC), which stimulates the expression of proteins needed for cell motility. These three pathways are schematized in fig 1.6. In more tissue specific contexts,

several other pathways can be activated including signal transducer and activator of transcription (STAT), p38 MAPK, Jun N-terminal kinase (JNK) and ribosomal protein S6 kinase 2 (RSK2) (see reviews by (Turner and Grose, 2010, Goetz and Mohammadi, 2013)).

In a developmental context, one important downstream FGF signaling cascade is the MAPK/ERK pathway, which has been shown to stimulate cellular proliferation (Ho and Dowdy, 2002). Interestingly, in different cellular contexts, MAPK signaling can result in cell cycle arrest and differentiation (Laprise et al., 2002, Pumiglia and Decker, 1997). This shows the importance of tissue specificity for different FGF signaling roles. In addition, signaling can be modulated by negative feedback. A good example of this is the Sprouty (SPRY) proteins. These proteins form hetero- and homo- oligomers, through their C-terminal domains, and are thought to compete with binding of adaptor proteins such as GRB2 and FRS2. In doing so, SPRYs can inhibit and modulate downstream FGF signaling (Casci et al., 1999, Ozaki et al., 2005).

To summarize, FGF signaling can lead to many different outcomes in different biological contexts. This complexity is generated by tissue specific expression of ligands and receptors, differing binding affinities between ligands and receptors and a vast array of downstream signaling pathways (Mohammadi et al., 2005).

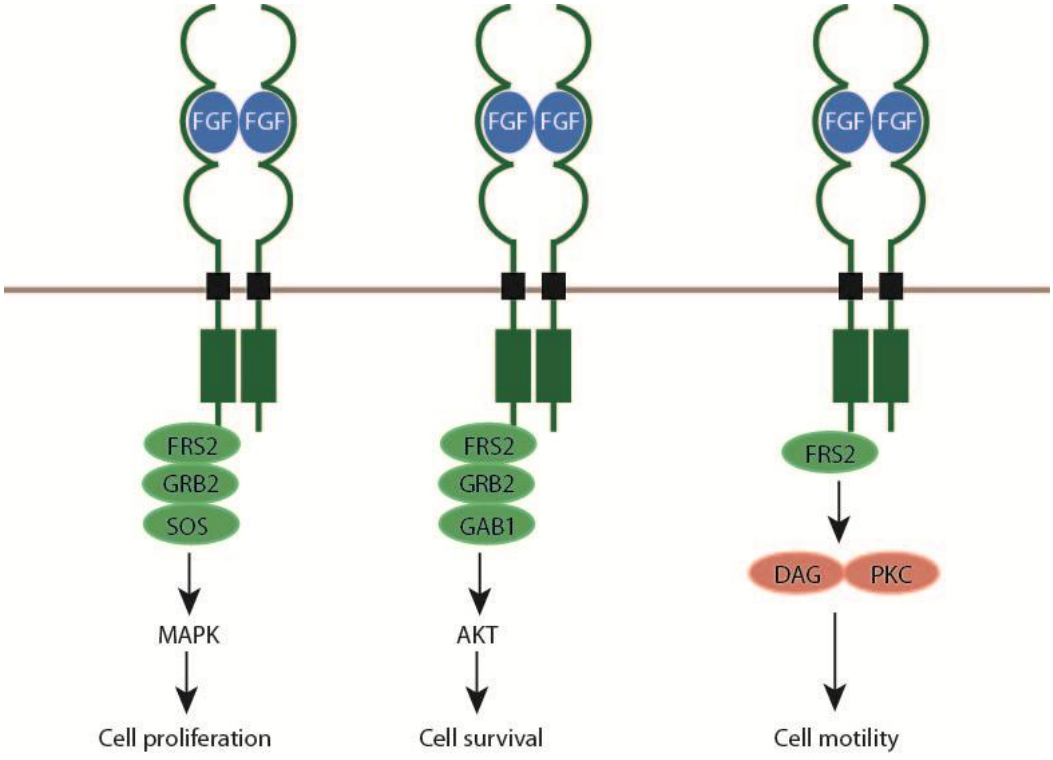

Figure 1.6 Key downstream pathways of FGF signaling

Receptor dimerization and signaling through the accessory proteins substrate 2 (FRS2), growth factor-receptor bound 2 (GRB2) and son of sevenless (SOS), initiate a MAPK signaling cascade to regulate cell proliferation

Signaling through the accessory proteins FRS2, GRB2 and GRB2-associated binding protein 1 (GAB1) initiates an AKT cascade needed to promote cell survival.

Signaling via FRS2 can also initiate a diacyglycerol (DAG) and protein kinase C (PKC) mediated cascades to control cell motility.

1.3 Hh, Wnt and Fgf in skeletal development

The signaling pathways described above have specific and well-defined roles in both endochondral and intramembranous ossification. Key signaling events discussed are schematized in Fig 1.7.

1.3.1 Signaling during endochondral ossification:

Pre-chondrogenic condensations

Prior to differentiation into chondrocytes, precursor cells undergo epithelial-mesenchymal transitions, which drive cellular condensations (Hall and Miyake, 2000). Condensed cells are densely packed as a result of upregulation of cell surface molecules, such as tenascin and heperan sulphate and adhesion molecules, such as N-CAM and N-cadherin. This enables cells to adhere to one another as a means of initiating condensations and establishing the condensation boundaries (Hall and Miyake, 2000). TGF-β and BMP receptors are expressed in pre-chondrogenic condensing mesenchyme but not differentiated chondrocytes themselves, implicating them in the formation of an inductive environment (Hall and Miyake, 2000).

One important transcription factor, SOX9, is expressed by condensing cells. It acts to initiate chondrogenesis in the place of ossification. SOX9 has roles in inhibiting RUNX2 activity via direct binding, and hence inactivation, as well as transcriptional repression and targeting for lysosomal degradation (Zhou et al., 2006, Yamashita et al., 2009, Cheng and Genever, 2010). This is one way in which cells are restricted from differentiating into osteoblasts. In addition to this, SOX9 is thought to make a physical complex with β-catenin. As a result of this, both proteins are inactivated, thus canonical Wnt signaling is thought to regulate condensations (Akiyama et al., 2004). The prediction is that as a result of the SOX9 and β-catenin interactions, as well as SOX9 and RUNX2 interactions, condensing cells are restricted to the endochondral pathway (Akiyama et al., 2004). The importance of this is seen in *Sox9* null mice, in which conditional inactivation in the limb bud results in an absence of long bone skeleton (Akiyama et al., 2002).

Chondrogenic Differentiation

Col2a1 expression induced by SOX9 is the hallmark of endochondral cartilage and *Col2a1* is required for proper chondrogenic development. As such, mice lacking functional regions of the gene have severely stunted cartilage development (Zhou et al., 1995). Given the important role of SOX9 in controlling *Col2a1* expression, and the role of β-catenin in regulating *Sox9* expression, it is suggested that canonical Wnt signaling controls chondrogenic onset in the growth plate (Akiyama et al., 2004, Bell et al., 1997).

Chondrogenic proliferation and hypertrophy

Proliferating chondrocytes express the same markers as resting chondrocytes (Leung et al., 2011). The characteristic columnar arrangements of proliferative chondrocytes are thought to be oriented by PCP signaling and in the absence of Prickle, columnar organization is lost (Yang et al., 2013). *Sox9* expression in proliferative chondrocytes is required to inhibit *Runx2* expression and activity in pre-hypertrophic chondrocytes. In this way it is believed to regulate transition from proliferation to pre-hypertrophy (Dy et al., 2012, Zhou et al., 2006).

FGF signaling is a key pathway in regulating the numbers of both proliferative and pre-hypertrophic chondrocytes in the developing growth plate. *Fgfr3* expression in proliferating chondrocytes inhibits both proliferation and hypertrophic onset (Murakami et al., 2004, Peters et al., 1993, Delezoide et al., 1998). Although multiple FGF ligands, including FGF7, -8, -17 and -18 have all been detected in the perichondrium of developing limbs, FGF18 is thought to be the key ligand that signals via the FGFR3 in this context (Mason et al., 1994, Xu et al., 1999, Liu et al., 2002, Ohbayashi et al., 2002). In keeping with the important role of FGFR3, mouse knockout and gain-of-function mutants have dwarfism and enlarged long bones respectively (Chen et al., 1999, Casci et al., 1999, Li et al., 1999, Su et al., 2010b).

Ihh signaling is another main pathway through which pre-hypertrophic and hypertrophic onset is regulated. This is expanded upon in chapter 4 but briefly, Ihh is secreted from hypertrophic chondrocytes and works in a feedback loop with parathyroid hormone-related protein (PTHrP) in order to regulate the numbers of chondrocytes committed to hypertrophy. Ihh expression in hypertrophic chondrocytes also stimulates blood vessel invasion, needed for osteoblast migration and differentiation as well as apoptosis of the zone of hypertrophy as new bone is being formed (Colnot et al., 2005). The importance of Ihh for chondrocyte maturation is best seen in *Ihh* null mutants, which have severe dysplasia of all skeletal elements. This is associated with a loss of COLX expression and absence of chondrocyte hypertrophy in the growth plate of the humerus at multiple embryonic ages (St-Jacques et al., 1999)

In humans, a common set of disorders called chondrodysplasias result in short endochondral. The most common is achondroplasia, also known as dwarfism. In these patients, chondrocyte maturation is perturbed during elongation of the long bones. This is due to gain of function mutations in *Fgfr3,* as is seen in FGFR3 mouse models. Additional skeletal abnormalities, including premature calvarial suture closure (craniosynostosis), can also be observed in chondrodysplasias. This will be the topic of chapter 5.

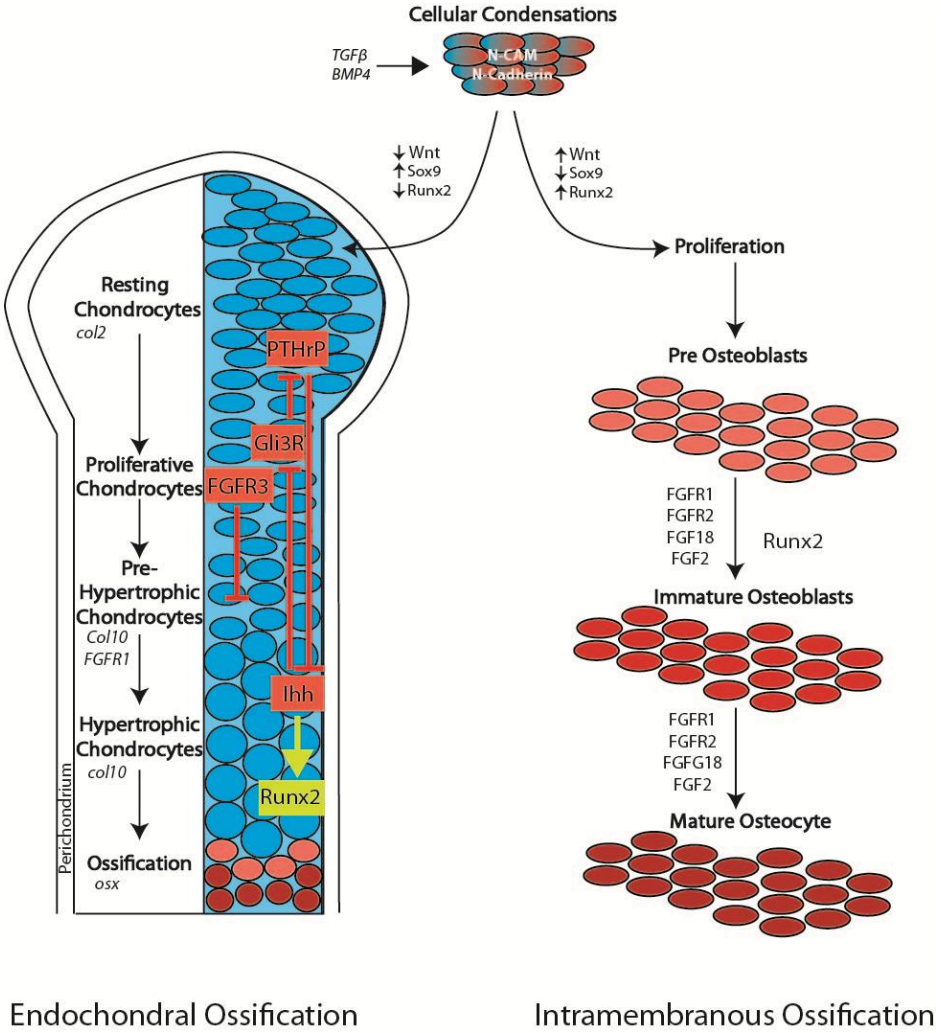

Figure 1.7 Pathways controlling endochondral and intramembranous ossification

Both processes are initiated by cellular condensations, which express adhesion molecules such as N-CAM and N Cahdherin. This is in part under the control of TGFβ and BMP4.

Endochondral ossification is associated with high *Sox9* expression coupled with low Wnt and Runx2. Precursors are then differentiated into resting chondrocytes, which abundantly express COL2. Resting chondrocytes proliferate in columnar orientations prior to pre- hypertrophic and hypertrophic differentiation. Hypertrophic chondrocytes abundantly express COL10. Chondrocyte maturation is under the control of two key pathways. Signaling through FGFR3 and via and Ihh-PTHrP negative feedback loop (described in the text). Hypertrophic chondrocytes are subsequently replaced by bone under the control of Runx2.

Intramembranous ossification is associated with low *Sox9* expression and high Wnt and Runx2. Cellular precursors proliferate and differentiate into the osteoblasts. Osteoblast maturation into osteocytes is under the control of Fgf signaling.

1.3.2 Signaling during intramembranous ossification

In pre-osteogenic condensations, contrary to chondrocyte differentiation, high levels of β-catenin degrades SOX9, which in turn allows *Runx2* expression (Akiyama et al., 2004, Zhou et al., 2006). This commits tissues to an osteogenic fate. In this way, Wnt signaling acts as a switch favoring intramembranous bone development over cartilage formation (Day et al., 2005, Akiyama et al., 2004).

Intramembranous ossification has been best described in the developing calvaria. Pre-osteogenic cells condense and directly differentiate into osteoblasts. This differentiation is dependent on maintenance of canonical Wnt signaling and as such it was shown that enhanced signaling resulted in excessive calvarial ossification in mice (Day et al., 2005). Initially, the calvaria grow as separate bones, with intervening joins known as calvarial sutures. The sutures are themselves sites of intramembranous bone formation (Opperman, 2000).

In humans, premature closure of the sutures results in craniosynostosis (expanded upon in chapter 3). Given the clinical significance of this, ossification at these sites has been very well characterised and multiple defects have been attributed to aberrant FGFR signaling. Signaling through FGFRs stimulates all levels of osteoblast maturation during intramembranous bone formation. Specifically, enhanced osteoblast differentiation, proliferation and maturation has been attributed to activating mutations in three of the FGFRs . Signaling via FGFR1 and FGFR2, however, are the must culpable (Muenke and Schell, 1995, Park et al., 1995, Webster and Donoghue, 1996).

FGFR1 is expressed in the calvarial mesenchyme and mature osteoblasts, whilst FGFR2 is expressed in differentiating osteoblasts (Hughes, 1997, Britto et al., 1998, Delezoide et al., 1998). Gain of function mutations in these receptors causes hyperactivation. These mutations in are typically dominant missense, in-frame insertions, or deletions resulting in constitutive receptor

activation, ligand independent dimerization, or receptor activation from inappropriate ligands (Wilkie, 1997, Britto et al., 2001, Wilkie and Morriss-Kay, 2001). For example, several mutation in FGFR1 and -2 cause synostosis via constitutive activation of FGFRs. These mutations stabilize disulphide bonds within the receptor, causing ligand independent dimerization(Neilson and Friesel, 1995, Wilkie et al., 1995, Galvin et al., 1996, Robertson et al., 1998).

1.4 The cilium

Abnormal formation or function of cilia results in a heterogeneous group of disorders known as ciliopathies (Veland et al., 2009). Recently, these have been associated with a variety of phenotypes ranging from cystic kidneys to obesity and mental retardation (Yoder, 2007, Han et al., 2014). Developmental defects are incredibly common and include defective skeletal development (expanded on in chapter 3) and organogenesis (well reviewed by (Goetz and Anderson, 2010). Cilia are finger-like, microtubule-based organelles, which project from the cell surface on almost every cell type of the human body. Structurally they are composed of a basal body, which anchors the cilium to the cell membrane; and a microtubule based body known as the axoneme.

There are two classes of cilia: motile or immotile. Motile cilia beat in coordinated waves, are present in large numbers, and have roles in fluid flow and clearance. For example, the cilia lining the trachea remove mucus from the airways while the cilia found in the fallopian tube are important in movement of the ovum (Engstrom, 1951, Halbert et al., 1976). Immotile cilia, also called primary cilia, are typically found singularly on the cell surface of most vertebrate cells and have very important roles in sensing the environment and in signal transduction. Microtubule organization within the axoneme differs between motile and primary cilia. Both have nine pairs of microtubules that project down the length of the axoneme, positioned around the circumference of the cilia. In addition, motile cilia have an additional pair positioned in the center (Pazour et al., 2005).

1.4.1 Ciliary Transport

Proper formation of cilia is dependent on intracellular transport of proteins. This transport machinery is required to move structural axonemal components, membrane proteins and signaling molecules throughout the cilium. Within the cilium, the transport machinery consists of intraflagellar transport proteins A and B (IFT-A/B) and their associated IFT machinery. Kinesin-2 motor complexes consist of two kinesin-2 family proteins (KIF), KIF3A and KIF3B, which drive trains of IFT-B up the axenome (anterograde transport); whilst dynein motor complexes drive trains of IFT-A back down (Pedersen and Rosenbaum, 2008, Pigino et al., 2009). Because the transport machinery is critical for maintenance of the cilium, loss of proper ciliogenesis or transport of cargo has very severe consequences.

1.4.2 Signaling pathways influenced by the primary cilium

The primary cilium is critically important in vertebrate signal transduction. During development, Gli processing during Hh signal transduction appears to be dependent on an intact cilium (Tukachinsky et al., 2010). In addition, it has been suggested to act as a 'switch' to modulate between canonical and non-canonical wnt signaling (Zhang et al., 2011).

Gli processing

As described above in section 1.2.2, the ratios of GliAs to GliRs modulates the output of Hh signaling. In vertebrates, this processing has been shown to be dependent on the cilium. In the absence of the Hh ligand, Glis are associated with a Hh signaling complex consisting of Suppressor of fused (SUFU), Costal 2 and Fused. This complex delivers Gli proteins to a kinase complex, consisting of multiple proteins including protein kinase A (PKA), Casein kinase I (CKI) and GSK3β. This protein complex is believed to associate with the base of the cilium (Sillibourne et al., 2002, Fumoto et al., 2006, Barzi et al., 2010). Subsequently, phosphorylation is necessary to promote ubiquitination, which targets Glis for cleavage into their repressor forms (Jiang, 2006). Conversely, in the presence of the Hh ligand, SMO activation results in transport of Gli2, Gli3 and SUFU to the tip of the cilium (Wen et al., 2010, Kim et al., 2009, Chen et al., 2009). This is coupled with the dissociation of full length Glis with SUFU (Tukachinsky et al., 2010). This

translocation through the cilium is thought to allow them to avoid post-transcriptional processing (Tukachinsky et al., 2010, Humke et al., 2010). Therefore, in the absence of a functioning cilium, full length Gli can not be processed into its activator or repressor forms (reviewed by (Briscoe and Therond, 2013).

Wnt and non-canonical Wnt Signaling

The cilium is suggested to modulate both the canonical and non-canonical PCP signaling pathways. During PCP signaling, Dvl must localize to the basal body for signal transduction (Gao and Chen, 2010). In ciliated MEFs, immunostaining reveals that DVL localizes with the basal body. Conversely, in unciliated MEFS, it did not. This was associated with a loss of PCP dependent processes such as a loss of cell polarization and significantly reduced cell movement (Zilber et al., 2013).

On the other hand, the authors also showed in un-ciliated MEFs, there was hyperactivation of the canonical wnt pathway. There was greater canonical signal output in response to Wnt ligand, seen with a TopFlash reporter assay. Furthermore, un-ciliated MEFs had a high concentration of β-catenin in cell nuclei, whilst in ciliated MEFs, it was restricted to the cytoplasm. (Zilber et al., 2013). This led the authors to speculate that in the absence of the cilium there is more DVL available to contribute to the canonical pathway (Zilber et al., 2013, Zhang et al., 2011). Together, this data suggests that the cilium as the ability to modulate both PCP and canonical wnt signaling in certain contexts. This raises the intriguing question of whether it could also act as a 'cellular switch' between the two pathways.

1.4.3 Ciliopathies

Given the important cellular and signaling functions of the primary cilium, ciliary dysfunction has been associated with a range of human phenotypes. These heterogeneous disorders are classified as ciliopathies (Veland et al., 2009). In recent times, these have been associated with a variety of phenotypes ranging from cystic kidneys to obesity and mental retardation (Yoder, 2007, Han et al., 2014).

Ciliopathic mouse models are generated by knocking out structural and transport proteins required for ciliary formation and function. These mouse models have been shown to have defects in Hh signaling. This is seen well in IFT mutants. *Kif3a* null embryos have a severe reduction in *Ptc1* expression, at e9.5. This is associated with spinal cord patterning defects similar to those seen in *Gli3* null mutants (Persson et al., 2002, Huangfu et al., 2003). In addition IFT88 mutants display polydactyly attributed to misexpression of downstream Shh targets in the developing limb bud, which is also seen in *Gli3* mutants, as well as neural tube patterning defects (Liu et al., 2005a, Babbs et al., 2008)

Loss of proteins required in the basal body such as Meckel syndrome type-1 (MKS1) and oro-facial digital syndrome type 1 (OFD1) is also associated with Hh defects. *OFD1* mutants have reduced *Shh, Ptc1* and *Gli1* expression in the neural tube. They also have polydactyly, which they speculate is from abnormal Gli3 processing (Ferrante et al., 2006). *Mks1* null embryos have similar phenotypes. In mouse mutants, Hh dependent neural tube patterning is abnormal and *Mks1* was shown to act downstream of *Ptc1*, suggesting Gli processing is abnormal (Weatherbee et al., 2009). Polydactyly is observed in both mutants. Although increased expression of *Shh, Ptc1* and *Gli1* was not detected in developing limb buds, downstream targets of Gli repression were reduced. This implies that defective Gli3 processing is driving polydactyly (Ferrante et al., 2006).

Ciliopathic mouse models have also shown defects in PCP signaling. *Bardet-Biedl Syndrome* (*BBS*) genes code for a variety of proteins, which localize to basal bodies and contribute to axonemal trafficking (Su et al., 2014, Ansley et al., 2003, Tobin and Beales, 2007). In mouse, loss of several of these genes resulted in PCP defects such as loss of cellular orientation in the cochlea and abnormal neural tube closure resulting in exencephaly (Ross et al., 2005).

The most striking phenotypes observed in ciliopathies are skeletal malformations such as truncations of the axial skeleton and craniofacial defects including craniosynostosis and a small lower jaw, which overlap

with those seen in achondroplasia and craniosynostosis syndromes (These are compared and described in chapter 7).

Skeletal phenotypes in ciliopathic mouse models are striking. *Mks1* mutants have a high arching palate, abnormal fusions between the ribs and the sternum as well as shortened and bowed hind limbs. In addition, reduced ossification of the calvaria is seen (Weatherbee et al., 2009). *Ofd1* mutants have a bifid and hyperossified sternum, as well as short limbs, craniosynostosis and a high arching palate (Ferrante et al., 2006).

Several of these phenotypes, such as craniosynostosis and short limbs are observed in chondrodysplasia and craniosynostosis syndromes. Chapter 3 aims to compare and contrast some of the underlying causes driving these phenotypes. This will be done using the *Fuzzy* mutant, which is a ciliopathic mouse model that has a variety of skeletal defects.

1.5 *Fuzzy*

In this project I will use the *Fuzzy* mutant, which is a ciliopathic mouse model. This mutant has a variety of signaling and skeletal defects, which are discussed in this section 1.5.3. For this reason it is a good model in which to study defective skeletogenesis in ciliopathies

My gene of interest in the project is *Fuzzy*. This gene was first identified in *Drosophila,* in which it was shown to regulate wing hair cell polarity and the numbers of hair cells (Collier and Gubb, 1997). The former observation suggests a role in planar cell polarity (PCP) signaling, which has historically been important for regulation of cellular orientation and polarity, whilst the later was attributed to a role in maintenance of cytoskeletal integrity which influences numbers of hair cells formed (Collier and Gubb, 1997, Tian et al., 2009). Since then, cellular roles have been further characterised and the Fuz protein is shown to have important roles in ciliogenesis. The Fuzzy gene is evolutionarily conserved and has been identified in a variety of organisms including *Xenopus*, mouse and human.

1.5.1 *Fuzzy expression*

In vertebrates, *Fuzzy* expression is detected in dorsal tissue and in key regions important for craniofacial development. In situ hybridization shows that Fuzzy mRNA is detected in the developing mouse embryo at e8.5 in the dorsal tissue surrounding the neural tube and the brain (Seo et al., 2011). At later stages, Zhang et al., using a LacZ knock-in allele as a reporter, show X-gal staining in dorsal tissue surrounding the neural tube. Later, at e11.5, expression is more concentrated in the brain, spinal cord and eyes but also weakly expressed in the heart and limbs. Staining then spreads more ventrally into craniofacial structures by e12.5 and can be seen in the oral epithelium and mesenchyme, as well as Meckel's cartilage. By e14.5 it is widely detected in many craniofacial tissues including the oral epithelium, mesenchyme, palate, tongue, Meckel's cartilage and the perichondrium. In addition, expression analysis in cell lines, by way of quantitative polymerase chain reaction (QPCR), also reveal an abundance in LS-8 (oral epithelial cells), MEFs, human embryonic kidney cells and human chondrocytes with weak expression in mouse dental mesenchyme cells (Zhang et al., 2011).

1.5.2 Cellular roles of FUZ

Studies in *Xenopus* and mouse have shed light on important cellular functions of the FUZ protein. Generally it appears to have roles in cellular trafficking. As a result of this, vesicular trafficking and secretion, as well as ciliogenesis are affected on manipulation of *Fuzzy*.

In order to determine the Fuz protein structure and function, Gray et al carried out a yeast-two-hybrid screen (Gray et al., 2009). Results from this analysis suggested an interaction with open reading frame 89 on human chromosome 1. Subsequent BLAST analysis predicted this to encode a GTPase similar to vesicle targeting Rab proteins, which was re-named as RSG1. Co-immunoprecipitation studies then confirmed an association with between Fuz and RSG1 (Gray et al., 2009). Further studies revealed that RSG1 is associated with the cilia basal bodies and necessary for ciliogenesis (Brooks and Wallingford, 2013, Gray et al., 2009)

Homology modeling by Gray *et al* revealed that the C-terminus of the *Xenopus* Fuz protein adopts a quaternary structure of 5 beta-sheets flanked by 5 alpha-helices reminiscent of a longin domain, which is also seen in a variety of membrane trafficking and membrane fusion proteins such as membrane-fusing SNARE proteins (Gray et al., 2009, Pryor et al., 2008, Rossi et al., 2004).

Roles in secretion and trafficking

Consistent with homology modeling showing the FUZ longin domain, morpholino-oligonucleotide (MO) treated *Xenopus* cells revealed abnormal exocytotic and trafficking behavior. Scanning electron microscopy on *Xenopus* goblet cells (mucus secreting cells), revealed a reduction in open exocytotic vesicles associated with reduction mucous granule secretion. This is consistent with a loss of vesicular membrane fusion (Gray et al., 2009). To confirm this, immunostaining for Intelectin2, which is a component of secreted mucus, was carried out in MO-treated embryos. In control samples, Intelectin2 was observed at and above the apical cell surface. In contrast, MO-treated cells, Intelectin2 accumulated below the apical cell surface only (Gray et al., 2009). In addition to this, Gray et al showed that interestingly, in *Fuzzy* morphants, vesicles could still fuse to one another. Together this data suggests that FUZ is needed for a subset of membrane fusions, and hence vesicular secretions in *Xenopus.*

More generally, FUZ has been associated with trafficking in the cytoplasm. In mouse embryonic fibroblasts (MEFs), FUZ localized with a small GTPase known as Rab8, which is essential for vesicular transport (Zilber et al., 2013, Nachury et al., 2007, Linder et al., 2007). Subsequently, Zilber et al showed that DVL, which is trafficked to the cilium in certain contexts, was absent from the basal body in *Fuzzy* mutant MEFs (Park et al., 2008, Mahuzier et al., 2012, Zilber et al., 2013).

Role in ciliogenesis

FUZ is now known to be a key regulator of ciliogenesis. Several imaging studies have reported loss or shortening of primary and motile cilia in *fuzzy* morpholino treated *Xenopus* embryos (Park et al., 2006, Gray et al., 2009). In

addition, on loss of *Fuzzy*, absence and shortening of cilia in mouse embryos has been documented in the notochord and limb buds at e11.5; the mandibular mesenchyme and Meckel's cartilage at e14.5; and dermal cells at e15.5 (Zhang et al., 2011, Gray et al., 2009, Heydeck et al., 2009, Pigino et al., 2009, Dai et al., 2011). These defects in ciliogenesis have been attributed to its role as a trafficking molecule. Rab8 (mentioned above) is not only important in vesicular trafficking but specifically trafficking of structural components to the ciliary axoneme (Nachury et al., 2007). Consistent with the association of FUZ and Rab8, overexpression of *Fuzzy* results in enhanced cilia length (Zilber et al., 2013).

Defective trafficking to the cilium gives FUZ important roles for transport of cargo on the axoneme. Brooks and Wallingford showed that in the absence of *Fuzzy,* anterograde transport within the cilia is defective, with no localization of IFT-A trains to the basal body or trafficking on the ciliary axoneme. Conversely, IFT-B trains were localized to the basal body. This unidirectional transport allows initial building of the cilium but over time creates a 'traffic-jam effect'. (Brooks and Wallingford, 2012, Gray et al., 2009). In keeping with this, it was shown in *Xenopus,* that *Fuzzy* knockdown causes a loss of calponin homology and microtubule-associated protein (CLAMP) localization to the ciliary tip (Brooks and Wallingford, 2012, Gray et al., 2009). CLAMP is involved in the building of microtubules and is associated with the ciliary axoneme. As such transport on the axoneme is compromised. Together this data reveals that FUZ is needed for cilial integrity and functionality.

1.5.3 Signaling perturbations and phenotypes in the *Fuzzy* mutant.

Given the important roles of the cilium for different signaling pathways, it is no surprise that signaling perturbations have been associated with dramatic phenotypes in *Fuzzy* mutants. The proposed role of FUZ with regards to these pathways are schematized in Fig 1.8.

Hh signaling

Proper Hh signal transduction is dependent on proper transport of Gli proteins on the ciliary axoneme. Given the role of FUZ in ciliogenesis, it is no

surprise that the *Fuzzy* mutant has been associated with abnormal HH signaling.

Previously we have shown that there is abnormal Gli processing in *Fuzzy* mutant heads at e9.0. Knock out of *Fuzzy* significantly increased levels of long form Gli proteins on loss of *Fuzzy*, indicative of a lack of Gli processing (Tabler et al., 2013). Consistent with this, we noted reduced expression of Hh signaling targets *Ptc1* and *Gli.* Loss of Gli processing was also observed by Heydeck et al, who showed that there was a huge increase in the amount of long form to repressor form Gli in *Fuzzy* mutant whole embryos and limb buds at e10.5 (Heydeck et al., 2009). In addition, at e14.5, in *Fuzzy* mutant mandibles, a reduction in downstream Hh gene expression such as *Shh, Gli1,* and *Ptch1* mRNA and protein was detected (Zhang et al., 2011).

Phenotypes associated with Hh signaling are observed in multiple developmental systems of the *Fuzzy* mutant. Defective limb and neural tube patterning, as well as abnormal skeletal development have all been observed.

The *Fuzzy* mutant has polydactyly. During the establishment of digit identity, a gradient of Gli3 is established to limit the number of digits formed (expanded upon in chapter 4). As such it was shown by Heydeck et al, that downstream targets of this gradient were all increased in *Fuzzy* mutant limb buds at e10.5. As a result of this, polydactyly in the *Fuzzy* mutant was attributed to abnormal Gli processing (Heydeck et al., 2009). In keeping with this suggestion, *Gli3* mutants also have polydactyly (Babbs et al., 2008).

Abnormal patterning of the spinal cord in the *Fuzzy* mutant has also been attributed to defective Hh signaling. Shh signaling is known to dictate dorsal-ventral patterning of the neural tube. In order to do this *Shh* is expressed in the floor plate, which is the most ventral structure of the spinal cord, and a gradient of expression is established with lower SHH in the more dorsal tissue. The strength of the signal specifies ventral cells into molecularly distinct domains by turning on different genes. In this way Shh

is important for neural tube patterning (well reviewed in (Sasai et al., 2014). Heydeck et al showed, with immunostaining, that there was a loss of SHH protein in the floor plate, as well as severely reduced expression of targets of the gradient, such as Foxa2 and Nkx2.2 (Heydeck et al., 2009, Heydeck and Liu, 2011).

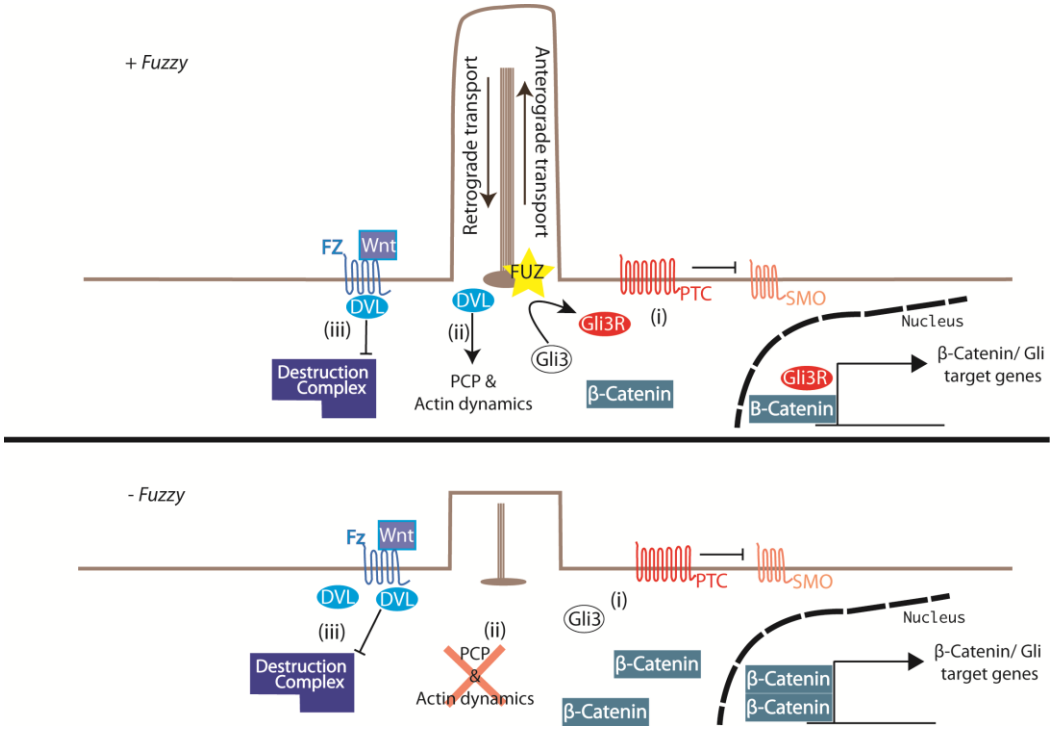

Figure 1.8 Schematic showing proposed cellular functions of FUZ

A) Signaling roles of FUZ in a normal cell. Three key pathways are thought to be influenced by FUZ activity.
(i) FUZ is needed for ciliary assembly. The cilium is needed for processing the long from Gli into a repressor (Gli3R). This causes repression of downstream target genes.
(ii) In non-canonical Wnt signaling, FUZ targets DVL the cilium. Cilia bound DVL is important in transducing PCP signals needed for cell polarity and actin dynamics.
(iii) During Canonical Wnt signaling, DVL is needed to repress the β-catenin destruction complex. This enables β-catenin to activate downstream transcription events.
B) In the absence of FUZ, cilia formation and trafficking is abnormal. This has knock on effects on signaling pathways described above.
(i) On Hh ligand binding, full length Gli3 is not processed, this results in less Gli3 repressor,
(ii) FUZ mediated localization of DVL to the cilium is inhibited causing a loss of PCP function.
(iii) Loss of DVL targeting the cilium results in a greater pool of cytoplasmic DVL. This is thought to increase β-catenin stability and thus enhance the effects of canonical Wnt signaling.

Canonical and PCP Wnt signaling

The link between PCP signaling and ciliogenesis is an intriguing one. In recent years, it has been suggested that DVL trafficking to the cilium is essential for proper ciliary polarity (Park et al., 2008). As such, it has been suggested that ciliogenesis may be in part regulated by PCP signaling (Wallingford, 2006). It has also been suggested that there are perturbations in both non-canonical Wnt PCP and canonical Wnt signaling. Consistent with the role of Fuz in membrane trafficking seen in *Xenopus* and in tissue culture, vesicular trafficking of DVL from the cytoplasm to the cilium is disrupted on loss of *Fuzzy* (Zilber et al., 2013). This is associated with an increase in cytoplasmic DVL and hyperactivity in response to Wnt ligand (Zilber et al., 2013). In addition, an upregulation of β-catenin and related target genes is seen in *Fuzzy* mutant mandibles at e14.5. As a result, Fuz is suggested to alter the balance between non-canonical and canonical wnt signaling (Zhang et al., 2011). Contrary to this, analysis of the skin of Fuzzy mutants revealed no changes in levels of Lef1, suggesting that this may be a tissue specific effect (Dai et al., 2011).

The *Fuzzy* mutant has many phenotypes associated with defective PCP signaling. Loss of the *Fuzzy* gene in *Drosophila* resulted in a loss of hair cell and compound eye cell orientation (Collier and Gubb, 1997). PCP dependent convergence and extension movements are also defective in the mouse embryos. An open neural tube, occasionally associated with exencephaly is typically observed, as well as a kinked tail and heart development with a single outflow tract. These phenotypes are attributed to varying degrees of PCP driven convergent extension defects (Wallingford, 2006, Guyot et al., 2011, Etheridge et al., 2008). In addition the role of *Fuzzy* in epidermal and dermal cells was shown via a lack of hair follicle differentiation in mouse, associated with abnormal PCP signaling (Dai et al., 2011).

A subset of phenotypes in the *Fuzzy* mutant have also been attributed to enhanced canonical Wnt signaling . It was suggested by Zhang et al, that increased proliferation in mouse MC at e14.5 was responsible for cartilage

bifurcation in the *Fuzzy* mutant (Zhang et al., 2011). This is highly debatable and is the topic of chapter 4.

Fgf Signaling

Recently we discovered aberrant FGF gene expression in the *Fuzzy* mutant. Typically at e9.0 *Fgf8* is expressed at the mid-hindbrain (MHB) boundary, frontonasal process and on lateral sides on the BA1 epithelium (See Fig 1.9). We showed that in *Fuzzy* mutants, the regions of *Fgf8* expression were expanded in all of these regions and this was associated with increased expression of downstream markers *erm1* and *Pea3.* Loss of *Fuz* in mouse mutants leads to maxillary hyperplasia and a high arching palate. We found that this phenotype was rescued on reduction of *Fgf8* expression in the *Fuzzy* mutant, suggesting that FGF increases were directly linked to the craniofacial phenotype. Fig 1.9 shows BA1 expansion of *Fgf8* expression.

In addition, we saw aberrant NC migration into BA1 as well as increased numbers of NC in the maxillary portion of BA1 at e9.5. As such we have proposed a model in which loss of Gli3 repressor allows *Fgf8* expansion in the regions described. Subsequently, NC migration into the maxillary portion of BA1 is increased resulting in maxillary hyperplasia and a high arching palate.

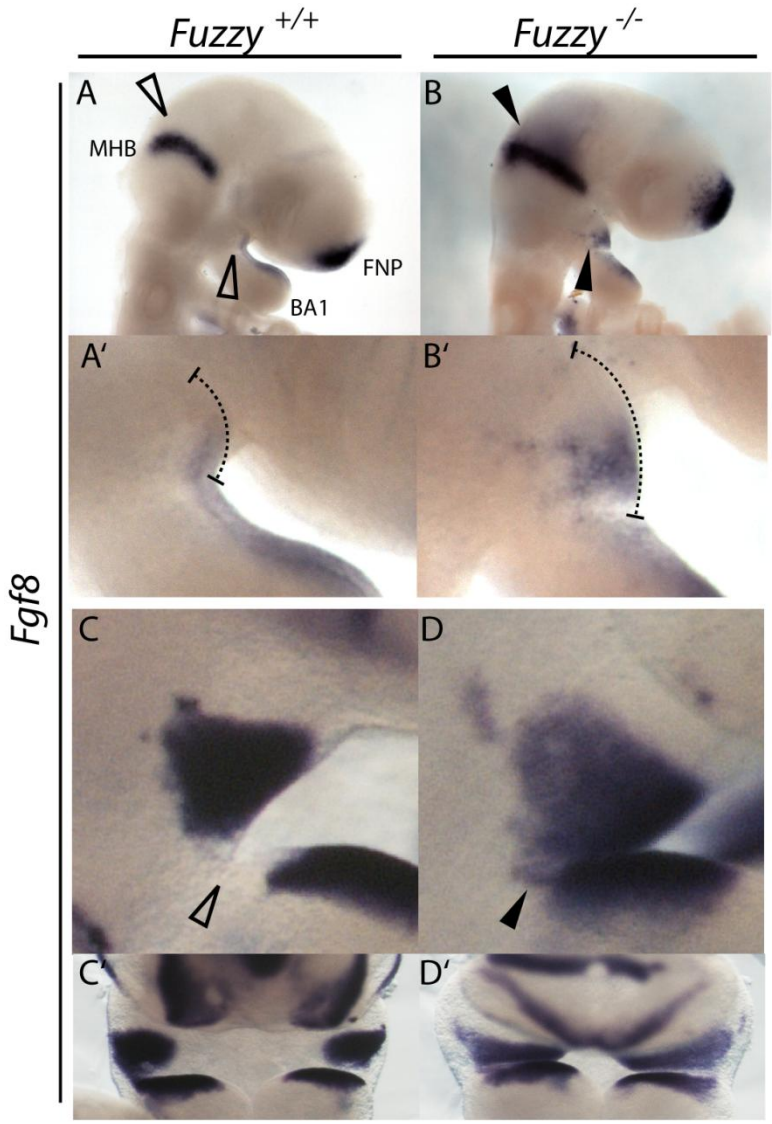

Figure 1.9 Taken from (Tabler et al., 2013) Lateral views of *Fgf8* expression

(A and B) Lateral views of *Fgf8* expression in e9.0 embryos. *Fgf8* is expressed in the midhindbrain boundary (MHB), frontonasal prominence (FNP), and the BA1 epithelium. In mutants, the region of *Fgf8* expression is expanded, indicated arrowheads.
(A' and B') Magnified lateral view of BA1. Brackets indicated *Fgf8* expression.
(C and D) Lateral view of BA1 in control and mutant embryos at e10.5. Arrowheads indicate increased region of *Fgf8* expression.
(E and F) Frontal view of *Fgf8* expression in e10.5 embryos. Note mediolateral expansion of mandibular *Fgf8* expression in the mutant.

Skeletal phenotypes

The most striking phenotypes in the *Fuzzy* mutant are in the skeleton. The mutant has been shown to have defects in almost all skeletal systems ranging from craniofacial elements such as calvarial synostosis and micrognathia, as well as short long bones, polydactyly, sternal ossification and neural tube closure defects (Gray et al., 2009, Tabler et al., 2013, Zhang et al., 2011, Zilber et al., 2013). These phenotypes have mostly been attributed to lack of cilia mediated Hh signaling. However, as described above, loss of cilia has consequences on a variety of signaling pathways. This project will look in depth at some of these phenotypes and attempt to determine molecular causes of these defects.

1.6 Project aims

Generally this project aims to further characterise skeletal malformations in the *fuzzy* mutant and investigate which signaling perturbations could be driving these malformations. In more detail, chapter aims are as follows:

- Chapter 3: Abnormal development of the long bones: In this chapter I document the phenotype seen in the long bones of *Fuzzy* mutants and attribute abnormal development to delayed chondrocyte hypertrophy.

- Chapter 4: Micrognathia in the *Fuzzy* mutant. In this chapter I demonstrate that several key steps in mandibular outgrowth that can lead to micrognathia. Notably abnormal NC distribution in the presumptive mandible coupled with abnormal medio-lateral patterning during early embryogenesis affects the position of the prechondrogenic condensations of Meckel's cartilage, resulting in premature fusion.

- Chapter 5: Hyperossification of the mandible. In this chapter I characterise abnormal bone deposition in the *Fuzzy* mutant, which has not been previously observed. I determine that genetic reduction

of *Fgf8* in the mutant rescues the phenotype implying defects in early embryogenesis, which contribute to abnormal ossification.

- Chapter 6 Characterization of skeletal malformations of the sternum, vertebra and calvaria: By comparing phenotypes observed in craniosynostosis syndromes, chondrodysplasias and ciliopathies, I will try to establish whether overlapping phenotypes reveal perturbations in common signaling pathways.

Chapter 2 Material and Methods

2.1 Animals

Work using genetically modified animals was conducted in accordance with the UK Animals (Scientific Procedures) act of 1986 and King's College London Research Ethics Committee. Work was carried out under project license (PPL) 70/6607 and 70/7441, with personal license number 70/22485.

2.1.1 Mouse strains

Mouse lines were maintained on a mixed genetic background and maintained as heterozygotes. Matings were set up by introducing male and female mice in the evening. Vaginal plug checks were carried out on subsequent mornings; embryonic day 0.5 (e0.5) was defined from noon on the day of plug detection. At appropriate ages, pregnant mothers were sacrificed by cervical dislocation and the uterus was dissected out into ice-cold phosphate buffered saline (PBS). Embryos were removed from yolk sacs whilst under a stereo-microscope (Leica Mz95)

2.1.1.1 Fuzzy mutant mice

Fuzzy mutant mice were generated as described by Gray et al (2009). A gene-trapping vector was inserted into the second exon of the *Fuzzy* gene (found on chromosome 7) in embryonic stem cells. It is predicted that this disrupts the transcription of the gene. Transcripts were selected by antibiotic resistance since the vector containing the gene trap contained a splice acceptor and neomycin resistant cassette (NEO). This enabled splicing to retain the NEO cassette. Vectors were microinjected into the blastocyst of C57BL/6 mice. This resulted in heterozygous $Fuz^{Gt(neo)}$ males and females, which were intercrossed to produce homozygous *fuzzy* mutants. Throughout the thesis they are denoted as $Fuzzy^{-/-}$.

2.1.1.3 Col2::LacZ reporter mice

A reporter mouse in which the *col2* promoter driving expression of the lacZ reporter gene was used to visualize col2 expression (Zhou et al., 1995).

2.1.1.3 Reduction of *FGF8*

Fgf8$^{L/+}$ mice have reduced *Fgf8* expression due to insertion of a *lacZ* cassette into the coding region of the *Fgf8* allele (Ilagan et al., 2006). These mice were intercrossed with heterozygous *Fuzzy* mice to generate compound *Fuzzy*$^{+/-}$*; Fgf8*$^{L/-}$ males, which were subsequently mates with *Fuzzy*$^{+/-}$ females.

2.1.2 Genotyping and genomic visualization

2.1.2.1 DNA preparation

Embryo tail tissue was used for DNA extraction. Tissue samples were digested at 55°C overnight in 250µl lysis buffer (50mM Tris pH8.0; 50mM EDTA; 50mM NaCL; 0.5% SDS) and 7.5µl of 20mg/ml proteinase K. DNA was precipitated using 5M NaCL and isolated using isopropanol. Resulting DNA was re-suspended in 500µl 0.1xTE.

2.1.2.2 DNA amplification

Standard polymerase chain reaction protocols were used to selectively amplify genomic DNA. The following reaction was used per sample.

Water:	5.55µl
5x reaction buffer:	2.5µl
$MgCl_2$:	1.5µl
dNTPs:	0.1µl
Primers:	0.75µl
Taq polymerase:	0.1µl
Genomic DNA:	2.0µl

The following PCR primers were used:

Gene	Allele	Direction	Primer	Product length
Fuzzy	Wildtype	Forward	AGTAGAGGCTCGGAGCCTTTA	295bp
	Wildtype	Reverse	TCACCTAAGCCAGGAACCACT	
	Mutant	Forward	AGTAGAGGCTCGGAGCCTTTA	220bp
	Mutant	Reverse	ATAAACCCTCTTGCAGTTGCA	
LacZ	Generic	Forward	TTTACAACGTCGTGACTG	700bp
	Generic	Reverse	TGATTTGTGTAGTCGGTT	

2.1.2.3 Agarose gel electrophoresis

Gels were made consisting of 2% agarose in 1x Tris-acetate buffer (TAE), which was also used as the running buffer during electrophoresis. DNA ladders of 1000bp were used to determine sample fragment sizes. Electrophoresis was carried out at 120V in a gel electrophoresis tank (alpha-laboratories) and gels were imaged using an ultraviolet transilluminator (BioDock-It™ Imaging system).

2.2 Histology

2.2.1 Tissue processing

Dissected embryos were fixed in 4% paraformaldehyde (PFA) in PBS overnight at 4°C. Embryos were then washed in PBS then underwent a graded series of ethanol dehydrations (25%, 50%, 70%, 95%) for half a day in each concentration. Ethanol was then replaced by histoclear and washed twice at room temperature followed by an hour incubation in 1:1 paraffin to histoclear mixture. Samples were then incubated at 60°C in paraffin for a minimum of 4 hours with a minimum of 4 solution changes. Samples were then embedded at appropriate orientations and stored at 4°C ready for sectioning.

2.2.2 Sectioning

Wax embedded samples were sectioned at 7µms on a microtome and disposable blades (Leica). Sections were either mounted continuously or

sequentially over several slides on superfrost plus slides (Thermo Scientific) using RNAse free water. Slides were dried on a heating block (Raymond A Lamb Hotplate) over night at 37°C and then stored at room temperature until further use.

2.2.3 Pico-Sirius red and Alcian Blue trichrome staining

Paraffin was removed from slides via 2x 10-minute incubations in histoclear and then re-hydrated through decreasing ethanol concentrations for 2 mins per concentration (100%; 90%; 70; and 50%). Slides were then washed in de-ionised water (dH_2O) and stained with Alcian Blue 8GX solution for 10 minutes (1% in 3% acetic acid, pH2.5; Fluka), which stains for glycosaminoglycans and mucopolysaccharides. Slides were then washed in running water for 10 mins and incubated in Ehlrich's Haematoxylin (Solmedia) for 2 mins to stain for cell nuclei and cytoplasm. Slides were again rinsed in dH_2O and then exposed to 2.5% phosphomolybdic acid for 10 mins prior to further dH_2O rinsing. Subsequently sections were incubated in Sirius Red solution (0.5% in saturated picric acid; Direct Red 80), to stain for bone, for one hour. Finally slides were rinsed twice in 0.5% acetic acid and de-hydrated over a graded series of ethanol. 3x 3-minute xylene washes were performed prior to mounting in DPX (Solmedia)

2.2.4 Imaging

Stained slides were imaged with a brightfield microscope (Zeiss AxioScop 2 Plus) with an attached camera (Zeiss AxioCam HRc). Axiovision software was used for photograph acquisition.

2.2.5 Cell counting

For each sample, cell counts were taken over 3 successive sections and averaged. A minimum of 3 samples were analyzed for each genotype.

2.3 Whole Mount Embryo Staining

2.3.1 X-gal Staining

Embryos were dissected from pregnant mothers and fixed in ice cold 4%PFA for 30mins. Samples were then washed in solution A (500ml 1x PBS with 1ml 1M $MgCl_2$) for 5 minutes followed by 15 minutes (both at room temperature). Samples were then incubated in solution B for 5 mins at room temp (50ml PBS with 500µl 10% deoxycholic acid, 1ml 10% Igepal and 50µl 1M $MgCl_2$). Finally samples were left in staining solution consisting of solution B with 5mM $K_3Fe(CN)_6$, 5mM $K_4Fe(CN)_6$ and 1mg/ml X-Gal at room temperature. Samples were checked regularly to ensure no over staining occurred. Once staining was finished, samples were then imaged (Section 2.3.5) or fixed for several days for optical projection tomography (OPT).

2.3.2 Optical projection tomography

After X-gal staining and fixation, embryos were thoroughly washed in PBS and suspended in 1% agarose in a petri dish. Once the agarose was set, excess agarose was trimmed away. The mount was washed with methanol and then the agarose block was attached with superglue. Once attached the agarose is further trimmed to ensure that the edges are flush with the mount. Sample and mount are then dehydrated and washed in methanol until no water is remaining in the agarose block and then washed a further time. Methanol is then replaced with 2 benzyl benzoate:1 benzyl alcohol (BBBA) and stored at room temperature away from light until the specimen is transparent. At this point the specimen is ready for imaging which took place in the OPT Scanner 3001 (Bioptonics). 3D image reconstruction was done using NRecon software (Bioptonics) and then the Bioptonics viewer (Bioptonics) was used for 3D image manipulation.

2.3.3 Cartilage Staining

Embryos younger then e15.5 were dissected into ice cold PBS and fixed in Bouins fixative (70% picric acid; 25% formaldehyde (37%) and 5% acetic acid) for 2 hours. Samples were then washed 6-8 times over 24 hours in 70% ethanol with 1% ammonium hydroxide until embryos are white.

Samples were then washed twice in 5% acetic acid for 1 hour each and then stained in 0.05% alcian blue 8XG (Fluka) in 5% acetic acid overnight. Post-staining, samples were washed in 100% methanol twice for an hour each and the cleared in BBBA until tissue was transparent.

2.3.4 Alizarin Red staining

Embryos older then E14.5, in which we wanted bone visualized as well as cartilage were dissected from pregnant mothers and skin and was dissected away. Samples were then fixed overnight in 95% ethanol at room temperature and then incubated with alcian blue staining solution for up to 48 hours. Post-fixation was carried out in 95% ethanol overnight at room temperature and then specimens were cleared in 2% potassium hydroxide (KOH) until slightly translucent. At this point, extraneous tissues are further removed and samples were incubated in alizarin red staining solution for 24-48 hours. After staining, samples are cleared in 1% KOH with 20% glycerol and then transferred to 50% ethanol with 50% glycerol for storage and imaging.

2.3.5 Imaging

Whole mount imaging was carried out using a stereoscope (Nikon SMZ1500) and photographs were taken with an attached camera (Nikon digital sight DS-Fi1).

2.4 RNA in situ hybridisation

All work with RNA was carried out in RNAse free conditions using autoclaved solutions and glassware.

2.4.1 DNA transformation into competent cells

Bacterial work was done with aseptic technique. DH5α competent cells (Invitrogen), stored at -80°C, were thawed on ice. 30µl of competent cells were mixed with approximately 1 µg/µl of stock plasmid. This mixture was incubated on ice for 20 mins and then heat shocked at 42°C for 30 seconds. Cells were then placed on ice again for 2 mins and then added to lysogeny

broth (LB) media to make a total volume of 500µl. This solution was incubated at 37°C for 30 mins. After this incubation, 100µl of cells were plated onto LB media with 100mg/ml ampicillin to select for resistant colonies. Cultures were grown over night and placed at 4°C until ready for amplification.

2.4.2 DNA amplification

Single colonies for amplification were isolated and transferred to either 15ml falcon tubes containing 5ml LB media; or 1l conical flasks containing 100ml LB media, both with 100mg/ml ampicillin. The former were used for mini preps and the latter for midi preps. Solutions were incubated overnight shaking at 225 rotations per minute (RPM) at 37°C. The next day plasmids were isolated from cultures using either the Qiaprep®Spin MiniprepKit or MidiprepKit, according to manufacturers instructions. Resultant DNA was quantified using a NanoDrop Lite Spectrophotometer (Thermo Scientific) and stored at -20°C.

2.4.3 Plasmid linearization

Plasmids were linearized using restriction enzymes with sites closest to the 5' end of the insert of interest (shown in table below). This was done in 100µl reactions as follows: 2µl restriction enzyme (as specified in table below), 20µg plasmid DNA, 1µl bovine serum albumin (BSA), 10µl 10x reaction buffer and water up to 100µl. Reactions happened at 37°C overnight. The next morning, samples were treated with 1µl of 20mg/ml proteinase K, 5µl of 10% SDS and water to make the total reaction volume 200µl. This was incubated at 55°C for 15 mins and then cleaned by adding 200µl phenol:chloroform, spinning at 13000 RPM on a table top centrifuge and then removing the top aqueous layer (approximately 180µl) into a clean eppendorf. DNA was then precipitated by adding 20µl of 3M sodium acetate and 200µl isopropanol. Samples were spun and supernatants were removed and cleaned with 70% ethanol before being re-suspended in 20µl RNAse free water. RNA was then quantified, again using the NanoDrop Lite Spectrophotometer (Thermo Scientific), and then stored at -20°C.

Probe	Restriction Enzyme	Antibiotic Resistance	Plasmid Vector	Insert Size	Polymerase Enzyme	Reference
mSox9	EcoR1	Ampicillin	pBSII^{SK}	525bp	T3	(Healy et al., 1999)
mIhh	BamH1	Ampicillin	pBSII^{SK}	1.8kbp	T7	(St-Jacques et al., 1999)
mRunx2	EcoR1	Ampicillin	pCMV5	1000bp	T7	(Xiao et al., 2005)
mBarx1	EcoR1	Ampicillin	pBSII^{SK}	951bp	T7	(Cobourne et al., 2004)

2.4.4 Digoxigenin labeled RNA probe synthesis

Probe synthesis reactions were carried out in total volumes of 50µl. Each reaction contained 3µl polymerase (as appropriate for each probe – see table above), 2µl of 40µg/µl RNAse inhibitor; 5µl Digoxigenin labeled NTPs, 1µg DNA template, 10µl of 5x reaction buffer, 5µl of 100mM DTT and water to make reaction volume 50µl. The reaction was incubated at for 2 hours at 37°C and then treated with 1µl DNAse1 for 20 mins at 37°C. The probe was then precipitated by adding 25µl of 8M lithium chloride and incubating at -20°C for 1-2 hours. Samples were spun at 13000 RPM on a tabletop centrifuge, the supernatant was removed and the sample washed in 70% ethanol before being resupsended in 55µl RNAse free water. Probe was then quantified with the Nanodrop (Thermo Scientific) and stored at -80°C.

2.4.5 Digoxigenin labeled in situ hybridization on paraffin sections.

In situ hybridisation with digoxigenin labeled probes was used to visualize gene expression. Paraffin was removed from slides by washing three times in xylene for 10 mins each. Slides were then re-hydrated through a series of ethanol concentrations, twice for 2mins each (100%, 95%, 70%) and then washed in RNAse free water twice and post-fixed in 4% PFA for 10mins. PFA was removed by washing twice in PBS for 5mins each and then samples were incubated with 4µg/ml proteinase K for 8mins. After a 5 minute PBS wash, slides were fixed again in 4% PFA followed by another PBS wash. Next, acetylation was carried to remove electric charge on the slides in order to reduce background staining. This was done using 50ml H_2O, with 625µl

triethanolamine (TEA), 130µl of 37% hydrochloric acid (HCL) and 125µl acetic anhydride. Slides were incubated for 10mins and then washed 3 times in PBS for 5mins each. Slides were again dehydrated through 70% and 95% ethanol and air-dried. During these dehydration steps 1µg of probe was added to 1ml of hybridisation solution. 100ml hybridization solution consists of the following:

Formamide	50ml
50% Dextran sulphate	20ml
50x Denhardt's solution	2ml
10mg/ml Yeast tRNA	2.5ml
5M NaCl	6ml
1M Tris-HCL pH8	2ml
0.5M EDTA	1ml
1M Sodium phosphate	1ml
20% Sarcosyl	5ml
Water	10.5ml

300µl of probe/hybridization solution was added to each slide and slides were subsequently covered with RNAse free coverslips and incubated at 65°C overnight in a humid chamber. Finally, 20X saline sodium citrate (SSC), pH7 in 1litre of water was prepared ready for use the next day. 20X SSC consists of 175.3g sodium chloride and 88.2g sodium acetate dissolved in water.

The next day, coverslips were removed in 5X SSC and washed in a high stringency wash, consisting of 50% formamide and 2X SSC, twice for 30mins at 65°C. Slides were then washed 3 times for 15mins each in RNAse buffer. This consists of 0.5M NaCl, 10mM Tris-HCL and 5mM EDTA pH8 made up in water. After the third wash, slides were incubated in RNAse buffer treated with 20mg/ml RNAse A (Invitrogen) for 30mins at 37°C. After this, again samples were washed in fresh RNAse buffer without RNAse A. High stringency washes are then repeated twice followed by washes in 2X SSC and then 0.1X SSC at 37°C for 15mins each. Then specimens were washed in

PBS Tween (PBTw), consisting of PBS and 0.1% Tween-20 for 15mins at room temperature. Finally slides were blocked for 1 hour in PBTw with 10% goat serum (GS) before incubating with alkaline phosphatase-coupled anti digoxigenin antibody (Boerhringer Mannheim), diluted at 1:5000 in PBTw with 1% GS, overnight at 4°C.

In order to visualize RNA expression, on the next day, slides are washed 4 times for 15mins in PBTw at room temperature. Then wash twice for 10mins each in NTMT buffer. 100ml NTMT buffer consists of the following:

5M NaCl	2ml
1ml Tris-HCL pH9.5	10ml
1M $Mgcl_2$	5ml
Tween-20	0.1ml
H_2O	82.9ml

Prior to addition of NTMT buffer add 0.5mg/ml levamisole in order to reduce background staining. After NTMT washes incubate slides in BM-purple AP substrate (Roche) with 0.5mg/ml levamisole and incubate in the dark at room temperature. Check slides every hour to ensure that over-staining does not occur. Once staining has finished, was slides in PBS twice for 5mins each and then counterstain in 0.005% fast red (Polyscientific) for 5mins. Finally dehydrate slides through 70%, 95% and 100% ethanol sequentially, incubate in xylene three times for 3mins each and then coverslip with DPX (Solmedia).

Chapter 3 Endochondral ossification in the *Fuzzy* mutant

3.1 Introduction

It has been previously observed that the *Fuzzy* mutant has short limbs and polydactyly (Tabler et al., 2013, Gray et al., 2009, Park et al., 2006). Individuals who have with a short stature as a result of reduced bone growth are described as having dwarfism. One of the most obvious phenotypes of dwarfism is delayed or reduced growth of the long bones resulting in short limbs relative to the trunk skeleton. Although in most cases of dwarfism, achondroplasia (enhanced FGFR signaling) is credited with being the causative factor, other signaling pathways have multiple roles in different aspects of limb development (Bellus et al., 1995, Elejalde and de Elejalde, 1985, Foldynova-Trantirkova et al., 2012). Both Hh and FGF signaling are essential for key steps of limb bud outgrowth, patterning and subsequent long bone elongation.

A series of epithelial-mesenchymal interactions regulates outgrowth of the limb. *Fgf10* expression in the mesenchyme initiates the budding of the limb mesenchyme, by stimulating cell survival and proliferation, and is believed to be responsible for inducing the apical ectodermal ridge (AER) (Ohuchi et al., 1997, Xu et al., 1998, Yonei-Tamura et al., 1999). This is an ectodermal thickening at the most distal tip of the limb bud, which overlies the mesenchyme.

The AER is a key signaling center, which controls outgrowth of the limb bud. Removal of this region corresponds to varying degrees of truncation of the distal limb skeleton in chick (Saunders, 1948). Addition of FGF proteins to the limb bud can substitute for loss of the AER (Niswander et al., 1993, Vogel et al., 1996). Whilst both *Fgf4* and *Fgf8* are expressed in the AER, *Fgf8* is the earliest detected in this region and is the key signal, whilst FGF4 can compensate in its absence to a certain degree (Crossley and Martin, 1995, Boulet et al., 2004). Recently it was shown that expression of these FGFs are

under the control of *Tbx5,* in the forelimb, and *Tbx4*, in the hind limb (Duboc and Logan, 2011).

Proximal and distal zones of the developing limb are established through a counteracting retinoid acid gradient, emerging from the proximal limb bud, which works against the FGF gradient from the AER. Thus it is believed that exposing limb bud mesenchyme to FGF8 commits them to a distal fate, whilst exposure to retinoic acid commits to a more proximal fate (Mercader et al., 2000, Niederreither et al., 2002, Niswander et al., 1993, Yashiro et al., 2004).

As well as initial limb bud expansion and proximal-distal outgrowth, polarity is tightly regulated to ensure the correct number of digits is formed. This is controlled from a signaling center called the zone of polarizing activity (ZPA). The ZPA is a key organizer of anterior-posterior patterning, located in the posterior limb bud mesenchyme. A gradient of Gli3 repressor expression from the anterior (high expression) to the posterior (low expression) limb bud is responsible for ensuring the correct spatial expression of genes driving more anterior versus more posterior digit identity, including *Pax9* and 5' *Hoxd* genes respectively (Wang et al., 2000, McGlinn et al., 2005, te Welscher et al., 2002b).

This Gli3 gradient is first set up through reciprocal antagonism between Gli3R, in anterior tissue, and *dHAND*, which is expressed in the more posterior limb bud (te Welscher et al., 2002a). In this way, *dHAND* subsequently activates *Shh* in the ZPA, which reduces Gli3 cleavage in the more posterior tissues, thus establishing a gradient of Gli3 from anterior to posterior (te Welscher et al., 2002b). Loss of *Shh* results in a single digit, whilst dual inactivation of *Shh* and *Gli3* results in polydactyly (te Welscher et al., 2002b). This implies that in the distal part of the developing limb bud, *Shh* acts to counteract effects of the Gli3-R in the developing limb to establish the number of digits formed (Litingtung et al., 2002).

Signaling from the AER and ZPA must occur at similar times to ensure correct patterning of the developing limb bud as it grows out. This is done via a positive feedback loop in which the *Shh* expressed in the ZPA signals to the distal mesenchyme. This activates *Fgf4* in the AER, which goes on to further stimulate *Shh* expression via gremlin mediated BMP4 antagonism in the ZPA (te Welscher et al., 2002b, Zuniga and Zeller, 1999).

Once the anterior-posterior and proximal-distal identities of the developing limb have been established, long bone formation occurs via endochondral ossification (described in the chapter 1). Elongation of the individual elements is driven by cartilage maturation in the center of the cartilaginous growth plate. A schematic showing the key roles of Hh and FGF in long bone formation is shown in fig 1.6.

As chondrocytes undergo hypertrophy they enlarge, as such, in mature chondrocytes, increases of cellular fluid volume by up to twenty times have been detected (Goldring et al., 2006). These cellular changes drive limb elongation (Goldring et al., 2006). Two key signaling pathways: Hh and Fgf control onset of cartilage hypertrophy. Ihh is the main ligand which is expressed in pre-hypertrophic and hypertrophic chondrocytes; its expression signifies and encourages hypertrophic maturation (St-Jacques et al., 1999). *Ihh* expression stimulates the expression of parathyroid related hormone protein (PTHrP), which in turn feeds back to inhibit Ihh expression. Via this feedback loop, the amount of hypertrophic chondrocyte differentiation is regulated and dictates the amount of longitudinal elongation (Chung et al., 2001). Interestingly, it was later discovered that Ihh activation of PTHrP is via inhibition of Gli3 mediated PTHrP repression (Koziel et al., 2005). Consistent with the importance of *Ihh* in long bone growth, *Ihh* null mice have severe shortening of the long bones, associated with a loss of proliferation and hypertrophy (St-Jacques et al., 1999).

FGF signaling is the other key regulator of cartilage maturation. *Fgf9, -8, -17, and -18* have all been detected in long bone chondrocytes (Mason et al., 1994, Xu et al., 1999, Ohbayashi et al., 2002). loss of FGF18 and -9 results in chondrogenic and osteogenic defects, such as a larger region of proliferative

and hypertrophic chondrocytes, and as such are thought to be the main FGFR3 ligands in this context (Liu et al., 2002, Ohbayashi et al., 2002, Hung et al., 2007). Signaling through the FGFR3 acts to regulate long bone elongation by limiting chondrocyte proliferation and hypertrophy (See Chapter 1). As such, animal models with gain of *Fgfr3* mutations, have severely stunted long bone growth (Chen et al., 1999, Wang et al., 1999). Consistent with this, missense gain of function mutations of FGFR3 have been identified as causative in chondrodysplasia syndromes in humans (Bellus et al., 1995, Elejalde and de Elejalde, 1985).

Interestingly, short limbs are occasionally observed in humans with certain ciliopathies such as Sensenbrenner and Ellis-Van Crevald syndromes, as well as mouse models of these same ciliopathies (Sensenbrenner et al., 1975, Pacheco et al., 2012). Therefore, short long bones are an example of an overlapping phenotype observed in both chondrodysplasia and ciliopathies. The former is attributed to gain of FGFR3 signaling whilst the mechanism driving the phenotype in ciliopathies and the *Fuzzy* mutant has not been explored in great detail. This chapter aims to fully characterise the onset of this phenotype in *Fuzzy* mutant mice, and to establish whether it is as a result of defective Hh or FGF signaling.

3.2 Results

3.2.1 Cartilaginous elements of *Fuzzy* mutant limbs are shorter than in wildtype controls from e13.5

Since it has been previously documented that the limbs of *Fuz* mutants are shorter then wildtype controls, I wanted to first characterise the defect in limb elongation. The maturation of resting chondrocytes into hypertrophic chondrocytes is believed to control the longitudinal elongation of the long bones (Goldring et al., 2006, St-Jacques et al., 1999). I carried out Alcian blue staining at e13.5, which is the age of hypertrophic onset in the limbs. Staining of wildtype and mutant forelimbs reveals that at this age, all of the cartilaginous elements of the mutants appear shorter (Fig 3.1 A and B). Quantification of the length of the radius (r) and humerus (h) reveal that both elements are significantly shorter in mutant embryos (Fig 3.1 C; $p=0.0443$ and $p=0.0004$ respectively; $n=4$). Polydactyly is also observed in the mutant forelimbs, which possess 8 digits as opposed to the normal 5 in the wildtype.

3.2.2 At e14.5, *Fuzzy* mutant limbs do not have obvious regions of chondrocyte hypertrophy

In wild-type embryo limbs, by e14.5, different stages of chondrocyte maturation within the growth plate are readily observable (Fig 3.2 A). Alcian blue staining in the wildtype limbs reveals regions with less Alcian blue colour retention, which correspond to chondrocyte hypertrophy (Fig 3.2 B, red arrowhead). All cartilaginous elements in the mutant forelimbs appear shorter then those in wildtype littermates and quantification of the radius and humorous reveals a clear statistical difference (Fig 3.2 C; $p<0.0001$; $n=5$).

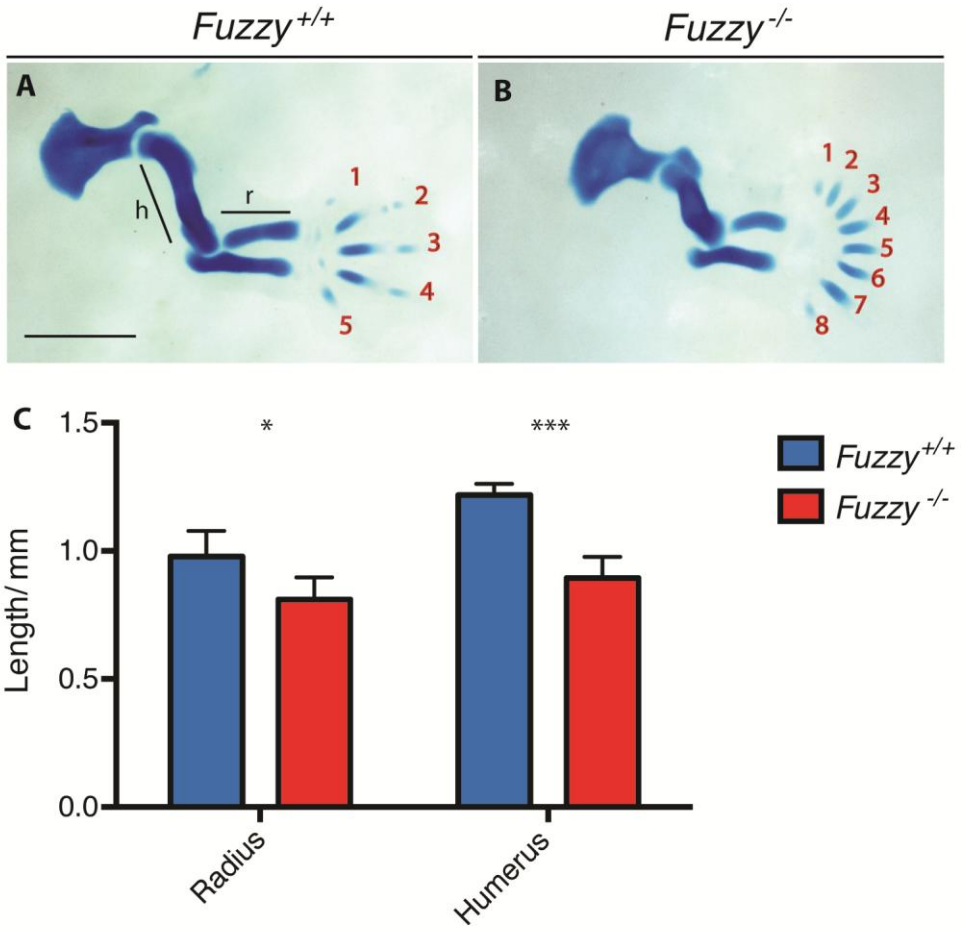

Figure 3.1 e13.5 *Fuzzy* mutants have polydactyly and shorter cartilaginous elements of the forelimbs.

(A and B) Alcian blue stained forelimbs of mutant and littermate control embryos at e13.5. The humerus (h) and radius (r) in the mutant (B) are shorter then the control (A). Polydactyly is observed in the limb of the mutant (8 digits compared to 5). Scale bar is 1mm.

(C) Quantification of the radius and humerus lengths between *Fuzzy* mutants and littermate controls. Both cartilaginous elements are shorter on loss of *Fuzzy*. (*P<0.05; ***P<0.0005); n=4).

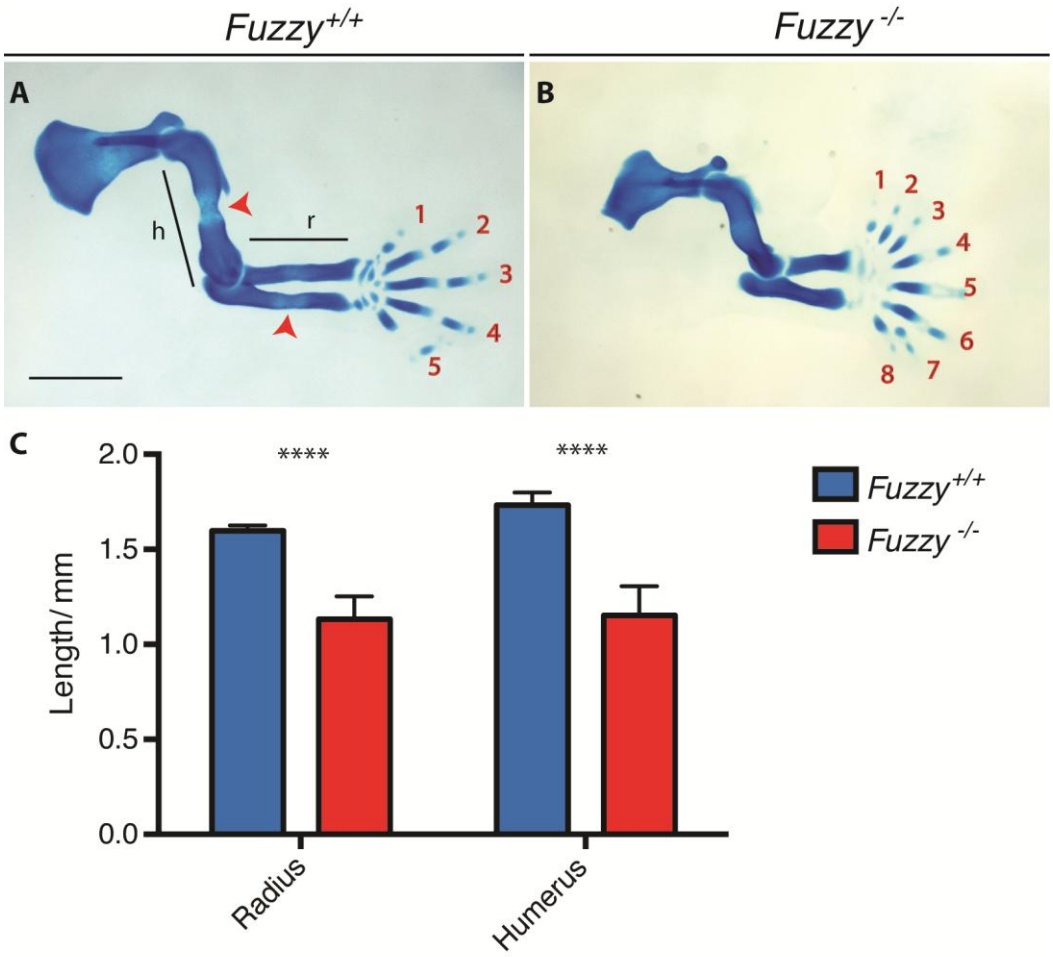

Figure 3.2 e14.5 *Fuzzy* mutants have shorter limbs and polydactyly.

(A and B) Alcian blue stained forelimbs of wildtype (A) and *Fuzzy* mutant (B) embryos at e14.5. Wildtype limbs have regions of hypertrophy (arrowheads) in the humerus (h) and radius (r), as well as 5 clear digits (numbered 1-5). *Fuzzy* mutants have shortened cartilaginous elements of the humerus and radius and polydactyly is also observed (B, numbered 1-8). Scale bar is 1mm.

(C) Quantification of the radius and the humerus lengths as shown in (A). Both the radii and humeri are shorter in mutant embryos (n=5, ****=$p<0.0001$).

3.2.3 *Fuzzy* mutant limbs have delayed chondrocyte maturation

Since chondrogenic hypertrophy is believed to drive longitudinal elongation I carried out trichrome staining on sagittal sections of wildtype and mutant radii at multiple stages. This enabled me to visualize the growth plate of the developing limbs (Fig 3.3). In wildtype limbs, by e14.5, a clear region of hypertrophic (hc), proliferative (pc) and resting chondrocytes (rc) can be observed (Fig 3.3 A). One day later at e15.5, the regions of hypertrophy and proliferation are clearly enlarged and bone collar formation is taking place surrounding the central region of hypertrophy (Fig 3.3 C, black asterisk). By e16.5, there is a clear boundary between the proliferative and hypertrophic chondrocytes and the region of bone deposition (Fig 3.3 E). In *Fuzzy* mutants, histology at e14.5 and e15.5 reveals that the chondrocytes of the radii have not yet progressed past the resting phase (Fig 3.3 B & D). It is not until e16.5 that we begin to see regions of stacked proliferating chondrocytes and hypertrophic chondrocytes suggesting a delay in hypertrophic onset (Fig 3.3 F).

3.2.4 *Fuzzy* mutant limbs have a loss of *Ihh* expression in developing long bones

During chondrocyte differentiation, the transcription factor *sox9* is expressed in resting chondrocytes while *Ihh*, a key regulator of chondrocyte terminal differentiation, is expressed in hypertrophic chondrocytes (St-Jacques et al., 1999). Since we observed a delay in hypertrophic onset we decided to examine the expression of both *Sox9* and *Ihh* (Fig 3.4). At e14.5 trichrome staining of transverse sections through the radius revealed three different stages of chondrocyte progression as seen in fig 3.3 A. *Sox9* expression in the wild-type is restricted to the resting chondrocytes (Fig 3.4 C), and *Ihh* expression is restricted to the hypertrophic chondrocytes (Fig 3.4 E). In comparison, in the mutant limb, *Sox9* expression appears to be expressed throughout the cartilaginous rod (Fig 3.4 D) and *Ihh* expression is massively diminished (Fig 3.4 F). This suggests that a loss of *Ihh* expression may be driving the short limb phenotype in the *Fuzzy* mutant.

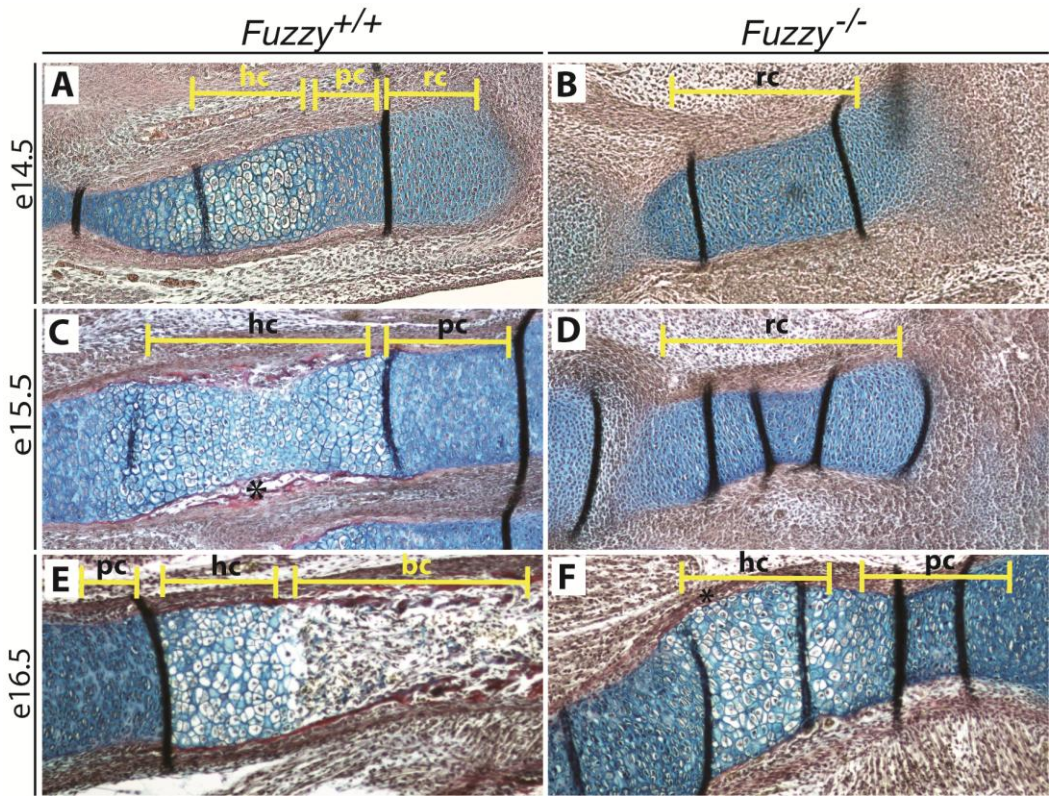

Figure 3.3 Delayed onset of hypertrophic chondrocytes in *Fuzzy* mutant limbs.

Trichrome staining showing cartilage in blue and bone in red in sagittal sections of radii, cartilage in blue. (A and B) E14.5 embryos. Wildtype embryos (A) have defined regions of resting (rc), proliferative (pc) and hypertrophic (hc) chondrocytes. The mutant radius (B) appears to only have resting chondrocytes.

(C and D) E15.5 embryos. In controls (C), the region of hypertrophy has expanded and is surrounded by the onset of bone formation (asterisk). Mutant forelimbs (D) only consist of resting chondrocytes at this stage.

(E and F) E16.5. Control samples (E) have a defined region of bone formation (bc) adjacent to the zone of hypertrophy. In mutant samples (F), chondrocytes have just acquired a hypertrophic morphology. Vertical black lines are histological artifacts.

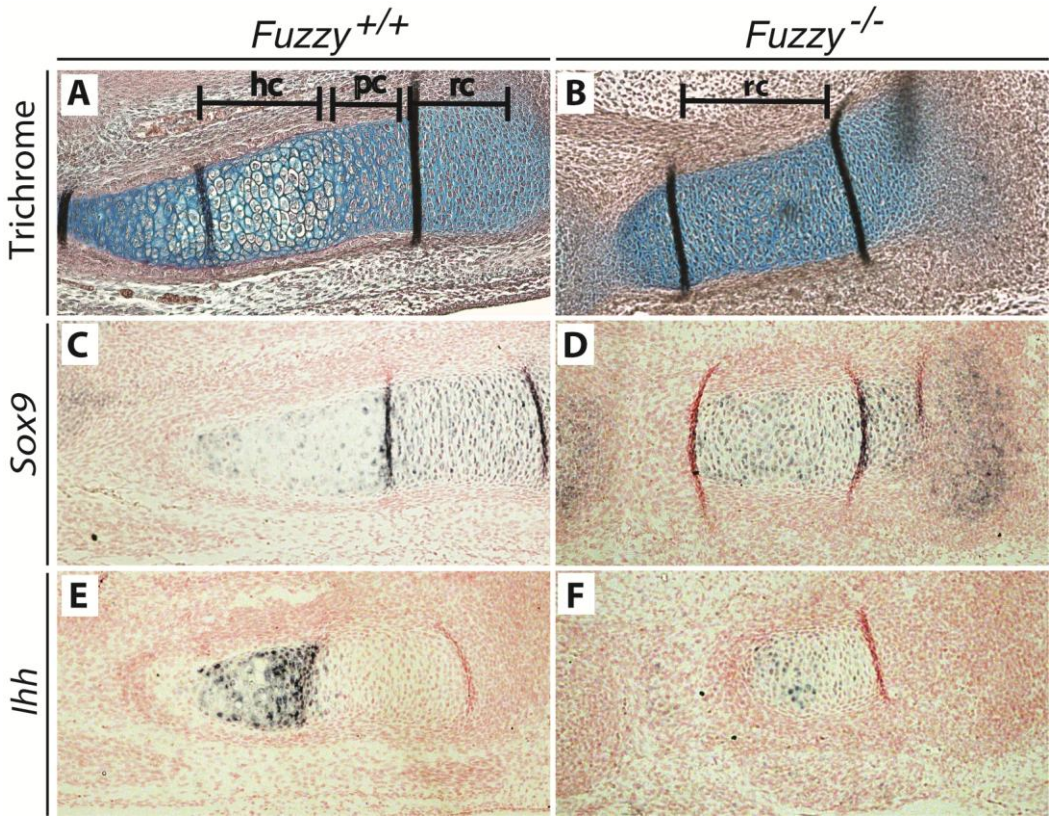

Figure 3.4 E14.5 *Fuzzy* mutants have diminished *Ihh* expression in radii

(A and B) Trichrome stained sagittal sections of radii, cartilage in blue. *Fuzzy* mutants (B) and littermate controls (A) at e14.5. 'hc' denotes region of hypertrophic chondrocytes and 'rc' represents region of resting chondrocytes. These are duplicates of Fig 3.3 A-B, for reference.

(C and D) mRNA *in situ* hybridisation for *Sox9* expression. *Sox9* expression is restricted to resting chondrocytes of wildtype radii (C). In mutant radii (D), *Sox9* is expressed throughout the cartilage.

(E and F) mRNA *in situ* hybridisation for *Ihh* expression. In wildtype limbs (E) Ihh is expressed in the region of hypertrophic chondrocytes. In mutants (F) *Ihh* is scarcely expressed.

3.2.5 *Fuzzy* mutant limbs have smaller regions of ossification

Since, during normal development, the cells in the region of hypertrophy are degraded and replaced by bone, and the *Fuzzy* mutant has delayed onset of hypertrophy, we would expect less ossification in mutants. To examine this we carried out Alizarin red staining for osteogenic calcification (Fig 3.5). At e18.5, in the wildtype forelimb, ossification of the humerus (h), radius (r), and ulna (u) is evident (Fig 3.5). Ossification of the phalanges is also under way (Fig 3.5 A, green arrowheads). In contrast, in the *Fuzzy* mutant limb, although some ossification is observed, regions of ossification are shorter in the mutant limbs and ossification of the phalanges has not yet begun (Fig 3.5 B). This observation is consistent with a delay in chondrocyte maturation.

3.2.6 Genetic reduction of *Fgf8* does not rescue the limb phenotype of the *Fuzzy* mutant.

We have previously shown that genetic reduction of *Fgf8* gene expression in the *Fuzzy* mutant rescues the phenotype of maxillary hyperplasia (Tabler et al., 2013). In addition, FGF signaling is the other key regulator of chondrocyte hypertrophy, with *Fgf8* having previously been detected in chondrocytes (Xu et al., 1999). This led us to ask whether genetic reduction of *Fgf8* rescues the short limb phenotype observed in our mutant. We tested this by genetically reducing the levels of *Fgf8* in our *Fuzzy* mutants using a null allele of *Fgf8* ($Fgf8^{LacZ/+}$). (Fig 3.6). In the wild-type embryo at e14.5, as has been described above, clear regions of chondrocyte maturation are observed (Fig 3.6 A; black arrowheads); whilst in the mutant, limbs are shorter and growth plate regions are less well defined (Fig 3.6 B; black arrowheads). Genetic reduction of *FGF8* does not rescue either the short limb phenotype or polydactyly (Fig 3.6 C). Panel 3.6 D shows a control sample, which is heterozygous for both *Fuzzy* and *Fgf8*. The limb is comparable to that of the wild type, which suggests that a reduced level of *Fgf8* alone has no effect on normal limb development.

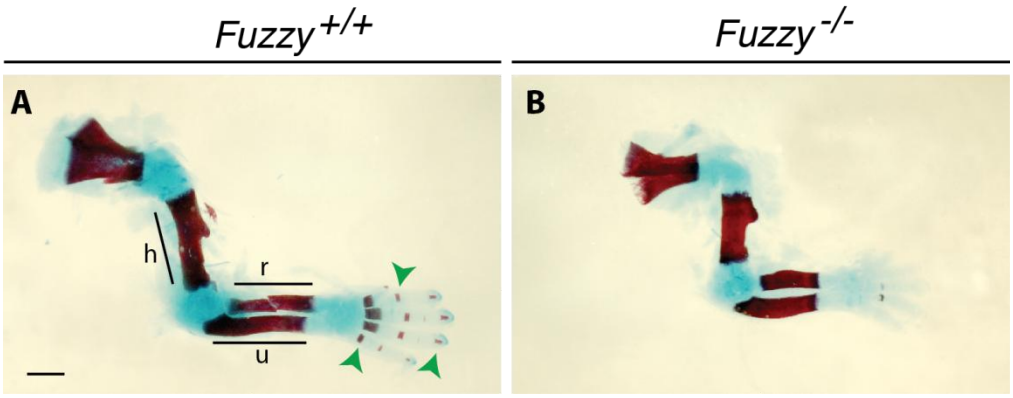

Figure 3.5 *Fuzzy* mutants have shorter regions of ossification

(A and B) Alizarin red staining for bone in forelimbs at e18.5. All skeletal elements of the long bone (humerus, radius and ulna; h, r and u respectively) can be seen in the wildtype sample (A). In addition, ossification of the phalanges is under way (green arrowheads; Fig 3.5 A). In the mutant (B), the ossified region of all skeletal elements is shorter and no ossification of the phalanges can be seen. Scale bar is 1mm.

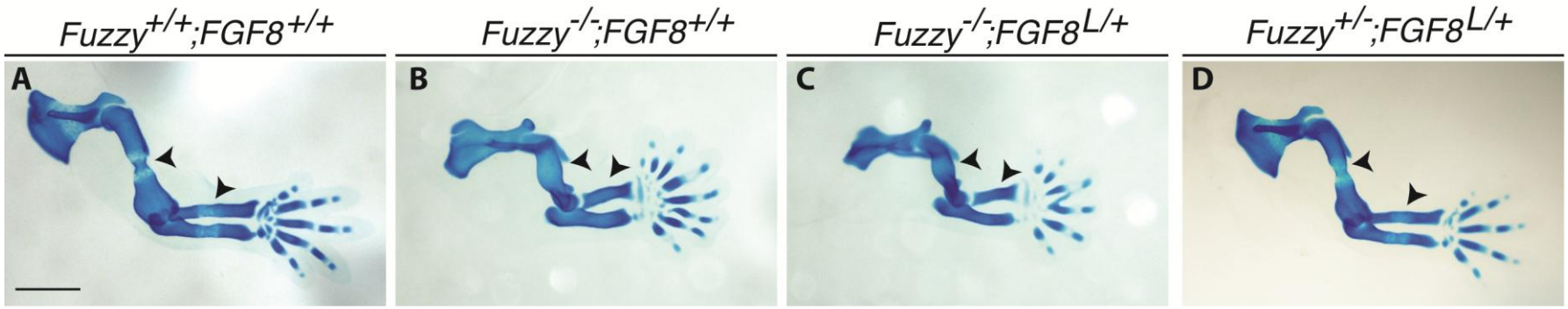

Figure 3.6 Reduction of *Fgf8* gene expression does not rescue the short limb phenotype in the *Fuzzy* mutant.

Alcian blue staining of forelimbs at e14.5.

(A) Wildtype forelimbs have clear regions of chondrocyte hypertrophy (black arrowheads) and 5 digits. (B) Loss of *Fuzzy* results in short limbs with less obvious regions of chondrocyte hypertrophy (black arrowheads) and polydactyly. (C) Reduction of *Fgf8* in the *Fuzzy* mutant does not rescue the short limb phenotype. Black arrowheads indicate less obvious regions of hypertrophy when compared with the wildtype. Embryos have polydactyly. (D) Control sample heterozygous for both Fuzzy and Fgf8 has is normal and identical to wild type (A). Limbs are normally sized with, no polydactyly, and obvious regions of hypertrophy (black arrowhead). Scale bar is 1mm.

3.2.7 Hypertrophic onset is also delayed in the basioccipitol bone

The developing limb bones are good models for endochondral ossification. In order to assess whether delayed chondrocyte maturation is likely to play a role in the developmental defects in other endochondral elements, I carried out histological staining on the basioccipitol bone of the cranial base between e13.5 and e16.5 (Fig 3.7). As was described in the developing radius, at e13.5 resting chondrocytes can be observed, these have progressed to hypertrophic chondrocytes at e14.5, and by e16.5 they are being replaced with newly forming bone (Fig 3.7 A, C, E). In the *Fuzzy* mutant however, resting chondrocytes are seen to persist from e13.5 to e14.5 (Fig 3.7 B and D). Strikingly, by e16.5, no bone deposition has taken place and chondrocytes are just beginning to undergo hypertrophy onset (Fig 3.7 F). This delay in hypertrophic onset is very similar to that seen in the long bone (Fig 3.3), suggesting a comparable mechanism driving lack of ossification and shortening in the cranial base.

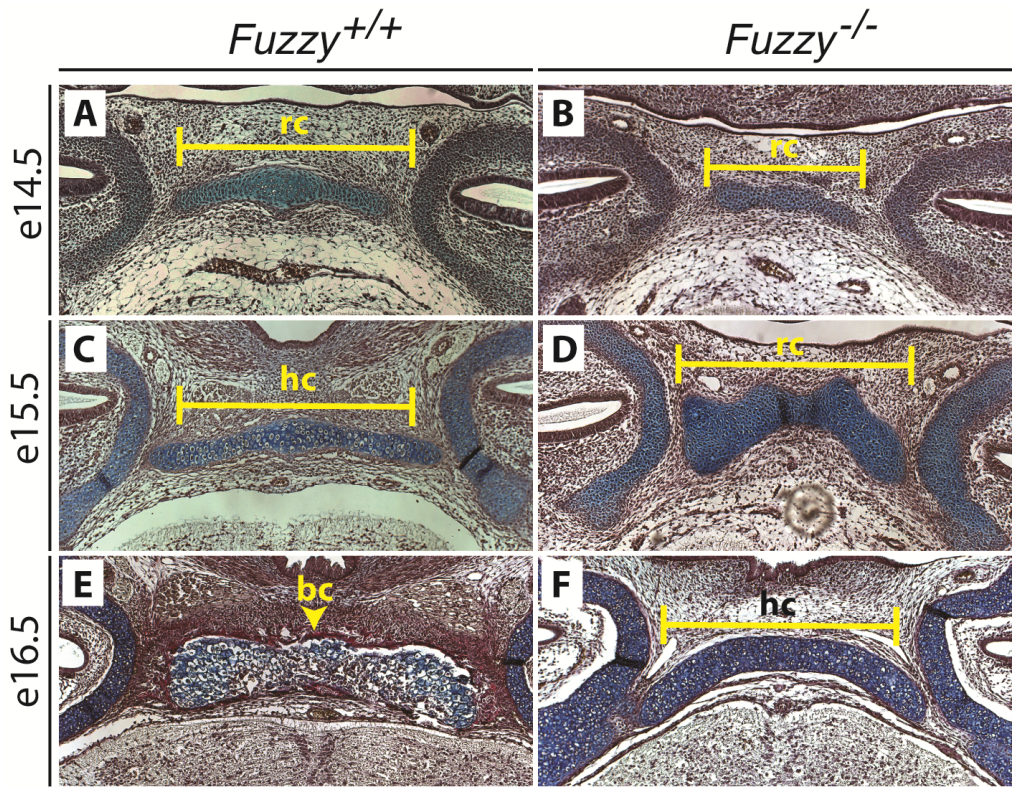

Figure 3.7 The basioccipitol bone of the *Fuzzy* mutant has delayed hypertrophic onset.

Frontal sections, trichrome staining, cartilage in blue.

(A and B) Basioccipitol of wildtype and mutant littermates at e13.5. At this age, resting chondrocytes (rc) are seen in both wildtype (A) and mutant (B) samples.

(C and D) By e14.5, chondrocytes in the wildtype (C) are becoming hypertrophic (hc), whereas the mutant chondrocytes (D) appear to be in the resting state.

(E and F) At e16.5, a clear bone collar (bc) is visible in the wildtype sample (E) with ossification, seen in red, surrounding the hypertrophic chondrocytes. In the mutant (F), chondrocytes are just beginning to undergo hypertrophy.

3.3 Discussion

Analysis carried out on the long bones of *fuzzy* mutants suggest that a loss of elongation is due to delayed chondrocyte maturation which also results in less ossification of the limb. My data suggests that a loss of *Ihh* expression may be driving this phenotype. As described above, *Ihh* expression is regulated by a negative feedback loop with PTHrP. The Gli3 repressor, which we previously showed to be up-regulated in the *Fuzzy* mutant, mediates this feedback loop (Tabler et al., 2013); see figure 5.8). The repressor acts to inhibit PTHrP expression during chondrocyte maturation (Koziel et al., 2005); hence loss of Gli3 repressor in the *Fuzzy* mutant, would result in a derepression of PTHrP and a subsequent inhibition of Ihh expression.

It is likely that in our *Fuzzy* mutant, the absence of the cilium means that binding of the Ihh ligand cannot regulate Gli3 repressor activity; this has previously been shown to delay chondrocyte maturation through both PTHrP dependent and independent mechanisms (Koziel et al., 2005). This model is supported by the observation that *Gli3* mutants have shortened long bones (Panman et al., 2005, Mo et al., 1997, Hui and Joyner, 1993, Johnson, 1967). Given the nature of Hh signaling, it could be suggested that reduced Ihh expression would result in increased formation of the Gli3 repressor (See Fig 3.8). However, in the absence of Gli processing in the *Fuzzy* mutant we would expect that we have no formation of the Gli3 repressor irrespective of Hh ligand binding. For this reason *Ihh* mutants have severely shortened long bones associated with a loss of PTHrP expression (St-Jacques et al., 1999); while, enhanced signaling through the PTHrP receptor also results in a delay of chondrocyte hypertrophy (Karp et al., 2000).

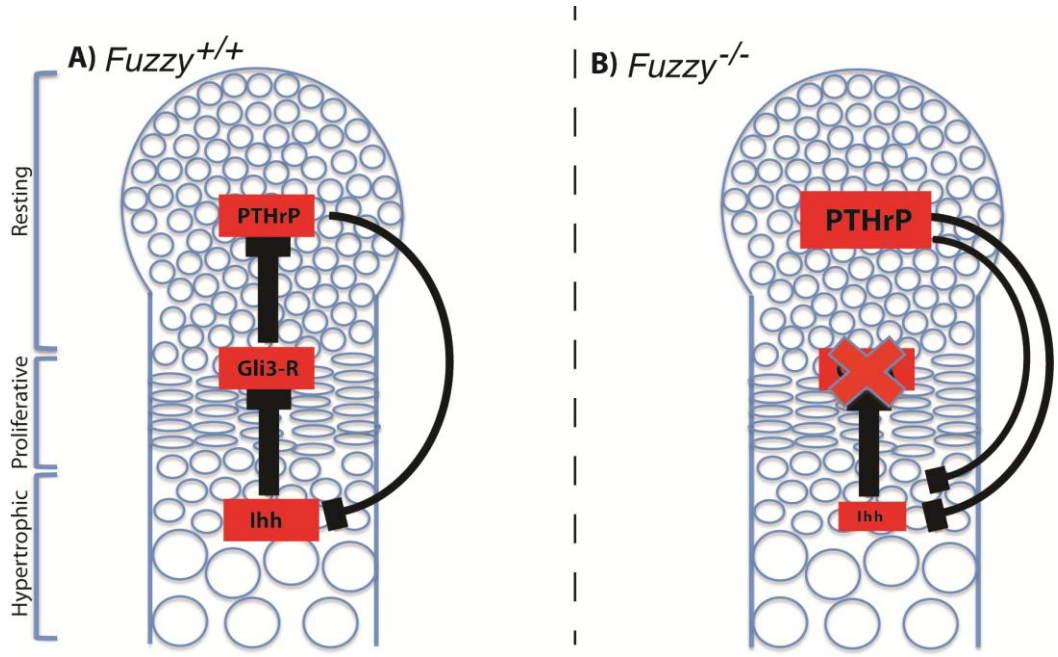

Figure 3.8 Predicted model for delayed onset of hypertrophy in *Fuzzy* mutant long bones.

A) In the wildtype situation, Ihh is expressed by, and stimulates the differentiation of hypertrophic chondrocytes. Hypertrophic cells express *Ihh*, which restricts the amount of Gli3 repressor. The Gli3 repressor is necessary for inhibition of PTHrP, which limits *Ihh* expression. In this way, the level of IHH and hence the number of hypertrophic chondrocytes is regulated.
B) In the Fuzzy mutant, we believe that a loss of the Gli3 repressor reduces the amount of PTHrP repression. Increased levels of PTHrP cause Ihh inhibition, ultimately resulting in fewer hypertrophic chondrocytes.

Interestingly, I observed shortening of the basioccipitol cartilage element via a delay in hypertrophy. It has been reported that loss of Gli3 causes reduced ossification in this element, which is in keeping with our observation of reduced hypertrophy (Bose et al., 2002); interestingly, in the basosphenoid, reduction in Gli2 causes a more severe shortening (Mo et al., 1997). This may be an example of tissue specific differences between relative contributions of Gli2 and Gli3 in skeletal development and could reflect the different origins of the limb, derived from the lateral plate mesoderm, and the basosphenoid bone, which derives from cephalic mesoderm. Along these same lines, mouse mutants lacking Gli2 have also been reported to have slight defects in long bone elongation and Gli2 has been shown to have roles in regulating chondrocyte hypertrophy (Mo et al., 1997, Joeng and Long, 2009). Although we have only showed altered processing of Gli3 in the *Fuzzy* mutant, this role for Gli2 in long bone development suggests that our mutant may also have defective Gli2 processing.

Another important aspect of limb development, as described in the introduction above, is the importance of Gli3 repression in patterning the digits. Mouse mutants for *Gli3*, as well as having short limbs, have polysyndactyly (Johnson, 1967, Hui and Joyner, 1993). In digit patterning, Shh signaling is required to restrict the levels of Gli3, which controls the number of fingers formed. For this reason, *Shh* mutants have only one digit and *Gli3* mutants have multiple (Chiang et al., 2001). Polydactyly observed in the *Fuzzy* mutant is also most likely due to the loss of the Gli3 repressor (Heydeck et al., 2009). Previous reports on the IFT88 hypomorph mutant, another ciliopathy mouse model, have reported polydactyly to be due to abnormal limb bud patterning as a result of to abnormal Gli3 regulation (Liu et al., 2005a). This study also reported lower levels of Gli1 and Ptc1 in their mutants, which we have also previously demonstrated in the *Fuzzy* mutant (Tabler et al., 2013).

Together, this data suggests that in the case of the shortened limbs of *Fuzzy* mutants, the main signaling defect is the regulation of Gli3R. It is important to remember, however, that in all of the developmental stages described in

this chapter, FGF signaling has significant contributions. This is a particularly important consideration since we have shown enhanced FGF8 signaling in the *Fuzzy* mutant (Tabler et al., 2013).

FGF signaling has multiple roles in chondrocyte maturation and specific roles with regards to regulation of chondrocyte hypertrophy. In mice, enhanced FGF signaling, specifically via hyper-activation of FGFR3 has been shown to result in a long bone phenotype which is very similar to that observed in the *Fuzzy* mutant, whereas diminished signaling through FGFR3 causes excessive long bone growth (Brodie and Deng, 2003). *Fgfr3* expression has been detected in proliferative and hypertrophic chondrocytes in the growth plate and mutations in this gene have been shown to be the most common cause of chondrodysplasia syndromes in humans (Peters et al., 1993, Delezoide et al., 1998, Rousseau et al., 1994, Shiang et al., 1994, Tavormina et al., 1995). These phenotypes have been re-created with activating mutations of FGFR3 in mice as well as constitutive activation of downstream FGF signaling components such as MEK1 (Li et al., 1999, Segev et al., 2000, Murakami et al., 2004). This is evidence to suggest that abnormal FGF signaling may contribute to the phenotypes we observe.

Due to this, and because FGF8 does in some contexts signal via binding to FGFR3, and also because reducing levels of FGF8 in the *Fuzzy* mutant rescues a hyperplastic maxilla (Tabler et al., 2013). We analyzed the limb phenotype in a *Fuzzy*$^{-/-}$;*Fgf8*$^{L/+}$ and Onset of hypertrophy was not restored. Even though *Fgf8* has been detected in rib chondrocytes at e14.5 and e15.5, it is not known to have roles in long bone elongation. In fact, loss of FGF18 results in a short long bone phenotype consistent with the suggestion that FGF18 is the key ligand that signals via FGFR3 to regulate chondrocyte hypertrophy (Ohbayashi et al., 2002)**.** No evidence to date suggests that one would expect altered expression of *Fgf18* in the *Fuzzy* mutant however this does not mean that the possibility can be ruled out. For this reason, further analysis of mutant limbs with manipulation of other FGF ligands, particularly FGF18, would be a logical next experiment in order to assess whether a loss in FGF signaling contributes to the phenotype observed.

Furthermore, these experiments would help determine whether there are any commonalities between the short limb phenotype observed in ciliopathies and chondrodysplasias; this is particularly important since FGFR3 signaling has been reported to inhibit *Ihh* expression in the growth plate (Naski et al., 1998, Chen et al., 2001).

With regards to patterning of the mutant limb bud, *Fgf8* is expressed in the AER and is said to be important for determining the homeotic identity of the skeletal elements in the developing limb. This works via a gradient of FGF expressed across the longitudinal plane of the limb with the cells exposed for longer adopting a more distal fate (Niswander et al., 1993). Previous experiments reveal that a loss of *Fgf8* expression in the mesenchyme causes a slight loss of ossification, whilst reduction in early limb ectoderm reduces proximal-distal limb bud growth, mainly by inhibiting growth of the most proximal limb element (the stylopod) development resulting in a short limb (Lewandoski et al., 2000). Since we do not see a homeotic transformation in the limb, and our *Fuzzy*$^{-/-}$*;FGF8*$^{L/+}$ compound mutants show no rescue of any limb phenotypes, combined with the fact that we observe no defects in the initial outgrowth of the limb bud, it is unlikely that enhanced FGF8 signaling contributes to the defects we have characterised.

In conclusion, it appears that the defective long bone elongation and digit patterning in the *Fuzzy* mutant are likely as a result of loss of regulation of the Gli3R and altered FGF signaling from the AER probably does not contribute to any of these phenotypes. It is likely that altered FGF signaling also does not contribute to lack of long bone elongation however analysis of expression of key FGFs required for limb bud growth or further compound mutants should be generated to confirm this. If indeed a loss of Gli3R were driving the *Fuzzy* long bone phenotype, then my data would suggest that there are different underlying causes to the phenotype in chondrodysplasias and ciliopathies.

Chapter 4 Micrognathia in the *Fuzzy* mutant

4.1 Introduction

Micrognathia, or small jaw, has an incidence of about 1:1000 births (Copel et al., 2012). In patients, the small jaw can cause misplacement of the tongue, which then obstructs palatal closure (Copel et al., 2012). In the most severe instances of micrognathia, an infant's feeding and breathing can be restricted. Later in life, the teeth may be misaligned due to space restrictions and agenesis of the condyle has also been reported (Gangopadhyay et al., 2012, Lam et al., 2014, Storm et al., 2005). Micrognathia is present in ciliopathies such as Meckel Gruber syndrome, Sensenbrenner syndrome, orofaciodigital syndrome and Bardet-Biedl syndrome (Brugmann et al., 2010, Bacino et al., 2012, Biswas et al., 2009, Beales et al., 1999). In addition, micrognathia is also associated with non-ciliopathic diseases such as Marfan syndrome, Treacher Collins syndrome and Pierre Robin Sequence (Ornek et al., 2012, Martelli-Junior et al., 2009, Buntinx et al., 1991, Summers et al., 2014). Interestingly it is also reported in rare chondrodysplasias such as Larsen-Like syndrome, kyphomelic dysplasia and thoracopelvic dysplasia (Orhan et al., 2008, Toledo et al., 1999, Hsieh et al., 1999, Dinno et al., 1976).

To date, etiology and physical mechanisms causing micrognathia during embryogenesis are unclear. Understanding how this phenotype arises is not only important from a clinical perspective but will also shed light on mechanisms of mandible growth and elongation, which are not fully understood. This chapter aims to identify underlying causes of micrognathia observed in the *Fuzzy* mutant, which act as a ciliopathic mouse model.

Micrognathia observed as a small Meckel's cartilage (MC), associated with ectopic rostral spikes of cartilage has previously been documented in the *Fuzzy* mutant (Zhang et al., 2011). However mechanisms driving this defect are not clear-cut. Perturbations in Hh and Wnt signaling have been observed in *Fuzzy* mutants (Zhang et al., 2011). At e14.5, in the mandible there were reduced levels of *Shh, Ptc1 and Gli1* in the mesenchyme, as well as less PTC1 in MC (Zhang et al., 2011). Additionally, increased levels of β-catenin and

LEF1 in the oral epithelium were noted, as well as increased expression of a Wnt-responsive luciferase (Topflash) in the oral mesenchyme (Zhang et al., 2011). As such increased proliferation seen in Meckel's cartilage was attributed to enhanced canonical wnt output (Zhang et al., 2011)

Meckel's cartilage is the initial skeletal support in the mandible. In the mouse, at approximately e8, CNC cells migrate laterally from the neural tube to populate the first branchial arch (BA1) (Kuo and Erickson, 2010). The mandibular and maxillary compartments are subsequently specified within BA1. Cells aggregate in two locations on either side of the midline of the presumptive mandible forming prechondrogenic condensation (Hall and Miyake, 1992). These differentiate into chondrocytes, which produce cartilage in bilateral rods running proximo-dorsally. At approximately e13.5, MC contains a mixed population of non-CNC cells and CNC cells (Chai et al., 2000). By e13.5 MC has adopted the characteristic 'V' shape, since the rods fuse at their distal tips forming the rostral process. The most proximal regions go on to form middle ear components such as the malleus and incus (Bhaskar et al., 1953, Frommer and Margolies, 1971). The cartilage then continues to elongate proximo-distally. Mechanisms driving elongation are largely unknown. However, FGFR3 dependent proliferation and levels of chondrocyte turnover are thought to be important (Havens et al., 2008, Ramaesh and Bard, 2003).

By e15.5, enlarged IHH and COLX secreting hypertrophic cells, similar to those observed in endochondral bones, can be observed in the distal half of MC in vivo and in cell culture (Shimo et al., 2004, Chung et al., 1995, Ishizeki et al., 1996, Yang et al., 2012). These cells appear to undergo autophagy at around e16.5 but are not replaced with ossified bone in a typical endochondral manner, and hence their contribution or role in mandible development is not truly known (Yang et al., 2012). As such there is a current debate as to how similar MC is compared to other endochondral cartilages.

Immature chondrocytes of the limbs express Rank-ligand (RANKL) and osteopontin (OPN), which are markers of bone onset, whereas MC chondrocytes do not (Sakakura et al., 2005). In addition, during chondrocyte hypertrophy in endochondral elements, the chondrocytes become heavily vascularized; a process which is not seen in hypertrophic-like cells of MC (Ishizeki et al., 1999, Shimada et al., 2003). Conversely, during hypertrophy, MC chondrocytes express RANKL, OPN and apoptotic markers, all of which are expressed in endochondral chondrocytes. As such, it has been suggested that some regions of MC give way to bone (Ishizeki et al., 1999, Trichilis and Wroblewski, 1997, Cheung et al., 2003). Interestingly, in tissue culture, chondrocytes were shown to differentiate into osteocytes (Ishizeki et al., 1996).

Instead, it is thought that bone formation takes place within a membranous sheath surrounding Meckel's cartilage. This persistent cartilaginous support, with the presence of hypertrophic-like cells and membranous deposition of bone, makes the ossification of the mandible a unique example of intramembranous ossification (This is expanded upon in chapter 6).

Mechanisms driving initial outgrowth of the mandible are not very well understood. Removal of the BA1 epithelium results in reduced mandibular outgrowth suggesting a role for epithelial to mesenchymal signals in BA1 (Richman and Tickle, 1989, Mina et al., 1994). Regional gene expression of *Msx* and *Bmp* genes in the mandibular arch contributes to zones of proliferation and medial cells appear to contribute more then their lateral neighbors during outgrowth of the mandibular arch in chick (Mina et al., 1994, McGonnell et al., 1998, Barlow and Francis-West, 1997). It is not known for sure if MC growth drives the elongation of the mandible however mice with *Sox9* null neural crest cells have a complete absence of Meckel's cartilage and severe micrognathia, suggesting that growth, at least in part, requires MC (Mori-Akiyama et al., 2003).

As described previously, cilia have important signaling roles and we have seen aberrant Hh and FGF signaling in our *Fuzzy* mutant (Tabler et al., 2013).

Abnormal Hh and FGF8 signaling are both associated with craniofacial malformations. Loss of *Shh* during embryogenesis results in a complete loss of craniofacial structures, while temporal reduction of Hedgehog signaling at later stages results in midline defects ranging from holoprosencephaly to cyclopia (Brugmann et al., 2010, Nanni et al., 1999, Babbs et al., 2008, Hu and Helms, 1999). Cobourne et al showed, in mandibular explant cultures, that Shh activity has essential roles in tooth bud formation (Cobourne et al., 2001). More specific to the mandibular growth, treatment of mandibular explant cultures with cyclopamine, a small molecule inhibitor of Hh signaling, leads to an inhibition of chondrogenic differentiation of Meckel's cartilage (Melnick et al., 2005). The Gli proteins themselves have also been shown to have redundant roles in mandibular development, since loss of Gli2 causes a truncation of the proximal mandible with a loss of incisors whilst loss of Gli3 alone does not appear to have any obvious mandibular phenotype. Compound mutants, however, have a severely shortened mandible (Veistinen et al., 2012, Mo et al., 1997).

Interestingly, SHH and FGF signaling are shown to work together to control patterning of BA1 in chick (Haworth et al., 2007). *Shh* is expressed in the more ventral endoderm, whilst *Fgf8* is expressed adjacent to this in the more dorsal ectoderm prior to BA specification in chick, (Haworth et al., 2007), In addition, *Fgf8* and *-9*, and *FGFR1* and *-2* are expressed in the mouse mandibular epithelium at e10.5 (Bachler and Neubuser, 2001). Furthermore, loss of Shh results in NC and mesenchymal cell death resulting in a smaller head in chick embryos as well as smaller BAs in mouse embryos (Ahlgren and Bronner-Fraser, 1999, Moore-Scott and Manley, 2005, Yamagishi et al., 2006). More over, in Shh null mice, a smaller BA1 was associated with a loss of epithelial *Fgf8* expression in BA1 at e9.5 (Yamagishi et al., 2006). This data suggests *Fgf8*-S*hh* interactions are important for initial BA outgrowth.

FGF8 has been shown to act as a NC survival factor and and has been shown to increase NC cell migration and proliferation within the developing face. In the developing maxilla, an increased domain of *Fgf8* expression in the

epithelium is associated with aberrant NC migration, whilst reduced expression in the developing mandibles is associated with extensive mesenchymal apoptosis in mice, as well as increased NC cell migration and proliferation within the mandible of the duck (Tabler et al., 2013, Abu-Issa et al., 2002, Trumpp et al., 1999). Further highlighting the importance of Fgf signaling in mandibular outgrowth and chondrogenesis, overexpression of *Fgf8* alters the polarity of MC condensation leading to ectopic and bifurcated Meckel's cartilage, while expression of dominant-negative FGFR3 results in a truncated and asymmetric mandible (Haworth et al., 2007, Havens et al., 2008). Taken together this data suggests that FGF8 is important for normal NC survival and migration during mandibular outgrowth and in addition, it has important roles in patterning the mandibular arch.

Another important role for *Fgf8* signaling is to specify different regions of tooth formation and establish medio-lateral spacing within the mandibular process. *FGF8* is expressed in the lateral mandibular epithelium, whilst medially in this same epithelium, *bone morphogenic protein-4* (*BMP4*), a member of the transforming growth factor beta superfamily, is expressed (Tucker et al., 1999). It is thought that the adjacent positioning of *FGF8* and *BMP4* regulate medio-lateral patterning within the mandibular primordia (Tucker et al., 1998, Bei and Maas, 1998). During this process, mesenchymal homeobox genes are expressed in strict temporo-spatial patterns. In molar forming regions, FGF8 drives BARX homeobox1 (*Barx1*) expression whilst in the medial incisor forming mesenchyme, BMP4 induces MSH homeobox 1 and 2 (*Msx-1* and *-2)* expression, which induces incisor formation (Barlow et al., 1999, Tucker et al., 1998, Cobourne and Sharpe, 2003).

We have previously shown defective Gli3 processing in the *Fuz*$^{-/-}$ embryos at e9.0, In addition, we note an expansion of *Fgf8* expression in the mid-hind brain boundary. Together, this leads to an increase in NC cell numbers. Later, during facial development, *Fuz* mutants also have an expansion of *Fgf8* expression in the BA1 epithelium (Tabler et al., 2013). Ordinarily, *Fgf8* is expressed in a stripe on lateral regions of the BA1 epithelium (see chapter 1; Fig 1.9). The best-characterised role of *Fgf8* in this context is in governing

mediolateral patterning of the mandible and positioning sites of tooth formation (Tucker et al., 1999, Tucker and Sharpe, 2004). Thus, we considered two possibilities: first, that ciliopathic mutations had altered medio-lateral patterning and constriction in BA1 due to increased neural crest cell numbers; and second, that the *Fgf8* increase might contribute to shape changes in the lower jaw. Our data shows that genetic reduction of the levels of *Fgf8* rescues micrognathia of the *Fuzzy* mutant. Altogether, our data documents several important stages in mandible formation and suggests a developmental sequence underlying ciliopathic micrognathia.

4.2 Results

4.2.1 The *Fuzzy* mutant has micrognathia which manifests as early as e10.5

We had previously observed that during development of the first branchial arch, *Fuzzy* mutant mice displayed a dramatically enlarged maxillary process, which subsequently led to development of a high arching palate (Tabler et al., 2013). It has also previously been observed that *Fuzzy* mutants had micrognathia (Fig 4.1 A & B, and (Gray et al., 2009). This raised the possibility that the enlargement of the maxillary domain came at the expense of the mandibular portion of BA1. Indeed, examining E10.5 mouse embryos, we noted that compared to littermate controls, the *Fuz* mutants were narrower in the mediolateral axis (Fig 4.1 C-D) and shorter in the dorsal-ventral axis (Fig 4.1 C'-D').

4.2.2 There is increased cell density and a larger region of *Sox9* expression on loss of *Fuzzy*

The size and density of prechondrogenic condensations are known to be important factors regulating the dimensions of the developing cartilage (Hall, 1992). We had previously shown an increase in neural crest cells in *Fuzzy* mutants (Tabler et al., 2013). But, as the mutant mandibular process appears smaller at e10.5, we asked whether cell packing was changed. To do this, we assessed the proximity of nuclei in the mandibular processes of e11.5 wildtype and mutant embryos. In mutant mandibular processes, cells appear closer together then in wildtype controls (Fig 4.2 A & B). As a result of this I counted cell nuclei in a fixed area of $0.2mm^2$ and found that cell density is significantly increased in *Fuzzy* mutants compared to controls (Fig 4.2 C; $p=0.0042$; $n=3$). This suggests an increase in condensing mesenchyme signifying the onset of chondrogenesis. Consistent with this, when we examined mRNA expression of *Sox9*, which marks prechondrogenic condensations, we found that expression was expanded toward the midline in mutants (Fig 4.2 D & E). Taken together these data suggest that during early mandibular development, there is increased cell packing associated with an abnormal region of prechondrogenic condensations, specifically spread towards the midline.

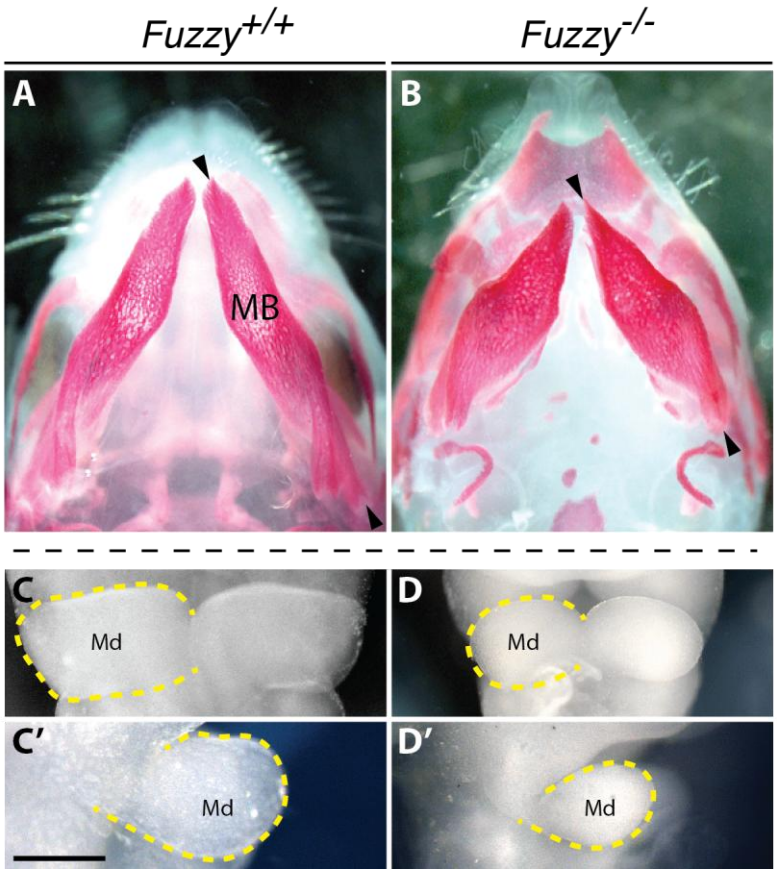

Figure 4.1 *Fuzzy* mutants exhibit micrognathia

(A and B) Ventral views of alizarin red stained heads at e18.5. The mandibular bone (MB) is demarcated between black arrowheads. The jaw of the *Fuzzy* mutant (B) is clearly shorter then that of the wildtype littermate (A).
(C and D) Frontal views of e10.5 embryos. Mandibular processes (Md) of BA1 are outlined in dashed yellow lines. The mutant mandible (D) is narrower and smaller then that of the wildtype (C).
(C' and D') Sagittal views of the mandibular process of BA1, outlined in dashed yellow lines. The mandible of the mutant (D') is smaller than littermate controls (C').

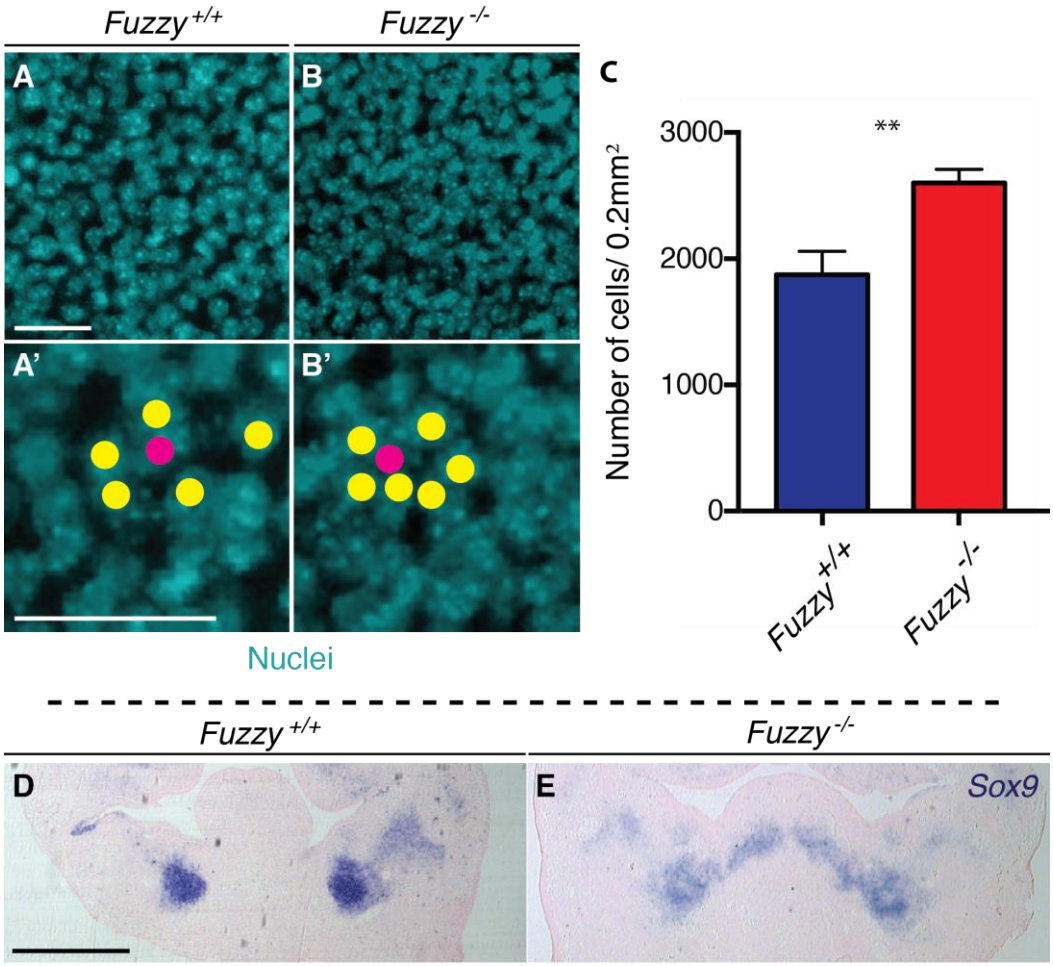

Figure 4.2 *Fuzzy* mutant mandibles have increased cell density at e11.5

(A and B) Frontal sections of the mandibular processes of mutant and control embryos. Nuclei are stained with Hoescht in cyan. Scale bar is 0.1mm.

(A' and B') Higher magnification of (A and B). An individual cell is highlighted in pink and its immediate neighbours are highlighted in yellow. Cells in mutant mandibles (B') are closer together then control samples (A'). Scale bar is 0.1mm.

(C) Quantification of the number of cells in an area of 0.2mm^2 in e11.5 mandibles. Mutants have a higher cell density ($p=0.0042$; $n=3$).

(D and E) mRNA *in situ* hybridization showing *Sox9* expression in mandibles of e12.5 embryos. (D) In control mandibles, *Sox9* expression corresponds to bilateral condensations of Meckel's cartilage. (E) In mutants, Sox9 expression occupies a larger area and is more spread towards the midline. Scale bar is 1mm.

4.2.3 Bilateral rods of MC are closer together by e11.5 and MC has prematurely fused by e12.5 in the *Fuzzy* mutant

Because of the expansion of *Sox9*, we decided to examine expression of *Col2*, which marks the cartilage precursors. To do this, we used a transgenic mouse carrying a β-galactosidase reporter under the control of the collagen II promoter (*Col2::lacZ*) (Zhou et al., 1995). When intercrossed with the *Fuz* mutants we observed that, at e11.5, the width of the mandibular process in mutants is significantly narrower then that of control littermates (p=0.013; n=4; Fig 5.3 A- C). Moreover, when we measure between the newly forming bilateral rods of Meckel's cartilage, we found that the distance at both the most distal and most proximal ends of MC were significantly narrower (Figure 4.2 C; distal: p=0.024 and proximal: p=0.017; n=4).

Because the mutant mandible is abnormally narrow, we considered the possibility that the bilateral rods of Meckel's cartilage might meet prematurely at the rostral process. To investigate this we again used *Col2::lacZ* reporter animals to mark the cartilaginous rods, this time using optical projection tomography (OPT) to visualize them in three dimensions. We see that at e12.5, Meckel's cartilage of the wildtype animals has not yet fully fused at the rostral process (Fig 4.3 E and E'). Strikingly, in the mutant littermates, the cartilage appears to be prematurely fused (Fig 4.3 F and F').

Quantification of the total proximo-distal length of the mandible between e12.5 to e16.5, reveal that at e12.5, there is no difference in length between wildtype and mutant mandibles. At e13.5 there is a trend of a shorter mandible in *Fuzzy* mutants and this difference in significant at e14.5 (p=0.0034; n=6) and e16.5 (p=0.0014, n=3).

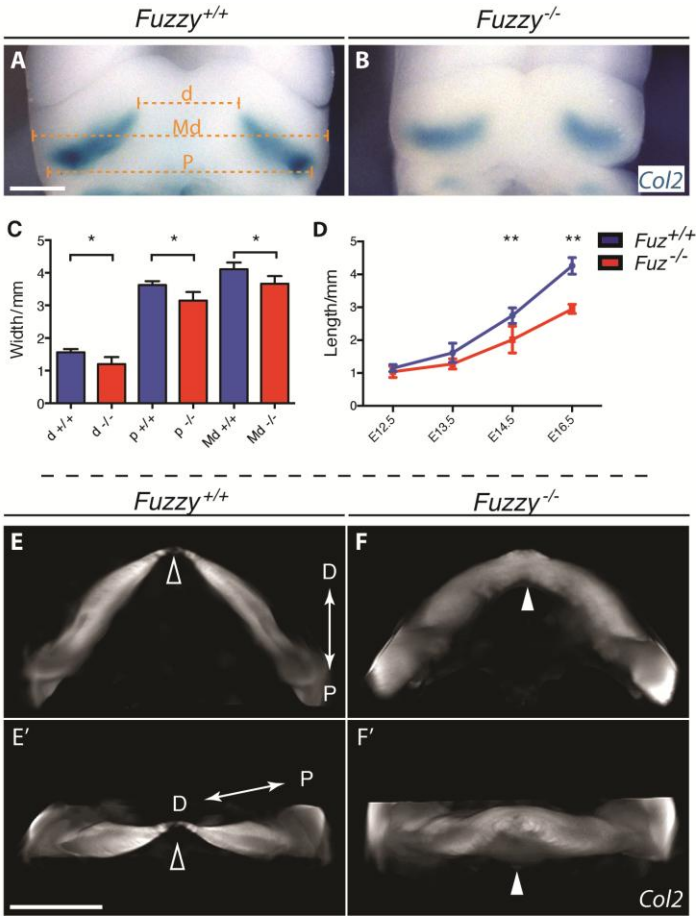

Figure 4.3 *Fuzzy* mutants have premature fusion of Meckel's cartilage at the rostral process

(A and B) Col2 expression in control and mutant mandibles at e11.5 seen with col2::lacZ reporter staining. Overall width of mandible (Md) as well as the most dorsal (d) and proximal (p) regions of col2 expression appear closer together in the mutant (B) when compared to control (A) mandibles. (C) Quantification of most dorsal, most proximal, and overall mandibular width in mutant and control embryos. All dimensions measured in the mutant are narrower then in control embryos ($p<0.05$; n=4). (D) Growth curve of the proximo-distal length of mandibles from e12.5 to e16.5. There is no real difference in length at e12.5 however by e13.5, mutant mandibles show a trend of being shorter. This difference is significant at e14.5 ($p=0.0034$; n=6) and e16.5 ($p=0.0014$; n=3). (E and F) Optical projection tomography of ventral views of col2 expression, which represent Meckel's cartilage. In control and mutant embryos most dorsal and proximal regions are indicated. (E) In control embryos the most dorsal region of Meckel's cartilage has not yet fused (open arrowhead). (F) In mutant embryos Meckel's cartilage has already fused in the midline (white arrowhead). (E' and F') Frontal views of col2 expression in control and mutant embryos. (E') In control samples col2 expression has not yet fused in the midline (open arrowhead). (F') In mutant samples, bilateral rods of Meckel's cartilage have prematurely fused at the most dorsal region (white arrowhead).

4.2.4 MC at the rostral process between e13.0 and e13.5

Since we saw premature fusion of MC at e12.5, we set out to document the consequences at later stages. At e13.0, in the wildtype, the rostral process had not yet fully fused. In the mutant, the rostral process appeared to be fused (red arrowhead; Fig 4.4 A & B). Half a day later, at e13.5, optical project tomographic (OPT) analysis of col2::lacZ reporter mice revealed wildtype MC developing into a characteristic 'V' shape, whereas the mutant cartilage appeared shorter and a prominent spike of cartilage could be seen protruding from the rostral process (red arrowhead) and the cartilage appears to be thicker towards the midline (green arrowheads) (Fig 4.4 C &D). These prominent rostral protrusions can also be seen in sagittal and frontal views (red arrowheads; Fig 4.4 E &F; Fig 4.4 G&H). Quantification of MC length (l) and distance between the bilateral rods of MC (d) at e13.5 reveal a slight trend that both parameters are shorter in the *Fuzzy* mutant however this difference is not significant (parameters measured are depicted in fig 4. 4 A). Taken together, these observations suggest a premature impact of MC causes the bilateral rods of cartilage to grow into one another at the rostral process causing an anterior thickening of the cartilage with 2 rostral spikes, which arise from each cartilaginous rod.

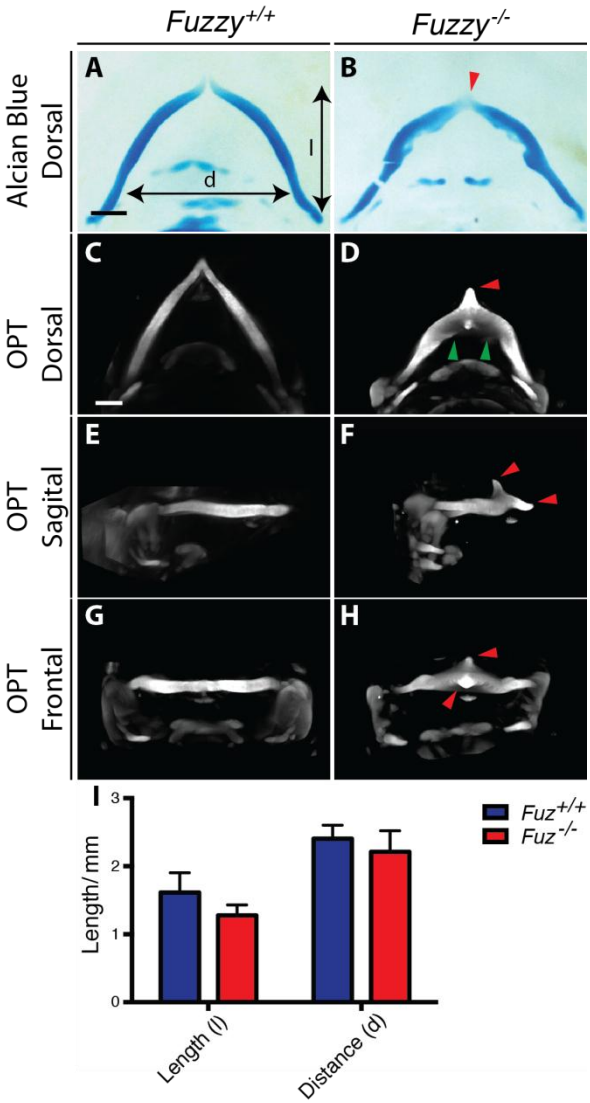

Figure 4.4 Meckel's cartilage of the *Fuzzy* mutant is malformed between e13.0 and e13.5.

(A and B) Dorsal view of Alcian blue stained Meckel's cartilage at e13.0. The most anterior portion of Meckel's cartilage is more fused in the mutant (red arrowhead, B), when compared to the control (A). Distance between the rods of MC (d) and the proximo-dorsal length of MC (l) represent distances measured in (I). (C and D) Dorsal view of 3D reconstructions of Col2 expression in Meckel's cartilage at e13.5. The wildtype MC (C) has a characteristic 'V' shape. The anterior of mutant Meckel's cartilage (D) is thickened towards the midline (green arrowheads) and the rostral process appears more pointed (red arrowhead).
(E and F) Sagittal views of Col2 expression at e13.5. The rostral process in the mutant (F) appears to have two prominent spikes protruding from the end (red arrowheads), which are not present in the wild type (E).
(G and H) Frontal view of col2 expression at e 13.5. Prominent spikes of the rostral process in the mutant (H) are highlighted with red arrowheads.
(I) Quantitation of the length (l) and distance between the two rods of Meckel's cartilage (d) as shown in (A). Mutant embryos show a trend of a shorter and narrower cartilage at e13.5 (n=4). Scale bar is 1mm.

4.2.5 MC is shorter and narrower at e14.5

Our observations above led us to consider the possibility that premature fusion of MC prevents elongation at later stages, thus constraining distal outgrowth of the mandible. Alcian blue staining of MC reveals the characteristic V shape in the wildtype, whilst the mutant cartilage appears shorter and a thickening of cartilage towards the midline is observed (Fig 4.5 A and B). 3D imaging of col2::lacZ reporter expression of MC at e14.5, similar to that seen at e13.5, shows a V shaped MC, which lies in one plane in the wildtype (Fig 4.5 C, E and G). In the *Fuzzy* mutant, as was seen at e13.5, there are two spiked protrusions of cartilage extending above and below the rostral process (Fig 4.5 D, F and H). Quantification of the proximodistal length and distance between the rods of MC (l and d shown in Fig 4.5 A), reveal that both parameters are significantly shorter in the *Fuzzy* mutant ($p=0.0034$ and $p=0.0381$ respectively; $n=6$; Fig 4.4 I). These observations follow on from the trend seen at e13.5, suggesting that premature fusion as early as e12.5 causes significant loss of elongation at later stages.

4.2.6 *Barx1* expression has a lateral to medial shift in the *Fuzzy* mutant mandible which is restored on reduction of *Fgf8*

We have previously shown that *Fuzzy* mutants have an expansion of *Fgf8* expression in the BA1 epithelium (Tabler et al., 2013). In BA1, *Fgf8* expression is thought to influence outgrowth of the maxillary and mandibular processes (Fish. 2014). Our previous data suggested that the maxillary phenotype could largely be attributed to an increase in cell numbers populating the dorsal component of BA1. However, the mandibular process did not show a similar expansion, and instead, was smaller. Therefore, I considered the possibility that FGF8 could contribute to the narrowing of the mandibular process. We tested this by looking at *Fuzzy*$^{-/-}$;*Fgf8*$^{L/+}$ compound mutants. I looked at expression of *Barx1* at e12.5, which is typically expressed in the lateral mandibular process, with no medial expression (Figure 545 A, (Tissier-Seta et al., 1995). In *Fuzzy* mutants, *Barx1* expression is clearly shifted toward the midline (Fig 4.6 B, black arrow). Interestingly, heterozygous loss of *Fgf8* was sufficient to restore normal medio-lateral placement of *Barx1* in the *Fuzzy* mutant mandible (compare Fig 4.6 C to B).

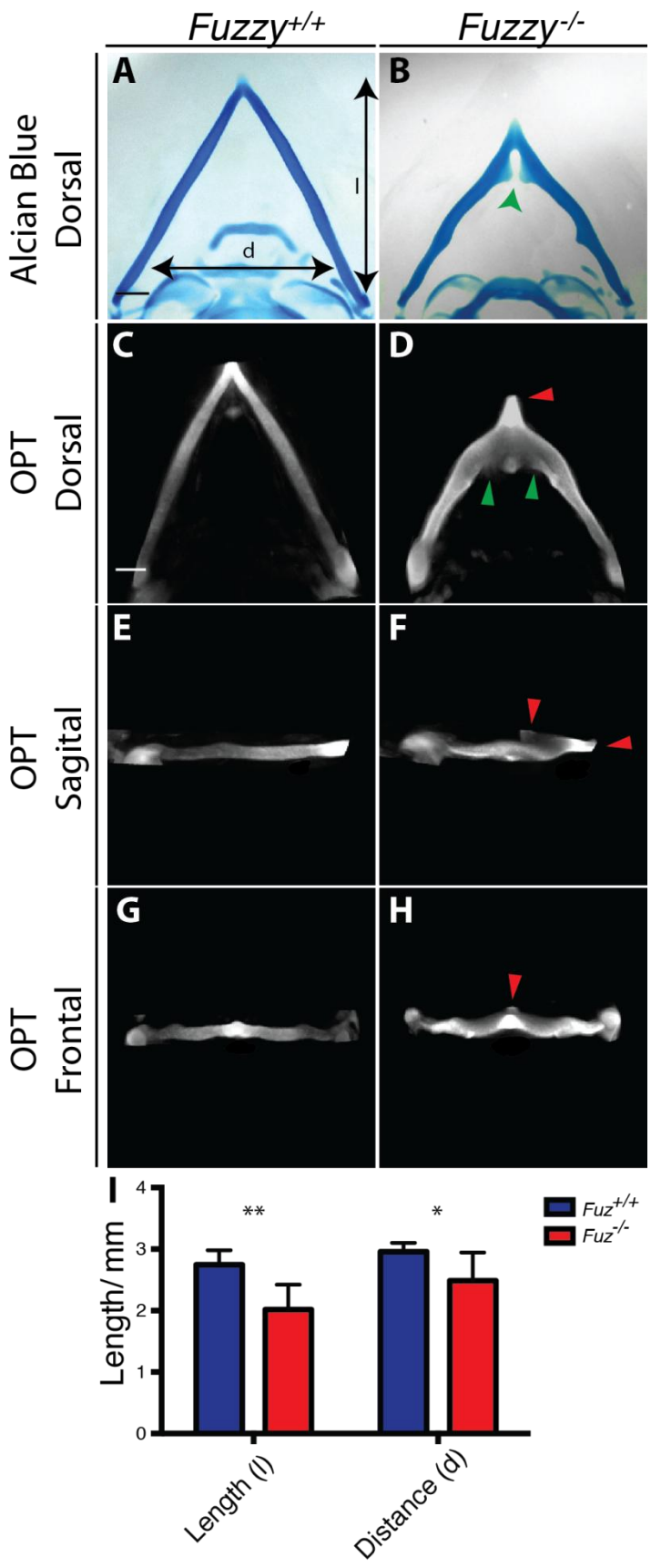
Fuzzy+/+
Fuzzy-/-
Alcian Blue Dorsal
OPT Dorsal
OPT Sagital
OPT Frontal
A
B
C
D
E
F
G
H
I
l
d
Length/ mm
**
*
Fuz+/+
Fuz-/-
Length (l)
Distance (d)

Figure 4.5 Meckel's cartilage of mutants is significantly shorter and there is a narrower distance between rods of cartilage at e14.5

(A and B) Alcian blue stained Meckel's cartilage at e14.5. Wild type cartilage is seen as a characteristic 'V' shape (A), whilst the mutant appears to have roughly the same shape but is visibly shorter (B). Green arrowhead in B shows a thickening towards the anterior portion of Meckel's cartilage. Arrows in (A) represent the dimensions quantified in (I).
(C and D) Stills from OPT reconstructions of Col2 expression visualized by means of a col2::lacZ reporter gene in Fuzzy mutant and littermate controls at e14.5. Wildtype cartilage (C) is a characteristic 'V' shape. In the Mutant (D), MC length appears visibly shorter. Green arrowheads show anterior thickening of Meckel's cartilage and red arrowhead shows anterior protrusions of Meckel's cartilage at the rostral process.
(E and F) Sagittal images of OPT reconstructions. Wildtype cartilage (E) sits in one plane, whilst mutant cartilage is noticeably shorter and has two spikes protruding from the rostral tip (red arrowheads).
(G and H) Frontal views of OPT reconstructions. In mutant MC (H), a spike of cartilage can be seen protruding above the plane of MC whilst wildtype MC does not protrude from its plane (G).
(I) Quantification of the length (l) and distance between the two rods of Meckel's cartilage (d) in *Fuzzy* mutants and control animals. Loss of *Fuzzy* results in a significantly shorter Meckel's cartilage ($p=0.0034$) with a narrower distance between the two cartilaginous rods ($p=0.0381$; $n=6$). Scale bar is 1mm.

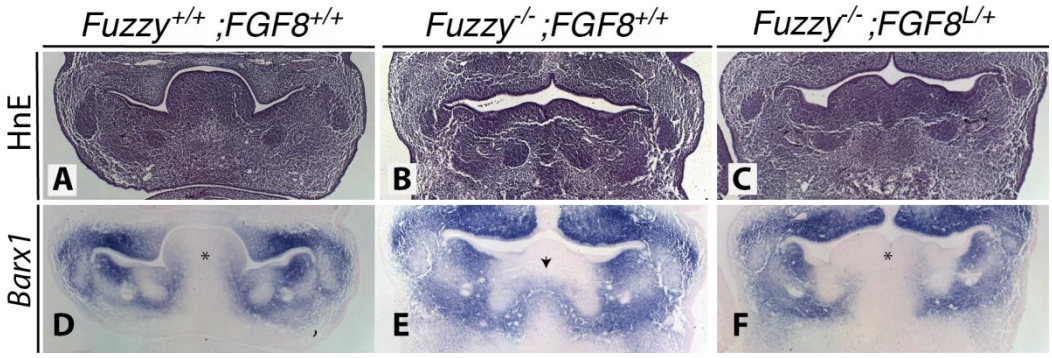

Figure 4.6 Medio-lateral spread of *Barx1* in the *Fuzzy* mutant is restored on reduction of *Fgf8*

(A-C) Reference slides showing haematoxylin and eosin stained frontal sections taken through the molar tooth bud of embryos at e12.5.

(D-F) *Barx1* expression in serial sections shown in (A-C). In the wildtype (D), *Barx1* expression is restricted to the lateral regions of the developing mandible and there is no expression in the tongue (asterisk). In the *Fuzzy* mutant (E), *Barx1* expression seems to be shifted towards the midline of the mandible (black arrow). The tongue is hypoplastic. On genetic reduction of *Fgf8* in the *Fuzzy* mutant (F), the lateral to medial shift of *Barx1* is rescued and it is not expressed in the midline or the tongue (black asterisk).

4.2.7 Genetic reduction of *Fgf8* in the *Fuzzy* mutant rescues the phenotype of MC

Since genetic reduction of *Fgf8* rescued the early mediolateral shift in expression of *Barx1*, I looked at MC at e14.5, again using alcian blue to mark the cartilage in compound mutants. As I showed previously, wild-type Meckel's cartilages have a characteristic 'V' shape while loss of *fuzzy* causes a shortening and narrowing of MC. (Fig 4.7 A and B). Fig 4.7 D shows that genetic reduction of *Fgf8* in the Fuzzy mutant rescues the phenotype of MC. The littermate control for this sample is a *Fuzzy* heterozygous embryo, which has no phenotype (Fig 4.7C). Quantification of the length (E), and the distance between bilateral rods of MC (F), reveal that whilst the differences between wildtype and *Fuzzy*$^{-/-}$ embryos are significantly different ($p=0.0027$ and $p=0.0169$ respectively; $n>3$), reduction of *Fgf8* partially restores these parameters (Fig 4.7 E and F). This observation combined with observations from early embryos suggests that abnormal mediolateral patterning, probably as a result of FGF8, influences MC positioning causing premature fusion and subsequent reduced elongation.

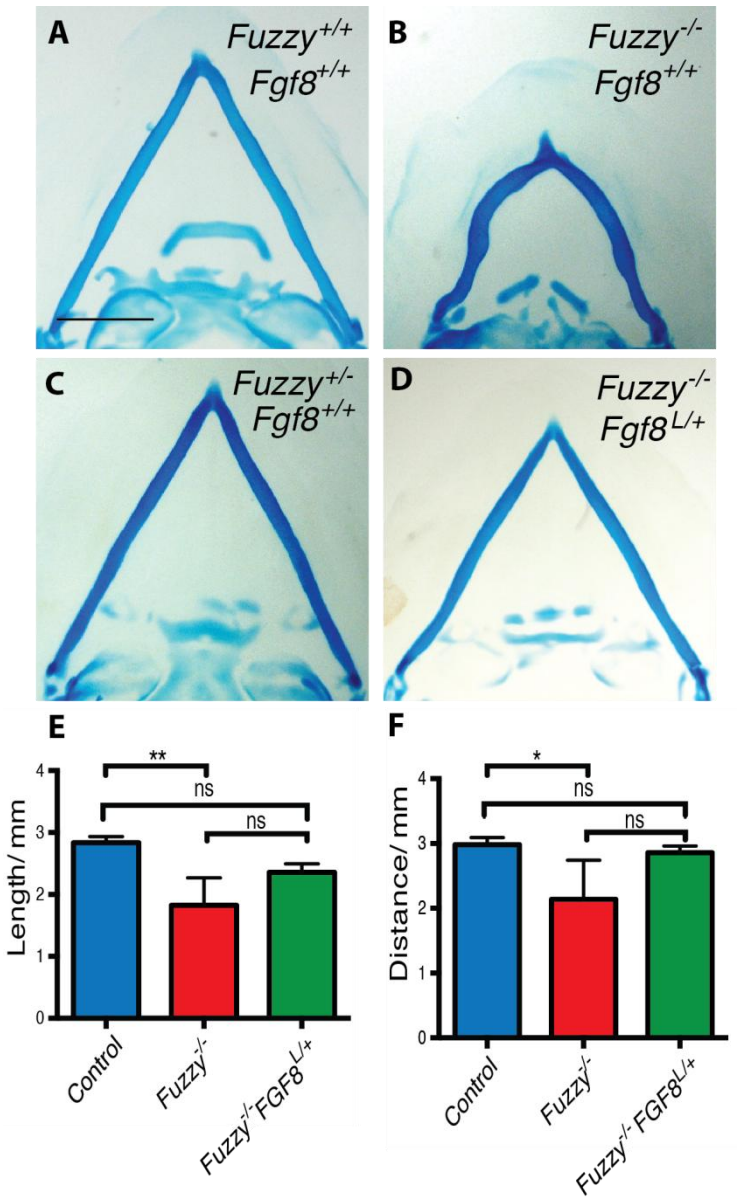

Figure 4.7 Reduction of *Fgf8* rescues the Meckel's cartilage phenotype of *Fuzzy* mutants

(A-D) Ventral views of Alcian blue stained Meckel's cartilage (MC) at e14.5. In control embryos (A), Meckel's cartilage can be seen as 2 bilateral rods, which are fused at the most rostral region. (B) Mutant Meckel's cartilage is noticeably shorter and is narrower between the rods of cartilage. (D) Reduction of *Fgf8* restores the shape of Meckel's cartilage. (C) is a littermate control for (D), revealing that heterozygous loss of both *Fuzzy* and *Fgf8* has no effect of Meckel's cartilage. (E) Quantification of the length of Meckel's cartilage. The length in *Fuzzy* mutants is shorter then control cartilages (p=0.0027; n=3). The length of compound mutant cartilages was not significantly different to control or mutant embryos. (H) Quantification of the width between bilateral rods of Meckel's cartilage. Measurements were taken at the most proximal region. Mutant width is significantly shorter then those of control samples (p=0.0169; n=3). Compound mutants reveal distances that are not significantly different to control samples. Scale bar is 1mm.

4.2.8 Hypertrophic chondrocytes and incisors are not seen in the mandible at e16.5 in *Fuzzy$^{-/-}$ and Fuzzy$^{-/-}$;Fgf8$^{L/+}$* mutants

During embryogenesis, Meckel's cartilage plays an important role in the placement and patterning of the mandibular skeleton. The jaw must continue growing even after Meckel's cartilage fuses at the rostral process. Previous reports suggest that late in gestation enlarged hypertrophic-like chondrocytes can be observed within Meckel's cartilage, which then presages chondrocyte degradation after birth (Bhaskar et al., 1953, Frommer and Margolies, 1971, Harada and Ishizeki, 1998) These cells appear to be induced by the developing incisors (Yang et al., 2012, Sakakura et al., 2005, Sakakura et al., 2007). This change in chondrocyte shape may contribute to further outgrowth of the mandible. In long bones, hypertrophic chondrocytes depend on *Ihh* signaling; Thus, we examined e16.5 mandibles to see if analogous events occur in Meckel's cartilage. As predicted, we noted enlarged chondrocytes in wildtype animals (Fig 4.8 A-A'). These were not found in mutants (Figure 4.8 B-B'), suggesting that lack of hypertrophy could also contribute to the micrognathia seen in the *Fuzzy* mutant.

The onset of chondrocyte hypertrophy s in MC is associated with the onset of incisor development (Yang et al., 2012). Frontal sections of wildtype and mutant mice at e16.5 reveal that the incisors, which can be clearly seen in the wildtype are not present in the mutant (Fig 4.8 C and D). Furthermore hypertrophic-like chondrocytes are clearly visible within Meckel's cartilage, whilst in the mutant only a few cells appear to be slightly enlarged (black arrowhead). Surprisingly, hypertrophic chondrocytes and the incisors are the only mandibular structures that are not rescued in *Fuz$^{-/-}$; Fgf8$^{L/+}$* compound mutants (Fig 4.8 E).

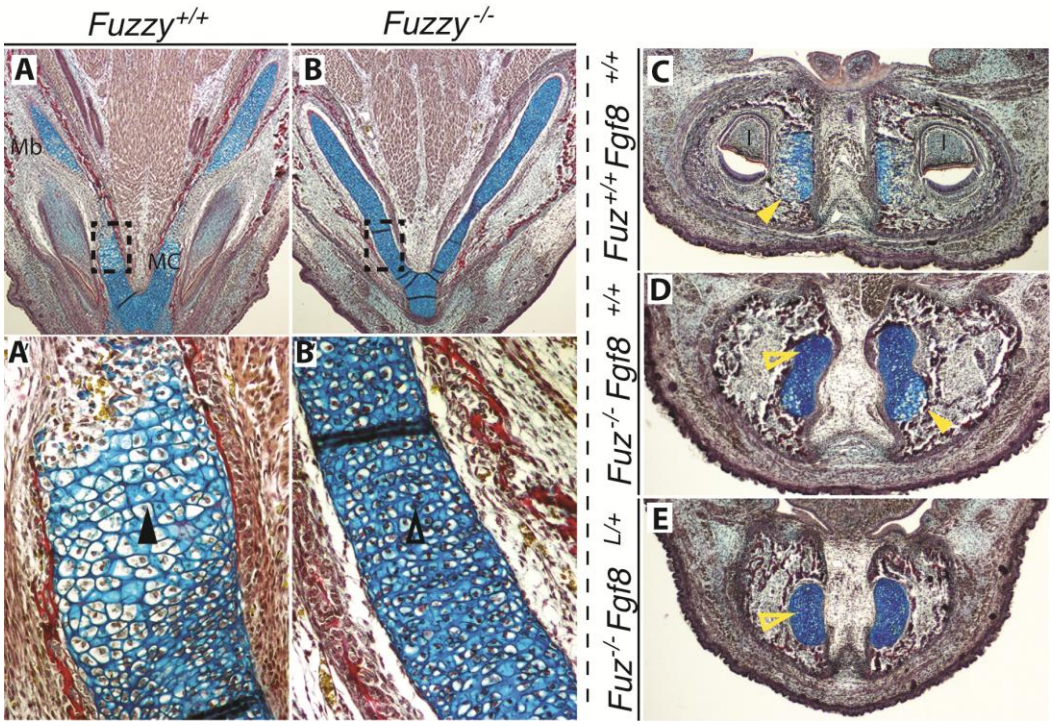

Figure 4.8 *Fuzzy* mutants lack of enlarged hypertrophic-like chondrocytes

(A-B) Trichrome staining of transverse sections of e16.5 embryos. Cartilage is stained in blue; mandibular bone is stained in red. Black boxes represent high magnification in A' and B'.

(A' and B') Higher magnifications of control and mutant Meckel's cartilage. Control sections (A') show enlarged hypertrophic-like chondrocytes (black arrowhead). Mutant sections do not have hypertrophic chondrocytes (open arrowhead).

(C-E) Trichrome staining of frontal sections of e16.5 embryos. Control sections (A) show hypertrophic chondrocytes, which have begun degrading. Two developing incisors (I) can be seen flanking MC. Fuzzy mutant cartilage (D), is mostly in the resting phase (open arrowhead) and has not yet begun to degrade. Discrete regions of MC are just beginning to undergo hypertrophy (black arrowhead). No incisors are present. In compound mutants (E), none of MC is yet undergoing hypertrophy (open arrowhead), and incisors are still not present.

4.2.9 *Ihh* is not expressed in *Fuzzy* mutant MC

I previously showed that in the mutant long bones, a loss of *Ihh* expression causes delayed elongation (Chapter 3). In addition, from e15.5, *Ihh* is expressed in hypertrophic-like chondrocytes in MC (Shimo et al., 2004). Therefore, because I see a loss of chondrocyte hypertrophy in mutant MC, I wanted to determine whether there is a disruption in a similar growth-plate like region in MC. To do this I looked at both *sox9* expression, which is expressed in immature chondrocytes, and *Ihh* expression, which is expressed in mature chondrocytes. In transverse sections of wildtype cartilage at e16.5, H & E staining reveals a region of enlarged hypertrophic–like chondrocytes adjacent to resting chondrocytes (Fig 5.9 A). In the mutant, only resting chondrocytes can be seen (Fig 5.8 B). In the wild-type, *Sox9* appears to be restricted to resting chondrocytes while *Ihh* expression is restricted to hypertrophic chondrocytes (Fig 5.9 C and E). In the mutant, however, *Sox9* is expressed throughout the cartilage and there is a clear absence of Ihh expression (Fig 4.9 D and F). This absence of chondrocyte maturation may be contributing to the micrognathic phenotypes.

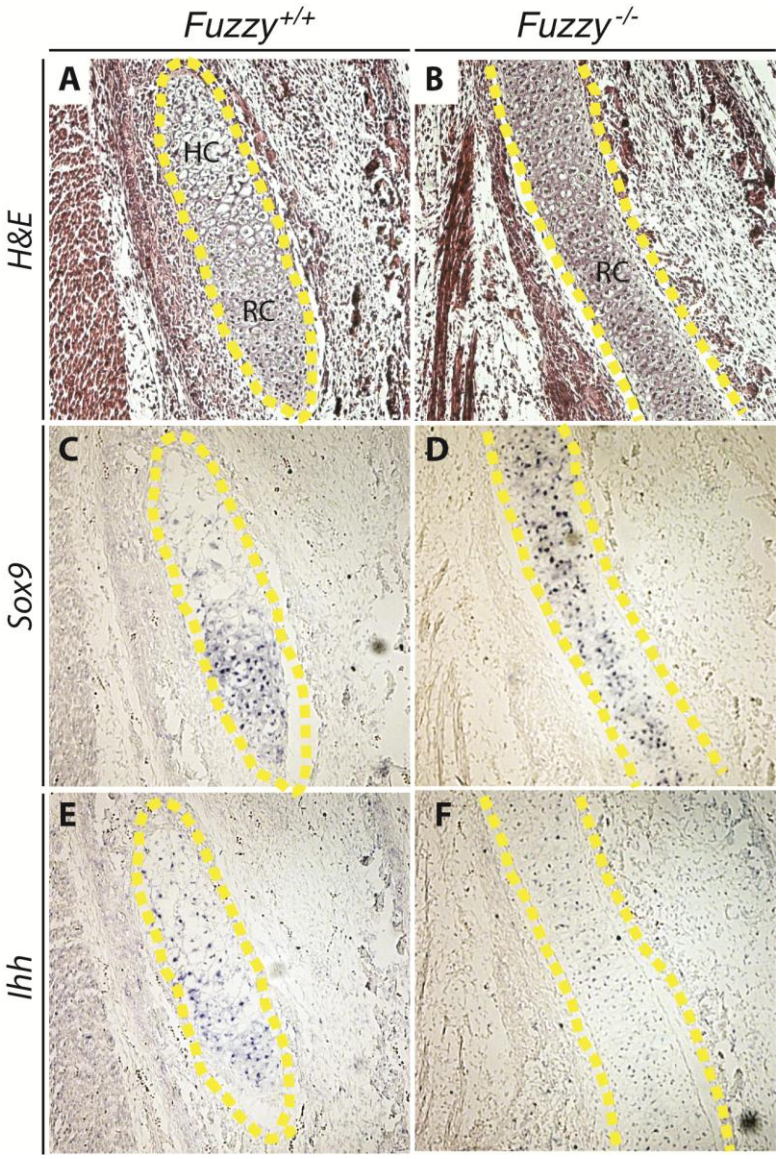

Figure 4.9 Meckel's cartilage of *Fuzzy* mutants does not undergo chondrocyte maturation

(A and B) Transverse views of MC from e16.5 embryos stained with haematoxylin and eosin. MC is outlined in dashed yellow line. (A) In the wild type cartilage chondrocytes within MC can be seen in both resting (RC) and hypertrophic (HC) states. (B) In the *Fuzzy* mutants, chondrocytes have not progressed to hypertrophy and they all appear to be in the resting state.
(C and D) Serial sections of (A and B) showing *Sox9* mRNA expression. In the wildtype (C), *Sox9* is restricted to the resting chondrocytes whilst in the mutant (D), *Sox9* is expressed throughout MC.
(E and F) Serial sections of (A and B) showing *Ihh* mRNA expression. In the wildtype embryos (E), *Ihh* expression is associated with hypertrophic chondrocytes. In *Fuzzy* mutants (F), *Ihh* is not expressed.

4.3 Discussion

Although micrognathia is fairly common, little is known about the etiology of this congenital anomaly. Micrognathia can be associated with ciliopathies; thus, we have turned to a ciliopathic mouse model to further our understanding of this phenotype. In particular, we consider a number of key steps during mandibular outgrowth: initial patterning of the first branchial arch, condensation of the mesenchyme destined to become Meckel's cartilage, fusion of Meckel's cartilage at the rostral process, and finally, hypertrophy of the chondrocytes. Our findings suggest that all of these steps in development can contribute to micrognathia, and that ciliopathic micrognathia may be due in part to aberrant FGF signaling (Summarized in Fig 4.10).

The majority of mesenchyme in the mandibular prominence is populated by cranial neural crest cells, which migrate from the posterior mesencephalon and the rostral hindbrain. As these cells are distributed within BA1, signaling cues, such as FGF, Hh and BMP, act to correctly position of developing facial structures in both the medio-lateral and anterior-posterior axes of the mandibular prominence (Barlow and Francis-West, 1997, Tucker et al., 1999, Ferguson et al., 2000, Abzhanov and Tabin, 2004). In *Fuzzy* mutants, the narrow mandible, combined with enhanced *Fgf8* expression toward the midline, leads to mispositioning of the mesenchymal condensations (Figure 4.2 A and B and Fig 4.10 A and B). Additional changes include increased local cell packing (Fig 4.2 A –C and Fig 4.10 C and D). My data suggests that these two factors combined leads to ectopic *Sox9* expression towards the midline (Fig 4.2 D and E and 4.10 E and F). This is consistent with observations that the *Fuzzy* mutant has increased proliferation and *Sox9* expression in MC at e14.5 (Zhang et al., 2011). As it has been suggested that increased cell density can result from neural crest migration into BA1, we propose that cellular changes in the Fuz mutants are in part due to the altered neural crest migration previously observed in the *Fuz* mutant mice (Smith and Schneider, 1998, Tabler et al., 2013). Interestingly, it was seen in duck and quail that pre-migratory NC cell numbers moving into the mandibular prominence have roles in regulating

mandible length, however on reduction of these cells, post-migratory NC can compensate (Fish et al., 2014). This is in keeping with our suggestion that perturbations occur in several key steps (summarized in Fig 4.10), and not simply one developmental defect that causes the overall micrognathic phenotype.

As the correct positioning of condensations is established, Meckel's cartilage forms bilaterally, elongating and fusing at the rostral process. Using the *Fuzz*y mutant, we can observe the physical consequences of a narrow mandible. In the mutant, the rods of Meckel's cartilage are positioned closer together then in the wildtype. As a result, they meet at the rostral tip at least one day earlier than their littermate controls (Fig 4.3 E-F'; Fig 4.10 E-H). Subsequently, the mutant cartilage fails to elongate appropriately, leading to a shorter, thicker Meckel's cartilage (Fig 5.4D, 5.5D). Frequently, this cartilage is also misshapen and twisted (Fig 5.7B) with two "spikes" emerging from the rostral tip (Fig 5.4F, 5.5F). Thus, it would appear that in the mutant, each cartilage rod continues to grow, but does so while constrained.

Many of the processes which contribute to micrognathia in the *Fuzzy* mutant have been shown to be influenced by FGF signaling. As described in the introduction, FGF signaling, particularly FGF8 have important roles in mandibular arch outgrowth and polarity. In cranial neural crest cells, conditional loss of FGF results in an increase in apoptosis and subsequent loss of BA1 derived skeletal elements (Trumpp et al., 1999). Conversely, FGF signaling from the frontonasal process stimulates neural crest cell proliferation (Szabo-Rogers et al., 2008). Subsequent polarity of the first branchial arch is also FGF8-dependent (Crump et al., 2004, Tucker et al., 1999, Cobourne and Sharpe, 2003).

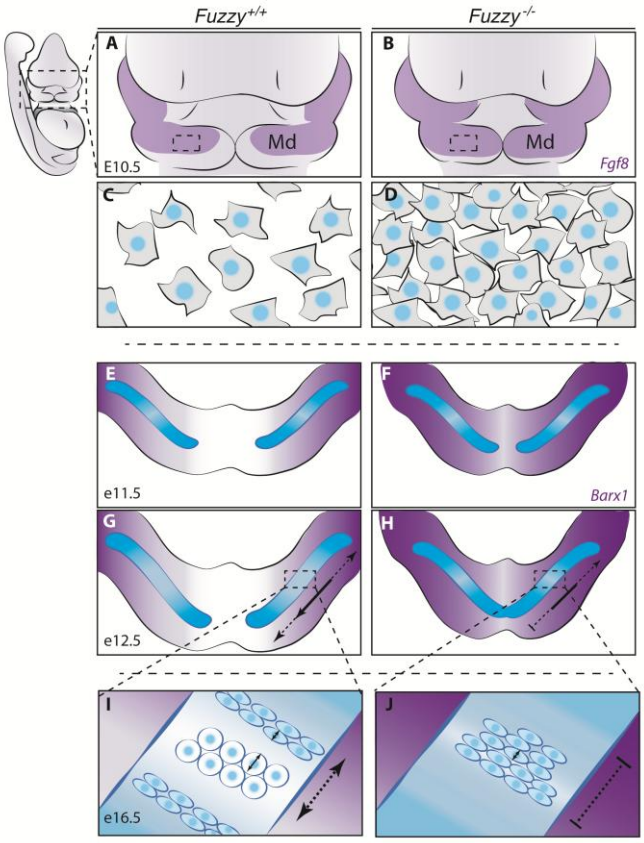

Figure 4.10 Proposed model for ciliopathic micrognathia in *Fuzzy* mutant mice

(A and B) Mandibular process of e10.5 embryos. (A) In normal situations, *Fgf8* expression (schematized in purple) is expressed on either side of the midline. In *Fuzzy* mutants, (B) *Fgf8* expression is expanded medially and the mandibular process is narrower.(C and D) represent cell packing in the mandibular process. (C) In wildtype situations, cells must be appropriately distributed. (D) In the mutant, there is increased cell density.
(E and F) represent the mandibular process at e11.5. (E) In wildtype embryos, bilateral rods of Meckel's cartilage are formed and *Barx1* expression is restricted to lateral regions. (F) In the mutant, the mandibular process is narrower then that of the wildtype and rods of cartilage are formed closer together. In addition, *Barx1* expression is also shifted to more medial regions representing a lateral to medial shift of tissue.
(G and H) show mandibles at e12.5. (G) In wild type embryos, rods of Meckel's cartilage are extended but have not yet fused in the midline. (H) In mutants the mandible is narrower then wild type mandibles and rods of Meckel's cartilage have prematurely fused at the rostral process.
(I and J) depict Meckel's cartilage at e16.5 (I) In wildtype embryos, a region of enlarged hypertrophic like chondrocytes are present and further contribute to mandibular elongation. (J) In mutants, enlarged chondrocytes cannot be seen.

Consistent with the widespread roles of FGF during sequential stages of jaw development, we found that heterozygous loss of *Fgf8* was sufficient to rescue the MC phenotype and restore medio-lateral patterning. Interestingly, *Tbx1* mutants, which have a loss of both *FGF8* and *FGF10*, have mild micrognathia (Jerome and Papaioannou, 2001, Vitelli et al., 2002). It was subsequently shown that these changes are probably as a result of abnormal mesodermal medio-lateral patterning in BA1 at e10.5 (Aggarwal et al., 2010). In contrast to our *Fuzzy* mutant, *FGF8* expression was shifted from medial positions to lateral positions, as were other medial markers (Aggarwal et al., 2010). This is particularly interesting since the *Fuzzy* mutant and *tbx1* mutant have similar mandibular phenotypes which appear to arise from opposing changes in *FGF8* expression (although that of the *Fuzzy* mutant is significantly more severe). Such an observation is hard to explain, especially since no real explanation as to how *Tbx1* loss causes micrognathia has been provided, however this further highlights the importance of proper mediolateral patterning and FGF8 in proper jaw formation. Our observations are backed up by those seen in compound Prx1 and Prx2 mutants in the chick which have a truncated mandible accompanied by lateral-medial shifts of *FGF8*, *Barx1* and other laterally expressed genes such as *Dlx5* (Balic et al., 2009).

It should be noted, however, that in addition to these processes described, additional mechanisms, such as apoptosis, might contribute to micrognathia. Micrognathia seen in conditional *Fgf8* knockouts was suggested to be in the absence of changes in proliferation of apoptosis (Aggarwal et al., 2010). Conversely, micrognathia seen by Balic et al was suggested to be from enhanced apoptosis from e10.5, causing loss of tissue in the medial mandibular prominence (Balic et al., 2009). Apoptosis linked to micrognathia has also been documented on loss of the *Obfc2b* gene, a DNA binding protein important for genomic stability. Loss of this gene is thought to cause micrognathia from increased apoptosis in skeletal tissue at e12.5 (Feldhahn et al., 2012). In support of this, FGF8 has been heavily implicated as a NC survival factor and along these same lines, loss of *Fgf8* was shown to result in a hypoplastic BA1 as a result of increased NC apoptosis (Abu-Issa et

al., 2002, Trumpp et al., 1999). Dose dependent effects of FGF8 may explain these differences in roles of Fgf8 with regards to apoptosis, during NC survival. Apoptotic pathways are activated on both loss of, and increased, *Fgf8* expression (Storm et al., 2003). This reveals the strict requirements and complicated role for FGF8 during early craniofacial development and may explain similarities in the *Fuzzy* mutant phenotype and loss of function *Fgf8* mutants. In support of this, electroporation of *Fgf2* into quail NC, reveals dose dependent responses with high doses inducing chondrogenesis and low doses causing upregulation of chondrogenic markers in the absence of actual differentiation (Petiot et al., 2002). These observations suggest that it would be a good idea to look at markers for apoptosis in the mandible of the Fuzzy mutant to establish whether this contributes the small mandibular prominence of BA1 that we see at e10.5 (Fig 4.1).

Additional signaling pathways may interplay with mechanisms described above. For example, mouse mutants for different *Tgfβ* subtypes have MC malformations. loss of *Tgfβ1*, which is known to be important in cartilage and bone formation, causes abnormal shaping of the rostral process, whilst loss of *TGFβ3* results in a smaller MC, thought to be due to reduced chondrocyte *col2* synthesis. This can be rescued with exogenous *TGFb3* application and is (Chai, 1994). Although it is a tentative link, given the complexity and multiple signaling pathway interactions that occur during mandibular development, convergence of *Fgf8* misregulation on other signaling interactions cannot be ruled out.

Once Meckel's cartilage has assumed it's characteristic inverted 'V' shape, it continues to elongate, suggesting additional mechanisms drive growth after rostral process fusion. In endochondral bone growth, chondrocyte enlargement drives further elongation. Shimo and colleagues have observed similar hypertrophic cells in Meckel's cartilage, but their function has been unclear (Shimo et al., 2004). These hypertrophic cells are associated with the onset of incisor development (Yang et al., 2012); indeed, *Fuz* mutants lack incisors and the accompanying hypertrophic chondrocytes (Figure 4.8 D)(Tabler et al., 2013, Zhang et al., 2011).

It is worth noting that the hypertrophic chondrocytes in Meckel's cartilage were not rescued in the compound mutants (Fig 6). The reasons for this are unclear. Whilst some groups have stated that the incisors are responsible for initiating chondrocyte maturation and subsequent degradation within Meckel's cartilage, others have stated that processes driving typical endochondral ossification, such as Ihh, PTHrP and colX expression are important (Shimo et al., 2004, Yang et al., 2012, Yamazaki et al., 1997). Since we see a loss of *Ihh* expression in developing mutant MC, (Fig 4.9 F) coupled with a lack of incisors (Fig 4.8 D), it is possible that a combination of the two is responsible for loss of chondrocyte maturation. I would postulate that the loss of Ihh expression is probably due to defective Gli3 processing which inhibits chondrocyte maturation, as described in the limbs (chapter 3); and subsequent to this, the lack of incisor development inhibits the degradation of these cartilages. This is supported by observations that reduction of FGF8 in the *Fuzzy* mutant does not rescue loss of hypertrophy in the developing long bones (Chapter 3, Fig 3.6) and developing incisors stimulate osteoclast differentiation (Wise et al., 2000, Kitahara et al., 2002). However, since mechanisms of chondrocyte maturation may be different between MC and endochondral elements, further work must be done to verify whether loss of MC hypertrophy is as a result of loss of incisors, or via the Ihh-PThRP feedback loop, or via both. It would be interesting to study this further by observing MC maturation in animal models lacking incisors but which have properly functioning cilia. Interestingly, Gli3 mutant mice also lack incisors (Mo et al., 1997). It is therefore possible that in our mutant, defective Gli3 processing could be driving both the lack of incisors and chondrocyte hypertrophy. Furthermore, the fact that Gli2 mutants have a more severe mandibular truncation then Gli3 mutants suggests that Gli2 processing may also be defective in the *Fuzzy* mutant (Mo et al., 1997). Further work examining relative levels of Gli proteins and activator:repressor ratios within the mandible will help to establish if this is the case. Another interesting way to determine this would be comparative analysis of *Fuzzy;Gli2 and Fuzzy;Gli3* compound mutants.

It is clear that growth of the mandible is complex, multistep process. Our analysis suggests that ciliopathic micrognathia arises in large part from aberrant FGF8 signaling during patterning of the first branchial arch. Furthermore, FGF signaling likely plays several additional roles in mandibular development, during the initiation and shaping of the chondrogenic condensations. Subsequently, several stages of mandibular development can go wrong resulting in micrognathia (summarized in fig 4.10).

As one final consideration, it was also mentioned that loss of *Fuzzy* was reported to cause increased canonical Wnt signaling and an increase in *Sox9* expression in the *Fuzzy* mutant (Zhang et al., 2011). The authors also suggested that these signaling changes cause the micrognathic phenotype. However, current consensus in the field is that low Wnt signaling is required to maintain *Sox9* expression so the observations made appear counter intuitive. In order to address this, more analysis into Wnt signaling in the mutant should be carried out. For example, it would be important to establish specifically when we see an increase in signaling. One possibility could be that increased in canonical Wnt activity seen at e14.5 could correspond to enhanced bone formation in the mandible (discussed further in chapter 6), since it is thought that Wnt signaling is a switch between cartilage and bone formation (Day et al., 2005). Thus, to further explore if Wnt signaling contributes to the micrognathic phenotype, further quantification of Wnt responsive markers, as well as regions of expression should be carried out at earlier and later time points. This is especially important since e14.5 is quite a dynamic time for MC development in terms of ossification, which is just starting is some regions. Furthermore, at e14.5 MC should already have formed its characteristic shape. I would suggest that analysis at earlier time points, such as that carried out in this chapter. Therefore, I would suggest that analysis carried out in this chapter is more definitive then that carried out by Zhang et al., and is more beneficial for establishing mechanisms driving the phenotype since it enables us to visualize what is happening during elongation as opposed to once it is already defective.

Our studies allow us to distinguish between the FGF dependent aspects of micrognathia (early patterning) versus FGF-independent events (chondrocyte maturation); and characterise key steps for proper mandible development that have not been described previously. Interesting further work would be to assess whether FGFs or Glis are integrating with other signaling pathways, such as TGFβ, in the etiology of micrognathia. Deciphering these interactions will be necessary for a full understanding of this pathological condition.

Chapter 5 Hyperossification of the mandible

5.1 Introduction

The skeletal element of the lower jaw is the mandibular bone. Functionally, it provides housing for the developing teeth and forms the temporomandibular joint, which is the articulation between the lower jaw and the cranium. In this way, abnormal ossification of the lower jaw could have serious consequences by affecting basic functions such as mastication and speech.

In humans, disorders in mandibular bone development are rare, with the majority causing cysts within the jaw or discontinuation of the bone. For example, haplo-insufficiency of *patched* causes odontogenic cysts on the mandible; whilst patients with magnesium deficiency are reported with increased levels of jaw osteoclastogenesis (Unden et al., 1996, Belluci et al., 2013). Although clinically hyperossification of the lower jaw is rarely described, syngnathia, which is fusion of the upper and lower jaw with unknown causes, is a rare anomaly that can occur as part of maxillofacial syndromes or on its own (Inman et al., 2013, Turksen et al., 2012).

Developmentally, mandibular skeletogenesis is a unique process which has aspects of both intramembranous and endochondral ossification. Development begins from NC derived mesenchyme, first seen at approximately e13.5, located laterally to the developing Meckel's cartilage (Ramaesh and Bard, 2003). It is generally thought that during normal bone formation, high Wnt signaling is required to switch between chondrogenic and osteogenic differentiation (Day et al., 2005). Consistent with this Wnt signaling has been shown to stimulate mandibular ossification (Leucht et al., 2008). During ossification, the proximal and distal bone fronts elongate and at the same time, the superior and inferior edges grow towards the midline to form an osseous membrane, which encapsulates Meckel's cartilage (Ramaesh and Bard, 2003). In a typical intramembranous manner, the cells at the periphery of the membrane proliferate much more then those in the mesenchyme causing bone formation to occur within the membranous

sheath (Tomo et al., 1997, Ramaesh and Bard, 2003). It has been suggested that MC plays a role in mandibular ossification but that role remains elusive. It was shown that the endothilin-converting-enzyme-1 knockout mouse lacks MC and the mandibular bone, whilst conditional *Sox9* mutants have complete absence of MC but a relatively normal mandibular bone, albeit severely micrognathic (Yanagisawa et al., 1998, Mori-Akiyama et al., 2003). This not only suggests that Meckel's cartilage has roles in elongating the jaw and creating space in which ossification can occur, but also implies that the mandibular bone formation is not entirely dependent on Meckel's cartilage formation.

To date, several differences between endochondral ossification and ossification of Meckel's cartilage have been documented. From around e15.5, chondrocytes of Meckel's cartilage undergo hypertrophic maturation, followed by autophagy, similar to that seen during endochondral ossification (Yang et al., 2012, Shimo et al., 2004, Roach et al., 2004). Similarly, hypertrophic cells of MC are shown to express the same successive markers of chondrocyte maturation seen in endochondral ossification, including *Col2* in resting chondrocytes and *Ihh* and *ColX* in hypertrophic chondrocytes (Shimo et al., 2004). Unlike in endochondral ossification, however, hypertrophic chondrocytes of Meckel's cartilage are not vascularized and infiltrated with osteocytes; it is simply degraded by early post-natal stages (Bhaskar et al., 1953). In mature chondrocytes of mouse MC, high levels of Rank-Ligand (RANKL) and osteoprotogenin (OPG) immunoreactivity is detected in MC. These proteins are not detected during these developmental stages in the hind limbs (Sakakura et al., 2005). Typically during bone development, RANKL will bind to the RANK receptor to stimulate osteoclastogenesis; to limit this process the 'decoy' receptor, OPG is synthesized, reducing osteoclastogenesis (Baud'huin et al., 2007). OPG secretion could therefore be a possible mechanism by which degradation of MC is limited to post-bone formation.

One other interesting aspect of mandibular ossification is the presence of a secondary cartilage called the mandibular symphisis. Secondary cartilages

are fibro-cartilaginous joints, which can undergo endochondral ossification and are typically associated with membranous bones (Trevisan and Scapino, 1976, Kjaer, 1975). In the mandible, the symphysis at the most distal region of the jaw exists between the two mandibular bones; in this way, there is a lack of ossification surrounding the rostral process (Trevisan and Scapino, 1976). In mice, it has been shown in compound *Ihh* and *Gli3* mutants, that formation of the symphisis is dependent on Ihh-Gli3 signaling, as occurs in the long bone growth plate. Specifically the Gli3 repressor was shown to inhibit chondrocyte maturation and proliferation at the distal tip (Sugito et al., 2011).

This chapter aims to characterise hyperossification observed in the mandible of the *Fuzzy* mutant. This phenotype of the lower jaw is rarely reported in humans.

5.2 Results

5.2.1 The mandibular bone is hyperossified and intertwined with Meckel's cartilage

Loss of *Fuzzy* has already been shown to cause a shortening of endochondral derived skeletal elements (See chapter 3). In Fig 5.1 A and B (Chapter 5), as well as the mandible of the *Fuzzy* mutant being shorter then the control, the bone of the mandible also appears to be thicker. Therefore, in order to characterise this malformation, I carried out trichrome staining on transverse and frontal sections of wildtype and mutant heads at e18.5. In transverse sections of wild-type animals, the mandibular bone (MB) is formed and ossification is taking place within a sheath of ossified tissue (Fig 5.1 A). The rostral process is the only region of Meckel's cartilage to not have bone formation around it. Conversely, in the *Fuzzy*_mutant, the mandibular bone appears to be much thicker with a loss of organization between the mandibular bone and Meckel's cartilage (Fig 5.1 B, yellow arrowhead). In addition there is clear ossification covering the rostral process. Frontal views of the wildtype reveal that Meckel's cartilage can be seen as a discreet rod running through the inside of the mandibular bone (Fig 5.1 C, black arrowhead), whilst in the mutant, MC can again be seen tangled with the bone (Fig 5.1 D, yellow arrowheads). In addition, the mandibular bone in the mutant appears to be larger in the rostrocaudal axis (Fig 5.1 D, black arrow).

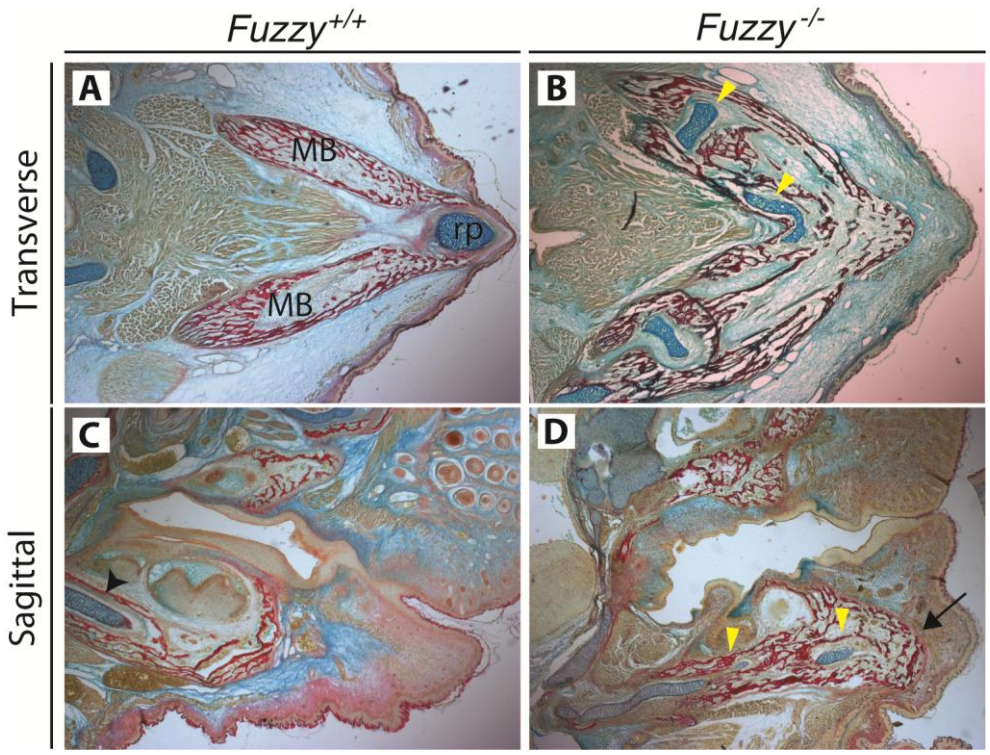

Figure 5.1 The mandible of the *Fuzzy* mutant is hyperossified and organization of Meckel's cartilage and the mandible bone is disrupted.

Trichrome stained sections of wildtype and mutant mandibles at e18.5. Cartilage is stained in blue and bone is stained in red. In the wildtype section (A and B) Transverse sections. (A) The two tubes of mandibular bone can be clearly seen independent of Meckel's cartilage. The rostral process (rp) can be seen at the most anterior tip. (B) In the mutant mandible bone is thicker and Meckel's cartilage can be seen encroaching into the bone (yellow arrowheads)

(C and D) Sagittal sections. (C) In the wildtype embryo, there is a clearly defined boundary between Meckel's cartilage and the surrounding mandibular bone (black arrowhead). (D) In the mutant, the boundary between cartilage and bone is less well defined (yellow arrowheads) and the bone appears to be thicker at the most distal point (black arrow).

5.2.2 *Runx2* expression is expanded in the *Fuzzy* mutant at e12.5 and e14.5

Runx2 is one of the key transcription factors that regulates bone formation by committing precursor cells to osteogenic differentiation. In normal situations, *Runx2* is expressed in pre-cartilaginous mesenchymal condensations of the mandible from as early as e10.5. By e12.5, this expression is suggested to be regulating osteoblast differentiation markers such as osterix (Shibata et al., 2004, Stricker et al., 2002). At e13.5, bone formation of the mandible has just started to commence (Ramaesh and Bard, 2003). For these reasons I decided to compare *Runx2* expression at e12.5 and e14.5. In frontal sections of wild-type embryos at e12.5, *Runx2* expression can be seen faintly in the mandibular mesenchyme (Fig 5.2 A). In the *Fuzzy* mutant, *Runx2* expression appears to be expanded in the rostrocaudal axis with ectopic expression in the tongue (Fig 5.2 B, green arrowhead). Two days later, at e14.5, in wildtype transverse sections, *runx2* is expressed around Meckel's cartilage and the incisors (Fig 5.2 C). Conversely, in the mutant, incisors are absent and *Runx2* is expressed throughout the mesenchyme (Fig 5.2 D). This data suggests that the *Fuzzy* mutant has more widespread *Runx2* expression then wildtype embryos.

5.2.3 Calcium deposition in the mandible appears closer to the midline in mutants

In order to visualize new bone formation in the mandible, calcein labeling was carried out. Calcein chemically binds to calcified tissue and can be visualized under green fluorescence. Pregnant females were injected twice, at e14.5 and e16.5, and sacrificed at e17.5. Calcium accumulation was assessed with fluorescent microscopy. Fig 5.3 A and B show ventral views of wild type and mutant heads. Fig 5.3 shows a fluorescent image of a wild-type sample in which calcium accumulation surrounds the two branches mandibular bone (yellow arrowheads). In the *Fuzzy* mutant, calcium accumulation is not restricted to each mandibular bone and appears to be more spread towards the midline, implying a shift in bone position (Fig 5.3 D, red arrowhead).

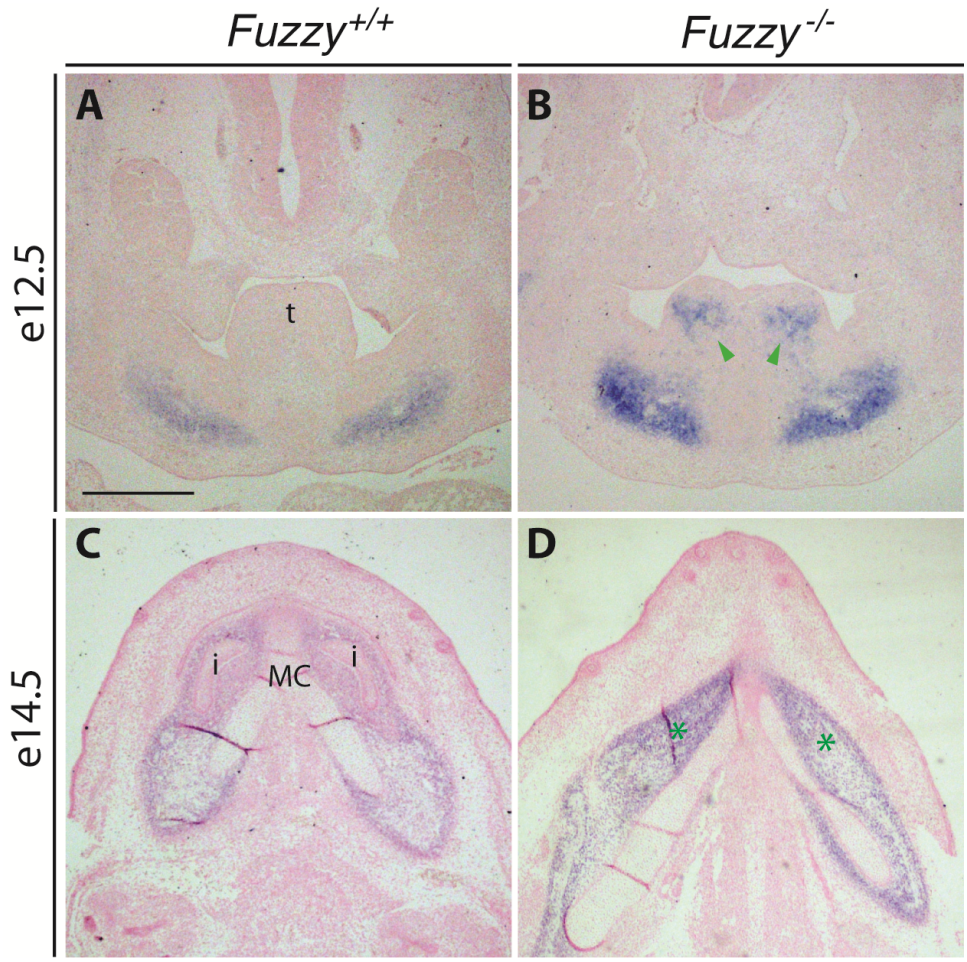

Figure 5.2 *Fuzzy* mutants have larger domains of *Runx2* expression

(A and B) Frontal sections of *Fuzzy* mutant and wildtype control embryos at e12.5 showing mRNA *in situ* hybridisation for *Runx2* expression. (A) In the control, *Runx2* is expressed in distinct domains in the developing mandible and is absent from the tongue (t). (B) *Runx2* appears to be more abundantly expressed in the mutant mandible. Ectopic expression can also be seen in the mutant tongue (green arrowheads).

(C and D) Transverse sections of Fuzzy mutants and littermate controls at e14.5. (C) In the control embryo, *Runx2* expression can be seen surrounding Meckel's cartilage (MC) and is absent in the incisors (i). In the mutant, *Runx2* appears to be more abundantly expressed, especially in the region of absent incisors (green asterisks). Scale bar is 0.5mm.

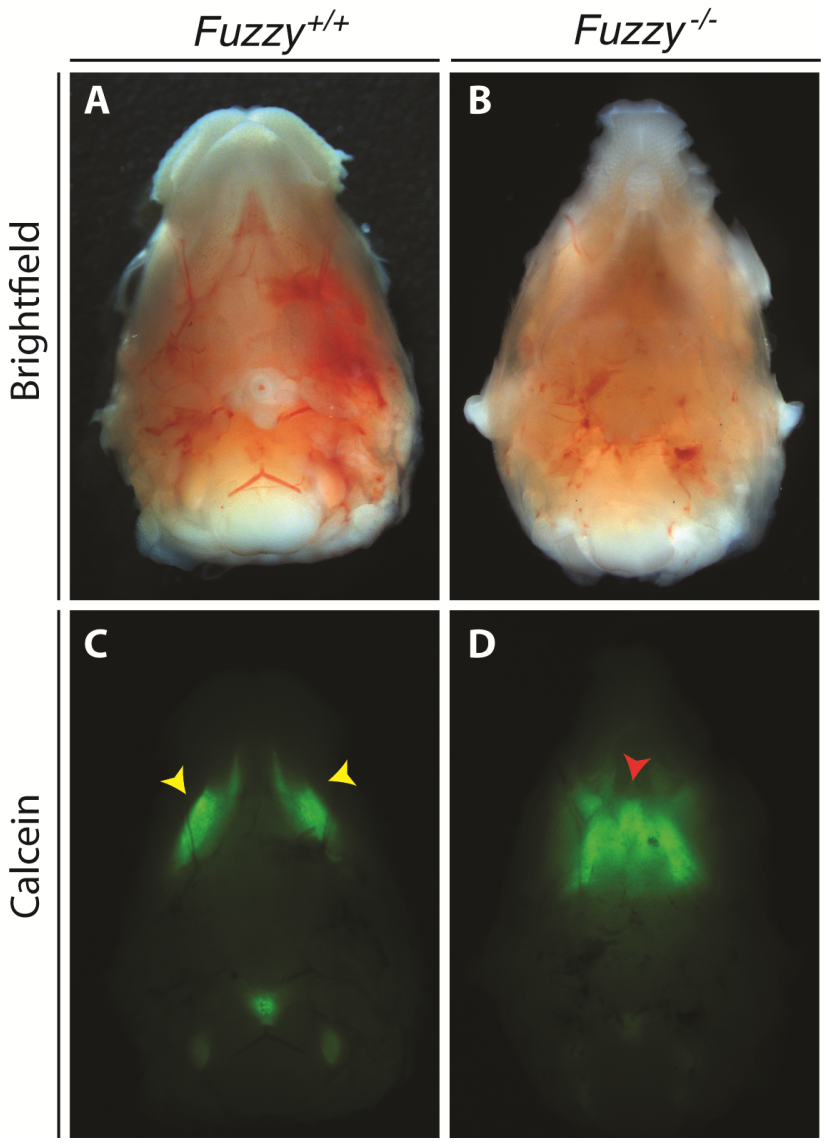

Figure 5.3 Calcein accumulation across the midline of *Fuzzy* mutants at e17.5

(A and B) Brightfield images of ventral views of wildtype and mutant heads. (C and D) Green fluorescence shows positive calcein labeling reflecting calcium deposition. (C) In the wildtype, calcein deposition occurs bilaterally in the mandibular bone (yellow arrowheads). (D) In mutants, calcein accumulation is more widespread and extends across the midline (red arrowhead).

5.2.4 Bone mineralization is seen in a larger region and is spread across the midline in the mutant mandible

In order to better visualize deposition in the mutant, calcein labeled embryos were sectioned. Dapi counterstained frontal sections of wildtype and mutant heads taken at the level of the molar tooth bud at e17.5 (Fig 5.4 A and B). Visualization of green fluorescence and hence calcium accumulation in these same sections are shown in Fig 6.4 C and D. GFP and Dapi merged images are shown in Fig 5.4 E and F. In the wildtype, Calceine accumulation is clearly seen on the lateral flanks of Meckel's cartilage (Fig 5.4 E). In the mutant however, the region of calcium accumulation surrounding Meckel's cartilage is noticeably larger (red asterisk) and there is ectopic ossification towards the midline (Fig 5.4 F; red arrowhead). Note that in this mutant sample, bilateral rods of Meckel's cartilage have clearly prematurely fused (Fig 5.4 F; yellow arrowhead; also note, premature MC fusion is discussed in chapter 4).

In order to further characterise the hyperossification of the mandible, we also carried out von Kossa staining for bone mineralization at e16.5. Transverse sections were taken at the level of the molar tooth bud. Fig 5.5 A and B show whole heads of wildtype and mutant embryos whilst A' and B' show magnified images of the mandibles. In the wildtype, positive Von Kossa staining (seen in black) surrounds Meckel's cartilage within a sheath but mineralization within this region is not complete (Fig 5.5 A and A'). Conversely, in the *Fuzzy* mutant, there is a lot more mineralization throughout the mandible and there is hyperossification across the midline (Fig 5.5 B and B', green arrowheads).

Taken together, calcein labeling and von Kossa staining reveals hyperossification of the mandible surrounding MC as well as a spread of ossified tissue towards the midline.

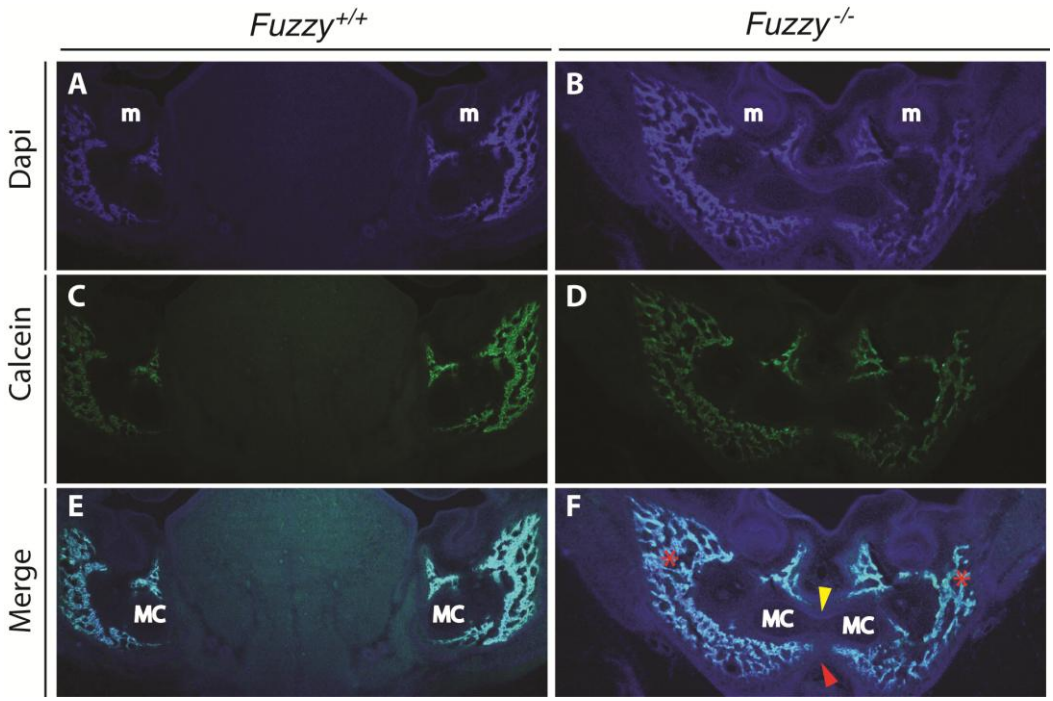

Figure 5.4 Excess calcium deposition in *Fuzzy* mutants at e17.5.

Calcein labelling shows calcium accumulation.

(A and B) Dapi stained frontal sections through the mandible of e17.5 mutant and littermate controls. Molar tooth buds are marked by 'm'.

(C and D) Calcein visualization in green channel shows hyperossification across the midline of Fuzzy mutants (D) compared to two discreet regions of mandibular ossification in the wildtype (C).

(E and F) Merged Dapi and GFP channels. In the wildtype (E), calcein accumulated in discreet regions surrounding Meckel's cartilage (MC). In the mutant (F), enlarged regions of calcein accumulation (red asterisks) are seen around each bar of Meckel's cartilage and towards the midline (red arrowhead). Fusion of Meckel's cartilage is also observed (yellow arrowhead).

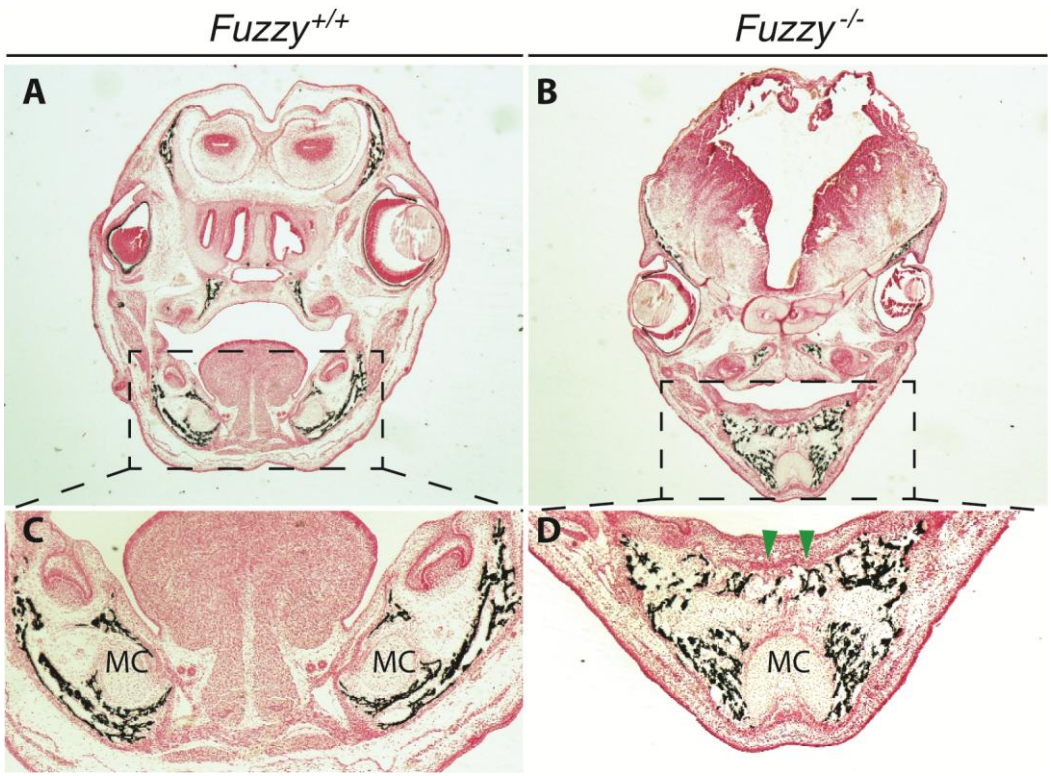

Figure 5.5 The *Fuzzy* mutant has increased mineralization across the midline of the mandible

Von Kossa staining marks bone in black. Eosin counterstain.

(A and B) Wild type and mutant littermates at e17.5.

(C and D) Enlarged images of regions highlighted in (A) and (B). (C) In the control embryo, mineralization is seen surrounding the two rods of Meckel's cartilage (MC). (D) In the mutant, mineralization is seen extending all the way across the midline of the mandible (green arrowheads, above MC).

5.2.6 Reduction of *Fgf8* in the *Fuzzy* mutant rescues mandibular hyperossification

Since Fgf8 has been shown to have roles in the regulation of *Runx2*, and reduction of *Fgf8* in the *Fuzzy* mutant rescues the phenotype of Meckel's cartilage, I wanted to see how reducing the levels of *Fgf8* affected the ossification phenotype in the mandible. As expected, in the wildtype, the Alizarin red stained mandible bone can be seen as two bilateral rods that are separated at the rostral process (Fig 5.6 A). In the *Fuzzy* mutant, as well as being shorter, the mandible appears thicker in the medio-lateral axis and is clearly ossified at the rostral process (Fig 5.6 b). In *Fuzzy*$^{-/-}$;*FGF8*$^{L/+}$ embryos, the length of the mandible is mostly restored (explained in chapter 5) and the medio-lateral width of each mandibular ossification does not appear to be as thick. In addition, ectopic ossification around the rostral process appears to be rescued (Fig 5.6 C). Compound mutants were also sectioned frontally at e16.5 and underwent tri-chrome staining. In the wildtype samples, as described previously, Alizarin red staining for mature bone can be seen in a sheath surrounding Meckel's cartilage with bone formation not fully occupying this region (Fig 5.6 D). In the *Fuzzy* mutant, the regions of alizarin red staining is much larger and there is more positive staining within the osseous sheath. Note fusion of bilateral rods of Meckel's cartilage as described in chapter 5. As predicted, reducing *Fgf8* gene expression in the mutant appears to rescue the hyperossification of the mandible. *Fuzzy* Compound mutant mandibles appear to be more similar to wildtype embryos with positive staining seen in a well defined sheath surrounding Meckel's cartilage, when compared to *Fuzzy* mutants, which have thicker mandibular bones and inappropriate ossification of the rostral process.

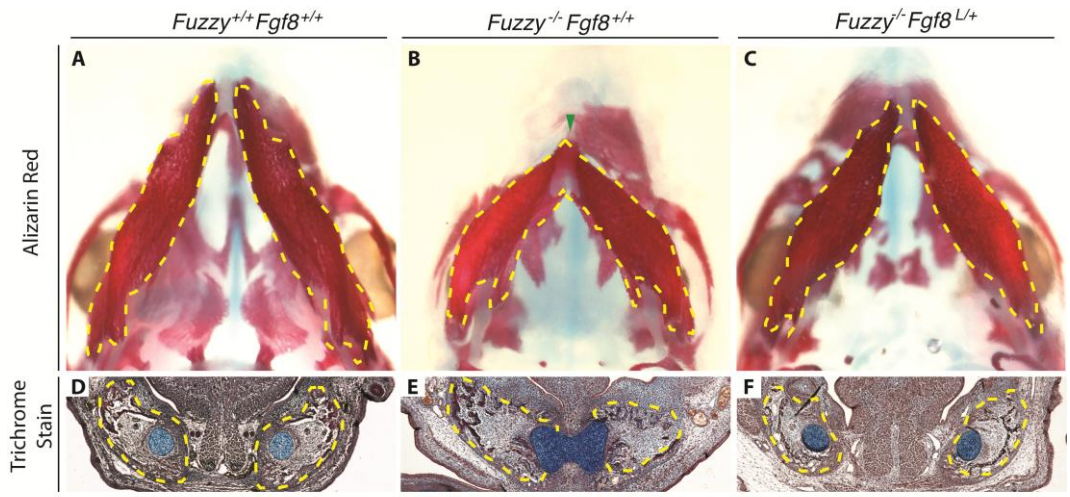

Figure 5.6 Mandibular hyperossification is rescued on reduction of *Fgf8* gene expression in the *Fuzzy* mutant

(A-C) Alizarin red staining marks bone in red. Ventral views mandibles at e16.5. One half of each mandible is outlined in a yellow dashed line. (A) In the control sample (A), the mandible can be seen as two bilateral rods of bone. (B) In the *Fuzzy* mutant, as previously described, the mandible is shorter. The bone is be thicker medio-laterally and the distal tips of each mandible bone are fused at the rostral process (green arrowhead). (C) In compound mutants, the ossification appears to be similar to the wild type. Although the bone is not as regularly shaped as in the wild type, the extent of mandibular thickening is mild.
(D-F) Trichrome stained sections show cartilages in blue and bone in red. Bone is outlined with yellow dotted lines. Frontal sections of E16.5 mouse mandibles, are taken at the level of the molars. The region of mandibular bone formation is outlined with a dashed yellow line. (D) In the control sample, the mandibular bone surroundS Meckel's cartilage. (E) In the *Fuzzy* mutant sample, the bone appears to be larger in the medio-lateral axis and does not encase Meckel's cartilage, which has prematurely fused. (F) Reduction of *Fgf8* gene expression in the mutant restores the appearance of the mandibular bone and distance between rods of MC.

5.3 Discussion

Results in this chapter reveal that the *Fuzzy* mutant has hyperossification of the mandible, which is spread towards the midline. This is an interesting phenotype since it is rarely described clinically. Our data indicates that prior to initiation of mandibular ossification at early developmental stages, there is an increased region of *Runx2* expression in mutants (Fig 6.2). Since *Runx2* is one of the key transcription factors committing mesenchymal stem cells to the osteoblast lineage, it is not surprising that this would lead to enhanced bone formation (Komori and Kishimoto, 1998, Komori, 2002). The outstanding question is how this upregulation of *Runx2* occurs.

The regulation of *Runx2* is complex and occurs on many levels. Transcriptional control is under the regulation of a variety of signaling molecules ranging from FGFs, specifically FGF2, to Retinoic acid and TGF-β signaling (Komori, 2005, Niger et al., 2013, Park et al., 2010). Adding complication to the issue of *Runx2* regulation, it has been shown to both positively and negatively regulate its own promoter (Drissi et al., 2000, Ducy et al., 1997); subsequently, post translational modifications, such as phosphorylation, further regulate activity (Selvamurugan et al., 2000).

Since in *Fuzzy* mutant, we see changes in *Runx2* expression from as early as e12.5, it is reasonable to postulate that early signaling changes are responsible. *Hand2*, typically associated with regulation of mandibular homeotic identity, is expressed in the medial epithelium of the developing mandible from as early as e10.5 and is shown to be important for craniofacial development, including the developing mandible and palate (Yanagisawa et al., 2003, Balic et al., 2009, Funato et al., 2009). From e13.5, *Hand2* and *Runx2* have been shown to co-localize and *Hand2* can inhibit *Runx2* binding to DNA, and hence regulate its activity (Funato et al., 2009). In chapter 4, I showed that *Fuzzy* mutants have a lateral to medial shift of *Barx1* expression implying either a loss of midline or change in tissue identity within the presumptive mandible. Along these lines, it can be proposed that early on we have a smaller domain of medial tissue, in which *Hand2* is normally expressed. It is therefore possible that loss of medial

tissue between e10.5 and e12.5 (since this is when we first see defects in the 1st branchial arch and changes in medio-lateral tissue markers, see chapter 5) can result in loss of *Runx2* regulation by *Hand2* and more osteoblastic commitment in the mandible. Giving weight to this hypothesis is the fact that loss of *Hand2* also results in cleft palate, micrognathia, and alobar tongue (which is something also observed in the *Fuzzy* mutant, data not shown). *Hand2* mutants also show mandibular hyperossification across the midline associated with increased regions of *Runx2* expression (Barron et al., 2011, Xiong et al., 2009, Funato et al., 2009, Liu et al., 2009). If this is the case, then, similar to micrognathia described, hyperossification of the mandible is as a result of early changes in *Fgf8* gene expression. In keeping with this, reduction of *Fgf8* in the *fuzzy* mutant appears to rescue most of the mandibular ossification phenotype. In order to determine if this is true it would be very interesting to look further at expression of medial and laterally expressed genes, including *Hand2*, in the mandible throughout development of the *Fuzzy* mutant.

While *Runx2* expression may be indirectly affected by mediolateral patterning changes in the *Fuzzy* mutant, is it also possible that FGF8 plays a more direct role in controlling *Runx2* expression. FGF8 has been shown to induce mouse myoblast cells to differentiate into osteoblasts and RUNX2 is known to be needed for intramembranous ossification (Omoteyama and Takagi, 2009, Komori et al., 1997, Lee et al., 1997, Mundlos et al., 1997). Furthermore, in tissue culture FGF8 has the ability to bind to all the FGFRs with highest affinity to *FGFR3* (Zhang et al., 2006). Although there are no published reports of FGFR3 signaling affecting the mandibular bone, FGFR3 hyperactivation has been associated with synostosis (Singh et al., 2014, Georgoulis et al., 2011). In addition, signaling through FGFR1 and -2 are known to be needed to promote osteoblast differentiation and maturation during craniosynostosis (Muenke and Schell, 1995, Park et al., 1995). It should therefore be considered that abarrent FGF signaling may directly causes upregulation of *Runx2* expression in the mutant mandible.

The lack of incisors in the *Fuzzy* mutant could also be a contributing factor to mandibular hyperossification. Fig 5.2 D shows *Runx2* expression in the

region where the incisors would normally be present. One possibility is that the tooth provides an inhibitory signal, and in its absence *Runx2* expression can expand. That said, rat mutants that lack incisors do not have mandibular hyperossification (Bhaskar et al., 1953).

Alternatively, Wnt signaling may play a role. It has been shown that application of Wnt10b, which activates canonical Wnt signaling, enhances osteoblast differentiation and leads to more mandibular bone at the expense of the incisors (Bennett et al., 2007). Since some reports state that canonical wnt signaling is enhanced in the *Fuzzy* mutant mandible at e14.5, it is possible that this contributes to the excessive ossification and loss of incisor we observe in the mutant (Zhang et al., 2011). Consistent with a possible role for Wnt driving this phenotype, a high bone density associated with an abnormally wide and deep mandible was observed in two related human patients, and attributed to gain of function mutations in LRP5, which is generally thought to induce wnt signaling (Boyden et al., 2002). Contribution of aberrant Wnt signaling can be tested in two ways. First, we could assess relative expression levels of Wnt target genes such as *Lef1* and *TCF*, by qPCR. Second, reducing the levels of Wnt signaling using a conditional deletion of *β-catenin* in NC cells (Wnt1::cre; β-catenin$^{fl/+}$; *Fuz*$^{-/-}$), may restore normal mandibular development. Subsequent phenotypic analysis would determine which aspects of mandibular hyperossification, if any, are influenced by aberrant Wnt signaling.

Another consideration for our phenotype is that enhanced bone formation towards the midline may be secondary to the smaller and narrower MC. This possibility is particularly interesting when one considers that the MC phenotype is rescued in compound mutants and the ossification phenotype is for the most part rescued. This is possible, however no reports have shown that MC is needed to regulate levels of mandibular ossification. In fact, in *Sox9* mouse mutants, which do not develop MC, the jaw is hypoplastic however ossification of the jaw is not spread towards the midline (Mori-Akiyama et al., 2003).

Thus far our mouse model has phenocopied many defects that are observed in mouse models and human patients of ciliopathies (described in chapters 3-5). It is therefore quite surprising that mandibular hyperossification of this nature has so rarely been described. Our data reveals that this ossification defect may be as a result of changes in early gene expression, which manifest in both the Meckel's cartilage phenotype described in chapter 5 and subsequent hyperossification. With this in mind, it is possible that the reason this phenotype has not been previously described is for two reasons. Firstly, the extent of hyperossification in the Fuzzy mutant is variable, so it is possible that in humans, those with more severe ciliopathies do not survive birth in which case mandibular hyperossification may not be assessed or may not even be developmentally complete depending on the stage at which the embryo dies. A good example of this is Meckel-Gruber syndrome, which has a 100% mortality rate (Alexiev et al., 2006). Secondly, many human patients of ciliopathies may not have been assessed for mandibular hyperossification. Therefore, this could provide new diagnostic criteria for assessment of ciliopathies.

Chapter 6 Additional skeletal phenotypes in the *Fuzzy* mutant

6.1 Introduction

6.1.1 Skeletal defects in ciliopathies

Ciliopathies are a broad class of disorders, which result from defects in proper cilia formation. Some ciliopathies are rare syndromic anomalies, which exhibit a range of skeletal defects. Patients may have limb phenotypes such as polydactyly, as is the case with Bardet-Biedl Syndrome, or defects in the endochondral bones, such as short limbs, short ribs and vertebral stenosis, as seen in Sensenbrenner and Ellis-van Creveld syndromes (David et al., 1999, Beales et al., 1999, Sensenbrenner et al., 1975, Young, 1989, Smith and Hand, 1958). In addition, some ciliopathies exhibit craniofacial malformations ranging from general changes in shape of the skull, seen in Bardet-Biedl syndrome and orofaciodigital (OFD) syndrome, to exencephaly, seen in Meckel-Gruber syndrome, and craniosynostosis, which has been reported in Sensenbrenner syndrome (Waters and Beales, 2011, Khalifa et al., 2012, Lin et al., 2013). Most skeletal ciliopathies are also reported to be associated with a cleft or high arching palate: the former seen in Meckel-Gruber and Joubert syndromes, the latter seen in Sensenbrenner, Bardet-Biedl and OFD syndromes (Myageri et al., 2013, Parelkar et al., 2013, Singh et al., 2011, Young, 1989, Beales et al., 1997, Shawky et al., 2013). Given the dependence of Hh signaling on proper functioning cilia, most of these phenotypes are attributed to changes in primary cilia-dependent transduction of Hedgehog signals. However the wide range of skeletal elements affected suggests a variety of signaling defects (Haycraft and Serra, 2008). Many phenotypically similar skeletal defects are observed in two other classes of skeletal disorders: the chondrodysplasias and the craniosynostosis syndromes.

6.1.2 FGF-related syndromes

Chondrodysplasia syndromes are characterised by truncation of the appendicular skeleton. These diseases arise from gain of function mutations of FGFR3 which typically acts to limit terminal differentiation of

chondrocytes, regulating long bone elongation, and hence growth (Cohen, 1998). As such, mouse mutants with enhanced FGFR3 signaling have shortening of most endochondral elements (Iwata et al., 2000). In humans, most mutations driving chondrodysplasias result in ligand-independent constitutive activation of FGF signaling and elevated tyrosine kinase activity. This may occur via aberrant FGFR dimerization or aberrant tyrosine kinase activity of the receptor (Naski et al., 1998, Neilson and Friesel, 1996, Webster and Donoghue, 1996). Examples of these disorders include achondroplasia, commonly referred to as dwarfism, hypochondroplasia and thanatophoric dysplasia (listed in order of severity).

In humans, the most striking phenotype is short long bones relative to the trunk skeleton, which is seen in all the chondrodysplasias. In addition, short ribs are also commonly seen in thanatophoric dysplasia and achondroplasia, whilst vertebral defects such as dysplastic vertebral bodies and vertebral fusions have been reported in chondrodysplasia punctata (Rimoin et al., 1970, Elejalde and de Elejalde, 1985, Khanna et al., 2001, Mason et al., 1994). The cranium, which consists of both endochondral and intramembranous bones, also exhibits craniofacial malformations. Skull shape changes are common due to reduced growth of the cranial base and craniosynostosis is frequently seen (Georgoulis et al., 2011, Cohen et al., 1985).

Craniosynostosis syndromes include disorders such as Apert syndrome, Pfeiffer syndrome and Crouzon syndrome. They are principally characterised by premature fusion of the cranial sutures associated with increased osteoblast maturation (De Pollack et al., 1996, Lomri et al., 1998). As described in chapter 1, signaling through FGFR1 and -2 stimulates osteoblastic differentiation and maturation, particularly during intramembranous bone formation. Hence, hyperactivation stimulates excessive bone formation. Clinically a ‘dome shape’ skull, as a result of craniosynostosis, and a high arching palate, are most commonly observed (Rynearson, 2000, Moore et al., 1995a). Malformations in the trunk skeleton have also been described with fusions of the cervical vertebra observed in Apert, Pfeiffer and Crouzon syndromes and short limbs and polydactyly

reported in Apert syndrome (Hemmer et al., 1987, Anderson et al., 1997, Cohen and Kreiborg, 1993).

It is clear that there is a great deal of phenotypic overlap between these skeletal syndromes (summarized in Yannakoudakis & Liu, 2014). Moreover, the *Fuzzy* mutant, which is a mouse model for ciliopathies, exhibits all of the phenotypes described. These similarities could suggest signals converging on deregulated FGF signaling in all of these syndromes. However, ciliopathy mouse phenotypes have commonly been attributed to abnormal Hh signaling while the role of aberrant FGF signaling is rarely explored. This chapter will document certain skeletal malformations of the *Fuzzy* mutant and compare them to those observed in FGF syndromes. In this way new light can be shed on underlying molecular changes driving defective skeletogenesis and enable us to establish whether individual phenotypes in these complex syndromes converge on similar genetic pathways. This chapter will mainly discuss phenotypes of the vertebra and the sternum as well as craniosynostosis. Phenotypes in the long bones and the mandible will be discussed in subsequent chapters.

6.1.3 Calvarial development

In mammals, the calvaria of the skull vault consists of paired frontal bones, paired parietal bones and the interparietal bone, which form from intramembranous ossification. The frontal bones are NC derived whilst the parietal bones are mesoderm derived. The interparietal bones consist of mixed NC and mesodermal cell populations (Morriss-Kay, 2001). Once these cells undergo intramembranous ossification, the bone fronts between them must fuse at the calvarial sutures.

Several signaling pathways have been implicated in the development of the calvarial bones and their sutures. FGF signaling is particularly important. FGF18 and -20 are expressed in the developing calvaria. *Fgf18* null mice have reduced calvarial ossification associated with a delayed onset of osteopontin and lower levels of proliferation in osteogenic cells. This suggests that FGF18 is important for proliferation and differentiation during

osteogenesis (Ohbayashi et al., 2002). The importance of FGFR1 and -2 in ossification of the suture are described above.

6.1.4 Sternal development

The sternum is classified as part of the appendicular skeleton given its mesenchymal origins in the lateral somatopleuric mesoderm (Chen, 1952, Scheuer and Black, 2004). Development initiates from two sternal primordia consisting of mesenchymal rods of condensations in the ventro-lateral body wall of the embryo (Chen, 1952). During development, these primordia elongate cranio-caudally to form sternal bars. From e12, these pre-cartilaginous bars migrate medially towards each other (Chen, 1952). By e14.5, the sternal bars begin to fuse in a cranial to caudal direction and cartilaginous regions in each bar can be seen and fusion is complete by e15.5 (Chen, 1952, Kaufman and Bard, 1999). These go on to chondrify across the midline and ultimately form one single rostral-caudal cartilaginous rod (Kaufman and Bard, 1999). Once chondrogenesis is complete, the sternal body, also known as the mesosternum, is segmented into sternebrae, which undergo endochondral ossification, at approximately e17.5. This happens from individual ossification centers running down the length of the manubrium (Chen, 1952, van der Merwe et al., 2013). The most caudal portion of the sternum (the xiphoid process) and fusions between sternebrae only ossify postnatally (Scheuer and Black, 2004). This is schematized in Fig 6.1.

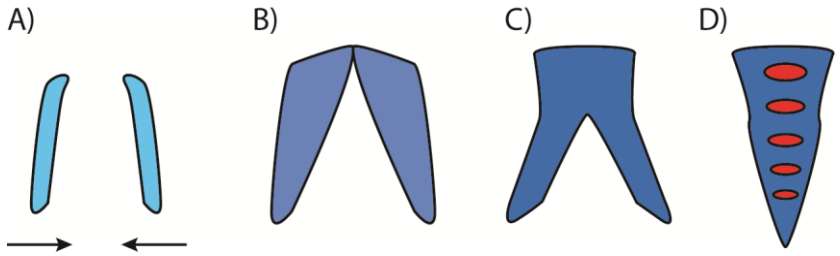

Figure 6.1 Schematic of sternal development

A) The sternum is originally made from two mesenchymal sternal rods which move towards the midline from around e12.

B) Sternal bars begin to fuse in a cranial-caudal direction from approximately e14.5.

C) Chondrogenesis across the midline forms a single cartilaginous sternum.

D) Subsequent ossification arises from individual ossification centres down the length of the sternum.

6.1.5 Vertebral development

The vertebral column, also known as the spine, can be anatomically subdivided into different regions: the cervical, the thoracic and the lumbar vertebra (listed rostral-caudal). Embryonically, it arises from two rods of paraxial mesoderm on either side of the neural tube which is segmented into somites arranged rostro-caudally. These somites go on to compartmentalize into sclerotome, syndetome, myotome and dermomyotome, which form the vertebra and ribs, tendons, skeletal muscle and dermis respectively (Tam and Trainor, 1994). Figure 6.2 A shows the outcome of somatic compartmentalization. During this process, the cells destined to become sclerotome, which ultimately form the vertebrae, undergo epithelial to mesenchymal transitions (Dockter and Ordahl, 1998). Shh signaling from the notochord and floor plate dictates dorso-ventral patterning, progenitor identity and spatial organization via a graded signal (Jeong and McMahon, 2005). All three Gli proteins are expressed in the early somites but this expression diverges when looking at discrete developmental regions. Gli2 is expressed in the sclerotome whilst Gli3 is expressed throughout the sclerotome and in the dermomyotome. It has been suggested that both Gli2 and Gli3 are required for *Pax1* and *Pax9* (early sclerotomal markers) induction, which stimulates *sox9* expression, and they display functional redundancy (Buttitta et al., 2003). In addition to sclerotome induction by Shh, FGF8 signaling from newly formed myotome goes on to specify a subset of the sclerotome into syndetome (Brent and Tabin, 2004, Gilbert, 2006).

Once the somites have been patterned, individual vertebra, which consist of a centrum (more ventral and develops next to the notochord) and a neural arch (more dorsal, develops adjacent to the spinal cord), form and together make up an individual vertebra,, which when aligned form the vertebral column (Hall, 2005). Each vertebra forms via endochondral ossification. Cartilaginous templates replace the mesenchyme of the primordial vertebra (schematized in Fig 6.2 B). It was shown that in the thoracic vertebrae, the centrum forms from two chondrogenic centers, which eventually fuse in the midline; this is followed by establishment of chondrogenic centers in the

neural arch, which go on to fuse with each other. This creates a cartilaginous vertebra surrounding a neural canal, in which the spinal cord will eventually sit. Once the cartilaginous template of the vertebra has been established, endochondral ossification occurs from different ossification centers (schematized in fig 6.2 B). In humans, different vertebral regions have different ossification centers. In the thoracic vertebrae, there is 1 primary ossification center in the centrum and two on either side in the neural arch. The 2nd cervical vertebrae has 5 primary ossification centers: the same three seen in the thoracic vertebrae and two additional centers just anterior to the centrum; whilst the first cervical vertebrae has 3 primary ossification centers, 1 in the anterior arch and 2 in the posterior arch. Secondary ossification centers form after puberty (Rosse and Gaddum-Rosee, 1997, Butler et al., 2012, Jinkins, 2000). A mature thoracic vertebra is schematized in figure 6.2 C.

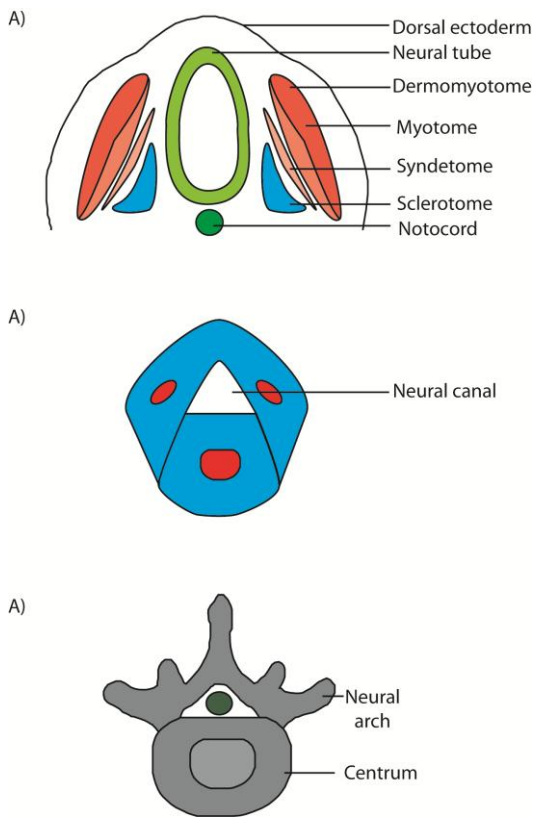

Figure 6.2 Schematic of vertebral chondrogenesis

A). Initially, the somite must me compartmentalized into different layers. The dermomyotome, myotome, syndetome and sclerotome. The sclerotome goes on to form the vertebra.

B) the cartilaginous precursors of a single vertebra has different ossification centers depending on its location in the body. This image depicts a thoracic vertebra with three ossification centers. Two in the future neural arch and one in the future centrum.

C) Ossification from these centers eventually forms continuous bone of the individual vertebra. The spinal cord runs in between the neural arch and centrum.

6.2 Results

6.2.1 *Fuzzy* mutants have coronal synostosis which cannot be rescued on reduction of *Fgf8*

We previously showed that genetic reduction of *Fgf8* can rescue a high arching palate observed in the *Fuzzy* mutant. In addition, *Fgf8* is expressed in the developing calvaria. We therefore wanted to see whether reducing *Fgf8* can rescue craniosynostosis previously documented in the mutant.

Using Alizarin red staining to mark the mineralized bone, we examined the coronal sutures or wildtype, *Fuzzy*$^{-/-}$ *and Fuzzy*$^{-/-}$*;Fgf8*$^{L/+}$ embryos at e16.5 (Fig 6.3). In the wild-type samples, a clear boundary between the developing frontal (f) and parietal (p) bones can be seen on either side of the coronal suture mesenchyme (Fig 6.3 A; black arrow). In *Fuzzy* mutant embryos, craniosynostosis can be observed and there is clear ossification between the frontal and parietal bone (Fig 6.3 B. yellow arrow). On genetic reduction of *Fgf8* in the *Fuzzy* mutant, craniosynostosis appears to be ameliorated. A clear boundary between frontal and parietal bones can be seen flanking un-ossified tissue (Fig 6.3 C; black arrow). There are, however, small patches in which ossification has encroached into the suture (Fig 6.3 C; yellow arrowhead). This suggests that although aberrant *Fgf8* expression may be responsible for the synostosis observed, other mechanisms may contribute on loss of *Fuzzy*.

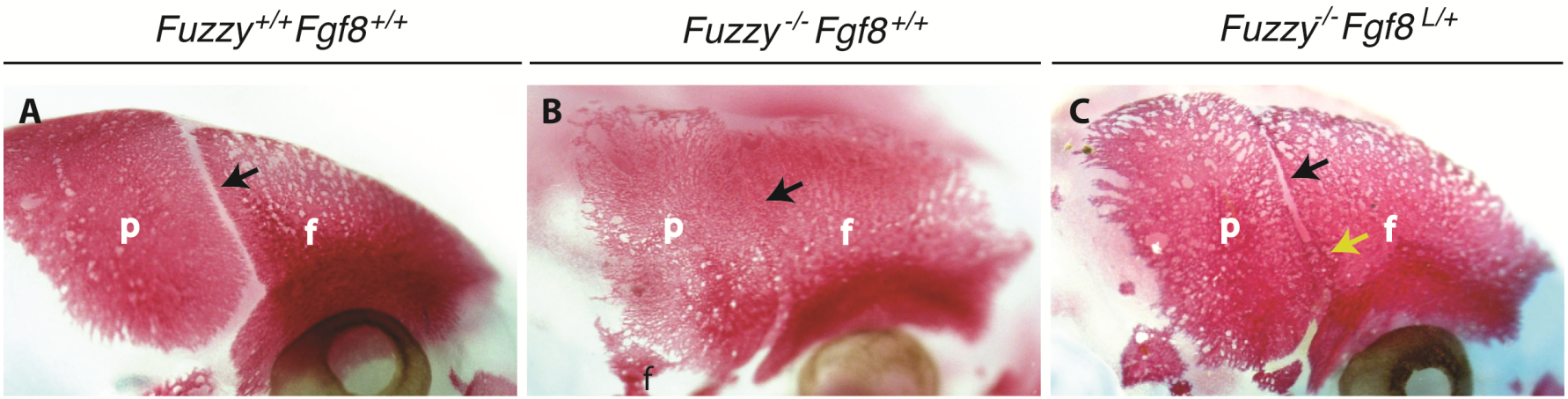

Figure 6.3 Craniosynostosis is observed in the *Fuzzy* mutant and is ameliorated on reduction of *Fgf8*

Bone is stained with Alizarin red.

A) Wildtype control embryo at e16.5. A clear suture with absence of ossification can be observed between the frontal (f) and parietal (p) bones (black arrows).

B) In the *Fuzzy* mutant at e16.5, the frontal and parietal bones have prematurely fused (black arrowhead denotes where the suture should be).

C) On genetic reduction of *Fgf8* in the *Fuzzy* mutant, the synostosis appears to be ameliorated as suture has not fused between the frontal and parietal bones. The black arrowhead shows an absence of synostosis whilst the yellow arrowhead shows some ossification encroaching into the suture.

6.2.1 *Fuzzy* mutants have vertebral stenosis and fusion of cervical vertebra

In order to characterise abnormal skeletal development of the vertebra, I looked at the developing cartilage and bone. Two different developmental times were chosen to try to determine the source of the phenotype. Cartilaginous precursors of the vertebra were visualized in e13.5 embryos by means of col2::lacZ reporter gene activity (Zhou et al., 1995). In the wild-type embryos, well-formed vertebral bodies can be seen regularly spaced down the length of the thoracic spinal cord (Fig 6.4 A; red arrowhead). In mutant embryos, chondrogenesis of the vertebral bodies appears to be absent (Fig 6.4 B, red asterisk), or if initiated appears to lack fusion of the two chondrogenic sites of the centrum (open red arrowhead).

By e18.5, in wildtype embryos, ossification of the vertebral bodies in the thoracic vertebra can be seen clearly under way down the length of the vertebra (Fig 6.4 C, yellow arrowhead). In the cervical vertebra, bone from the 2 primary ossification centers of the vertebral arch appears regularly spaced on either side of the midline (Fig 6.4 C, black arrowheads). In the mutant embryos, ossification of the centrum is clearly absent (Fig 6.4 D, yellow asterisk) and there is clear fusion of the cervical vertebra (CV). Taken together, these data suggest that underlying cartilage abnormalities may be responsible for the later defects in ossification.

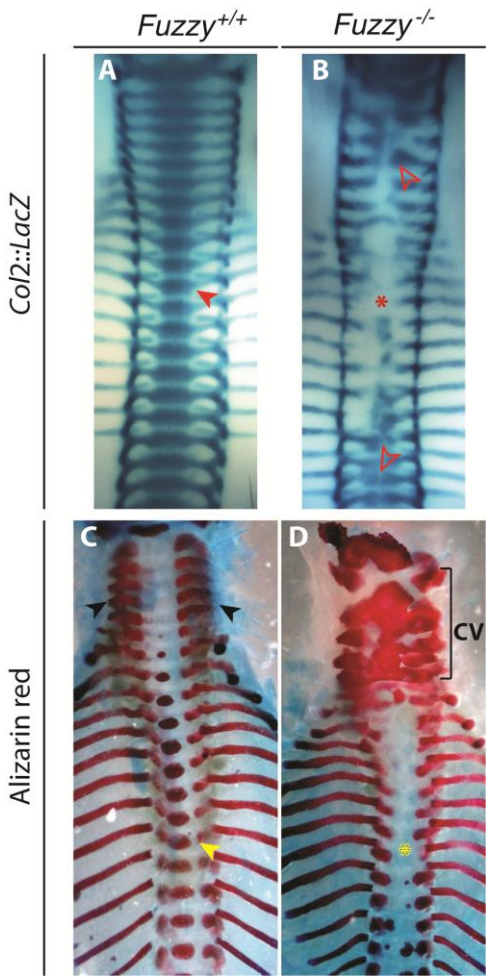

Figure 6.4 Chondrogenesis and ossification of the vertebra in the *Fuzzy* mutant is abnormal

(A and B) Dorsal images of vertebral columns of wildtype and mutant embryos at e13.5 showing cartilage visualized with a *Col2*::*lacZ* reporter gene. (A) In the wild type, chondrogenesis of the vertebral bodies is normal and has fused in the midline (red arrowhead). (B) In the mutant, cartilage appears to be either absent (red asterisk), or has failed to fuse in the midline (hollow red arrowhead).

(C and D) Dorsal images of alizarin red stained bone in vertebral columns of wildtype and *Fuzzy* mutant embryos at e18.5. (C) In the wildtype, ossification of the vertebral arch of the cervical vertebra appears normally sized and regularly spaced apart (black arrowheads). Ossification of the vertebral bodies is well under way (yellow arrowhead). (D) In the mutant, there is obvious fusion of the cervical vertebra (CV) while ossification of the vertebral bodies is absent (yellow asterisk).

6.2.3 Reduction of *Fgf8* in the *Fuzzy* mutant does not rescue the cartilage phenotype of the vertebral column

Since we previously showed elevated levels of FGF8 signaling driving a maxillary phenotype in the *Fuzzy* mutant, and since FGFR3, one of the receptors for FGF8, is expressed in the developing spine, we decided to see whether an increase in FGF has roles in the vertebral phenotype of the *Fuzzy* mutant (Peters et al, 1993)(Tabler et al., 2013, Peters et al., 1993). Fig 6.5 shows alcian blue stained vertebral columns from e14.5 embryos. In the wildtype specimen, fusion of the centrum in the midline appears normal in both the cervical vertebra (Fig 6.5 A; asterisk) and the thoracic vertebra (black arrowhead). In the *Fuzzy*$^{-/-}$ specimen, the centra of the cervical vertebrae and the thoracic vertebrae are not fused at the midline (Fig 6.5 B; black asterisk). Reduction of *Fgf8* gene dose in the *Fuzzy* mutant does not rescue the vertebral phenotype. Lack of fusion in the cervical and thoracic vertebrae is very obvious (black asterisk and arrowhead respectively; Fig 6.5 C). As an additional control, panel (Fig 6.5 D) shows a heterozygous *Fgf8* animal, which appears normal.

6.2.4 *Fuzzy* mutants have a cleft sternum with excess ossification

In order to characterise defective sternal development in the Fuzzy mutant, cartilage and bone were visualized at two different stages. The cartilaginous development of the sternum was visualized with Alcian blue staining at e15.5, whilst ossification was visualized with Alizarin red staining at e18.5. At e15.5 (Fig 6.6 A), the frontal views of the wild type sternum reveal fusion of the sternal bars. Seven pairs of ribs can be seen attached to the sternal bars. In the *Fuzzy* mutant littermate, the sternal bars have failed to fuse in the midline and the sternum is clearly cleft (Fig 6.6 B, black arrow). Later observations, at e18.5, reveal that in the wildtype sample individual ossification centers in the sternebrae can be seen (Fig 6.6 C). In the mutant at this age, the sternum is still clearly cleft (black arrow) but the sternebrae are ectopically ossified on either side of the midline (Fig 6.6 D).

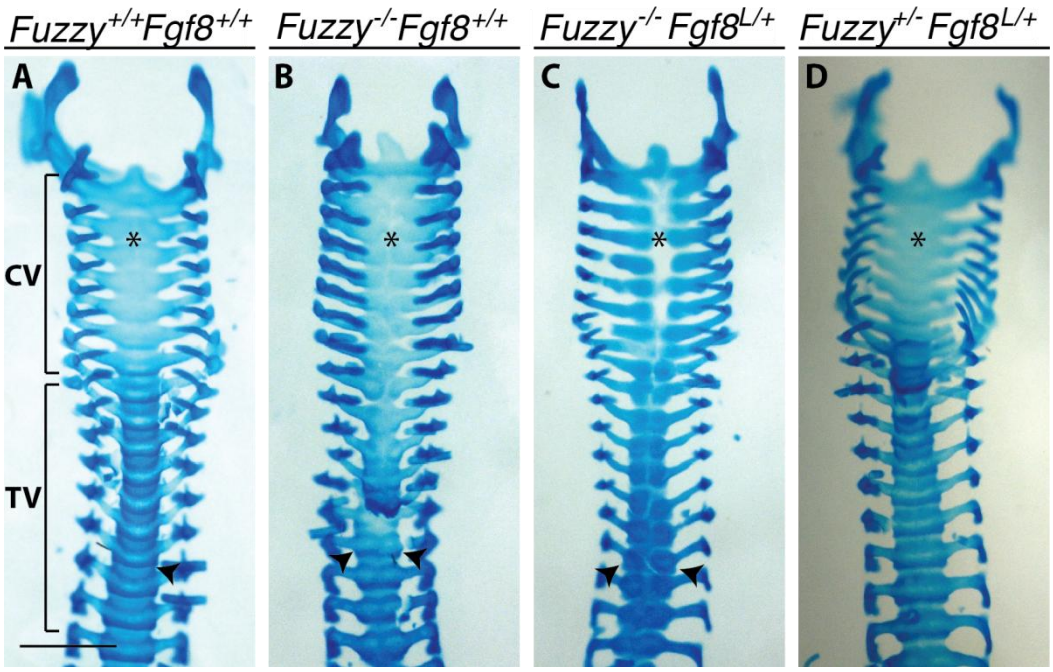

Figure 6.5 Reduction of *Fgf8* does not rescue the vertebral phenotype

Ventral views of alcian blue stained cartilage of vertebral columns from e14.5 embryos. Cervical vertebrae (CV); thoracic vertebrae (TV).

(A) Wild type animal. Normal fusion of the centrum can be seen in the midline of both the cervical (asterisk) and thoracic (arrowhead) vertebrae.

(B) The *Fuzzy* mutant vertebra has incomplete fusion of the centrum of both the cervical (asterisk) and thoracic (arrowhead) vertebrae. (A) and (B) are littermates.

(C) Reduction of *Fgf8* does not rescue the mutant phenotype. Incomplete fusion of the centrum is still visible in the cervical and thoracic vertebrae (asterisk and arrowheads respectively).

(D) Heterozygous *Fgf8 animals have* vertebra that are indistinguishable from the wild type. (C) and (D) are littermates. Scale bar is 1mm.

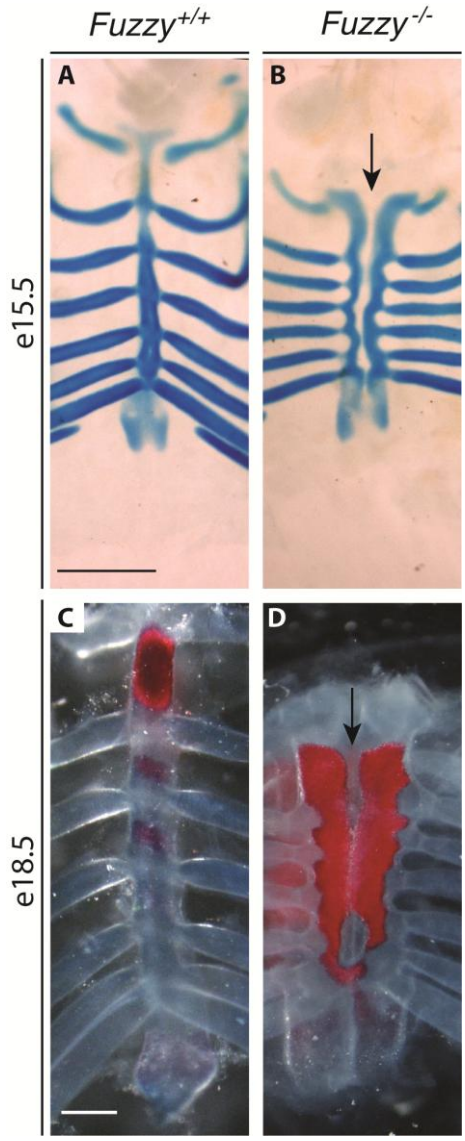

Figure 6.6 The sternum of *Fuzzy* mutants is bifid and hyperossified

(A and B) Frontal images of alcian blue stained cartilage in mutant and littermate control sterna. (A) In the control sample, the sternum has already fused and appears as a single cartilaginous rod. (B) In mutants, the sternum is shorter and bifid. Black arrow shows the sternal cleft.

(C and D) Frontal views of alizarin red stained bone in mutant and littermate control sternums. (C) In the wildtype, discrete regions of ossification can be seen. (D) In the mutant, the sternum is shorter and bifid (black arrow) and is hyperossified. Scale bar is 1mm.

6.2.5 Reduction of *Fgf8* gene expression in the *Fuzzy* mutant does not rescue the sternal phenotype.

In order to assess the effect of reducing *Fgf8* gene expression on the sternal phenotype, we carried out Alcian blue staining on compound embryos at e14.5. At this stage, in the wildtype, the two sternal rods are just about to fuse (Fig 6.7 A). In the *Fuzzy*$^{-/-}$ mutant, the sternal bars have not come together (Fig 6.7 B, black arrow) and they appear shorter (Fig 6.7 B). This phenotype appears similar on reduction of *Fgf8,* in that the sternal bars still appear shorter and there is a clear lack of fusion in the midline (Fig 6.7 C, black arrowhead).

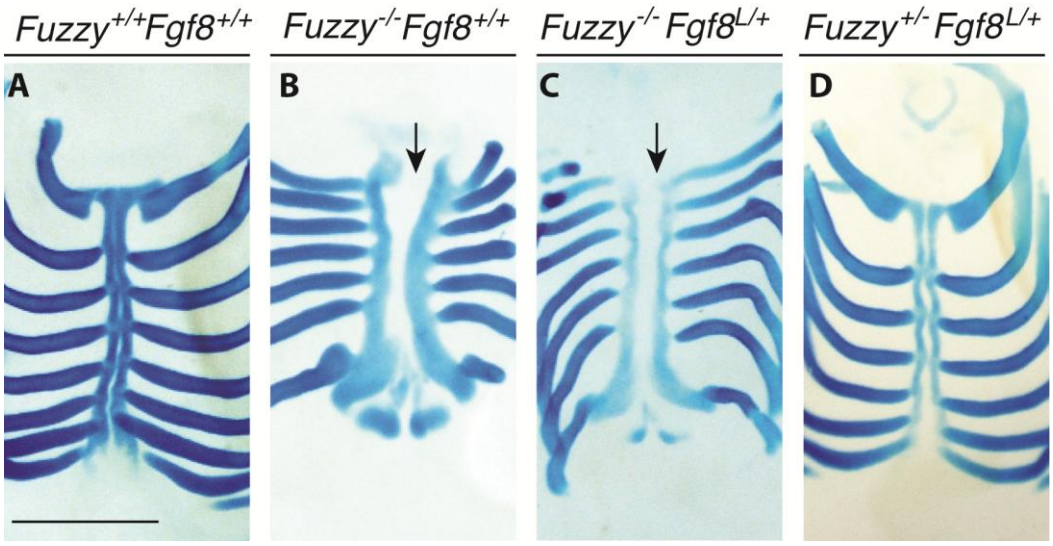

Figure 6.7 Genetic reduction of *Fgf8* does not rescue the cartilaginous sternal phenotype in the Fuzzy mutant

E14.5 animals, cartilage is stained with alcian blue.

A) Frontal view of wild type sternum shows sternal bars are fusing in the midline.

B) In the *Fuzzy* mutant, the sternal bars are shorter and have not yet met in the midline. Black arrow shows clefting. (A) and (B) are littermates.

C) Likewise on reduction of *Fgf8*, sternal bars have not yet met in the midline.

D) As an additional control, *Fuzzy* and *Fgf8* double heterozygotes are similar to the wild type control, as sternal bars are just meeting at the midline. Scale bar is 1mm.

6.3 Discussion

6.3.1 Craniosynostosis

Coronal craniosynostosis is observed in the *Fuzzy* mutant and the craniosynostosis syndromes. In the craniosynostosis syndromes, the majority of Apert syndrome cases are due to mutations in FGFR2 (Wilkie et al., 1995), whereas mutations of Pfeiffer and Crouzon syndromes are more varied but still result from FGFR hyperactivation (Muenke et al., 1994, Schell et al., 1995). Craniosynostosis can arise from activating mutations in all three of the main FGFRs (Ibrahimi et al., 2004). Mutations in FGFR1 and 2 have been most recognized as causing craniosynostosis; as such, in Apert syndrome, FGFR2 mutations are seen to cause enhanced osteoblast differentiation either in the absence of an FGF ligand or by increasing affinity to the FGF ligand (Lomri et al., 1998, Lemonnier et al., 2000). Similarly gain of FGFR2 function in Crouzon syndrome has been shown to increase osteoblast proliferation (Galvin et al., 1996). Interestingly, some Apert and Crouzon patients have been reported to have lower levels of *FGFR2* expression as a result of either negative feedback, or FGF ligand-receptor induced receptor internalization (Bresnick and Schendel, 1995, Bresnick and Schendel, 1998, Estival et al., 1996). In keeping with the key role of RUNX2 for osteoblast differentiation, *FGFR1* mutations in mouse have been shown to cause upregulation of osteoblastic markers such as *Runx2* and osteocalcin in association with synostosis (Zhou et al., 2000).

Craniosynostosis is also seen in the chondrodysplasias but the reasons why have not been well characterised. As described above, FGFR3 is the main culprit in these disorders, limiting hypertrophy during endochondral ossification resulting in reduced bone mass (Su et al., 2010a). Although the calvaria do not form via this mechanism, it may be possible that signaling through this receptor has a stimulatory effect on osteoblasts in the calvarial sutures. In keeping with this idea, patients with Muenke syndrome, which have gain of FGFR3 mutations, have craniosynostosis (Singh et al., 2014, Georgoulis et al., 2011). Since the only intramembranous bones in which FGFR3 is expressed are the calvaria, this could represent an example in which FGFRs exert tissue specific functions (Rice et al., 2000). All of this

evidence together shows that enhanced FGFR activity acts to stimulate osteoblastic activity at the calvarial sutures resulting in craniosynostosis seen in both chondrodysplasias and craniosynostosis syndromes.

Given that *Runx2* is a key regulator of bone formation, it is no surprise that early onset is associated with craniosynostosis (Maeno et al., 2011). As described in chapter 1, FGFR signaling is an important regulator of intramembranous bone formation at various stages of osteoblast differentiation and proliferation. Constitutively active FGFR1 causes craniosynostosis associated with an increase in *runx2,* and constitutively active FGFR2 activity also stimulates *Runx2* expression (Zhou et al., 2000, Suh et al., 2014). Furthermore, in tissue culture experiments, it was shown that exogenous application of FGF4 results in increased transcriptional activity of RUNX2, proposed to be via the inositol polyphosphate and PKC cascade. (Niger et al., 2013, Grillo et al., 2014). Interestingly, exogenous FGF8 treatment of bone cells also upregulates *Runx2* expression, apparently also via activation of the PKC pathway (Kim et al., 2003, Kim et al., 1998). Thus it seems that multiple FGF-FGFR ligand combinations act to stimulate osteoblast maturation via *Runx2.*

Ciliopathies such as Sensenbrenner syndrome and cranioectodermal dysplasia can manifest with craniosynostosis but the mechanisms behind this have not been explored (Levin et al., 1977). Analysis in the Fuzzy mutant suggests that synostosis is at least in part due to aberrant *Fgf8* expression. Both *Fgf8* and *Gli3* are expressed in the calvarial sutures at e15.5 (Xu et al., 1999). Loss of *Gli3* is shown to cause synostosis by upregulating *Runx2* and subsequent osteogenic differentiation (Tanimoto et al., 2012, Veistinen et al., 2012, Rice et al., 2010). By way of speculation, it is possible that loss of the Gli3 repressor could be accompanied by an increase in *Fgf8* expression, as we saw in BA1. Subsequent increases in *Fgf8* could be driving *Runx2* upregulation. This hypothesis is supported by my observations that genetic reduction of *FGF8* in the *Fuzzy* mutant appears to ameliorate the observed craniosynostosis (Fig 3.1C; (Xu et al., 1999). Thus, this suggests that aberrant FGF8 expression may contribute to the phenotype in the *Fuzzy*

mutants and ciliopathy patients. This does not however explain why synostosis is not fully rescued.

One interesting possibility to explain this could be that in the sutures, the Gli3 repressor may be regulating other FGFs. Craniosynostosis in Gli3 mutants can be due to enhanced ERK-MAP kinase signaling downstream of FGF2, ultimately causing *runx2* upregulation (Park et al., 2010, Niger et al., 2013). It is therefore feasible that in our mutant, aberrant Gli3 processing may also converge on misregulation of FGF2. If this were the case we would expect a more complete rescue in compound mutants in which FGF2 and FGF8 have been reduced. Along these same lines, it could be speculated that Gli3 could regulate other FGFs, which are important in processes of intramembranous ossification, such as FGF4, but have not previously been thought to be regulated by Glis (Kim et al., 1998). Along these same lines, FGF 2 , -4 and -9 are all found in the sutural mesenchyme (Britto et al., 2001, Kim et al., 1998, Rice et al., 2000). This could be tested by comparing the expression of the different Fgfs between wild type and *Fuzzy* mutants. Furthermore, one could analyze *Fuzzy* compound mutants in which other FGFs have been genetically reduced.

As a final thought, another explanation behind the incomplete rescue in our *Fuzzy*$^{-/-}$*; FGF8*$^{L/+}$ compound mutants could be due to the involvement of other signaling pathways. The BMP signaling pathway has been known to stimulate ossification. This has been seen by ectopic bone formation on application of recombinant BMPs *in vivo* and *in vitro* (Wang et al., 1990, Myllyla et al., 2014). Interestingly, it was shown that Gli3 mutants, which have craniosynostosis, lose Gli3 repression of BMP signaling (Tanimoto et al., 2012). It should therefore not be ruled out that improper Gli3 regulation of the BMP signaling pathway could contribute to craniosynostosis observed in our mutant mice.

In summary, craniosynostosis has been associated with upregulation of *Runx2* through both FGF dependent and FGF independent means, as described above. The presence of sutural mesenchyme in the *Fuzzy*$^{-/-}$;*Fgf8*$^{L/+}$

compound mutants suggest that in part excessive FGF8 signaling is driving our phenotype. More work must be done to determine additional causes contributing to lack of complete rescue such as Gli regulation of other FGFs or other signaling pathways such as BMP. These observations have interesting implications when comparing craniosynostosis syndromes and craniosynostosis observed in chondrodysplasias and ciliopathies. Typically in the craniosynostosis syndromes, enhanced osteoblast differentiation and proliferation via excessive FGFR1 and FGFR2 signaling has been attributed to craniosynostosis; whilst synostosis seen in chondrodysplasia is probably due to enhanced signaling through the FGFR3. My observations suggest that similar craniosynostotic phenotypes observed between FGF syndromes and ciliopathies may arise through different mechanisms.

6.3.2 Defective vertebral development

Vertebral chondrogenic phenotype

My data reveals an interesting vertebral phenotype in the *Fuzzy* mutant. In both the cervical and thoracic vertebra, it appears that cartilage formation occurs, however chondrogenesis appears defective in the midline in that there is a lack of fusion of the vertebral bodies (Fig 6.4). With regards to ossification, the cervical vertebra appears fused whereas there is a loss of ossified vertebral bodies in the midline of the thoracic vertebra.

Glis have important roles in early patterning of the developing vertebrae, and compound Gli mutant analysis reveals the need for both the Gli3 repressor and Gli2 activator in *sox9* induction during chondrogenesis of the sclerotome (Buttitta et al., 2003). Interestingly, cartilage preparations in *Gli3* mutant mice reveal similar vertebral phenotypes to those seen in the *Fuzzy* mutant, with loss of cartilage formation towards the midline (Mo et al., 1997). Compound mutants in which both *Gli2* and *Gli3* are knocked out have exacerbated phenotypes and it has been suggested that in some vertebral regions, in the absence of the Gli3 repressor, Gli2 is functionally redundant and can acting as a repressor. Likewise in the absence of the Gli2 activator, Gli3 can compensate (Buttitta et al., 2003, Mo et al., 1997). Moreover, both chondrogenic and myogenic markers (*Pax1* and *Myf5* respectively) are

mixed in the mesenchyme of *Gli2* and *Gli3* mutants which suggest a loss of organization of cell types; an observation also seen in *Smo*$^{-/-}$;*Gli3*$^{-/-}$ compound embryos (Wijgerde et al., 2002, Buttitta et al., 2003). Since these cells are organized in response to Shh, it has been suggested that the *Gli2*$^{-/-}$*;Gli3*$^{-/-}$ compound mutants cannot respond to Hh signaling and thus represent a default state independent of Hh activity (Buttitta et al., 2003). This is also what we would expect in the *Fuzzy* mutant given the need for the cilium to process Gli proteins in response to Hh ligand.

It is reported that Glis induce *sox9* via regulation of *Pax1* gene expression. Consistent with this, *Pax1* mutants have similar chondrogenic defects in their vertebral columns (Wallin et al., 1994, Murtaugh et al., 1999, Buttitta et al., 2003). Moreover, given that the severity of the *Fuzzy* mutant phenotype is worse then that seen in *Gli2* or *Gli3* mutant, and the proposed redundancy between Gli2 and Gli3 activity, I propose that not only is Gli3 processing defective, but also Gli2 function, which has not been previously described in the *Fuzzy* mutant.

Another interesting point is the role of FGF8 signaling from the myotome. In this instance, *Shh* from the notochord induces *Fgf8* expression in the myotome. Subsequently, this goes on to specify a subset of sclerotome to differentiate into tendon forming syndetome. Syndetome is formed at the expense of cartilage forming sclerotome (Brent et al., 2003, Brent and Tabin, 2004). Since we have seen both an upregulation of *Fgf8* expression and a loss of ability for the Shh ligand to regulate Glis in the *Fuzzy* mutant, it could be proposed that loss of midline cartilage formation may be due to enhanced syndetome formation at the expense of sclerotome. This, however, is unlikely since genetic reduction of *FGF8* in the *Fuzzy* mutant does not rescue the vertebral phenotype, and there has been no evidence for Gli regulation of FGF8 expression in the developing somites. In order to test this I would look for increased presence of syndetome markers such as scleraxis.

Vertebral ossification phenotype

Defective ossification seems to affect the vertebral body in the thoracic vertebra and the neural arches in the cervical vertebrae. These two defects appear in *Gli2* and *Gli3* knock out mice (Mo et al., 1997). *Gli2* mutant mice have very few vertebral bodies whilst the cervical neural arches appear normal and unfused. Conversely, *Gli3* mutants have only slightly smaller vertebral bodies then wild type. Interestingly they display cervical vertebral anomalies in that 1st and 2nd neural arches are fused and the rest are malformed (Mo et al., 1997). These differences can be explained given the different expression domains of the Glis in the developing embryo. *Gli2* is expressed in medial sclerotome cells adjacent to the expression of pax1, which is an important signal to specify centrum development. *Gli3*, however, is expressed in the more lateral regions adjacent to *Pax9*, which is important for neural arch development (Goulding et al., 1994). The lack of vertebral bodies in the *Gli2* mutants resembles the phenotype of the *Pax1* knockout mouse and the cervical fusions observed in *Gli3* mutants resembles that seen in *Pax9* mutants (Peters et al., 1999, Wallin et al., 1994). Since knock out of each *Gli* alone causes relatively mild phenotypes compared to that of the double knock out, it reveals functional redundancy between the two.
These observations suggest that the ossification phenotype could be secondary to the loss of chondrogenesis resulting from misregulation of *Pax* genes as explained above.

It should also be considered that as well as ossification effects being secondary to cartilaginous defects, there may be a loss cartilage maturation, which contributes to the phenotype. This is plausible given that Gli proteins have been implicated in controlling cartilage maturation and the spine forms through endochondral ossification (Miao et al., 2004). During vertebral development, *Gli2* is expressed more in the medial sclerotome while *Gli3* is expressed more laterally. This would explain why Gli2 mutants have more obvious ossification defects in the vertebral bodies compared to the neural arches, which are malformed on loss of Gli3 (Mo et al., 1997). To assess whether cartilage maturation as well as chondrogenic induction is

defective in *Fuzzy* mutants, analysis for key markers for different stages of cartilage maturation should be carried out.

We, and others, have previously reported that *Fuzzy* mutants have defective neural tube closure (Gray et al., 2009, Tabler et al., 2013). Moreover, occasionally fatal human ciliopathies such as Meckel-Gruber syndrome are seen with neural tube anomalies, and mouse models lacking ciliary components, such as IFT proteins have abnormal neural tube closure (Huangfu and Anderson, 2005, Van Allen et al., 1993). It could be postulated that this lack of closure is inhibiting chondrogenic fusion of the vertebral bodies in the midline. Previously it has been suggested that cilia, and hence FUZ, are required for proper PCP signaling (see chapter 1). As well as this, in *Xenopu*s, PCP-dependent convergent extension is required for proper neural tube closure (Wallingford and Harland, 2002). This evidence could imply that defective ciliogenesis in the *Fuzzy* mutant inhibits neural tube closure by altering PCP signaling. One could therefore suggest that defective vertebral development is secondary to defective neural tube closure. However, DVL mutants, which have open neural tubes and mild defects in somite segmentation, have ossified vertebral bodies that are disorganized in their spacing (Hamblet et al., 2002). This is in contrast to the lack of vertebral bodies in the *Fuzzy* mutants, which suggests that our phenotype is more complicated than abnormal PCP signaling during neural tube closure.

Surprisingly, many craniosynostosis patients have progressive cervical spine fusions. Two thirds exhibit fusions of the C5-C6 segment and C2-C3 fusions have also been reported in Saethre-Chotzen and Pfeiffer syndrome (Hemmer et al., 1987, Moore et al., 1995b, Moore et al., 1995a, Anderson et al., 1997). Again, this would implicate FGF signaling in the onset of vertebral fusions.

Chondrodysplasias generally have no reports of spinal ossification defects however spinal stenosis has been reported in rhizomelic chondrodysplasia punctata patients (Khanna et al., 2001). Furthermore, mouse models with enhanced FGFR3 signaling have premature fusions between ossification

centers of the vertebra but no fusions of individual vertebrae as is seen in the *Fuzzy* mutant (Matsushita et al., 2009). This is interesting since typically, activating FGFR3 mutations result in reduced bone mass of endochondral elements (Su et al., 2010a). However this has been put down to the importance of FGFR3 signaling in controlling bony fusions between various synchondroses (Su et al., 2010a, Matsushita et al., 2009). Molecular causes of these vertebral anomalies are unknown but it is reasonable to speculate that they arise from abnormal FGFR signaling. Therefore, if these defects have any similarities to those in the *Fuzzy* mutant vertebra, it would suggest a novel link between cilia, Gli proteins and FGF regulation.

Vertebral phenotype summary

In summary, my observations suggest a correlation between defective Gli processing in the developing vertebra and abnormal vertebral development in the *Fuzzy* mutant. Since chondrogenesis of the vertebra appears to have at least partially occurred, it can be suggested that initial chondrogenic induction is not defective, however it is still not clear which endochondral stages are being affected. In addition, it has been suggested that Gli2 and Gli3 play differential roles in cervical versus thoracic vertebral ossification. Since we see defects in both subsets of vertebrae, it is possible that we are also getting defective Gli2 processing in our mutant, which we have not previously shown. This is highly plausible given the roles of proper ciliogenesis in Gli2 processing as well as Gli3 processing. If these observations are correct then it would imply that vertebral phenotypes observed are independent of abnormal FGF or PCP signaling or defective neural tube closure.

6.3.3 Abnormal sternal development

In humans, failure of sternal bar fusion causes congenital sternal clefts. These are rare birth defects that are reported to be more common in females then males, with an incomplete cleft being more common then a complete cleft (Acastello et al., 2003). This birth defect is usually isolated; however, sternal clefts have occasionally been observed in association with other congenital anomalies such as ventral hernias, absent pericardium and cervicofacial hemangioma to name a few (Acastello et al., 2003, Bernhardt et

al., 1968, Cantrell et al., 1958, Aytac and Saylam, 1976, Ishikawa et al., 2002). To date no genetic, teratogenic or nutritional cause driving this phenotype has been identified.

Abnormal sternal development in the *Fuzzy* mutant manifests as a bifid sternum with hyperossification. Mouse mutants with defective ephrin signaling (ephrinB1-EphB) show occasional lack of sternal bar fusion with occasional fusion of ossification centers, but none as severe as in the *Fuzzy* mutant(Compagni et al., 2003). This is possibly because ephrin signaling has been implicated in many aspects of tissue movements in both skeletal and non- skeletal tissues as well as being expressed at sites of tissue fusion (Poliakov et al., 2004). Thus defective signaling could inhibit proper sternal bar movement or fusion in the midline (Compagni et al., 2003, Dimidschstein et al., 2013).

Along the same line, a cleft sternum, with small sternal rods, has been observed in mice with enhanced Shh signaling, which typically results in reduced levels of Gli3 repressor and increased levels of Gli2 activator (Tavella et al., 2004). This suggests a role for Glis in elongation and fusion of the sternal rods in the midline. In keeping with this, loss of GSK3β, which is required for Gli3 processing, also results in a cleft sternum (Liu et al., 2007). Interestingly, both these mouse mutants also have a loss of sternal ossification centers, which is in contrast to the hyper-ossification observed in the *fuzzy* mutant.

Although the Gli3 mutant mouse sternal phenotype is very similar to that of the *Fuzzy* mutant: the sternum is bifid with extensive ossification covering the length of each unfused sternal bar. Interestingly in Gli2 mutants, there is no failure of sternal bar fusion but compound Gli2 and Gli3 mutants have both a bifid sternum and sternal hyperossification (Mo et al., 1997). Furthermore, conditional mouse mutants lacking *Kif3a* in the dermis and lateral plate mesoderm also have a bifid sternum with fused ossification centers (the former being more severe then the later) (Kolpakova-Hart et al., 2007). The reasons between these discrepancies in ossification phenotypes

are unknown. However, in the absence of proper sternal bar fusion in the midline, two ossification centers may form on either side of the midline, causing excessive ossification (Scheuer and Black, 2004).

Shh mutants have reduced ossification, whilst *Gli3* mutants have hyperossification. Since Shh activity causes reduction of the Gli3 repressor, one could speculate that Shh activity stimulates ossification and in response, Gli3 is needed to regulate this process. Indeed, Shh ligand binding has been shown to stimulate osteogenesis in tissue culture experiments and in mouse fibroblasts transfected with *Shh* cDNA (Iwamoto et al., 1999, Kinto et al., 1997).

Interestingly, other observations in mice suggest that the phenotype of hyperossification could also be due to disregulation of FGF signaling. Gain of FGFR1 expression in mouse models leads to small fusions between ossification centers in normal 'fused' sternum; whilst gain of FGFR2 mutations have a delay in sternal bar fusion followed by more pronounced fusions of ossification centers (Hajihosseini et al., 2004, Hajihosseini et al., 2001). A mouse model of Apert syndrome with gain-of-function FGFR2 also has fusions of ossification centers (Wang et al., 2005b). Furthermore, mouse models for achondroplasia are also reported to have sternebral fusion, as do mice in which FGFR3 has been fused to the intracellular domain of FGFR1 (Wang et al., 2001). It is believed that this phenotype arises from a lack of FGFR regulation of joint segmentation resulting in hyperossification down the length of the sternum. This link between defective FGF signaling and sternal ossification has been observed in humans with Noonan syndrome, which is caused by a mutation in SH2 domain-containing protein tyrosine phosphatase (SHP-2), which a key regulator of the FGF-Ras-MAPK pathway (Hoeffel et al., 1981, Tartaglia et al., 2002).

Although there is no rescue or amelioration of the cartilaginous phenotype in *Fuzzy*$^{-/-}$*;Fgf8*$^{L/+}$ compound embryos, there are ossification similarities between Gli mutant mice, and aberrant FGF signaling described above. This raises an intriguing question of whether Gli processing may converge on

FGF signaling as is described in the maxilla of the *fuzzy* mutant. To determine this properly the link between Gli protein function and transcriptional regulation of other Fgfs in the sternum must be further assessed.

6.3.4 Final remarks

It would appear that all of the skeletal phenotypes described in this chapter arise from either abnormal FGF or Hh signaling, or a combination of both. The *Fuzzy* mutant has provided us with a model system in which, in some instances at least, defective Gli processing results in excessive FGF signaling. To date we have only shown this relationship with regards to FGF8 regulation during early brain development stages. But, time permitting, it would be interesting to examine FGF expression in the axial skeleton in the absence of Gli proteins.

A greater understanding of molecular mechanisms driving different phenotypes across the spectrum of disorders described will enable better classification of diseases. In turn, this will undoubtedly provide the opportunity for improved therapy as well as better understanding of different phenotypes to expect and classify. For example, Der Kaloustian and colleagues in 2001 describe a human patient with a variety of skeletal defects including micrognathia, a short neck, which could be caused by cervical vertebra fusions, widely spaced nipples, which could be caused from a cleft sternum, and polydactyly (Der Kaloustian et al., 2001). The authors of this paper suggest that this is a new syndrome yet to be described. Given what I have described above, I would speculate that this patient has classical hallmarks of a skeletal ciliopathy; furthermore, in the future, ciliopathy patients could be screened for defects in multiple skeletal elements including the sternum and vertebra.

Chapter 7 Final Discussion

7.1 Summary Of Observations

Observations made in this project have shed interesting light on how development of a variety of skeletal structures is affected in the ciliopathic *Fuzzy* mutant mouse. These observations are summarized as follows.

- Craniosynostosis in the *Fuzzy* mutant can be partially rescued by genetic reduction of *Fgf8*. This phenotype probably arises from loss of Gli processing causing and an upregulation of *runx2.* My data suggests different molecular causes driving craniosynostosis in FGF-related syndromes and ciliopathies.
- Vertebral chondrogenic defects in the *Fuzzy* mutant may be secondary to abnormal neural tube closure. Different ossification defects are observed between cervical and thoracic vertebra with the former showing vertebral fusions and the latter manifesting with lack of ossification centers. These differences may reflect novel defects in Gli2 processing in the *Fuzzy* mutant and the relative importance for Gli2 in development of thoracic vertebrae versus more importance for Gli3 in development of cervical vertebrae.
- Abnormal sternal bar fusion in the mutant may be due to a loss of planar cell polarity as well as defective Gli regulation of FGF signaling. Subsequent hyperossification probably occurs as a result sternal clefting.
- Abnormal elongation of endochondral elements is probably due to a loss of Gli3 repressor activity causing delayed onset of chondrocyte hypertrophic maturation.
- Analysis of micrognathia in the *Fuzzy* mutant reveals several key steps which have not previously been described in the context of mandibular elongation, including the importance of proper medio-lateral patterning; proper cell packing and chondrogenic condensation positioning in the presumptive mandible. Medio-lateral patterning, at least, is dependent on proper *Fgf8* expression. Finally, we suggest the importance of chondrocyte hypertrophy for

elongation from approximately e15.5, which is independent of abnormal FGF8 expression.

- The mandible is hyperossified in the *Fuzzy* mutant; a phenotype which has not been previously described in ciliopathies. This appears to be due to an early expansion in *runx2* expression and can be largely rescued on genetic reduction of FGF8.

7.2 Variability in the phenotypes of the *Fuzzy* mutant

The *Fuzzy* mutant provides us with a great model organism in which to study ciliopathies and downstream signaling pathways that are dysfunctional as a result of loss of cilia formation and function. The developmental defects in *Fuzzy* mutant are widespread but do not encompass all phenotypes observed in ciliopathies: in particular, defects in the motile cilia are not seen. For example, *situs inversus* is a disease in which symmetry of internal organs within the body is reversed. This is typically associated with defects in motile cilia and is established as early as nodal establishment during gastrulation (El Zein et al., 2003, Nonaka et al., 1998). This defect may not be observed in *Fuzzy* because we do not know whether or not *Fuzzy* is expressed at such early stages since the earliest expression analysis only covers e8.5-e9.5 (Seo et al., 2011). Interestingly ciliopathy patients and mouse models display varied severity in the phenotypes that arise. This probably reflects differences in the roles of affected proteins in ciliogenesis and axonemal transport. In addition to this, some cilial components are only expressed in tissue specific contexts. For example the polycystin 1 receptor is only found on the cilia of the kidney (Peters et al., 1996). As such, mutations in this gene result in polycystic kidneys but no defects in internal patterning (Karcher et al., 2005). With this logic, it could be suggested that FUZ has roles in formation of only a subset of cilia. In keeping with this suggestion, it has been seen that there is tissue specific functional roles for cilia since there is significant variability in cilial stability in different tissues, and in fact between organisms, although there is structural conservation, there is diversity in the over all ciliary proteome. It has been suggested that in addition to the core structural units of the cilium, there may be organism specific and tissue specific structural adaptations

(Ostrowski et al., 2002, Pazour et al., 2005, Smith et al., 2005). In order to assess how these factors may influence variability when comparing our phenotype with other ciliopathies, better characterization of *Fuzzy* gene expression in a variety of different tissue and in a stage series dependent manner would be beneficial.

As a general observation, one could suggest that apart from the limbs, the majority of phenotypes affected are NC derived structures. This is not surprising since *Fuzzy* expression at e9.5 is in the neural axis, which is the site of NC formation. The argument against this is that defective endochondral elements are not neural crest derived. Although *Fuzzy* expression has not yet been visualized in long bones, we would suggest that *Fuz* must be expressed in pre-hypertrophic chondrocytes. This bears further analysis.

There is also variability of phenotypes within the *Fuzzy* mutant itself. Defects in endochondral ossification appear to be consistent. However, the craniofacial malformations are more variable in their severity. Craniofacial development is an extremely complex process under the regulation of many signaling molecules. Proper formation of craniofacial structures is essential for vertebrate life and as such, there are many reports of functional redundancy between signaling molecules; for example FGF4, -8 and -9 are known to demonstrate functional redundancy during tooth development (Kettunen and Thesleff, 1998). With this in mind it is very possible that other proteins can compensate to varying degrees in the absence of the Fuzzy protein. A good example of this is Inturned (INTU), which was also first described as a PCP effector in *Drosophila,* and is structurally homologous to FUZ (Collier and Gubb, 1997, Park et al., 1996). In *Xenopus, Intu* is expressed in the same regions as *Fuzzy* and its loss also causes similar defects in neural tube closure, loss of ciliogenesis and PCP signaling (Park et al., 2006). Similarly, in the mouse, loss of *inturned* phenocopies loss of *Fuzzy* and can compensate in its absence during neural tube convergent extension but not patterning (Heydeck and Liu, 2011). This idea is given more strength when one considers that in the *Fuzzy* mutant, quantitation of

cilia reveals that they are not entirely absent and some remaining cilia are shortened. This implies that there may still by be some residual ciliary function in *Fuzzy* mutants (Zhang et al., 2011).

7.3 Implications for Glis in development

Gli2 and Gli3 can be processed into both repressor and activator forms although Gli3 conversion to a repressor, and Gli2 conversion to an activator are the most common modifications during Hh signaling. Different Gli activators and repressors work in tissue specific contexts to differentially control downstream target gene transcription. For example, the Gli3 repressor has been shown to regulate FGF gene expression in patterning of the dorsal telencephalon, in which it restricts expression of FGF -3, -15, -17 and -18, whilst in the developing limb bud it controls FGF4 (te Welscher et al., 2002b, Rash and Grove, 2007). Adding further complexity to Gli activity, in some contexts such as Gli regulation of *Runx2* expression, the total balance of Gli3 repressor and Gli2 activator ultimately controls the overall transcriptional output (Shimoyama et al., 2007, Ohba et al., 2008, Komori, 2011).

Observations made throughout this project provide examples of differential Gli regulation of different tissues. For example, I and others suggest, in the developing spine, that Gli3 may have more important roles in regulating cervical vertebral development whilst Gli2 may have more important roles in regulating thoracic vertebral development (Chapter 3 and (Mo et al., 1997)). Tissue specificity of FGF regulation of Gli3 is also apparent when comparing the mandible and the limbs of *Fuzzy*$^{-/-}$;*Fgf8*$^{L/+}$ compound mutants. The fact that we have rescue of the Meckel's cartilage but no differences in the limbs, even though FGF8 is very important in the development of both of these structures suggests that Gli misregulation only converges on aberrant *Fgf8* regulation in a tissue specific context.

One interesting question that arises from this observation is why we don't see micrognathia in *Gli3* mutant mice (Mo et al., 1997). This is especially interesting since patients with Greig cephalopolysndactyly syndrome

(GCPS), which is known to be due to a loss of function mutations in Gli3, do not have micrognathia (Debeer et al., 2007, Vortkamp et al., 1991). Gli3 mouse mutants have several phenotypes in common with the *Fuzzy* mutant including exencephaly, cleft palate, polydactyly and short long bones (Johnson, 1967). Gli3 heterozygotes alone have no obvious mandibular phenotypes however compound homozygous Gli2 and heterozygous Gli3 mutants have a truncated mandible. This probably reflects a shift in the overall activating and repressive balance of Gli2 and Gli3 transcription factors in the *Fuzzy* mutant suggesting that a fine balance of the two must exist in the developing mandible for proper formation. If this is true this suggests a previously undescribed role for Gli2 in mandibular development.

7.4 Regulation of FGFs

Our previous data has attributed loss of Gli3 repressor formation to upregulation of *FGF8* (Tabler et al., 2013). The Gli3 repressor has previously been shown to control *FGF8* expression in the first branchial arch and indeed loss of Gli3 from e9.5 through to e10.5 results in increased domains of FGF8 expression (Aoto et al., 2002).

The important role for FGF8 in early mandibular patterning has been well documented in chapters 1 and 5. In keeping with these important roles, I have attributed micrognathia in the *Fuzzy* mutant to enhanced *FGF8* expression driving abnormal medio-lateral patterning. It has been shown in mouse models with knock out of the Gli3 repressor, that craniosynostosis observed is a result of upregulation of *FGF2*, which inhibits *runx2* (Rice et al., 2010). This suggests that a subset of the phenotypes we observe may be due to Gli misregulation of general *Fgf* expression. That said, I would suggest that, since many phenotypes can be rescued by genetic reduction of *Fgf8,* this is the main ligand regulated by Gli3 in developmental contexts studied in this project. Conversely, craniosynostosis and hyperossification of the mandible were partially rescued. This could have several causes. Firstly, because the level of FGF8 reduction in *Fuzzy*$^{-/-}$;*Fgf8*$^{L/+}$ compound mutants may not be enough to alleviate FGF8 over-expression in these tissues; and secondly, due to misregulation of other FGFs regulating *Runx2* in these

tissues. In order to assess whether other Fgfs are indeed misregulated in the *Fuzzy* mutant, mutants specific for different FGFs, such as Fgf2, can be crossed with the *Fuzzy* mutant and exacerbation of amelioration of phenotypes can be assessed.

Further justifying these experiments is that fact that preliminary observations of the mutant trachea see a loss of cartilaginous rings. It has been suggested that Shh signaling activates *FGF10* expression and FGF10 acts as an activator-dependent inhibitor of Shh in order to control periodic patterning of the cartilage rings (Sala et al., 2011). In this way, one could imagine a scenario in which abnormal Gli processing in the *Fuzzy* mutant disrupts the Shh-FGF10 interaction causing loss of cartilage ring formation. This scenario is speculation and more work into understanding the nature of Shh mediated *Fgf10* regulation must be carried out in order to fully understand how and if this signaling interaction is perturbed in the *Fuzzy* mutant.

7.5 Wnt signaling defects in the *Fuzzy* mutant

Throughout this project, I have attributed many skeletal phenotypes to abnormal Gli processing and subsequent misregulation of FGF transcription. Previous reports on the *Fuzzy* mutant have also focused on its role in PCP signaling. This is logical given the subset of phenotypes which can be attributed to malfunction of this pathway, such as an abnormal outflow track of the heart, defective neural tube closure in mice, as well as loss of convergent extension seen in *Xenopus* (Gray et al., 2009, Wallingford and Harland, 2002). It is therefore possible that defective PCP signaling may be contributing to some of the phenotypes observed.

A case can also be made for PCP involvement in the mandibular malformations. We previously showed that maxillary hyperplasia is due to aberrant NCC migration into the maxillary portion of BA1 (Tabler et al., 2013). My observations on defective MC development show that abnormal medio-lateral patterning and increased cell density contribute to micrognathia by inducing precocious and out of place Meckel's cartilage

condensations, (Chapter 5). This does not address the role of abnormal NC migration into the mandibular portion of BA1 which should be considered since we showed by fluorescent activated cell sorting (FACS) analysis that there are increased numbers of NCCs in the *Fuzzy* mutant (Tabler et al., 2013).

Zebrafish embryos lacking PCP components lose chondrocyte convergent extension during cartilage outgrowth. In addition, these mutants have defects in secretion from chondrocytes, resulting in misshapen craniofacial elements (LeClair et al., 2009). Furthermore, in *Xenopus,* convergent extension is suggested to play a role in growth of Meckel's cartilage; and in addition to this, *frizzled* mutants have a slightly shorter mandible, suggesting that PCP plays a role in jaw extension but not an overriding one (Park et al., 2006, Kamel et al., 2013). With this in mind, it is possible to imagine a scenario in the *fuzzy* mutant in which defective PCP signaling or convergent extension dependent tissue movements contribute to the craniofacial phenotypes.

Earlier in development, PCP signaling is also involved in proper NC cell movement (Mayor and Theveneau, 2014). Hence, in our mutant, abnormal PCP could contribute to abnormal NC migration seen in Tabler et al. This situation seems plausible given previous observations that craniofacial abnormalities in Bardet Biedl Syndrome have been partly attributed to abnormal NC migration (Tobin et al., 2008). On the other hand, this abnormal NC migration could also arise from enhanced FGF8 chemo-attraction from the BA1 epithelium, as FGF8 has previously been suggested to play this role in cranial NC and cardiac NC cells (Kubota and Ito, 2000, Sato et al., 2011).

During abnormal development of the sternum in the *Fuzzy* mutant, we see a loss of fusion of the sternal bars. A similar phenotype is observed in mouse mutants lacking Dachsous 1 (a core PCP component) and it is suggested that this is a direct result of defective convergent extension (Mao et al., 2011). Similarly, these authors observe defects in vertebral formation, attributed to

defective convergent extension however this appears to be speculation. During development of the sternum, cartilaginous structures must move towards each other and fuse (Chapter 7). Guided tissue movements of this nature, such as neural tube closure and axon guidance, are well characterised to occur via PCP driven convergent extension (Ybot-Gonzalez et al., 2007, Wang and Nathans, 2007). Along these same lines, PCP signaling is suggested to control the organization of proliferating chondrocytes into their characteristic columns and as such, loss of *Frizzled* results in altered shape of the long bones in chick (Yang et al., 2013). Given the cellular role of Fuz and its purported roles in localization of PCP components to the cilia, it can be suggested that defective PCP signaling contributes to a subset of the phenotypes observed. Further understanding how PCP signaling is altered during the development of these structures can ultimately enable us to establish a developmental hierarchy to determine which pathways are more important in the development of different tissues and organs.

Canonical Wnt signaling is also reported to be enhanced on loss of *Fuzzy in vivo* and *in vitro* (Zilber et al., 2013, Zhang et al., 2011). As a result of this, it has been suggested that Fuz mediates canonical Wnt signaling. Since this pathway regulates *Sox9* expression, one may expect excessive cartilage formation in the *Fuzzy* mutant. Although this doesn't seem to be the case, the fact that the *Fuzzy* promoter itself has 11 binding sites for Wnt responsive elements and can physically bind to endogenous β-catenin in tissue culture, supports this theory (Zhang et al., 2011).

There are several possible explanations for this. Firstly, potential canonical Wnt hyperactivation may be below a threshold needed exert downstream effects. Secondly, the effects from other signaling changes (notably Fgf and Hh) may be so critical that effects from Wnt changes may not be as obvious. Thirdly, as discussed above, Fuz may have tissue specific roles. Consistent with this, loss of *Fuzzy* resulted in no increases in Wnt target genes in the dermal cells of mouse embryos (Dai et al., 2011). One other interesting thought is that FUZ may use b-catenin as a means of regulating its own expression. Since increased levels of b-catenin have been detected, its

possible that this could be going directly to the *Fuzzy* promoter creating a feedback loop to maintain *Fuzzy* expression (Zhang et al., 2011)

7.6 Endochondral versus intramembranous ossification

My observations in the long bones and basosphenoid of the cranial base suggest that shortening of these elements in the mutant is as a result of loss of Gli3 mediated *Ihh* expression (Chapter 4). Since elongation of all endochondral elements is mediated via this feedback loop it is not unreasonable to suggest that all of these structures are probably affected in the same way. One outstanding question with regards to defective endochondral ossification in the *Fuzzy* mutant is whether defective FGF signaling also contributes to the phenotype, given that signaling through FGFR3 is also important for regulation of chondrocyte hypertrophy and FGF8 is known to bind to this receptor in certain contexts (Jacques et al., 2007, Wilkie et al., 2002). This doesn't seem likely since none of the endochondral defects are rescued in *Fuzzy*$^{-/-}$;*Fgf8*$^{L/+}$ compound mutants. That said, the main FGF ligand that binds to FGFR3 during hypertrophic regulation are believed to be FGF18 and -9 and it cannot be ruled out that abnormal Gli processing may result in misregulation of these FGF ligands.

Taken together, these observations suggest that in our *Fuzzy* mutant, and therefore, potentially in ciliopathies, shortened endochondral skeletal elements are attributed to the role of Gli3 in the Ihh-PTHrP feedback loop. Hyperossification of intramembranous ossification can be attributed convergence of Gli transcription factors on FGF, particularly FGF8, signaling. This consideration is particularly interesting when looking at a mouse model in which the Kif3a transport complex is conditionally knocked out in cartilage only. This mutant has very similar endochondral defects to the *Fuzzy* mutant, such as shortened long bones and cranial base malformations associated with a loss of hypertrophic maturation and excess ossification of intramembranous elements (Koyama '07). Interestingly ciliopathy patients and mouse models display varied severity

and variability of which phenotypes arise. This probably reflects differential importance of affected proteins in ciliogenesis.

Intramembranous skeletal elements in the *Fuzzy* mutants all appear quite similar in their defects. Craniosynostosis is observed and both the maxilla and the mandible appear to be hyperossified (Tabler et al., 2013) & chapter 5). The fact that genetic reduction of *Fgf8* in *Fuzzy* ameliorates all of these defects suggests that aberrant FGF8 regulation is key to driving this. I showed in chapter 5 that mandibular hyperossification is associated with increased *Runx2* expression and *Runx2* overexpression has previously been associated with craniosynostosis. These observations suggest that abnormal *Runx2* activation could be driving these phenotypes. Indeed, in *Gli3* mutants, craniosynostosis associated with *Runx2* upregulation is also observed (Rice et al., 2010).

The key outstanding question, however, is whether excessive FGFR activation contributes to these phenotypes, especially given the important roles of FGFR1 and -2 in various stages of osteoblast maturation during intramembranous ossification and *Runx2* regulation (Discussed in chapter 1, section 1.3.2).

7.7 FGF syndromes versus ciliopathies and other syndromic diseases

Skeletal phenotypes observed in the *Fuzzy* mutant are observed in many different diseases and as part of several seemingly unrelated syndromes. As I have described previously, there is particular overlap between the craniosynostosis syndromes, chondrodysplasias and ciliopathies. Comparing phenotypes observed in these disorders will aid in establishing similarities between molecular causes driving these phenotypes as a means of greater understanding phenotypic overlap. For example, I suggest in chapter 4 that short long bones seen in ciliopathies are probably due to loss of Gli3 repression in the Ihh-PTHrP feedback loop whilst the molecular causes of short limbs in achondroplasias are known to be as a result of FGFR3 hyperactivation.

Finally, analyzing the phenotype of the *Fuzzy* mutant in detail may provide us with novel phenotypic criteria with which to assess ciliopathies and to better understand these syndromes. A good example of this is seen in chapter 6 in which I characterise mandibular hyperossification in the *Fuzzy* mutant, which has not previously been described in ciliopathy patients.

Overall, comparative analysis of different overlapping phenotypes will provide better molecular understanding of syndromic diseases. Comparing animal models with patient case studies, as shown in Table 1, is a powerful way to determine these links. In addition, this type of analysis can provide us with improved criteria for diagnostics of diseases, which arise from multiple complex signaling interactions.

	Affected structure						
	Skull/Face	**Palate**	**Limb/Hand**	**Vertebra**	**Rib/Thorax**	**Sternum**	**Refs.**
Ciliopathies							
Human							
Meckel	encephalocele	C	PD	?	-	-	20
Bardet-Biedl	Shape change	HA	PD, SD	scoliosis	-	-	37
Joubert	-	C?	-	Cervical fusion	-	-	28
OFD1	Shape change	HA	PD	-	-	-	20
Jeune	-	-	PD	Cervical stenosis	irregular	bulge	9, 38
Sensenbrenner	SS	HA	SL, PD	-	Short ribs	-	13, 39–41
Ellis-Van Creveld	-	-	SL, PD	-	Short ribs	-	42
Mouse Models							
Meckel: *MKS1*^{hlb614}/*MKS1*^{krc}	-	C	-	-	-	bifid, fused	35, 43
Ellis-van Creveld: *EVC*	-	-	SL	Fusions	Short ribs	-	44, 45
Orofacial Digital: *OFD1*	-	C	SL, PD	-	-	bifid, fused	46, 47
Sensenbrenner: *WDR35*	-	-	-	-	Short ribs	-	48
Ciliopathy: *Fuz*	CS	HA	SL, PD	Cervical fusion	Short ribs	Fused, bifid	14, 16–18
Craniosynostosis							
Human							
Apert	CS	HA	SD	Cervical fusion	-	-	19, 49
Crouzon	CS	HA	SL, SD	Cervical fusion	-	-	21, 50
Pfeiffer	CS	HA	SD	Cervical fusion	-	-	22, 23
Mouse Models							
Crouzon/Pfeiffer: *Fgfr2c*^{C342Y}	CS	C	-	-	-	Fused	51, 52
Pfeiffer: Tg(*Fgfr1*^{P252R})	CS	-	PD	Homeotic transformation	-	Fusions	27
Apert: *Fgfr2*$^{IIIc/\Delta}$	CS	-	-	-	-	Fused	29, 53
Apert: *Fgfr2*^{S252W}	CS	C	-	-	-	Fusions	30
Chondrodysplasia							
Human							
Chondrodysplasia punctata 2	variable	-	SL	Scoliosis fusions	calcified	calcified	20
Hypochondroplasia	variable	-	SL	stenosis	-	-	53
Thanatophoric dysplasia	-	-	SL	flattened	Short ribs	-	54
Achondroplasia	Small base	-	SL	stenosis	Small chest	-	55
Mouse Models							
Achondroplasia: *Fgfr3*^{G374R}	-	-	SL	Cervical fusion	-	-	56
Thanatophoric Dysplasia: FGFR3369	-	-	SL	-	Short ribs	-	57

Abbreviations: SS, sagittal synostosis; CS, coronal synostosis; C, cleft palate; HA, high arched palate; PD, polydactyly; SD, syndactyly; SL, short limbs

Table 1 Taken from Yannakoudakis and Liu, 2013

Table shows skeletal phenotypes seen in FGF related syndromes and ciliopathies. References indicated refer to the paper, which is in the appendix.

Chapter 8 References

ABU-ISSA, R., SMYTH, G., SMOAK, I., YAMAMURA, K. & MEYERS, E. N. 2002. Fgf8 is required for pharyngeal arch and cardiovascular development in the mouse. *Development,* 129**,** 4613-25.

ABZHANOV, A. & TABIN, C. J. 2004. Shh and Fgf8 act synergistically to drive cartilage outgrowth during cranial development. *Dev Biol,* 273**,** 134-48.

ACASTELLO, E., MAJLUF, R., GARRIDO, P., BARBOSA, L. M. & PEREDO, A. 2003. Sternal cleft: a surgical opportunity. *J Pediatr Surg,* 38**,** 178-83.

ADOLPHE, C., NIEUWENHUIS, E., VILLANI, R., LI, Z. J., KAUR, P., HUI, C. C. & WAINWRIGHT, B. J. 2014. Patched 1 and patched 2 redundancy has a key role in regulating epidermal differentiation. *J Invest Dermatol,* 134**,** 1981-90.

AGGARWAL, V. S., CARPENTER, C., FREYER, L., LIAO, J., PETTI, M. & MORROW, B. E. 2010. Mesodermal Tbx1 is required for patterning the proximal mandible in mice. *Dev Biol,* 344**,** 669-81.

AHLGREN, S. C. & BRONNER-FRASER, M. 1999. Inhibition of sonic hedgehog signaling in vivo results in craniofacial neural crest cell death. *Curr Biol,* 9**,** 1304-14.

AKIYAMA, H., CHABOISSIER, M. C., MARTIN, J. F., SCHEDL, A. & DE CROMBRUGGHE, B. 2002. The transcription factor Sox9 has essential roles in successive steps of the chondrocyte differentiation pathway and is required for expression of Sox5 and Sox6. *Genes Dev,* 16**,** 2813-28.

AKIYAMA, H., LYONS, J. P., MORI-AKIYAMA, Y., YANG, X., ZHANG, R., ZHANG, Z., DENG, J. M., TAKETO, M. M., NAKAMURA, T., BEHRINGER, R. R., MCCREA, P. D. & DE CROMBRUGGHE, B. 2004. Interactions between Sox9 and beta-catenin control chondrocyte differentiation. *Genes Dev,* 18**,** 1072-87.

ALEXIEV, B. A., LIN, X., SUN, C. C. & BRENNER, D. S. 2006. Meckel-Gruber syndrome: pathologic manifestations, minimal diagnostic criteria, and differential diagnosis. *Arch Pathol Lab Med,* 130**,** 1236-8.

ANDERSON, P. J., HALL, C., EVANS, R. D., HARKNESS, W. J., HAYWARD, R. D. & JONES, B. M. 1997. The cervical spine in Crouzon syndrome. *Spine (Phila Pa 1976),* 22**,** 402-5.

ANSLEY, S. J., BADANO, J. L., BLACQUE, O. E., HILL, J., HOSKINS, B. E., LEITCH, C. C., KIM, J. C., ROSS, A. J., EICHERS, E. R., TESLOVICH, T. M., MAH, A. K., JOHNSEN, R. C., CAVENDER, J. C., LEWIS, R. A., LEROUX, M. R., BEALES, P. L. & KATSANIS, N. 2003. Basal body dysfunction is a likely cause of pleiotropic Bardet-Biedl syndrome. *Nature,* 425**,** 628-33.

AOTO, K., NISHIMURA, T., ETO, K. & MOTOYAMA, J. 2002. Mouse GLI3 regulates Fgf8 expression and apoptosis in the developing neural tube, face, and limb bud. *Dev Biol,* 251**,** 320-32.

AYTAC, A. & SAYLAM, A. 1976. Successful surgical repair of congenital total cleft sternum with partial ectopia cordis. *Thorax,* 31**,** 466-9.

BABBS, C., FURNISS, D., MORRISS-KAY, G. M. & WILKIE, A. O. 2008. Polydactyly in the mouse mutant Doublefoot involves altered Gli3

processing and is caused by a large deletion in cis to Indian hedgehog. *Mech Dev,* 125**,** 517-26.
BACHLER, M. & NEUBUSER, A. 2001. Expression of members of the Fgf family and their receptors during midfacial development. *Mech Dev,* 100**,** 313-6.
BACINO, C. A., DHAR, S. U., BRUNETTI-PIERRI, N., LEE, B. & BONNEN, P. E. 2012. WDR35 mutation in siblings with Sensenbrenner syndrome: a ciliopathy with variable phenotype. *Am J Med Genet A,* 158A**,** 2917-24.
BALIC, A., ADAMS, D. & MINA, M. 2009. Prx1 and Prx2 cooperatively regulate the morphogenesis of the medial region of the mandibular process. *Dev Dyn,* 238**,** 2599-613.
BARLOW, A. J., BOGARDI, J. P., LADHER, R. & FRANCIS-WEST, P. H. 1999. Expression of chick Barx-1 and its differential regulation by FGF-8 and BMP signaling in the maxillary primordia. *Dev Dyn,* 214**,** 291-302.
BARLOW, A. J. & FRANCIS-WEST, P. H. 1997. Ectopic application of recombinant BMP-2 and BMP-4 can change patterning of developing chick facial primordia. *Development,* 124**,** 391-8.
BARRON, F., WOODS, C., KUHN, K., BISHOP, J., HOWARD, M. J. & CLOUTHIER, D. E. 2011. Downregulation of Dlx5 and Dlx6 expression by Hand2 is essential for initiation of tongue morphogenesis. *Development,* 138**,** 2249-59.
BARZI, M., BERENGUER, J., MENENDEZ, A., ALVAREZ-RODRIGUEZ, R. & PONS, S. 2010. Sonic-hedgehog-mediated proliferation requires the localization of PKA to the cilium base. *J Cell Sci,* 123**,** 62-9.
BAUD'HUIN, M., DUPLOMB, L., RUIZ VELASCO, C., FORTUN, Y., HEYMANN, D. & PADRINES, M. 2007. Key roles of the OPG-RANK-RANKL system in bone oncology. *Expert Rev Anticancer Ther,* 7**,** 221-32.
BEALES, P. L., ELCIOGLU, N., WOOLF, A. S., PARKER, D. & FLINTER, F. A. 1999. New criteria for improved diagnosis of Bardet-Biedl syndrome: results of a population survey. *J Med Genet,* 36**,** 437-46.
BEALES, P. L., WARNER, A. M., HITMAN, G. A., THAKKER, R. & FLINTER, F. A. 1997. Bardet-Biedl syndrome: a molecular and phenotypic study of 18 families. *J Med Genet,* 34**,** 92-8.
BEENKEN, A. & MOHAMMADI, M. 2009. The FGF family: biology, pathophysiology and therapy. *Nat Rev Drug Discov,* 8**,** 235-53.
BEI, M. & MAAS, R. 1998. FGFs and BMP4 induce both Msx1-independent and Msx1-dependent signaling pathways in early tooth development. *Development,* 125**,** 4325-33.
BELL, D. M., LEUNG, K. K., WHEATLEY, S. C., NG, L. J., ZHOU, S., LING, K. W., SHAM, M. H., KOOPMAN, P., TAM, P. P. & CHEAH, K. S. 1997. SOX9 directly regulates the type-II collagen gene. *Nat Genet,* 16**,** 174-8.
BELLUCI, M. M., SCHOENMAKER, T., ROSSA-JUNIOR, C., ORRICO, S. R., DE VRIES, T. J. & EVERTS, V. 2013. Magnesium deficiency results in an increased formation of osteoclasts. *J Nutr Biochem,* 24**,** 1488-98.
BELLUS, G. A., MCINTOSH, I., SMITH, E. A., AYLSWORTH, A. S., KAITILA, I., HORTON, W. A., GREENHAW, G. A., HECHT, J. T. & FRANCOMANO, C. A. 1995. A recurrent mutation in the tyrosine kinase domain of fibroblast growth factor receptor 3 causes hypochondroplasia. *Nat Genet,* 10**,** 357-9.

BELLUSCI, S., GRINDLEY, J., EMOTO, H., ITOH, N. & HOGAN, B. L. 1997. Fibroblast growth factor 10 (FGF10) and branching morphogenesis in the embryonic mouse lung. *Development,* 124**,** 4867-78.
BENNETT, C. N., OUYANG, H., MA, Y. L., ZENG, Q., GERIN, I., SOUSA, K. M., LANE, T. F., KRISHNAN, V., HANKENSON, K. D. & MACDOUGALD, O. A. 2007. Wnt10b increases postnatal bone formation by enhancing osteoblast differentiation. *J Bone Miner Res,* 22**,** 1924-32.
BERNARD, P., TANG, P., LIU, S., DEWING, P., HARLEY, V. R. & VILAIN, E. 2003. Dimerization of SOX9 is required for chondrogenesis, but not for sex determination. *Hum Mol Genet,* 12**,** 1755-65.
BERNHARDT, L. C., MEYER, T. & YOUNG, W. P. 1968. Bifid sternum. Case report and surgical management. *J Thorac Cardiovasc Surg,* 55**,** 758-60.
BHASKAR, S. N., WEINMANN, J. P. & SCHOUR, I. 1953. Role of Meckel's cartilage in the development and growth of the rat mandible. *J Dent Res,* 32**,** 398-410.
BISWAS, A., GHOSH, J. K., SINHA, M. K., BASU, K. & CHATTERJEE, S. 2009. Mohr-Claussen syndrome or oro-facial-digital syndrome (OFDS) type-II. *J Pak Med Assoc,* 59**,** 484-6.
BOSE, J., GROTEWOLD, L. & RUTHER, U. 2002. Pallister-Hall syndrome phenotype in mice mutant for Gli3. *Hum Mol Genet,* 11**,** 1129-35.
BOULET, A. M., MOON, A. M., ARENKIEL, B. R. & CAPECCHI, M. R. 2004. The roles of Fgf4 and Fgf8 in limb bud initiation and outgrowth. *Dev Biol,* 273**,** 361-72.
BOYDEN, L. M., MAO, J., BELSKY, J., MITZNER, L., FARHI, A., MITNICK, M. A., WU, D., INSOGNA, K. & LIFTON, R. P. 2002. High bone density due to a mutation in LDL-receptor-related protein 5. *N Engl J Med,* 346**,** 1513-21.
BRAND-SABERI, B. & CHRIST, B. 2000. Evolution and development of distinct cell lineages derived from somites. *Curr Top Dev Biol,* 48**,** 1-42.
BRENT, A. E., SCHWEITZER, R. & TABIN, C. J. 2003. A somitic compartment of tendon progenitors. *Cell,* 113**,** 235-48.
BRENT, A. E. & TABIN, C. J. 2004. FGF acts directly on the somitic tendon progenitors through the Ets transcription factors Pea3 and Erm to regulate scleraxis expression. *Development,* 131**,** 3885-96.
BRESNICK, S. & SCHENDEL, S. 1995. Crouzon's disease correlates with low fibroblastic growth factor receptor activity in stenosed cranial sutures. *J Craniofac Surg,* 6**,** 245-8.
BRESNICK, S. & SCHENDEL, S. 1998. Apert's syndrome correlates with low fibroblast growth factor receptor activity in stenosed cranial sutures. *J Craniofac Surg,* 9**,** 92-5.
BRISCOE, J. & THEROND, P. P. 2013. The mechanisms of Hedgehog signalling and its roles in development and disease. *Nat Rev Mol Cell Biol,* 14**,** 416-29.
BRITTO, J. A., CHAN, J. C., EVANS, R. D., HAYWARD, R. D., THOROGOOD, P. & JONES, B. M. 1998. Fibroblast growth factor receptors are expressed in craniosynostotic sutures. *Plast Reconstr Surg,* 101**,** 540-3.
BRITTO, J. A., EVANS, R. D., HAYWARD, R. D. & JONES, B. M. 2001. From genotype to phenotype: the differential expression of FGF, FGFR, and TGFbeta genes characterizes human cranioskeletal development and

reflects clinical presentation in FGFR syndromes. *Plast Reconstr Surg,* 108**,** 2026-39; discussion 2040-6.
BRODIE, S. G. & DENG, C. X. 2003. Mouse models orthologous to FGFR3-related skeletal dysplasias. *Pediatr Pathol Mol Med,* 22**,** 87-103.
BROOKS, E. R. & WALLINGFORD, J. B. 2012. Control of vertebrate intraflagellar transport by the planar cell polarity effector Fuz. *J Cell Biol,* 198**,** 37-45.
BROOKS, E. R. & WALLINGFORD, J. B. 2013. The Small GTPase Rsg1 is important for the cytoplasmic localization and axonemal dynamics of intraflagellar transport proteins. *Cilia,* 2**,** 13.
BRUGMANN, S. A., CORDERO, D. R. & HELMS, J. A. 2010. Craniofacial ciliopathies: A new classification for craniofacial disorders. *Am J Med Genet A,* 152A**,** 2995-3006.
BUMCROT, D. A., TAKADA, R. & MCMAHON, A. P. 1995. Proteolytic processing yields two secreted forms of sonic hedgehog. *Mol Cell Biol,* 15**,** 2294-303.
BUNTINX, I. M., WILLEMS, P. J., SPITAELS, S. E., VAN REEMPST, P. J., DE PAEPE, A. M. & DUMON, J. E. 1991. Neonatal Marfan syndrome with congenital arachnodactyly, flexion contractures, and severe cardiac valve insufficiency. *J Med Genet,* 28**,** 267-73.
BUTLER, P., MITCHEL, A. & HEALY, J. C. 2012. *Applied Radilogical Anatomy,* Cmbridge, University Press.
BUTTITTA, L., MO, R., HUI, C. C. & FAN, C. M. 2003. Interplays of Gli2 and Gli3 and their requirement in mediating Shh-dependent sclerotome induction. *Development,* 130**,** 6233-43.
CANTRELL, J. R., HALLER, J. A. & RAVITCH, M. M. 1958. A syndrome of congenital defects involving the abdominal wall, sternum, diaphragm, pericardium, and heart. *Surg Gynecol Obstet,* 107**,** 602-14.
CASCI, T., VINOS, J. & FREEMAN, M. 1999. Sprouty, an intracellular inhibitor of Ras signaling. *Cell,* 96**,** 655-65.
CHAI, Y., JIANG, X., ITO, Y., BRINGAS, P., JR., HAN, J., ROWITCH, D. H., SORIANO, P., MCMAHON, A. P. & SUCOV, H. M. 2000. Fate of the mammalian cranial neural crest during tooth and mandibular morphogenesis. *Development,* 127**,** 1671-9.
CHAMOUN, Z., MANN, R. K., NELLEN, D., VON KESSLER, D. P., BELLOTTO, M., BEACHY, P. A. & BASLER, K. 2001. Skinny hedgehog, an acyltransferase required for palmitoylation and activity of the hedgehog signal. *Science,* 293**,** 2080-4.
CHEN, J. M. 1952. Studies on the morphogenesis of the mouse sternum. II. Experiments on the origin of the sternum and its capacity for self-differentiation in vitro. *J Anat,* 86**,** 387-401.
CHEN, L., ADAR, R., YANG, X., MONSONEGO, E. O., LI, C., HAUSCHKA, P. V., YAYON, A. & DENG, C. X. 1999. Gly369Cys mutation in mouse FGFR3 causes achondroplasia by affecting both chondrogenesis and osteogenesis. *J Clin Invest,* 104**,** 1517-25.
CHEN, L., LI, C., QIAO, W., XU, X. & DENG, C. 2001. A Ser(365)-->Cys mutation of fibroblast growth factor receptor 3 in mouse downregulates Ihh/PTHrP signals and causes severe achondroplasia. *Hum Mol Genet,* 10**,** 457-65.
CHEN, M. H., WILSON, C. W., LI, Y. J., LAW, K. K., LU, C. S., GACAYAN, R., ZHANG, X., HUI, C. C. & CHUANG, P. T. 2009. Cilium-independent

regulation of Gli protein function by Sufu in Hedgehog signaling is evolutionarily conserved. *Genes Dev,* 23**,** 1910-28.
CHENG, A. & GENEVER, P. G. 2010. SOX9 determines RUNX2 transactivity by directing intracellular degradation. *J Bone Miner Res,* 25**,** 2680-9.
CHEUNG, J. O., GRANT, M. E., JONES, C. J., HOYLAND, J. A., FREEMONT, A. J. & HILLARBY, M. C. 2003. Apoptosis of terminal hypertrophic chondrocytes in an in vitro model of endochondral ossification. *J Pathol,* 201**,** 496-503.
CHIANG, C., LITINGTUNG, Y., HARRIS, M. P., SIMANDL, B. K., LI, Y., BEACHY, P. A. & FALLON, J. F. 2001. Manifestation of the limb prepattern: limb development in the absence of sonic hedgehog function. *Dev Biol,* 236**,** 421-35.
CHRIST, B. & ORDAHL, C. P. 1995. Early stages of chick somite development. *Anat Embryol (Berl),* 191**,** 381-96.
CHUNG, K. S., PARK, H. H., TING, K., TAKITA, H., APTE, S. S., KUBOKI, Y. & NISHIMURA, I. 1995. Modulated expression of type X collagen in Meckel's cartilage with different developmental fates. *Dev Biol,* 170**,** 387-96.
CHUNG, U. I., SCHIPANI, E., MCMAHON, A. P. & KRONENBERG, H. M. 2001. Indian hedgehog couples chondrogenesis to osteogenesis in endochondral bone development. *J Clin Invest,* 107**,** 295-304.
CLARK, A. M., GARLAND, K. K. & RUSSELL, L. D. 2000. Desert hedgehog (Dhh) gene is required in the mouse testis for formation of adult-type Leydig cells and normal development of peritubular cells and seminiferous tubules. *Biol Reprod,* 63**,** 1825-38.
CLARKE, B. 2008. Normal bone anatomy and physiology. *Clin J Am Soc Nephrol,* 3 Suppl 3**,** S131-9.
CLEMENT, V., SANCHEZ, P., DE TRIBOLET, N., RADOVANOVIC, I. & RUIZ I ALTABA, A. 2007. HEDGEHOG-GLI1 signaling regulates human glioma growth, cancer stem cell self-renewal, and tumorigenicity. *Curr Biol,* 17**,** 165-72.
COBOURNE, M. T., HARDCASTLE, Z. & SHARPE, P. T. 2001. Sonic hedgehog regulates epithelial proliferation and cell survival in the developing tooth germ. *J Dent Res,* 80**,** 1974-9.
COBOURNE, M. T., MILETICH, I. & SHARPE, P. T. 2004. Restriction of sonic hedgehog signalling during early tooth development. *Development,* 131**,** 2875-85.
COBOURNE, M. T. & SHARPE, P. T. 2003. Tooth and jaw: molecular mechanisms of patterning in the first branchial arch. *Arch Oral Biol,* 48**,** 1-14.
COHEN, M. M., JR. 1998. Achondroplasia, hypochondroplasia and thanatophoric dysplasia: clinically related skeletal dysplasias that are also related at the molecular level. *Int J Oral Maxillofac Surg,* 27**,** 451-5.
COHEN, M. M., JR. & KREIBORG, S. 1993. Skeletal abnormalities in the Apert syndrome. *Am J Med Genet,* 47**,** 624-32.
COHEN, M. M., JR., WALKER, G. F. & PHILLIPS, C. 1985. A morphometric analysis of the craniofacial configuration in achondroplasia. *J Craniofac Genet Dev Biol Suppl,* 1**,** 139-65.
COHN, M. J. & TICKLE, C. 1996. Limbs: a model for pattern formation within the vertebrate body plan. *Trends Genet,* 12**,** 253-7.

COLLIER, S. & GUBB, D. 1997. Drosophila tissue polarity requires the cell-autonomous activity of the fuzzy gene, which encodes a novel transmembrane protein. *Development,* 124**,** 4029-37.
COLNOT, C., DE LA FUENTE, L., HUANG, S., HU, D., LU, C., ST-JACQUES, B. & HELMS, J. A. 2005. Indian hedgehog synchronizes skeletal angiogenesis and perichondrial maturation with cartilage development. *Development,* 132**,** 1057-67.
COMPAGNI, A., LOGAN, M., KLEIN, R. & ADAMS, R. H. 2003. Control of skeletal patterning by ephrinB1-EphB interactions. *Dev Cell,* 5**,** 217-30.
CONG, F., SCHWEIZER, L. & VARMUS, H. 2004. Wnt signals across the plasma membrane to activate the beta-catenin pathway by forming oligomers containing its receptors, Frizzled and LRP. *Development,* 131**,** 5103-15.
COPEL, J. A., D'ALTON, M. E., GRATACOS, E., PLATT, L. D., TUTSCHEK, B., FELTOVICH, H. & ODIBO, A. O. 2012. *Obstetric Imaging,* San Diego, Elsevier.
CROSSLEY, P. H. & MARTIN, G. R. 1995. The mouse Fgf8 gene encodes a family of polypeptides and is expressed in regions that direct outgrowth and patterning in the developing embryo. *Development,* 121**,** 439-51.
CRUMP, J. G., MAVES, L., LAWSON, N. D., WEINSTEIN, B. M. & KIMMEL, C. B. 2004. An essential role for Fgfs in endodermal pouch formation influences later craniofacial skeletal patterning. *Development,* 131**,** 5703-16.
DAI, D., ZHU, H., WLODARCZYK, B., ZHANG, L., LI, L., LI, A. G., FINNELL, R. H., ROOP, D. R. & CHEN, J. 2011. Fuz controls the morphogenesis and differentiation of hair follicles through the formation of primary cilia. *J Invest Dermatol,* 131**,** 302-10.
DAVID, A., BITOUN, P., LACOMBE, D., LAMBERT, J. C., NIVELON, A., VIGNERON, J. & VERLOES, A. 1999. Hydrometrocolpos and polydactyly: a common neonatal presentation of Bardet-Biedl and McKusick-Kaufman syndromes. *J Med Genet,* 36**,** 599-603.
DAY, T. F., GUO, X., GARRETT-BEAL, L. & YANG, Y. 2005. Wnt/beta-catenin signaling in mesenchymal progenitors controls osteoblast and chondrocyte differentiation during vertebrate skeletogenesis. *Dev Cell,* 8**,** 739-50.
DE POLLACK, C., RENIER, D., HOTT, M. & MARIE, P. J. 1996. Increased bone formation and osteoblastic cell phenotype in premature cranial suture ossification (craniosynostosis). *J Bone Miner Res,* 11**,** 401-7.
DEBEER, P., DEVRIENDT, K., DE SMET, L., DERAVEL, T., GONZALEZ-MENESES, A., GRZESCHIK, K. H. & FRYNS, J. P. 2007. The spectrum of hand and foot malformations in patients with Greig cephalopolysyndactyly. *J Child Orthop,* 1**,** 143-50.
DELEZOIDE, A. L., BENOIST-LASSELIN, C., LEGEAI-MALLET, L., LE MERRER, M., MUNNICH, A., VEKEMANS, M. & BONAVENTURE, J. 1998. Spatio-temporal expression of FGFR 1, 2 and 3 genes during human embryo-fetal ossification. *Mech Dev,* 77**,** 19-30.
DER KALOUSTIAN, V. M., PELLETIER, M., COSTA, T., BLACKSTON, D. R. & OUDJHANE, K. 2001. A new syndrome with craniofacial and skeletal dysmorphisms and developmental delay. *Clin Dysmorphol,* 10**,** 87-93.

DIMIDSCHSTEIN, J., PASSANTE, L., DUFOUR, A., VAN DEN AMEELE, J., TIBERI, L., HRECHDAKIAN, T., ADAMS, R., KLEIN, R., LIE, D. C., JOSSIN, Y. & VANDERHAEGHEN, P. 2013. Ephrin-B1 controls the columnar distribution of cortical pyramidal neurons by restricting their tangential migration. *Neuron,* 79**,** 1123-35.

DINNO, N., SHEARER, L. & WEISSKOPF, B. 1976. Chondrodysplastic dwarfism, cleft palate and micrognathia in a neonate, a new syndrome? *European Journal of Pediatrics,* 123**,** 39-42.

DOCKTER, J. L. & ORDAHL, C. P. 1998. Determination of sclerotome to the cartilage fate. *Development,* 125**,** 2113-24.

DRISSI, H., LUC, Q., SHAKOORI, R., CHUVA DE SOUSA LOPES, S., CHOI, J. Y., TERRY, A., HU, M., JONES, S., NEIL, J. C., LIAN, J. B., STEIN, J. L., VAN WIJNEN, A. J. & STEIN, G. S. 2000. Transcriptional autoregulation of the bone related CBFA1/RUNX2 gene. *J Cell Physiol,* 184**,** 341-50.

DUBAND, J. L., MONIER, F., DELANNET, M. & NEWGREEN, D. 1995. Epithelium-mesenchyme transition during neural crest development. *Acta Anat (Basel),* 154**,** 63-78.

DUBOC, V. & LOGAN, M. P. 2011. Regulation of limb bud initiation and limb-type morphology. *Dev Dyn,* 240**,** 1017-27.

DUCY, P., ZHANG, R., GEOFFROY, V., RIDALL, A. L. & KARSENTY, G. 1997. Osf2/Cbfa1: a transcriptional activator of osteoblast differentiation. *Cell,* 89**,** 747-54.

DY, P., WANG, W., BHATTARAM, P., WANG, Q., WANG, L., BALLOCK, R. T. & LEFEBVRE, V. 2012. Sox9 directs hypertrophic maturation and blocks osteoblast differentiation of growth plate chondrocytes. *Dev Cell,* 22**,** 597-609.

EL ZEIN, L., OMRAN, H. & BOUVAGNET, P. 2003. Lateralization defects and ciliary dyskinesia: lessons from algae. *Trends Genet,* 19**,** 162-7.

ELEJALDE, B. R. & DE ELEJALDE, M. M. 1985. Thanatophoric dysplasia: fetal manifestations and prenatal diagnosis. *Am J Med Genet,* 22**,** 669-83.

ENGSTROM, H. 1951. The structure of tracheal cilia. *Acta Otolaryngol,* 39**,** 364-6.

ENLOW, D. H. 1962. Functions of the Haversian system. *Am J Anat,* 110**,** 269-305.

ESTIVAL, A., MONZAT, V., MIQUEL, K., GAUBERT, F., HOLLANDE, E., KORC, M., VAYSSE, N. & CLEMENTE, F. 1996. Differential regulation of fibroblast growth factor (FGF) receptor-1 mRNA and protein by two molecular forms of basic FGF. Modulation of FGFR-1 mRNA stability. *J Biol Chem,* 271**,** 5663-70.

ETHERIDGE, S. L., RAY, S., LI, S., HAMBLET, N. S., LIJAM, N., TSANG, M., GREER, J., KARDOS, N., WANG, J., SUSSMAN, D. J., CHEN, P. & WYNSHAW-BORIS, A. 2008. Murine dishevelled 3 functions in redundant pathways with dishevelled 1 and 2 in normal cardiac outflow tract, cochlea, and neural tube development. *PLoS Genet,* 4**,** e1000259.

FELDHAHN, N., FERRETTI, E., ROBBIANI, D. F., CALLEN, E., DEROUBAIX, S., SELLERI, L., NUSSENZWEIG, A. & NUSSENZWEIG, M. C. 2012. The hSSB1 orthologue Obfc2b is essential for skeletogenesis but dispensable for the DNA damage response in vivo. *EMBO J,* 31**,** 4045-56.

FERGUSON, C. A., TUCKER, A. S. & SHARPE, P. T. 2000. Temporospatial cell interactions regulating mandibular and maxillary arch patterning. *Development,* 127**,** 403-12.
FERRANTE, M. I., ZULLO, A., BARRA, A., BIMONTE, S., MESSADDEQ, N., STUDER, M., DOLLE, P. & FRANCO, B. 2006. Oral-facial-digital type I protein is required for primary cilia formation and left-right axis specification. *Nat Genet,* 38**,** 112-7.
FISH, J. L., SKLAR, R. S., WORONOWICZ, K. C. & SCHNEIDER, R. A. 2014. Multiple developmental mechanisms regulate species-specific jaw size. *Development,* 141**,** 674-84.
FOLDYNOVA-TRANTIRKOVA, S., WILCOX, W. R. & KREJCI, P. 2012. Sixteen years and counting: the current understanding of fibroblast growth factor receptor 3 (FGFR3) signaling in skeletal dysplasias. *Hum Mutat,* 33**,** 29-41.
FROMMER, J. & MARGOLIES, M. R. 1971. Contribution of Meckel's cartilage to ossification of the mandible in mice. *J Dent Res,* 50**,** 1260-7.
FUMOTO, K., HOOGENRAAD, C. C. & KIKUCHI, A. 2006. GSK-3beta-regulated interaction of BICD with dynein is involved in microtubule anchorage at centrosome. *EMBO J,* 25**,** 5670-82.
FUNATO, N., CHAPMAN, S. L., MCKEE, M. D., FUNATO, H., MORRIS, J. A., SHELTON, J. M., RICHARDSON, J. A. & YANAGISAWA, H. 2009. Hand2 controls osteoblast differentiation in the branchial arch by inhibiting DNA binding of Runx2. *Development,* 136**,** 615-25.
GALLERA, J. 1971. Primary induction in birds. *Adv Morphog,* 9**,** 149-80.
GALLET, A., RUEL, L., STACCINI-LAVENANT, L. & THEROND, P. P. 2006. Cholesterol modification is necessary for controlled planar long-range activity of Hedgehog in Drosophila epithelia. *Development,* 133**,** 407-18.
GALVIN, B. D., HART, K. C., MEYER, A. N., WEBSTER, M. K. & DONOGHUE, D. J. 1996. Constitutive receptor activation by Crouzon syndrome mutations in fibroblast growth factor receptor (FGFR)2 and FGFR2/Neu chimeras. *Proc Natl Acad Sci U S A,* 93**,** 7894-9.
GANGOPADHYAY, N., MENDONCA, D. A. & WOO, A. S. 2012. Pierre robin sequence. *Semin Plast Surg,* 26**,** 76-82.
GAO, B., SONG, H., BISHOP, K., ELLIOT, G., GARRETT, L., ENGLISH, M. A., ANDRE, P., ROBINSON, J., SOOD, R., MINAMI, Y., ECONOMIDES, A. N. & YANG, Y. 2011. Wnt signaling gradients establish planar cell polarity by inducing Vangl2 phosphorylation through Ror2. *Dev Cell,* 20**,** 163-76.
GAO, C. & CHEN, Y. G. 2010. Dishevelled: The hub of Wnt signaling. *Cell Signal,* 22**,** 717-27.
GARZON-ALVARADO, D. A., GUTIERREZ, M. L. & CALIXTO, L. F. 2014. A computational model of clavicle bone formation: a mechano-biochemical hypothesis. *Bone,* 61**,** 132-7.
GEORGOULIS, G., ALEXIOU, G. & PRODROMOU, N. 2011. Achondroplasia with synostosis of multiple sutures. *Am J Med Genet A,* 155A**,** 1969-71.
GILBERT, S. F. 2006. *Developmental Biology,* Massachusets USA, Sinaur Associates Inc.
GOETZ, R. & MOHAMMADI, M. 2013. Exploring mechanisms of FGF signalling through the lens of structural biology. *Nat Rev Mol Cell Biol,* 14**,** 166-80.

GOETZ, R., NAKADA, Y., HU, M. C., KUROSU, H., WANG, L., NAKATANI, T., SHI, M., ELISEENKOVA, A. V., RAZZAQUE, M. S., MOE, O. W., KURO-O, M. & MOHAMMADI, M. 2010. Isolated C-terminal tail of FGF23 alleviates hypophosphatemia by inhibiting FGF23-FGFR-Klotho complex formation. *Proc Natl Acad Sci U S A,* 107**,** 407-12.

GOETZ, S. C. & ANDERSON, K. V. 2010. The primary cilium: a signalling centre during vertebrate development. *Nat Rev Genet,* 11**,** 331-44.

GOLDFARB, M. 2005. Fibroblast growth factor homologous factors: evolution, structure, and function. *Cytokine Growth Factor Rev,* 16**,** 215-20.

GOLDRING, M. B., TSUCHIMOCHI, K. & IJIRI, K. 2006. The control of chondrogenesis. *J Cell Biochem,* 97**,** 33-44.

GOULDING, M., LUMSDEN, A. & PAQUETTE, A. J. 1994. Regulation of Pax-3 expression in the dermomyotome and its role in muscle development. *Development,* 120**,** 957-71.

GRAY, R. S., ABITUA, P. B., WLODARCZYK, B. J., SZABO-ROGERS, H. L., BLANCHARD, O., LEE, I., WEISS, G. S., LIU, K. J., MARCOTTE, E. M., WALLINGFORD, J. B. & FINNELL, R. H. 2009. The planar cell polarity effector Fuz is essential for targeted membrane trafficking, ciliogenesis and mouse embryonic development. *Nat Cell Biol,* 11**,** 1225-32.

GRIGORYAN, T., WEND, P., KLAUS, A. & BIRCHMEIER, W. 2008. Deciphering the function of canonical Wnt signals in development and disease: conditional loss- and gain-of-function mutations of beta-catenin in mice. *Genes Dev,* 22**,** 2308-41.

GRILLO, L., GRECO, D., PETTINATO, R., AVOLA, E., POTENZA, N., CASTIGLIA, L., SPALLETTA, A., AMATA, S., DI BENEDETTO, D., LUCIANO, D., ROMANO, C. & FICHERA, M. 2014. Increased FGF3 and FGF4 gene dosage is a risk factor for craniosynostosis. *Gene,* 534**,** 435-9.

GUYOT, M. C., BOSOI, C. M., KHARFALLAH, F., REYNOLDS, A., DRAPEAU, P., JUSTICE, M., GROS, P. & KIBAR, Z. 2011. A novel hypomorphic Looptail allele at the planar cell polarity Vangl2 gene. *Dev Dyn,* 240**,** 839-49.

HAJIHOSSEINI, M. K., LALIOTI, M. D., ARTHAUD, S., BURGAR, H. R., BROWN, J. M., TWIGG, S. R., WILKIE, A. O. & HEATH, J. K. 2004. Skeletal development is regulated by fibroblast growth factor receptor 1 signalling dynamics. *Development,* 131**,** 325-35.

HAJIHOSSEINI, M. K., WILSON, S., DE MOERLOOZE, L. & DICKSON, C. 2001. A splicing switch and gain-of-function mutation in FgfR2-IIIc hemizygotes causes Apert/Pfeiffer-syndrome-like phenotypes. *Proc Natl Acad Sci U S A,* 98**,** 3855-60.

HALBERT, S. A., TAM, P. Y., ADAMS, R. J. & BLANDAU, R. J. 1976. An analysis of the mechanisms of egg transport in the ampulla of the rabbit oviduct. *Gynecol Invest,* 7**,** 306-20.

HALL, B. K. 2005. *Bones and Cartilage,* San Diego, Elsevier.

HALL, B. K. & MIYAKE, T. 1992. The membranous skeleton: the role of cell condensations in vertebrate skeletogenesis. *Anat Embryol (Berl),* 186**,** 107-24.

HALL, B. K. & MIYAKE, T. 2000. All for one and one for all: condensations and the initiation of skeletal development. *Bioessays,* 22**,** 138-47.

HAMBLET, N. S., LIJAM, N., RUIZ-LOZANO, P., WANG, J., YANG, Y., LUO, Z., MEI, L., CHIEN, K. R., SUSSMAN, D. J. & WYNSHAW-BORIS, A. 2002. Dishevelled 2 is essential for cardiac outflow tract development, somite segmentation and neural tube closure. *Development,* 129**,** 5827-38.

HAN, Y. & LEFEBVRE, V. 2008. L-Sox5 and Sox6 drive expression of the aggrecan gene in cartilage by securing binding of Sox9 to a far-upstream enhancer. *Mol Cell Biol,* 28**,** 4999-5013.

HAN, Y. M., KANG, G. M., BYUN, K., KO, H. W., KIM, J., SHIN, M. S., KIM, H. K., GIL, S. Y., YU, J. H., LEE, B. & KIM, M. S. 2014. Leptin-promoted cilia assembly is critical for normal energy balance. *J Clin Invest,* 124**,** 2193-7.

HARADA, Y. & ISHIZEKI, K. 1998. Evidence for transformation of chondrocytes and site-specific resorption during the degradation of Meckel's cartilage. *Anat Embryol (Berl),* 197**,** 439-50.

HAVENS, B. A., VELONIS, D., KRONENBERG, M. S., LICHTLER, A. C., OLIVER, B. & MINA, M. 2008. Roles of FGFR3 during morphogenesis of Meckel's cartilage and mandibular bones. *Dev Biol,* 316**,** 336-49.

HAWORTH, K. E., WILSON, J. M., GREVELLEC, A., COBOURNE, M. T., HEALY, C., HELMS, J. A., SHARPE, P. T. & TUCKER, A. S. 2007. Sonic hedgehog in the pharyngeal endoderm controls arch pattern via regulation of Fgf8 in head ectoderm. *Dev Biol,* 303**,** 244-58.

HAYCRAFT, C. J. & SERRA, R. 2008. Cilia involvement in patterning and maintenance of the skeleton. *Curr Top Dev Biol,* 85**,** 303-32.

HE, X., SAINT-JEANNET, J. P., WANG, Y., NATHANS, J., DAWID, I. & VARMUS, H. 1997. A member of the Frizzled protein family mediating axis induction by Wnt-5A. *Science,* 275**,** 1652-4.

HEALY, C., UWANOGHO, D. & SHARPE, P. T. 1999. Regulation and role of Sox9 in cartilage formation. *Dev Dyn,* 215**,** 69-78.

HEMMER, K. M., MCALISTER, W. H. & MARSH, J. L. 1987. Cervical spine anomalies in the craniosynostosis syndromes. *Cleft Palate J,* 24**,** 328-33.

HEYDECK, W. & LIU, A. 2011. PCP effector proteins inturned and fuzzy play nonredundant roles in the patterning but not convergent extension of mammalian neural tube. *Dev Dyn,* 240**,** 1938-48.

HEYDECK, W., ZENG, H. & LIU, A. 2009. Planar cell polarity effector gene Fuzzy regulates cilia formation and Hedgehog signal transduction in mouse. *Dev Dyn,* 238**,** 3035-42.

HO, A. & DOWDY, S. F. 2002. Regulation of G(1) cell-cycle progression by oncogenes and tumor suppressor genes. *Curr Opin Genet Dev,* 12**,** 47-52.

HOEFFEL, J. C., PERNOT, C. & JUNCKER, P. 1981. Radiologic patterns of the sternum in Noonan's syndrome with congenital heart defect. *Am J Dis Child,* 135**,** 1044-6.

HSIEH, Y. Y., CHANG, C. C., TSAI, H. D., YANG, T. C., LEE, C. C. & TSAI, C. H. 1999. The prenatal diagnosis of Pierre-Robin sequence. *Prenat Diagn,* 19**,** 567-9.

HU, D. & HELMS, J. A. 1999. The role of sonic hedgehog in normal and abnormal craniofacial morphogenesis. *Development,* 126**,** 4873-84.

HUANGFU, D. & ANDERSON, K. V. 2005. Cilia and Hedgehog responsiveness in the mouse. *Proc Natl Acad Sci U S A,* 102**,** 11325-30.

HUANGFU, D., LIU, A., RAKEMAN, A. S., MURCIA, N. S., NISWANDER, L. & ANDERSON, K. V. 2003. Hedgehog signalling in the mouse requires intraflagellar transport proteins. *Nature,* 426**,** 83-7.
HUGHES, S. E. 1997. Differential expression of the fibroblast growth factor receptor (FGFR) multigene family in normal human adult tissues. *J Histochem Cytochem,* 45**,** 1005-19.
HUI, C. C. & JOYNER, A. L. 1993. A mouse model of greig cephalopolysyndactyly syndrome: the extra-toesJ mutation contains an intragenic deletion of the Gli3 gene. *Nat Genet,* 3**,** 241-6.
HUMKE, E. W., DORN, K. V., MILENKOVIC, L., SCOTT, M. P. & ROHATGI, R. 2010. The output of Hedgehog signaling is controlled by the dynamic association between Suppressor of Fused and the Gli proteins. *Genes Dev,* 24**,** 670-82.
HUNG, I. H., YU, K., LAVINE, K. J. & ORNITZ, D. M. 2007. FGF9 regulates early hypertrophic chondrocyte differentiation and skeletal vascularization in the developing stylopod. *Dev Biol,* 307**,** 300-13.
IBRAHIMI, O. A., ZHANG, F., ELISEENKOVA, A. V., LINHARDT, R. J. & MOHAMMADI, M. 2004. Proline to arginine mutations in FGF receptors 1 and 3 result in Pfeiffer and Muenke craniosynostosis syndromes through enhancement of FGF binding affinity. *Hum Mol Genet,* 13**,** 69-78.
ILAGAN, R., ABU-ISSA, R., BROWN, D., YANG, Y. P., JIAO, K., SCHWARTZ, R. J., KLINGENSMITH, J. & MEYERS, E. N. 2006. Fgf8 is required for anterior heart field development. *Development,* 133**,** 2435-45.
INMAN, K. E., PURCELL, P., KUME, T. & TRAINOR, P. A. 2013. Interaction between Foxc1 and Fgf8 during mammalian jaw patterning and in the pathogenesis of syngnathia. *PLoS Genet,* 9**,** e1003949.
ISHIKAWA, N., HIRANUMA, C., SATO, H., UENO, Y., SEKI, M. & YAMAMOTO, M. 2002. Congenital sternal cleft with patent ductus arteriosus: report of a case. *Surg Today,* 32**,** 66-8.
ISHIZEKI, K., SAITO, H., SHINAGAWA, T., FUJIWARA, N. & NAWA, T. 1999. Histochemical and immunohistochemical analysis of the mechanism of calcification of Meckel's cartilage during mandible development in rodents. *J Anat,* 194 (Pt 2)**,** 265-77.
ISHIZEKI, K., TAKIGAWA, M., NAWA, T. & SUZUKI, F. 1996. Mouse Meckel's cartilage chondrocytes evoke bone-like matrix and further transform into osteocyte-like cells in culture. *Anat Rec,* 245**,** 25-35.
ITOH, N. & ORNITZ, D. M. 2008. Functional evolutionary history of the mouse Fgf gene family. *Dev Dyn,* 237**,** 18-27.
IWAMOTO, M., ENOMOTO-IWAMOTO, M. & KURISU, K. 1999. Actions of hedgehog proteins on skeletal cells. *Crit Rev Oral Biol Med,* 10**,** 477-86.
IWATA, T., CHEN, L., LI, C., OVCHINNIKOV, D. A., BEHRINGER, R. R., FRANCOMANO, C. A. & DENG, C. X. 2000. A neonatal lethal mutation in FGFR3 uncouples proliferation and differentiation of growth plate chondrocytes in embryos. *Hum Mol Genet,* 9**,** 1603-13.
JACQUES, B. E., MONTCOUQUIOL, M. E., LAYMAN, E. M., LEWANDOSKI, M. & KELLEY, M. W. 2007. Fgf8 induces pillar cell fate and regulates cellular patterning in the mammalian cochlea. *Development,* 134**,** 3021-9.
JEONG, J. & MCMAHON, A. P. 2005. Growth and pattern of the mammalian neural tube are governed by partially overlapping feedback activities

of the hedgehog antagonists patched 1 and Hhip1. *Development,* 132**,** 143-54.
JEROME, L. A. & PAPAIOANNOU, V. E. 2001. DiGeorge syndrome phenotype in mice mutant for the T-box gene, Tbx1. *Nat Genet,* 27**,** 286-91.
JIANG, J. 2006. Regulation of Hh/Gli signaling by dual ubiquitin pathways. *Cell Cycle,* 5**,** 2457-63.
JINKINS, J. R. 2000. *Atlas of Neuroradiologic Embryology,* Lippincott, Williams & Wilkins.
JOENG, K. S. & LONG, F. 2009. The Gli2 transcriptional activator is a crucial effector for Ihh signaling in osteoblast development and cartilage vascularization. *Development,* 136**,** 4177-85.
JOHNSON, D. R. 1967. Extra-toes: anew mutant gene causing multiple abnormalities in the mouse. *J Embryol Exp Morphol,* 17**,** 543-81.
KALININA, J., BYRON, S. A., MAKARENKOVA, H. P., OLSEN, S. K., ELISEENKOVA, A. V., LAROCHELLE, W. J., DHANABAL, M., BLAIS, S., ORNITZ, D. M., DAY, L. A., NEUBERT, T. A., POLLOCK, P. M. & MOHAMMADI, M. 2009. Homodimerization controls the fibroblast growth factor 9 subfamily's receptor binding and heparan sulfate-dependent diffusion in the extracellular matrix. *Mol Cell Biol,* 29**,** 4663-78.
KAMEL, G., HOYOS, T., ROCHARD, L., DOUGHERTY, M., KONG, Y., TSE, W., SHUBINETS, V., GRIMALDI, M. & LIAO, E. C. 2013. Requirement for frzb and fzd7a in cranial neural crest convergence and extension mechanisms during zebrafish palate and jaw morphogenesis. *Developmental Biology,* 381**,** 423-433.
KARCHER, C., FISCHER, A., SCHWEICKERT, A., BITZER, E., HORIE, S., WITZGALL, R. & BLUM, M. 2005. Lack of a laterality phenotype in Pkd1 knock-out embryos correlates with absence of polycystin-1 in nodal cilia. *Differentiation,* 73**,** 425-32.
KARP, S. J., SCHIPANI, E., ST-JACQUES, B., HUNZELMAN, J., KRONENBERG, H. & MCMAHON, A. P. 2000. Indian hedgehog coordinates endochondral bone growth and morphogenesis via parathyroid hormone related-protein-dependent and -independent pathways. *Development,* 127**,** 543-8.
KAUFMAN, M. H. & BARD, J. B. 1999. *The anatomical basis of mouse development,* Texas, Gulf professional publishing.
KAVRAN, J. M., WARD, M. D., OLADOSU, O. O., MULEPATI, S. & LEAHY, D. J. 2010. All mammalian Hedgehog proteins interact with cell adhesion molecule, down-regulated by oncogenes (CDO) and brother of CDO (BOC) in a conserved manner. *J Biol Chem,* 285**,** 24584-90.
KETTUNEN, P. & THESLEFF, I. 1998. Expression and function of FGFs-4, -8, and -9 suggest functional redundancy and repetitive use as epithelial signals during tooth morphogenesis. *Dev Dyn,* 211**,** 256-68.
KHALIFA, O., RAHBEENI, Z., ALHASHMI, N. & ALMANE, K. 2012. Oral-facial-digital syndrome type 1: unique radiological findings. *Clin Dysmorphol,* 21**,** 77-9.
KHANNA, A. J., BRAVERMAN, N. E., VALLE, D. & SPONSELLER, P. D. 2001. Cervical stenosis secondary to rhizomelic chondrodysplasia punctata. *Am J Med Genet,* 99**,** 63-6.
KIBAR, Z., VOGAN, K. J., GROULX, N., JUSTICE, M. J., UNDERHILL, D. A. & GROS, P. 2001. Ltap, a mammalian homolog of Drosophila Strabismus/Van

Gogh, is altered in the mouse neural tube mutant Loop-tail. *Nat Genet,* 28**,** 251-5.
KIM, H. J., KIM, J. H., BAE, S. C., CHOI, J. Y., KIM, H. J. & RYOO, H. M. 2003. The protein kinase C pathway plays a central role in the fibroblast growth factor-stimulated expression and transactivation activity of Runx2. *J Biol Chem,* 278**,** 319-26.
KIM, H. J., RICE, D. P., KETTUNEN, P. J. & THESLEFF, I. 1998. FGF-, BMP- and Shh-mediated signalling pathways in the regulation of cranial suture morphogenesis and calvarial bone development. *Development,* 125**,** 1241-51.
KIM, J., KATO, M. & BEACHY, P. A. 2009. Gli2 trafficking links Hedgehog-dependent activation of Smoothened in the primary cilium to transcriptional activation in the nucleus. *Proc Natl Acad Sci U S A,* 106**,** 21666-71.
KINTO, N., IWAMOTO, M., ENOMOTO-IWAMOTO, M., NOJI, S., OHUCHI, H., YOSHIOKA, H., KATAOKA, H., WADA, Y., YUHAO, G., TAKAHASHI, H. E., YOSHIKI, S. & YAMAGUCHI, A. 1997. Fibroblasts expressing Sonic hedgehog induce osteoblast differentiation and ectopic bone formation. *FEBS Lett,* 404**,** 319-23.
KITAHARA, Y., SUDA, N., KURODA, T., BECK, F., HAMMOND, V. E. & TAKANO, Y. 2002. Disturbed tooth development in parathyroid hormone-related protein (PTHrP)-gene knockout mice. *Bone,* 30**,** 48-56.
KJAER, I. 1975. Histochemical investigations on the symphysis menti in the human fetus related to fetal skeletal maturation in the hand and foot. *Acta Anat (Basel),* 93**,** 606-33.
KNECHT, A. K. & BRONNER-FRASER, M. 2002. Induction of the neural crest: a multigene process. *Nat Rev Genet,* 3**,** 453-61.
KOLPAKOVA-HART, E., JINNIN, M., HOU, B., FUKAI, N. & OLSEN, B. R. 2007. Kinesin-2 controls development and patterning of the vertebrate skeleton by Hedgehog- and Gli3-dependent mechanisms. *Dev Biol,* 309**,** 273-84.
KOMORI, T. 2002. Runx2, a multifunctional transcription factor in skeletal development. *J Cell Biochem,* 87**,** 1-8.
KOMORI, T. 2005. Regulation of skeletal development by the Runx family of transcription factors. *J Cell Biochem,* 95**,** 445-53.
KOMORI, T. 2011. Signaling networks in RUNX2-dependent bone development. *J Cell Biochem,* 112**,** 750-5.
KOMORI, T. & KISHIMOTO, T. 1998. Cbfa1 in bone development. *Curr Opin Genet Dev,* 8**,** 494-9.
KOMORI, T., YAGI, H., NOMURA, S., YAMAGUCHI, A., SASAKI, K., DEGUCHI, K., SHIMIZU, Y., BRONSON, R. T., GAO, Y. H., INADA, M., SATO, M., OKAMOTO, R., KITAMURA, Y., YOSHIKI, S. & KISHIMOTO, T. 1997. Targeted disruption of Cbfa1 results in a complete lack of bone formation owing to maturational arrest of osteoblasts. *Cell,* 89**,** 755-64.
KOZIEL, L., WUELLING, M., SCHNEIDER, S. & VORTKAMP, A. 2005. Gli3 acts as a repressor downstream of Ihh in regulating two distinct steps of chondrocyte differentiation. *Development,* 132**,** 5249-60.
KUBOTA, Y. & ITO, K. 2000. Chemotactic migration of mesencephalic neural crest cells in the mouse. *Dev Dyn,* 217**,** 170-9.

KUO, B. R. & ERICKSON, C. A. 2010. Regional differences in neural crest morphogenesis. *Cell Adh Migr,* 4**,** 567-85.
LABONNE, C. & BRONNER-FRASER, M. 1998. Neural crest induction in Xenopus: evidence for a two-signal model. *Development,* 125**,** 2403-14.
LAM, D. J., TABANGIN, M. E., SHIKARY, T. A., URIBE-RIVERA, A., MEINZEN-DERR, J. K., DE ALARCON, A., BILLMIRE, D. A. & GORDON, C. B. 2014. Outcomes of mandibular distraction osteogenesis in the treatment of severe micrognathia. *JAMA Otolaryngol Head Neck Surg,* 140**,** 338-45.
LAPRISE, P., CHAILLER, P., HOUDE, M., BEAULIEU, J. F., BOUCHER, M. J. & RIVARD, N. 2002. Phosphatidylinositol 3-kinase controls human intestinal epithelial cell differentiation by promoting adherens junction assembly and p38 MAPK activation. *J Biol Chem,* 277**,** 8226-34.
LECLAIR, E. E., MUI, S. R., HUANG, A., TOPCZEWSKA, J. M. & TOPCZEWSKI, J. 2009. Craniofacial skeletal defects of adult zebrafish Glypican 4 (knypek) mutants. *Dev Dyn,* 238**,** 2550-63.
LEE, B., THIRUNAVUKKARASU, K., ZHOU, L., PASTORE, L., BALDINI, A., HECHT, J., GEOFFROY, V., DUCY, P. & KARSENTY, G. 1997. Missense mutations abolishing DNA binding of the osteoblast-specific transcription factor OSF2/CBFA1 in cleidocranial dysplasia. *Nat Genet,* 16**,** 307-10.
LEE, J. J., EKKER, S. C., VON KESSLER, D. P., PORTER, J. A., SUN, B. I. & BEACHY, P. A. 1994. Autoproteolysis in hedgehog protein biogenesis. *Science,* 266**,** 1528-37.
LEMONNIER, J., DELANNOY, P., HOTT, M., LOMRI, A., MODROWSKI, D. & MARIE, P. J. 2000. The Ser252Trp fibroblast growth factor receptor-2 (FGFR-2) mutation induces PKC-independent downregulation of FGFR-2 associated with premature calvaria osteoblast differentiation. *Exp Cell Res,* 256**,** 158-67.
LEUCHT, P., KIM, J. B. & HELMS, J. A. 2008. Beta-catenin-dependent Wnt signaling in mandibular bone regeneration. *J Bone Joint Surg Am,* 90 Suppl 1**,** 3-8.
LEUNG, V. Y., GAO, B., LEUNG, K. K., MELHADO, I. G., WYNN, S. L., AU, T. Y., DUNG, N. W., LAU, J. Y., MAK, A. C., CHAN, D. & CHEAH, K. S. 2011. SOX9 governs differentiation stage-specific gene expression in growth plate chondrocytes via direct concomitant transactivation and repression. *PLoS Genet,* 7**,** e1002356.
LEVIN, L. S., PERRIN, J. C., OSE, L., DORST, J. P., MILLER, J. D. & MCKUSICK, V. A. 1977. A heritable syndrome of craniosynostosis, short thin hair, dental abnormalities, and short limbs: cranioectodermal dysplasia. *J Pediatr,* 90**,** 55-61.
LEWANDOSKI, M., SUN, X. & MARTIN, G. R. 2000. Fgf8 signalling from the AER is essential for normal limb development. *Nat Genet,* 26**,** 460-3.
LI, C., CHEN, L., IWATA, T., KITAGAWA, M., FU, X. Y. & DENG, C. X. 1999. A Lys644Glu substitution in fibroblast growth factor receptor 3 (FGFR3) causes dwarfism in mice by activation of STATs and ink4 cell cycle inhibitors. *Hum Mol Genet,* 8**,** 35-44.
LIN, A. E., TRAUM, A. Z., SAHAI, I., KEPPLER-NOREUIL, K., KUKOLICH, M. K., ADAM, M. P., WESTRA, S. J. & ARTS, H. H. 2013. Sensenbrenner syndrome (Cranioectodermal dysplasia): clinical and molecular

analyses of 39 patients including two new patients. *Am J Med Genet A,* 161A**,** 2762-76.
LINDER, M. D., URONEN, R. L., HOLTTA-VUORI, M., VAN DER SLUIJS, P., PERANEN, J. & IKONEN, E. 2007. Rab8-dependent recycling promotes endosomal cholesterol removal in normal and sphingolipidosis cells. *Mol Biol Cell,* 18**,** 47-56.
LITINGTUNG, Y., DAHN, R. D., LI, Y., FALLON, J. F. & CHIANG, C. 2002. Shh and Gli3 are dispensable for limb skeleton formation but regulate digit number and identity. *Nature,* 418**,** 979-83.
LIU, A., WANG, B. & NISWANDER, L. A. 2005a. Mouse intraflagellar transport proteins regulate both the activator and repressor functions of Gli transcription factors. *Development,* 132**,** 3103-11.
LIU, K. J., ARRON, J. R., STANKUNAS, K., CRABTREE, G. R. & LONGAKER, M. T. 2007. Chemical rescue of cleft palate and midline defects in conditional GSK-3beta mice. *Nature,* 446**,** 79-82.
LIU, N., BARBOSA, A. C., CHAPMAN, S. L., BEZPROZVANNAYA, S., QI, X., RICHARDSON, J. A., YANAGISAWA, H. & OLSON, E. N. 2009. DNA binding-dependent and -independent functions of the Hand2 transcription factor during mouse embryogenesis. *Development,* 136**,** 933-42.
LIU, W., SELEVER, J., MURALI, D., SUN, X., BRUGGER, S. M., MA, L., SCHWARTZ, R. J., MAXSON, R., FURUTA, Y. & MARTIN, J. F. 2005b. Threshold-specific requirements for Bmp4 in mandibular development. *Dev Biol,* 283**,** 282-93.
LIU, Z., XU, J., COLVIN, J. S. & ORNITZ, D. M. 2002. Coordination of chondrogenesis and osteogenesis by fibroblast growth factor 18. *Genes Dev,* 16**,** 859-69.
LOMRI, A., LEMONNIER, J., HOTT, M., DE PARSEVAL, N., LAJEUNIE, E., MUNNICH, A., RENIER, D. & MARIE, P. J. 1998. Increased calvaria cell differentiation and bone matrix formation induced by fibroblast growth factor receptor 2 mutations in Apert syndrome. *J Clin Invest,* 101**,** 1310-7.
MAENO, T., MORIISHI, T., YOSHIDA, C. A., KOMORI, H., KANATANI, N., IZUMI, S., TAKAOKA, K. & KOMORI, T. 2011. Early onset of Runx2 expression caused craniosynostosis, ectopic bone formation, and limb defects. *Bone,* 49**,** 673-82.
MAHUZIER, A., GAUDE, H. M., GRAMPA, V., ANSELME, I., SILBERMANN, F., LEROUX-BERGER, M., DELACOUR, D., EZAN, J., MONTCOUQUIOL, M., SAUNIER, S., SCHNEIDER-MAUNOURY, S. & VESQUE, C. 2012. Dishevelled stabilization by the ciliopathy protein Rpgrip1l is essential for planar cell polarity. *J Cell Biol,* 198**,** 927-40.
MAO, Y., MULVANEY, J., ZAKARIA, S., YU, T., MORGAN, K. M., ALLEN, S., BASSON, M. A., FRANCIS-WEST, P. & IRVINE, K. D. 2011. Characterization of a Dchs1 mutant mouse reveals requirements for Dchs1-Fat4 signaling during mammalian development. *Development,* 138**,** 947-57.
MARTELLI-JUNIOR, H., COLETTA, R. D., MIRANDA, R. T., BARROS, L. M., SWERTS, M. S. & BONAN, P. R. 2009. Orofacial features of Treacher Collins syndrome. *Med Oral Patol Oral Cir Bucal,* 14**,** E344-8.
MASON, I. J., FULLER-PACE, F., SMITH, R. & DICKSON, C. 1994. FGF-7 (keratinocyte growth factor) expression during mouse development

suggests roles in myogenesis, forebrain regionalisation and epithelial-mesenchymal interactions. *Mech Dev,* 45**,** 15-30.
MATISE, M. P., EPSTEIN, D. J., PARK, H. L., PLATT, K. A. & JOYNER, A. L. 1998. Gli2 is required for induction of floor plate and adjacent cells, but not most ventral neurons in the mouse central nervous system. *Development,* 125**,** 2759-70.
MATSUSHITA, T., WILCOX, W. R., CHAN, Y. Y., KAWANAMI, A., BUKULMEZ, H., BALMES, G., KREJCI, P., MEKIKIAN, P. B., OTANI, K., YAMAURA, I., WARMAN, M. L., GIVOL, D. & MURAKAMI, S. 2009. FGFR3 promotes synchondrosis closure and fusion of ossification centers through the MAPK pathway. *Hum Mol Genet,* 18**,** 227-40.
MAYOR, R. & THEVENEAU, E. 2014. The role of the non-canonical Wnt-planar cell polarity pathway in neural crest migration. *Biochem J,* 457**,** 19-26.
MCGLINN, E., VAN BUEREN, K. L., FIORENZA, S., MO, R., POH, A. M., FORREST, A., SOARES, M. B., BONALDO MDE, F., GRIMMOND, S., HUI, C. C., WAINWRIGHT, B. & WICKING, C. 2005. Pax9 and Jagged1 act downstream of Gli3 in vertebrate limb development. *Mech Dev,* 122**,** 1218-33.
MCGONNELL, I. M., CLARKE, J. D. & TICKLE, C. 1998. Fate map of the developing chick face: analysis of expansion of facial primordia and establishment of the primary palate. *Dev Dyn,* 212**,** 102-18.
MELNICK, M., WITCHER, D., BRINGAS, P., JR., CARLSSON, P. & JASKOLL, T. 2005. Meckel's cartilage differentiation is dependent on hedgehog signaling. *Cells Tissues Organs,* 179**,** 146-57.
MERCADER, N., LEONARDO, E., PIEDRA, M. E., MARTINEZ, A. C., ROS, M. A. & TORRES, M. 2000. Opposing RA and FGF signals control proximodistal vertebrate limb development through regulation of Meis genes. *Development,* 127**,** 3961-70.
MIAO, D., LIU, H., PLUT, P., NIU, M., HUO, R., GOLTZMAN, D. & HENDERSON, J. E. 2004. Impaired endochondral bone development and osteopenia in Gli2-deficient mice. *Exp Cell Res,* 294**,** 210-22.
MIKELS, A. J. & NUSSE, R. 2006. Purified Wnt5a protein activates or inhibits beta-catenin-TCF signaling depending on receptor context. *PLoS Biol,* 4**,** e115.
MINA, M., UPHOLT, W. B. & KOLLAR, E. J. 1994. Enhancement of avian mandibular chondrogenesis in vitro in the absence of epithelium. *Arch Oral Biol,* 39**,** 551-62.
MO, R., FREER, A. M., ZINYK, D. L., CRACKOWER, M. A., MICHAUD, J., HENG, H. H., CHIK, K. W., SHI, X. M., TSUI, L. C., CHENG, S. H., JOYNER, A. L. & HUI, C. 1997. Specific and redundant functions of Gli2 and Gli3 zinc finger genes in skeletal patterning and development. *Development,* 124**,** 113-23.
MOHAMMADI, M., OLSEN, S. K. & IBRAHIMI, O. A. 2005. Structural basis for fibroblast growth factor receptor activation. *Cytokine Growth Factor Rev,* 16**,** 107-37.
MONTCOUQUIOL, M., RACHEL, R. A., LANFORD, P. J., COPELAND, N. G., JENKINS, N. A. & KELLEY, M. W. 2003. Identification of Vangl2 and Scrb1 as planar polarity genes in mammals. *Nature,* 423**,** 173-7.
MOORE, M. H., CANTRELL, S. B., TROTT, J. A. & DAVID, D. J. 1995a. Pfeiffer syndrome: a clinical review. *Cleft Palate Craniofac J,* 32**,** 62-70.

MOORE, M. H., LODGE, M. L. & CLARK, B. E. 1995b. Spinal anomalies in Pfeiffer syndrome. *Cleft Palate Craniofac J,* 32**,** 251-4.
MOORE-SCOTT, B. A. & MANLEY, N. R. 2005. Differential expression of Sonic hedgehog along the anterior-posterior axis regulates patterning of pharyngeal pouch endoderm and pharyngeal endoderm-derived organs. *Dev Biol,* 278**,** 323-35.
MORI-AKIYAMA, Y., AKIYAMA, H., ROWITCH, D. H. & DE CROMBRUGGHE, B. 2003. Sox9 is required for determination of the chondrogenic cell lineage in the cranial neural crest. *Proc Natl Acad Sci U S A,* 100**,** 9360-5.
MORRISON, S. J. & SCADDEN, D. T. 2014. The bone marrow niche for haematopoietic stem cells. *Nature,* 505**,** 327-34.
MORRISS-KAY, G. M. 2001. Derivation of the mammalian skull vault. *J Anat,* 199**,** 143-51.
MUENKE, M. & SCHELL, U. 1995. Fibroblast-growth-factor receptor mutations in human skeletal disorders. *Trends Genet,* 11**,** 308-13.
MUENKE, M., SCHELL, U., HEHR, A., ROBIN, N. H., LOSKEN, H. W., SCHINZEL, A., PULLEYN, L. J., RUTLAND, P., REARDON, W., MALCOLM, S. & ET AL. 1994. A common mutation in the fibroblast growth factor receptor 1 gene in Pfeiffer syndrome. *Nat Genet,* 8**,** 269-74.
MUNDLOS, S., OTTO, F., MUNDLOS, C., MULLIKEN, J. B., AYLSWORTH, A. S., ALBRIGHT, S., LINDHOUT, D., COLE, W. G., HENN, W., KNOLL, J. H., OWEN, M. J., MERTELSMANN, R., ZABEL, B. U. & OLSEN, B. R. 1997. Mutations involving the transcription factor CBFA1 cause cleidocranial dysplasia. *Cell,* 89**,** 773-9.
MURAKAMI, S., BALMES, G., MCKINNEY, S., ZHANG, Z., GIVOL, D. & DE CROMBRUGGHE, B. 2004. Constitutive activation of MEK1 in chondrocytes causes Stat1-independent achondroplasia-like dwarfism and rescues the Fgfr3-deficient mouse phenotype. *Genes Dev,* 18**,** 290-305.
MURDOCH, B., DELCONTE, C. & GARCIA-CASTRO, M. I. 2012. Pax7 lineage contributions to the mammalian neural crest. *PLoS One,* 7**,** e41089.
MURDOCH, J. N., DOUDNEY, K., PATERNOTTE, C., COPP, A. J. & STANIER, P. 2001. Severe neural tube defects in the loop-tail mouse result from mutation of Lpp1, a novel gene involved in floor plate specification. *Hum Mol Genet,* 10**,** 2593-601.
MURTAUGH, L. C., CHYUNG, J. H. & LASSAR, A. B. 1999. Sonic hedgehog promotes somitic chondrogenesis by altering the cellular response to BMP signaling. *Genes Dev,* 13**,** 225-37.
MYAGERI, A., GRAMPUROHIT, V. & RAO, R. 2013. Meckel gruber syndrome: report of two cases with review of literature. *J Family Med Prim Care,* 2**,** 106-8.
MYLLYLA, R. M., HAAPASAARI, K. M., LEHENKARI, P. & TUUKKANEN, J. 2014. Bone morphogenetic proteins 4 and 2/7 induce osteogenic differentiation of mouse skin derived fibroblast and dermal papilla cells. *Cell Tissue Res,* 355**,** 463-70.
NACHURY, M. V., LOKTEV, A. V., ZHANG, Q., WESTLAKE, C. J., PERANEN, J., MERDES, A., SLUSARSKI, D. C., SCHELLER, R. H., BAZAN, J. F., SHEFFIELD, V. C. & JACKSON, P. K. 2007. A core complex of BBS proteins cooperates with the GTPase Rab8 to promote ciliary membrane biogenesis. *Cell,* 129**,** 1201-13.

NAKASHIMA, K., ZHOU, X., KUNKEL, G., ZHANG, Z., DENG, J. M., BEHRINGER, R. R. & DE CROMBRUGGHE, B. 2002. The novel zinc finger-containing transcription factor osterix is required for osteoblast differentiation and bone formation. *Cell,* 108**,** 17-29.

NANNI, L., MING, J. E., BOCIAN, M., STEINHAUS, K., BIANCHI, D. W., DIE-SMULDERS, C., GIANNOTTI, A., IMAIZUMI, K., JONES, K. L., CAMPO, M. D., MARTIN, R. A., MEINECKE, P., PIERPONT, M. E., ROBIN, N. H., YOUNG, I. D., ROESSLER, E. & MUENKE, M. 1999. The mutational spectrum of the sonic hedgehog gene in holoprosencephaly: SHH mutations cause a significant proportion of autosomal dominant holoprosencephaly. *Hum Mol Genet,* 8**,** 2479-88.

NASKI, M. C., COLVIN, J. S., COFFIN, J. D. & ORNITZ, D. M. 1998. Repression of hedgehog signaling and BMP4 expression in growth plate cartilage by fibroblast growth factor receptor 3. *Development,* 125**,** 4977-88.

NEILSON, K. M. & FRIESEL, R. 1996. Ligand-independent activation of fibroblast growth factor receptors by point mutations in the extracellular, transmembrane, and kinase domains. *J Biol Chem,* 271**,** 25049-57.

NEILSON, K. M. & FRIESEL, R. E. 1995. Constitutive activation of fibroblast growth factor receptor-2 by a point mutation associated with Crouzon syndrome. *J Biol Chem,* 270**,** 26037-40.

NG, L. J., WHEATLEY, S., MUSCAT, G. E., CONWAY-CAMPBELL, J., BOWLES, J., WRIGHT, E., BELL, D. M., TAM, P. P., CHEAH, K. S. & KOOPMAN, P. 1997. SOX9 binds DNA, activates transcription, and coexpresses with type II collagen during chondrogenesis in the mouse. *Dev Biol,* 183**,** 108-21.

NIEDERREITHER, K., VERMOT, J., SCHUHBAUR, B., CHAMBON, P. & DOLLE, P. 2002. Embryonic retinoic acid synthesis is required for forelimb growth and anteroposterior patterning in the mouse. *Development,* 129**,** 3563-74.

NIGER, C., LUCIOTTI, M. A., BUO, A. M., HEBERT, C., MA, V. & STAINS, J. P. 2013. The regulation of runt-related transcription factor 2 by fibroblast growth factor-2 and connexin43 requires the inositol polyphosphate/protein kinase Cdelta cascade. *J Bone Miner Res,* 28**,** 1468-77.

NISWANDER, L., TICKLE, C., VOGEL, A., BOOTH, I. & MARTIN, G. R. 1993. FGF-4 replaces the apical ectodermal ridge and directs outgrowth and patterning of the limb. *Cell,* 75**,** 579-87.

NODEN, D. M. 1983. The role of the neural crest in patterning of avian cranial skeletal, connective, and muscle tissues. *Dev Biol,* 96**,** 144-65.

NODEN, D. M. 1988. Interactions and fates of avian craniofacial mesenchyme. *Development,* 103 Suppl**,** 121-40.

NODEN, D. M. 1992. Vertebrate craniofacial development: novel approaches and new dilemmas. *Curr Opin Genet Dev,* 2**,** 576-81.

NONAKA, S., TANAKA, Y., OKADA, Y., TAKEDA, S., HARADA, A., KANAI, Y., KIDO, M. & HIROKAWA, N. 1998. Randomization of left-right asymmetry due to loss of nodal cilia generating leftward flow of extraembryonic fluid in mice lacking KIF3B motor protein. *Cell,* 95**,** 829-37.

ODGAARD, A. 1997. Three-dimensional methods for quantification of cancellous bone architecture. *Bone,* 20**,** 315-28.

OHBA, S., KAWAGUCHI, H., KUGIMIYA, F., OGASAWARA, T., KAWAMURA, N., SAITO, T., IKEDA, T., FUJII, K., MIYAJIMA, T., KURAMOCHI, A., MIYASHITA, T., ODA, H., NAKAMURA, K., TAKATO, T. & CHUNG, U. I. 2008. Patched1 haploinsufficiency increases adult bone mass and modulates Gli3 repressor activity. *Dev Cell,* 14**,** 689-99.

OHBAYASHI, N., SHIBAYAMA, M., KUROTAKI, Y., IMANISHI, M., FUJIMORI, T., ITOH, N. & TAKADA, S. 2002. FGF18 is required for normal cell proliferation and differentiation during osteogenesis and chondrogenesis. *Genes Dev,* 16**,** 870-9.

OHUCHI, H., NAKAGAWA, T., YAMAMOTO, A., ARAGA, A., OHATA, T., ISHIMARU, Y., YOSHIOKA, H., KUWANA, T., NOHNO, T., YAMASAKI, M., ITOH, N. & NOJI, S. 1997. The mesenchymal factor, FGF10, initiates and maintains the outgrowth of the chick limb bud through interaction with FGF8, an apical ectodermal factor. *Development,* 124**,** 2235-44.

OLSEN, B. R., REGINATO, A. M. & WANG, W. 2000. Bone development. *Annu Rev Cell Dev Biol,* 16**,** 191-220.

OLSEN, S. K., LI, J. Y., BROMLEIGH, C., ELISEENKOVA, A. V., IBRAHIMI, O. A., LAO, Z., ZHANG, F., LINHARDT, R. J., JOYNER, A. L. & MOHAMMADI, M. 2006. Structural basis by which alternative splicing modulates the organizer activity of FGF8 in the brain. *Genes Dev,* 20**,** 185-98.

OMOTEYAMA, K. & TAKAGI, M. 2009. FGF8 regulates myogenesis and induces Runx2 expression and osteoblast differentiation in cultured cells. *J Cell Biochem,* 106**,** 546-52.

OPPERMAN, L. A. 2000. Cranial sutures as intramembranous bone growth sites. *Dev Dyn,* 219**,** 472-85.

ORHAN, D., BALCI, S., DEREN, O., UTINE, E. G., BASARAN, A. & KALE, G. 2008. Prenatally diagnosed lethal type Larsen-like syndrome associated with bifid tongue. *Turk J Pediatr,* 50**,** 395-9.

ORNEK, D., AYDIN, G. B., KAHVECI, K., CICEK, F. & DIKMEN, B. 2012. Anesthetic management of a child with both Marfan syndrome and Turner syndrome. *J Anesth,* 26**,** 442-4.

ORR-URTREGER, A., BEDFORD, M. T., BURAKOVA, T., ARMAN, E., ZIMMER, Y., YAYON, A., GIVOL, D. & LONAI, P. 1993. Developmental localization of the splicing alternatives of fibroblast growth factor receptor-2 (FGFR2). *Dev Biol,* 158**,** 475-86.

OSTROWSKI, L. E., BLACKBURN, K., RADDE, K. M., MOYER, M. B., SCHLATZER, D. M., MOSELEY, A. & BOUCHER, R. C. 2002. A proteomic analysis of human cilia: identification of novel components. *Mol Cell Proteomics,* 1**,** 451-65.

OSUMI-YAMASHITA, N., NINOMIYA, Y. & ETO, K. 1997. Mammalian craniofacial embryology in vitro. *Int J Dev Biol,* 41**,** 187-94.

OZAKI, K., MIYAZAKI, S., TANIMURA, S. & KOHNO, M. 2005. Efficient suppression of FGF-2-induced ERK activation by the cooperative interaction among mammalian Sprouty isoforms. *J Cell Sci,* 118**,** 5861-71.

PACHECO, M., VALENCIA, M., CAPARROS-MARTIN, J. A., MULERO, F., GOODSHIP, J. A. & RUIZ-PEREZ, V. L. 2012. Evc works in chondrocytes and osteoblasts to regulate multiple aspects of growth plate development in the appendicular skeleton and cranial base. *Bone,* 50**,** 28-41.

PAN, Y. & WANG, B. 2007. A novel protein-processing domain in Gli2 and Gli3 differentially blocks complete protein degradation by the proteasome. *J Biol Chem,* 282**,** 10846-52.
PANMAN, L., DRENTH, T., TEWELSCHER, P., ZUNIGA, A. & ZELLER, R. 2005. Genetic interaction of Gli3 and Alx4 during limb development. *Int J Dev Biol,* 49**,** 443-8.
PARELKAR, S. V., KAPADNIS, S. P., SANGHVI, B. V., JOSHI, P. B., MUNDADA, D. & OAK, S. N. 2013. Meckel-Gruber syndrome: A rare and lethal anomaly with review of literature. *J Pediatr Neurosci,* 8**,** 154-7.
PARK, H. L., BAI, C., PLATT, K. A., MATISE, M. P., BEEGHLY, A., HUI, C. C., NAKASHIMA, M. & JOYNER, A. L. 2000. Mouse Gli1 mutants are viable but have defects in SHH signaling in combination with a Gli2 mutation. *Development,* 127**,** 1593-605.
PARK, O. J., KIM, H. J., WOO, K. M., BAEK, J. H. & RYOO, H. M. 2010. FGF2-activated ERK mitogen-activated protein kinase enhances Runx2 acetylation and stabilization. *J Biol Chem,* 285**,** 3568-74.
PARK, T. J., HAIGO, S. L. & WALLINGFORD, J. B. 2006. Ciliogenesis defects in embryos lacking inturned or fuzzy function are associated with failure of planar cell polarity and Hedgehog signaling. *Nat Genet,* 38**,** 303-11.
PARK, T. J., MITCHELL, B. J., ABITUA, P. B., KINTNER, C. & WALLINGFORD, J. B. 2008. Dishevelled controls apical docking and planar polarization of basal bodies in ciliated epithelial cells. *Nat Genet,* 40**,** 871-9.
PARK, W. J., LIU, J., SHARP, E. J. & ADLER, P. N. 1996. The Drosophila tissue polarity gene inturned acts cell autonomously and encodes a novel protein. *Development,* 122**,** 961-9.
PARK, W. J., MEYERS, G. A., LI, X., THEDA, C., DAY, D., ORLOW, S. J., JONES, M. C. & JABS, E. W. 1995. Novel FGFR2 mutations in Crouzon and Jackson-Weiss syndromes show allelic heterogeneity and phenotypic variability. *Hum Mol Genet,* 4**,** 1229-33.
PATHI, S., PAGAN-WESTPHAL, S., BAKER, D. P., GARBER, E. A., RAYHORN, P., BUMCROT, D., TABIN, C. J., BLAKE PEPINSKY, R. & WILLIAMS, K. P. 2001. Comparative biological responses to human Sonic, Indian, and Desert hedgehog. *Mech Dev,* 106**,** 107-17.
PAZOUR, G. J., AGRIN, N., LESZYK, J. & WITMAN, G. B. 2005. Proteomic analysis of a eukaryotic cilium. *J Cell Biol,* 170**,** 103-13.
PEDERSEN, L. B. & ROSENBAUM, J. L. 2008. Intraflagellar transport (IFT) role in ciliary assembly, resorption and signalling. *Curr Top Dev Biol,* 85**,** 23-61.
PEPINSKY, R. B., ZENG, C., WEN, D., RAYHORN, P., BAKER, D. P., WILLIAMS, K. P., BIXLER, S. A., AMBROSE, C. M., GARBER, E. A., MIATKOWSKI, K., TAYLOR, F. R., WANG, E. A. & GALDES, A. 1998. Identification of a palmitic acid-modified form of human Sonic hedgehog. *J Biol Chem,* 273**,** 14037-45.
PERSSON, M., STAMATAKI, D., TE WELSCHER, P., ANDERSSON, E., BOSE, J., RUTHER, U., ERICSON, J. & BRISCOE, J. 2002. Dorsal-ventral patterning of the spinal cord requires Gli3 transcriptional repressor activity. *Genes Dev,* 16**,** 2865-78.
PETERS, D. J., SPRUIT, L., KLINGEL, R., PRINS, F., BAELDE, H. J., GIORDANO, P. C., BERNINI, L. F., DE HEER, E., BREUNING, M. H. & BRUIJN, J. A. 1996.

Adult, fetal, and polycystic kidney expression of polycystin, the polycystic kidney disease-1 gene product. *Lab Invest,* 75**,** 221-30.
PETERS, H., WILM, B., SAKAI, N., IMAI, K., MAAS, R. & BALLING, R. 1999. Pax1 and Pax9 synergistically regulate vertebral column development. *Development,* 126**,** 5399-408.
PETERS, K., ORNITZ, D., WERNER, S. & WILLIAMS, L. 1993. Unique expression pattern of the FGF receptor 3 gene during mouse organogenesis. *Dev Biol,* 155**,** 423-30.
PETIOT, A., FERRETTI, P., COPP, A. J. & CHAN, C. T. 2002. Induction of chondrogenesis in neural crest cells by mutant fibroblast growth factor receptors. *Dev Dyn,* 224**,** 210-21.
PIGINO, G., GEIMER, S., LANZAVECCHIA, S., PACCAGNINI, E., CANTELE, F., DIENER, D. R., ROSENBAUM, J. L. & LUPETTI, P. 2009. Electron-tomographic analysis of intraflagellar transport particle trains in situ. *J Cell Biol,* 187**,** 135-48.
POLIAKOV, A., COTRINA, M. & WILKINSON, D. G. 2004. Diverse roles of eph receptors and ephrins in the regulation of cell migration and tissue assembly. *Dev Cell,* 7**,** 465-80.
PORTER, J. A., EKKER, S. C., PARK, W. J., VON KESSLER, D. P., YOUNG, K. E., CHEN, C. H., MA, Y., WOODS, A. S., COTTER, R. J., KOONIN, E. V. & BEACHY, P. A. 1996. Hedgehog patterning activity: role of a lipophilic modification mediated by the carboxy-terminal autoprocessing domain. *Cell,* 86**,** 21-34.
PRYOR, P. R., JACKSON, L., GRAY, S. R., EDELING, M. A., THOMPSON, A., SANDERSON, C. M., EVANS, P. R., OWEN, D. J. & LUZIO, J. P. 2008. Molecular basis for the sorting of the SNARE VAMP7 into endocytic clathrin-coated vesicles by the ArfGAP Hrb. *Cell,* 134**,** 817-27.
PUMIGLIA, K. M. & DECKER, S. J. 1997. Cell cycle arrest mediated by the MEK/mitogen-activated protein kinase pathway. *Proc Natl Acad Sci U S A,* 94**,** 448-52.
RAMAESH, T. & BARD, J. B. 2003. The growth and morphogenesis of the early mouse mandible: a quantitative analysis. *J Anat,* 203**,** 213-22.
RASH, B. G. & GROVE, E. A. 2007. Patterning the dorsal telencephalon: a role for sonic hedgehog? *J Neurosci,* 27**,** 11595-603.
RICE, D. P., ABERG, T., CHAN, Y., TANG, Z., KETTUNEN, P. J., PAKARINEN, L., MAXSON, R. E. & THESLEFF, I. 2000. Integration of FGF and TWIST in calvarial bone and suture development. *Development,* 127**,** 1845-55.
RICE, D. P., CONNOR, E. C., VELTMAAT, J. M., LANA-ELOLA, E., VEISTINEN, L., TANIMOTO, Y., BELLUSCI, S. & RICE, R. 2010. Gli3Xt-J/Xt-J mice exhibit lambdoid suture craniosynostosis which results from altered osteoprogenitor proliferation and differentiation. *Hum Mol Genet,* 19**,** 3457-67.
RICHMAN, J. M. & TICKLE, C. 1989. Epithelia are interchangeable between facial primordia of chick embryos and morphogenesis is controlled by the mesenchyme. *Dev Biol,* 136**,** 201-10.
RIMOIN, D. L., HUGHES, G. N., KAUFMAN, R. L., ROSENTHAL, R. E., MCALISTER, W. H. & SILBERBERG, R. 1970. Endochondral ossification in achondroplastic dwarfism. *N Engl J Med,* 283**,** 728-35.
ROACH, H. I., AIGNER, T. & KOURI, J. B. 2004. Chondroptosis: a variant of apoptotic cell death in chondrocytes? *Apoptosis,* 9**,** 265-77.

ROBERTSON, S. C., MEYER, A. N., HART, K. C., GALVIN, B. D., WEBSTER, M. K. & DONOGHUE, D. J. 1998. Activating mutations in the extracellular domain of the fibroblast growth factor receptor 2 function by disruption of the disulfide bond in the third immunoglobulin-like domain. *Proc Natl Acad Sci U S A,* 95**,** 4567-72.

ROSS, A. J., MAY-SIMERA, H., EICHERS, E. R., KAI, M., HILL, J., JAGGER, D. J., LEITCH, C. C., CHAPPLE, J. P., MUNRO, P. M., FISHER, S., TAN, P. L., PHILLIPS, H. M., LEROUX, M. R., HENDERSON, D. J., MURDOCH, J. N., COPP, A. J., ELIOT, M. M., LUPSKI, J. R., KEMP, D. T., DOLLFUS, H., TADA, M., KATSANIS, N., FORGE, A. & BEALES, P. L. 2005. Disruption of Bardet-Biedl syndrome ciliary proteins perturbs planar cell polarity in vertebrates. *Nat Genet,* 37**,** 1135-40.

ROSSE, C. & GADDUM-ROSEE, P. 1997. *Hollinshead's textbook of anatomy,* Lippincott, Williams & Wilkins

.

ROSSI, V., BANFIELD, D. K., VACCA, M., DIETRICH, L. E., UNGERMANN, C., D'ESPOSITO, M., GALLI, T. & FILIPPINI, F. 2004. Longins and their longin domains: regulated SNAREs and multifunctional SNARE regulators. *Trends Biochem Sci,* 29**,** 682-8.

ROUSSEAU, F., BONAVENTURE, J., LEGEAI-MALLET, L., PELET, A., ROZET, J. M., MAROTEAUX, P., LE MERRER, M. & MUNNICH, A. 1994. Mutations in the gene encoding fibroblast growth factor receptor-3 in achondroplasia. *Nature,* 371**,** 252-4.

RUIZ I ALTABA, A. 1999. Gli proteins encode context-dependent positive and negative functions: implications for development and disease. *Development,* 126**,** 3205-16.

RYNEARSON, R. D. 2000. Case report: orthodontic and dentofacial orthopedic considerations in Apert's syndrome. *Angle Orthod,* 70**,** 247-52.

SAKAKURA, Y., HOSOKAWA, Y., TSURUGA, E., IRIE, K. & YAJIMA, T. 2007. In situ localization of gelatinolytic activity during development and resorption of Meckel's cartilage in mice. *Eur J Oral Sci,* 115**,** 212-23.

SAKAKURA, Y., TSURUGA, E., IRIE, K., HOSOKAWA, Y., NAKAMURA, H. & YAJIMA, T. 2005. Immunolocalization of receptor activator of nuclear factor-kappaB ligand (RANKL) and osteoprotegerin (OPG) in Meckel's cartilage compared with developing endochondral bones in mice. *J Anat,* 207**,** 325-37.

SALA, F. G., DEL MORAL, P. M., TIOZZO, C., ALAM, D. A., WARBURTON, D., GRIKSCHEIT, T., VELTMAAT, J. M. & BELLUSCI, S. 2011. FGF10 controls the patterning of the tracheal cartilage rings via Shh. *Development,* 138**,** 273-82.

SASAI, N., KUTEJOVA, E. & BRISCOE, J. 2014. Integration of signals along orthogonal axes of the vertebrate neural tube controls progenitor competence and increases cell diversity. *PLoS Biol,* 12**,** e1001907.

SATO, A., SCHOLL, A. M., KUHN, E. N., STADT, H. A., DECKER, J. R., PEGRAM, K., HUTSON, M. R. & KIRBY, M. L. 2011. FGF8 signaling is chemotactic for cardiac neural crest cells. *Dev Biol,* 354**,** 18-30.

SAUNDERS, J. W., JR. 1948. The proximo-distal sequence of origin of the parts of the chick wing and the role of the ectoderm. *J Exp Zool,* 108**,** 363-403.

SCHELL, U., HEHR, A., FELDMAN, G. J., ROBIN, N. H., ZACKAI, E. H., DE DIE-SMULDERS, C., VISKOCHIL, D. H., STEWART, J. M., WOLFF, G., OHASHI, H. & ET AL. 1995. Mutations in FGFR1 and FGFR2 cause familial and sporadic Pfeiffer syndrome. *Hum Mol Genet,* 4**,** 323-8.

SCHEUER, L. & BLACK, S. 2004. *The Juvenile Skeleton,* New York, Elsevier Academic Pres.

SCHLESSINGER, J., PLOTNIKOV, A. N., IBRAHIMI, O. A., ELISEENKOVA, A. V., YEH, B. K., YAYON, A., LINHARDT, R. J. & MOHAMMADI, M. 2000. Crystal structure of a ternary FGF-FGFR-heparin complex reveals a dual role for heparin in FGFR binding and dimerization. *Mol Cell,* 6**,** 743-50.

SCHLESSINGER, K., HALL, A. & TOLWINSKI, N. 2009. Wnt signaling pathways meet Rho GTPases. *Genes Dev,* 23**,** 265-77.

SEGEV, O., CHUMAKOV, I., NEVO, Z., GIVOL, D., MADAR-SHAPIRO, L., SHEININ, Y., WEINREB, M. & YAYON, A. 2000. Restrained chondrocyte proliferation and maturation with abnormal growth plate vascularization and ossification in human FGFR-3(G380R) transgenic mice. *Hum Mol Genet,* 9**,** 249-58.

SELVAMURUGAN, N., PULUMATI, M. R., TYSON, D. R. & PARTRIDGE, N. C. 2000. Parathyroid hormone regulation of the rat collagenase-3 promoter by protein kinase A-dependent transactivation of core binding factor alpha1. *J Biol Chem,* 275**,** 5037-42.

SENSENBRENNER, J. A., DORST, J. P. & OWENS, R. P. 1975. New syndrome of skeletal, dental and hair anomalies. *Birth Defects Orig Artic Ser,* 11**,** 372-9.

SEO, J. H., ZILBER, Y., BABAYEVA, S., LIU, J., KYRIAKOPOULOS, P., DE MARCO, P., MERELLO, E., CAPRA, V., GROS, P. & TORBAN, E. 2011. Mutations in the planar cell polarity gene, Fuzzy, are associated with neural tube defects in humans. *Hum Mol Genet,* 20**,** 4324-33.

SHAWKY, R. M., ELSAYED, S. M., ABD-ELKHALEK, H. S. & GAD, S. 2013. Oral-facial-digital syndrome type II: Transitional type between Mohr and Varadi. *Egyptian Journal of Medical Human Genetics,* 14**,** 311-315.

SHEN, G. 2005. The role of type X collagen in facilitating and regulating endochondral ossification of articular cartilage. *Orthod Craniofac Res,* 8**,** 11-7.

SHIANG, R., THOMPSON, L. M., ZHU, Y.-Z., CHURCH, D. M., FIELDER, T. J., BOCIAN, M., WINOKUR, S. T. & WASMUTH, J. J. 1994. Mutations in the transmembrane domain of FGFR3 cause the most common genetic form of dwarfism, achondroplasia. *Cell,* 78**,** 335-342.

SHIBATA, S., SUDA, N., YODA, S., FUKUOKA, H., OHYAMA, K., YAMASHITA, Y. & KOMORI, T. 2004. Runx2-deficient mice lack mandibular condylar cartilage and have deformed Meckel's cartilage. *Anat Embryol (Berl),* 208**,** 273-80.

SHIMADA, M., YAMAMOTO, M., WAKAYAMA, T., ISEKI, S. & AMANO, O. 2003. Different expression of 25-kDa heat-shock protein (Hsp25) in Meckel's cartilage compared with other cartilages in the mouse. *Anat Embryol (Berl),* 206**,** 163-73.

SHIMO, T., KANYAMA, M., WU, C., SUGITO, H., BILLINGS, P. C., ABRAMS, W. R., ROSENBLOOM, J., IWAMOTO, M., PACIFICI, M. & KOYAMA, E. 2004. Expression and roles of connective tissue growth factor in Meckel's cartilage development. *Dev Dyn,* 231**,** 136-47.

SHIMOYAMA, A., WADA, M., IKEDA, F., HATA, K., MATSUBARA, T., NIFUJI, A., NODA, M., AMANO, K., YAMAGUCHI, A., NISHIMURA, R. & YONEDA, T. 2007. Ihh/Gli2 signaling promotes osteoblast differentiation by regulating Runx2 expression and function. *Mol Biol Cell,* 18**,** 2411-8.
SILLIBOURNE, J. E., MILNE, D. M., TAKAHASHI, M., ONO, Y. & MEEK, D. W. 2002. Centrosomal Anchoring of the Protein Kinase CK1δ Mediated by Attachment to the Large, Coiled-coil Scaffolding Protein CG-NAP/AKAP450. *Journal of Molecular Biology,* 322**,** 785-797.
SIMKIN, J. E., ZHANG, D., ROLLO, B. N. & NEWGREEN, D. F. 2013. Retinoic acid upregulates ret and induces chain migration and population expansion in vagal neural crest cells to colonise the embryonic gut. *PLoS One,* 8**,** e64077.
SINGH, A., GOYAL, M., KUMAR, S., KRESS, W. & KAPOOR, S. 2014. Phenotypic Variability in Two Families of Muenke Syndrome with FGFR3 Mutation. *Indian J Pediatr*.
SINGH, P., GORAYA, J. S., SAGGAR, K. & AHLUWALIA, A. 2011. A report of Joubert syndrome in an infant, with literature review. *J Pediatr Neurosci,* 6**,** 44-7.
SMITH, H. L. & HAND, A. M. 1958. Chondroectodermal dysplasia (Ellis-van Creveld syndrome); report of two cases. *Pediatrics,* 21**,** 298-307.
SMITH, J. C., NORTHEY, J. G., GARG, J., PEARLMAN, R. E. & SIU, K. W. 2005. Robust method for proteome analysis by MS/MS using an entire translated genome: demonstration on the ciliome of Tetrahymena thermophila. *J Proteome Res,* 4**,** 909-19.
SMITH, K. K. & SCHNEIDER, R. A. 1998. Have gene knockouts caused evolutionary reversals in the mammalian first arch? *Bioessays,* 20**,** 245-55.
SMOLICH, B. D., MCMAHON, J. A., MCMAHON, A. P. & PAPKOFF, J. 1993. Wnt family proteins are secreted and associated with the cell surface. *Mol Biol Cell,* 4**,** 1267-75.
ST-JACQUES, B., HAMMERSCHMIDT, M. & MCMAHON, A. P. 1999. Indian hedgehog signaling regulates proliferation and differentiation of chondrocytes and is essential for bone formation. *Genes Dev,* 13**,** 2072-86.
STECCA, B., MAS, C., CLEMENT, V., ZBINDEN, M., CORREA, R., PIGUET, V., BEERMANN, F. & RUIZ, I. A. A. 2007. Melanomas require HEDGEHOG-GLI signaling regulated by interactions between GLI1 and the RAS-MEK/AKT pathways. *Proc Natl Acad Sci U S A,* 104**,** 5895-900.
STORM, A. L., JOHNSON, J. M., LAMMER, E., GREEN, G. E. & CUNNIFF, C. 2005. Auriculo-condylar syndrome is associated with highly variable ear and mandibular defects in multiple kindreds. *Am J Med Genet A,* 138A**,** 141-5.
STORM, E. E., RUBENSTEIN, J. L. & MARTIN, G. R. 2003. Dosage of Fgf8 determines whether cell survival is positively or negatively regulated in the developing forebrain. *Proc Natl Acad Sci U S A,* 100**,** 1757-62.
STRICKER, S., FUNDELE, R., VORTKAMP, A. & MUNDLOS, S. 2002. Role of Runx genes in chondrocyte differentiation. *Dev Biol,* 245**,** 95-108.
SU, N., SUN, Q., LI, C., LU, X., QI, H., CHEN, S., YANG, J., DU, X., ZHAO, L., HE, Q., JIN, M., SHEN, Y., CHEN, D. & CHEN, L. 2010a. Gain-of-function mutation in FGFR3 in mice leads to decreased bone mass by affecting

both osteoblastogenesis and osteoclastogenesis. *Hum Mol Genet,* 19**,** 1199-210.
SU, N., XU, X., LI, C., HE, Q., ZHAO, L., LI, C., CHEN, S., LUO, F., YI, L., DU, X., HUANG, H., DENG, C. & CHEN, L. 2010b. Generation of Fgfr3 conditional knockout mice. *Int J Biol Sci,* 6**,** 327-32.
SU, X., DRISCOLL, K., YAO, G., RAED, A., WU, M., BEALES, P. L. & ZHOU, J. 2014. Bardet-Biedl syndrome proteins 1 and 3 regulate the ciliary trafficking of polycystic kidney disease 1 protein. *Hum Mol Genet,* 23**,** 5441-51.
SUGITO, H., SHIBUKAWA, Y., KINUMATSU, T., YASUDA, T., NAGAYAMA, M., YAMADA, S., MINUGH-PURVIS, N., PACIFICI, M. & KOYAMA, E. 2011. Ihh signaling regulates mandibular symphysis development and growth. *J Dent Res,* 90**,** 625-31.
SUH, Y. J., BAE, H. S., CHOI, J. Y., LEE, J. H., KIM, M. J., KIM, S., RYOO, H. M. & BAEK, S. H. 2014. A novel FGFR2 mutation in tyrosine kinase II domain, L617F, in Crouzon syndrome. *J Cell Biochem,* 115**,** 102-10.
SUMMERS, J., LUDWIG, J. & KANZE, D. 2014. Pierre robin sequence in a neonate with suckling difficulty and weight loss. *J Am Osteopath Assoc,* 114**,** 727-31.
SZABO-ROGERS, H. L., GEETHA-LOGANATHAN, P., NIMMAGADDA, S., FU, K. K. & RICHMAN, J. M. 2008. FGF signals from the nasal pit are necessary for normal facial morphogenesis. *Dev Biol,* 318**,** 289-302.
TABLER, J. M., BARRELL, W. B., SZABO-ROGERS, H. L., HEALY, C., YEUNG, Y., PERDIGUERO, E. G., SCHULZ, C., YANNAKOUDAKIS, B. Z., MESBAHI, A., WLODARCZYK, B., GEISSMANN, F., FINNELL, R. H., WALLINGFORD, J. B. & LIU, K. J. 2013. Fuz Mutant Mice Reveal Shared Mechanisms between Ciliopathies and FGF-Related Syndromes. *Dev Cell,* 25**,** 623-35.
TALMAGE, R. V. 1970. Morphological and physiological considerations in a new concept of calcium transport in bone. *Am J Anat,* 129**,** 467-76.
TAM, P. P. & TRAINOR, P. A. 1994. Specification and segmentation of the paraxial mesoderm. *Anat Embryol (Berl),* 189**,** 275-305.
TANAKA, K., KITAGAWA, Y. & KADOWAKI, T. 2002. Drosophila segment polarity gene product porcupine stimulates the posttranslational N-glycosylation of wingless in the endoplasmic reticulum. *J Biol Chem,* 277**,** 12816-23.
TANIMOTO, Y., VEISTINEN, L., ALAKURTTI, K., TAKATALO, M. & RICE, D. P. 2012. Prevention of premature fusion of calvarial suture in GLI-Kruppel family member 3 (Gli3)-deficient mice by removing one allele of Runt-related transcription factor 2 (Runx2). *J Biol Chem,* 287**,** 21429-38.
TAO, Q., YOKOTA, C., PUCK, H., KOFRON, M., BIRSOY, B., YAN, D., ASASHIMA, M., WYLIE, C. C., LIN, X. & HEASMAN, J. 2005. Maternal wnt11 activates the canonical wnt signaling pathway required for axis formation in Xenopus embryos. *Cell,* 120**,** 857-71.
TARTAGLIA, M., KALIDAS, K., SHAW, A., SONG, X., MUSAT, D. L., VAN DER BURGT, I., BRUNNER, H. G., BERTOLA, D. R., CROSBY, A., ION, A., KUCHERLAPATI, R. S., JEFFERY, S., PATTON, M. A. & GELB, B. D. 2002. PTPN11 mutations in Noonan syndrome: molecular spectrum, genotype-phenotype correlation, and phenotypic heterogeneity. *Am J Hum Genet,* 70**,** 1555-63.

TAVELLA, S., BITICCHI, R., SCHITO, A., MININA, E., DI MARTINO, D., PAGANO, A., VORTKAMP, A., HORTON, W. A., CANCEDDA, R. & GAROFALO, S. 2004. Targeted expression of SHH affects chondrocyte differentiation, growth plate organization, and Sox9 expression. *J Bone Miner Res,* 19**,** 1678-88.

TAVORMINA, P. L., SHIANG, R., THOMPSON, L. M., ZHU, Y. Z., WILKIN, D. J., LACHMAN, R. S., WILCOX, W. R., RIMOIN, D. L., COHN, D. H. & WASMUTH, J. J. 1995. Thanatophoric dysplasia (types I and II) caused by distinct mutations in fibroblast growth factor receptor 3. *Nat Genet,* 9**,** 321-8.

TE WELSCHER, P., FERNANDEZ-TERAN, M., ROS, M. A. & ZELLER, R. 2002a. Mutual genetic antagonism involving GLI3 and dHAND prepatterns the vertebrate limb bud mesenchyme prior to SHH signaling. *Genes Dev,* 16**,** 421-6.

TE WELSCHER, P., ZUNIGA, A., KUIJPER, S., DRENTH, T., GOEDEMANS, H. J., MEIJLINK, F. & ZELLER, R. 2002b. Progression of vertebrate limb development through SHH-mediated counteraction of GLI3. *Science,* 298**,** 827-30.

TIAN, G., ZHOU, Y., HAJKOVA, D., MIYAGI, M., DINCULESCU, A., HAUSWIRTH, W. W., PALCZEWSKI, K., GENG, R., ALAGRAMAM, K. N., ISOSOMPPI, J., SANKILA, E. M., FLANNERY, J. G. & IMANISHI, Y. 2009. Clarin-1, encoded by the Usher Syndrome III causative gene, forms a membranous microdomain: possible role of clarin-1 in organizing the actin cytoskeleton. *J Biol Chem,* 284**,** 18980-93.

TISSIER-SETA, J. P., MUCCHIELLI, M. L., MARK, M., MATTEI, M. G., GORIDIS, C. & BRUNET, J. F. 1995. Barx1, a new mouse homeodomain transcription factor expressed in cranio-facial ectomesenchyme and the stomach. *Mech Dev,* 51**,** 3-15.

TOBIN, J. L. & BEALES, P. L. 2007. Bardet-Biedl syndrome: beyond the cilium. *Pediatr Nephrol,* 22**,** 926-36.

TOBIN, J. L., DI FRANCO, M., EICHERS, E., MAY-SIMERA, H., GARCIA, M., YAN, J., QUINLAN, R., JUSTICE, M. J., HENNEKAM, R. C., BRISCOE, J., TADA, M., MAYOR, R., BURNS, A. J., LUPSKI, J. R., HAMMOND, P. & BEALES, P. L. 2008. Inhibition of neural crest migration underlies craniofacial dysmorphology and Hirschsprung's disease in Bardet-Biedl syndrome. *Proc Natl Acad Sci U S A,* 105**,** 6714-9.

TOLEDO, C., NAVARRO-BARROS, R., ALBA, L. & MUNOZ, E. 1999. Kyphomelic dysplasia: a report of a family with an autosomal dominant pattern. *Ann Genet,* 42**,** 170-3.

TOMO, S., OGITA, M. & TOMO, I. 1997. Development of mandibular cartilages in the rat. *Anat Rec,* 249**,** 233-9.

TRAINOR, P. A. 2005. Specification and patterning of neural crest cells during craniofacial development. *Brain Behav Evol,* 66**,** 266-80.

TREVISAN, R. A. & SCAPINO, R. P. 1976. Secondary cartilages in growth and development of the symphysis menti in the hamster. *Acta Anat (Basel),* 94**,** 40-58.

TRICHILIS, A. & WROBLEWSKI, J. 1997. Expression of p53 and hsp70 in relation to apoptosis during Meckel's cartilage development in the mouse. *Anat Embryol (Berl),* 196**,** 107-13.

TRUMPP, A., DEPEW, M. J., RUBENSTEIN, J. L., BISHOP, J. M. & MARTIN, G. R. 1999. Cre-mediated gene inactivation demonstrates that FGF8 is

required for cell survival and patterning of the first branchial arch. *Genes Dev,* 13**,** 3136-48.
TUCKER, A. & SHARPE, P. 2004. The cutting-edge of mammalian development; how the embryo makes teeth. *Nat Rev Genet,* 5**,** 499-508.
TUCKER, A. S., MATTHEWS, K. L. & SHARPE, P. T. 1998. Transformation of tooth type induced by inhibition of BMP signaling. *Science,* 282**,** 1136-8.
TUCKER, A. S., YAMADA, G., GRIGORIOU, M., PACHNIS, V. & SHARPE, P. T. 1999. Fgf-8 determines rostral-caudal polarity in the first branchial arch. *Development,* 126**,** 51-61.
TUKACHINSKY, H., LOPEZ, L. V. & SALIC, A. 2010. A mechanism for vertebrate Hedgehog signaling: recruitment to cilia and dissociation of SuFu-Gli protein complexes. *J Cell Biol,* 191**,** 415-28.
TURKSEN, Z., OZAKPINAR, H. R. & TELLIOGLU, A. T. 2012. A case of syngnathia, cleft palate and hypospadias: an isolated case or syndromic syngnathism? *J Craniomaxillofac Surg,* 40**,** 8-10.
TURNER, N. & GROSE, R. 2010. Fibroblast growth factor signalling: from development to cancer. *Nat Rev Cancer,* 10**,** 116-29.
TUSON, M., HE, M. & ANDERSON, K. V. 2011. Protein kinase A acts at the basal body of the primary cilium to prevent Gli2 activation and ventralization of the mouse neural tube. *Development,* 138**,** 4921-30.
UNDEN, A. B., HOLMBERG, E., LUNDH-ROZELL, B., STAHLE-BACKDAHL, M., ZAPHIROPOULOS, P. G., TOFTGARD, R. & VORECHOVSKY, I. 1996. Mutations in the human homologue of Drosophila patched (PTCH) in basal cell carcinomas and the Gorlin syndrome: different in vivo mechanisms of PTCH inactivation. *Cancer Res,* 56**,** 4562-5.
VAN ALLEN, M. I., KALOUSEK, D. K., CHERNOFF, G. F., JURILOFF, D., HARRIS, M., MCGILLIVRAY, B. C., YONG, S. L., LANGLOIS, S., MACLEOD, P. M., CHITAYAT, D. & ET AL. 1993. Evidence for multi-site closure of the neural tube in humans. *Am J Med Genet,* 47**,** 723-43.
VAN DER MERWE, A. E., WESTON, D. A., OOSTRA, R. J. & MAAT, G. J. 2013. A review of the embryological development and associated developmental abnormalities of the sternum in the light of a rare palaeopathological case of sternal clefting. *Homo,* 64**,** 129-41.
VEISTINEN, L., TAKATALO, M., TANIMOTO, Y., KESPER, D. A., VORTKAMP, A. & RICE, D. P. 2012. Loss-of-Function of Gli3 in Mice Causes Abnormal Frontal Bone Morphology and Premature Synostosis of the Interfrontal Suture. *Front Physiol,* 3**,** 121.
VELAND, I. R., AWAN, A., PEDERSEN, L. B., YODER, B. K. & CHRISTENSEN, S. T. 2009. Primary cilia and signaling pathways in mammalian development, health and disease. *Nephron Physiol,* 111**,** p39-53.
VITELLI, F., LINDSAY, E. A. & BALDINI, A. 2002. Genetic dissection of the DiGeorge syndrome phenotype. *Cold Spring Harb Symp Quant Biol,* 67**,** 327-32.
VOGEL, A., RODRIGUEZ, C. & IZPISUA-BELMONTE, J. C. 1996. Involvement of FGF-8 in initiation, outgrowth and patterning of the vertebrate limb. *Development,* 122**,** 1737-50.
VORTKAMP, A., GESSLER, M. & GRZESCHIK, K. H. 1991. GLI3 zinc-finger gene interrupted by translocations in Greig syndrome families. *Nature,* 352**,** 539-40.

VYAS, N., GOSWAMI, D., MANONMANI, A., SHARMA, P., RANGANATH, H. A., VIJAYRAGHAVAN, K., SHASHIDHARA, L. S., SOWDHAMINI, R. & MAYOR, S. 2008. Nanoscale organization of hedgehog is essential for long-range signaling. *Cell,* 133**,** 1214-27.

WALLIN, J., WILTING, J., KOSEKI, H., FRITSCH, R., CHRIST, B. & BALLING, R. 1994. The role of Pax-1 in axial skeleton development. *Development,* 120**,** 1109-21.

WALLINGFORD, J. B. 2006. Planar cell polarity, ciliogenesis and neural tube defects. *Hum Mol Genet,* 15 Spec No 2**,** R227-34.

WALLINGFORD, J. B. & HARLAND, R. M. 2002. Neural tube closure requires Dishevelled-dependent convergent extension of the midline. *Development,* 129**,** 5815-25.

WANG, B., FALLON, J. F. & BEACHY, P. A. 2000. Hedgehog-regulated processing of Gli3 produces an anterior/posterior repressor gradient in the developing vertebrate limb. *Cell,* 100**,** 423-34.

WANG, E. A., ROSEN, V., D'ALESSANDRO, J. S., BAUDUY, M., CORDES, P., HARADA, T., ISRAEL, D. I., HEWICK, R. M., KERNS, K. M., LAPAN, P. & ET AL. 1990. Recombinant human bone morphogenetic protein induces bone formation. *Proc Natl Acad Sci U S A,* 87**,** 2220-4.

WANG, J., MARK, S., ZHANG, X., QIAN, D., YOO, S. J., RADDE-GALLWITZ, K., ZHANG, Y., LIN, X., COLLAZO, A., WYNSHAW-BORIS, A. & CHEN, P. 2005a. Regulation of polarized extension and planar cell polarity in the cochlea by the vertebrate PCP pathway. *Nat Genet,* 37**,** 980-5.

WANG, Q., GREEN, R. P., ZHAO, G. & ORNITZ, D. M. 2001. Differential regulation of endochondral bone growth and joint development by FGFR1 and FGFR3 tyrosine kinase domains. *Development,* 128**,** 3867-76.

WANG, Y. & NATHANS, J. 2007. Tissue/planar cell polarity in vertebrates: new insights and new questions. *Development,* 134**,** 647-58.

WANG, Y., SPATZ, M. K., KANNAN, K., HAYK, H., AVIVI, A., GORIVODSKY, M., PINES, M., YAYON, A., LONAI, P. & GIVOL, D. 1999. A mouse model for achondroplasia produced by targeting fibroblast growth factor receptor 3. *Proc Natl Acad Sci U S A,* 96**,** 4455-60.

WANG, Y., XIAO, R., YANG, F., KARIM, B. O., IACOVELLI, A. J., CAI, J., LERNER, C. P., RICHTSMEIER, J. T., LESZL, J. M., HILL, C. A., YU, K., ORNITZ, D. M., ELISSEEFF, J., HUSO, D. L. & JABS, E. W. 2005b. Abnormalities in cartilage and bone development in the Apert syndrome FGFR2(+/S252W) mouse. *Development,* 132**,** 3537-48.

WANG, Y., ZHOU, Z., WALSH, C. T. & MCMAHON, A. P. 2009. Selective translocation of intracellular Smoothened to the primary cilium in response to Hedgehog pathway modulation. *Proc Natl Acad Sci U S A,* 106**,** 2623-8.

WATERS, A. M. & BEALES, P. L. 2011. Ciliopathies: an expanding disease spectrum. *Pediatr Nephrol,* 26**,** 1039-56.

WEATHERBEE, S. D., NISWANDER, L. A. & ANDERSON, K. V. 2009. A mouse model for Meckel syndrome reveals Mks1 is required for ciliogenesis and Hedgehog signaling. *Hum Mol Genet,* 18**,** 4565-75.

WEBSTER, M. K. & DONOGHUE, D. J. 1996. Constitutive activation of fibroblast growth factor receptor 3 by the transmembrane domain point mutation found in achondroplasia. *EMBO J,* 15**,** 520-7.

WEN, X., LAI, C. K., EVANGELISTA, M., HONGO, J. A., DE SAUVAGE, F. J. & SCALES, S. J. 2010. Kinetics of hedgehog-dependent full-length Gli3 accumulation in primary cilia and subsequent degradation. *Mol Cell Biol,* 30**,** 1910-22.

WIJGERDE, M., MCMAHON, J. A., RULE, M. & MCMAHON, A. P. 2002. A direct requirement for Hedgehog signaling for normal specification of all ventral progenitor domains in the presumptive mammalian spinal cord. *Genes Dev,* 16**,** 2849-64.

WILKIE, A. O. 1997. Craniosynostosis: genes and mechanisms. *Hum Mol Genet,* 6**,** 1647-56.

WILKIE, A. O. & MORRISS-KAY, G. M. 2001. Genetics of craniofacial development and malformation. *Nat Rev Genet,* 2**,** 458-68.

WILKIE, A. O., PATEY, S. J., KAN, S. H., VAN DEN OUWELAND, A. M. & HAMEL, B. C. 2002. FGFs, their receptors, and human limb malformations: clinical and molecular correlations. *Am J Med Genet,* 112**,** 266-78.

WILKIE, A. O., SLANEY, S. F., OLDRIDGE, M., POOLE, M. D., ASHWORTH, G. J., HOCKLEY, A. D., HAYWARD, R. D., DAVID, D. J., PULLEYN, L. J., RUTLAND, P. & ET AL. 1995. Apert syndrome results from localized mutations of FGFR2 and is allelic with Crouzon syndrome. *Nat Genet,* 9**,** 165-72.

WILLERT, K., BROWN, J. D., DANENBERG, E., DUNCAN, A. W., WEISSMAN, I. L., REYA, T., YATES, J. R., 3RD & NUSSE, R. 2003. Wnt proteins are lipid-modified and can act as stem cell growth factors. *Nature,* 423**,** 448-52.

WISE, G. E., LUMPKIN, S. J., HUANG, H. & ZHANG, Q. 2000. Osteoprotegerin and osteoclast differentiation factor in tooth eruption. *J Dent Res,* 79**,** 1937-42.

XIAO, G., JIANG, D., GE, C., ZHAO, Z., LAI, Y., BOULES, H., PHIMPHILAI, M., YANG, X., KARSENTY, G. & FRANCESCHI, R. T. 2005. Cooperative interactions between activating transcription factor 4 and Runx2/Cbfa1 stimulate osteoblast-specific osteocalcin gene expression. *J Biol Chem,* 280**,** 30689-96.

XIONG, W., HE, F., MORIKAWA, Y., YU, X., ZHANG, Z., LAN, Y., JIANG, R., CSERJESI, P. & CHEN, Y. 2009. Hand2 is required in the epithelium for palatogenesis in mice. *Dev Biol,* 330**,** 131-41.

XU, J., LAWSHE, A., MACARTHUR, C. A. & ORNITZ, D. M. 1999. Genomic structure, mapping, activity and expression of fibroblast growth factor 17. *Mech Dev,* 83**,** 165-78.

XU, X., WEINSTEIN, M., LI, C., NASKI, M., COHEN, R. I., ORNITZ, D. M., LEDER, P. & DENG, C. 1998. Fibroblast growth factor receptor 2 (FGFR2)-mediated reciprocal regulation loop between FGF8 and FGF10 is essential for limb induction. *Development,* 125**,** 753-65.

YAMAGISHI, C., YAMAGISHI, H., MAEDA, J., TSUCHIHASHI, T., IVEY, K., HU, T. & SRIVASTAVA, D. 2006. Sonic hedgehog is essential for first pharyngeal arch development. *Pediatr Res,* 59**,** 349-54.

YAMASHITA, S., ANDOH, M., UENO-KUDOH, H., SATO, T., MIYAKI, S. & ASAHARA, H. 2009. Sox9 directly promotes Bapx1 gene expression to repress Runx2 in chondrocytes. *Exp Cell Res,* 315**,** 2231-40.

YAMAZAKI, K., SUDA, N. & KURODA, T. 1997. Immunohistochemical localization of parathyroid hormone-related protein in developing mouse Meckel's cartilage and mandible. *Arch Oral Biol,* 42**,** 787-94.

YANAGISAWA, H., CLOUTHIER, D. E., RICHARDSON, J. A., CHARITE, J. & OLSON, E. N. 2003. Targeted deletion of a branchial arch-specific enhancer reveals a role of dHAND in craniofacial development. *Development,* 130**,** 1069-78.

YANAGISAWA, H., YANAGISAWA, M., KAPUR, R. P., RICHARDSON, J. A., WILLIAMS, S. C., CLOUTHIER, D. E., DE WIT, D., EMOTO, N. & HAMMER, R. E. 1998. Dual genetic pathways of endothelin-mediated intercellular signaling revealed by targeted disruption of endothelin converting enzyme-1 gene. *Development,* 125**,** 825-36.

YANG, R. T., ZHANG, C., LIU, Y., ZHOU, H. H. & LI, Z. B. 2012. Autophagy prior to chondrocyte cell death during the degeneration of Meckel's cartilage. *Anat Rec (Hoboken),* 295**,** 734-41.

YANG, T., BASSUK, A. G. & FRITZSCH, B. 2013. Prickle1 stunts limb growth through alteration of cell polarity and gene expression. *Dev Dyn,* 242**,** 1293-306.

YANNAKOUDAKIS, B. Z. & LIU, K. J. 2013. Common skeletal features in rare diseases: New links between ciliopathies and FGF-related syndromes. *Rare dis,* 1:e27109

YASHIRO, K., ZHAO, X., UEHARA, M., YAMASHITA, K., NISHIJIMA, M., NISHINO, J., SAIJOH, Y., SAKAI, Y. & HAMADA, H. 2004. Regulation of retinoic acid distribution is required for proximodistal patterning and outgrowth of the developing mouse limb. *Dev Cell,* 6**,** 411-22.

YBOT-GONZALEZ, P., SAVERY, D., GERRELLI, D., SIGNORE, M., MITCHELL, C. E., FAUX, C. H., GREENE, N. D. & COPP, A. J. 2007. Convergent extension, planar-cell-polarity signalling and initiation of mouse neural tube closure. *Development,* 134**,** 789-99.

YEH, B. K., IGARASHI, M., ELISEENKOVA, A. V., PLOTNIKOV, A. N., SHER, I., RON, D., AARONSON, S. A. & MOHAMMADI, M. 2003. Structural basis by which alternative splicing confers specificity in fibroblast growth factor receptors. *Proc Natl Acad Sci U S A,* 100**,** 2266-71.

YODER, B. K. 2007. Role of primary cilia in the pathogenesis of polycystic kidney disease. *J Am Soc Nephrol,* 18**,** 1381-8.

YONEI-TAMURA, S., ENDO, T., YAJIMA, H., OHUCHI, H., IDE, H. & TAMURA, K. 1999. FGF7 and FGF10 directly induce the apical ectodermal ridge in chick embryos. *Dev Biol,* 211**,** 133-43.

YOUNG, I. D. 1989. Cranioectodermal dysplasia (Sensenbrenner's syndrome). *J Med Genet,* 26**,** 393-6.

ZENG, X., GOETZ, J. A., SUBER, L. M., SCOTT, W. J., JR., SCHREINER, C. M. & ROBBINS, D. J. 2001. A freely diffusible form of Sonic hedgehog mediates long-range signalling. *Nature,* 411**,** 716-20.

ZHANG, X., IBRAHIMI, O. A., OLSEN, S. K., UMEMORI, H., MOHAMMADI, M. & ORNITZ, D. M. 2006. Receptor specificity of the fibroblast growth factor family. The complete mammalian FGF family. *J Biol Chem,* 281**,** 15694-700.

ZHANG, Z., WLODARCZYK, B. J., NIEDERREITHER, K., VENUGOPALAN, S., FLOREZ, S., FINNELL, R. H. & AMENDT, B. A. 2011. Fuz regulates craniofacial development through tissue specific responses to signaling factors. *PLoS One,* 6**,** e24608.

ZHOU, G., GAROFALO, S., MUKHOPADHYAY, K., LEFEBVRE, V., SMITH, C. N., EBERSPAECHER, H. & DE CROMBRUGGHE, B. 1995. A 182 bp fragment of the mouse pro alpha 1(II) collagen gene is sufficient to

direct chondrocyte expression in transgenic mice. *J Cell Sci,* 108 (Pt 12)**,** 3677-84.
ZHOU, G., ZHENG, Q., ENGIN, F., MUNIVEZ, E., CHEN, Y., SEBALD, E., KRAKOW, D. & LEE, B. 2006. Dominance of SOX9 function over RUNX2 during skeletogenesis. *Proc Natl Acad Sci U S A,* 103**,** 19004-9.
ZHOU, Y. X., XU, X., CHEN, L., LI, C., BRODIE, S. G. & DENG, C. X. 2000. A Pro250Arg substitution in mouse Fgfr1 causes increased expression of Cbfa1 and premature fusion of calvarial sutures. *Hum Mol Genet,* 9**,** 2001-8.
ZHU, J., GARRETT, R., JUNG, Y., ZHANG, Y., KIM, N., WANG, J., JOE, G. J., HEXNER, E., CHOI, Y., TAICHMAN, R. S. & EMERSON, S. G. 2007. Osteoblasts support B-lymphocyte commitment and differentiation from hematopoietic stem cells. *Blood,* 109**,** 3706-12.
ZILBER, Y., BABAYEVA, S., SEO, J. H., LIU, J. J., MOOTIN, S. & TORBAN, E. 2013. The PCP effector Fuzzy controls cilial assembly and signaling by recruiting Rab8 and Dishevelled to the primary cilium. *Mol Biol Cell,* 24**,** 555-65.
ZUNIGA, A. & ZELLER, R. 1999. Gli3 (Xt) and formin (ld) participate in the positioning of the polarising region and control of posterior limb-bud identity. *Development,* 126**,** 13-21.

Chapter 9 Appendix

Developmental Cell
Article

Fuz Mutant Mice Reveal Shared Mechanisms between Ciliopathies and FGF-Related Syndromes

Jacqueline M. Tabler,[1,6] William B. Barrell,[1] Heather L. Szabo-Rogers,[1,5,7] Christopher Healy,[1,5] Yvonne Yeung,[1] Elisa Gomez Perdiguero,[2] Christian Schulz,[2] Basil Z. Yannakoudakis,[1] Aida Mesbahi,[1] Bogdan Wlodarczyk,[3] Frederic Geissmann,[2] Richard H. Finnell,[3] John B. Wallingford,[4] and Karen J. Liu[1,*]
[1]Department of Craniofacial Development and Stem Cell Biology, Dental Institute
[2]Centre for the Cellular and Molecular Biology of Inflammation
King's College London, London SE1 9RT, UK
[3]Dell Pediatric Research Institute, Departments of Nutritional Sciences, Chemistry, and Biochemistry, The University of Texas at Austin, Austin, TX 78723, USA
[4]Howard Hughes Medical Institute and Section of Molecular Cell and Developmental Biology and Institute for Cellular and Molecular Biology, The University of Texas at Austin, Austin, TX 78712, USA
[5]These authors contributed equally to this work
[6]Present address: Section of Molecular Cell and Developmental Biology, University of Texas, Austin, TX 78712, USA
[7]Present address: Department of Oral Biology, Center for Craniofacial Regeneration, University of Pittsburgh, Pittsburgh, PA 15260, USA
*Correspondence: karen.liu@kcl.ac.uk
http://dx.doi.org/10.1016/j.devcel.2013.05.021

SUMMARY

Ciliopathies are a broad class of human disorders with craniofacial dysmorphology as a common feature. Among these is high arched palate, a condition that affects speech and quality of life. Using the ciliopathic *Fuz* mutant mouse, we find that high arched palate does not, as commonly suggested, arise from midface hypoplasia. Rather, increased neural crest expands the maxillary primordia. In *Fuz* mutants, this phenotype stems from dysregulated Gli processing, which in turn results in excessive craniofacial *Fgf8* gene expression. Accordingly, genetic reduction of *Fgf8* ameliorates the maxillary phenotypes. Similar phenotypes result from mutation of oral-facial-digital syndrome 1 (*Ofd1*), suggesting that aberrant transcription of *Fgf8* is a common feature of ciliopathies. High arched palate is also a prevalent feature of fibroblast growth factor (FGF) hyperactivation syndromes. Thus, our findings elucidate the etiology for a common craniofacial anomaly and identify links between two classes of human disease: FGF-hyperactivation syndromes and ciliopathies.

INTRODUCTION

Craniofacial dysmorphology is a common component of the ciliopathy disease spectrum, but while defective neural crest (NC) cell migration has been implicated in Bardet-Biedl Syndrome (BBS) (Tobin et al., 2008), little else is known about the underlying developmental processes in ciliopathy-associated craniofacial defects. Among the more consistent craniofacial phenotypes in ciliopathies is the presence of a high arched palate (Beales et al., 1999). In this condition, the palate is characterized by a pronounced median groove, but the roof of the mouth remains intact across the midline. This condition is often referred to as a "pseudo-cleft." Later in life, a high arched palate is also associated with secondary dental anomalies, such as postnatal gingival swelling and crowding of the molars. These defects can impair speech and complicate intubation, a major concern for craniofacial patients who frequently require multiple surgeries during childhood. Thus, high arched palate has a significant impact on patients' quality of life.

The etiology of high arched palate remains obscure. One long-held hypothesis proposes that the arch arises from a midface hypoplasia causing insufficient maxillary growth and subsequent compression of the upper dental arch (Hennekam et al., 2010; Kreiborg and Cohen, 1992; Slaney et al., 1996). However, recent morphometric analyses suggest that this may not be true (Martínez-Abadías et al., 2010). Although a chemically induced rat model has existed for several decades, the embryological progression of the phenotype is unknown (Lorente et al., 1981). Surprisingly, no genetic model of high arched palate has yet been reported, so the underlying cellular and anatomical causes remain unknown and developmental hypotheses are untested.

Clinical observations also complicate our picture of high arched palate, as this defect is associated with a variety of seemingly unrelated syndromes (Hayward et al., 2004; Hennekam et al., 2010; Kreiborg and Cohen, 1992; Vadiati Saberi and Shakoorpour, 2011). For example, though rarely mentioned in the literature, high arched palate is a central feature in many ciliopathies, including BBS, oral-facial-digital syndromes (OFD types I and IV), Joubert syndrome, and Sensenbrenner syndrome (Beales et al., 1999; Hennekam et al., 2010; Moore et al., 2005; Prattichizzo et al., 2008; Sensenbrenner et al., 1975; Somlo et al., 1993). In fact, 88% of BBS patients present with high arched palate, and many also display associated dental crowding and soft tissue swellings (Beales et al., 1999). High arched palate is also consistently observed in an array of syndromes characterized by dysregulation of fibroblast growth factor (FGF) signaling or downstream components such as the Ras kinase (Goodwin et al., 2012). Examples include Apert, Crouzon, Muenke, and cardio-facio-cutaneous syndromes (Agochukwu

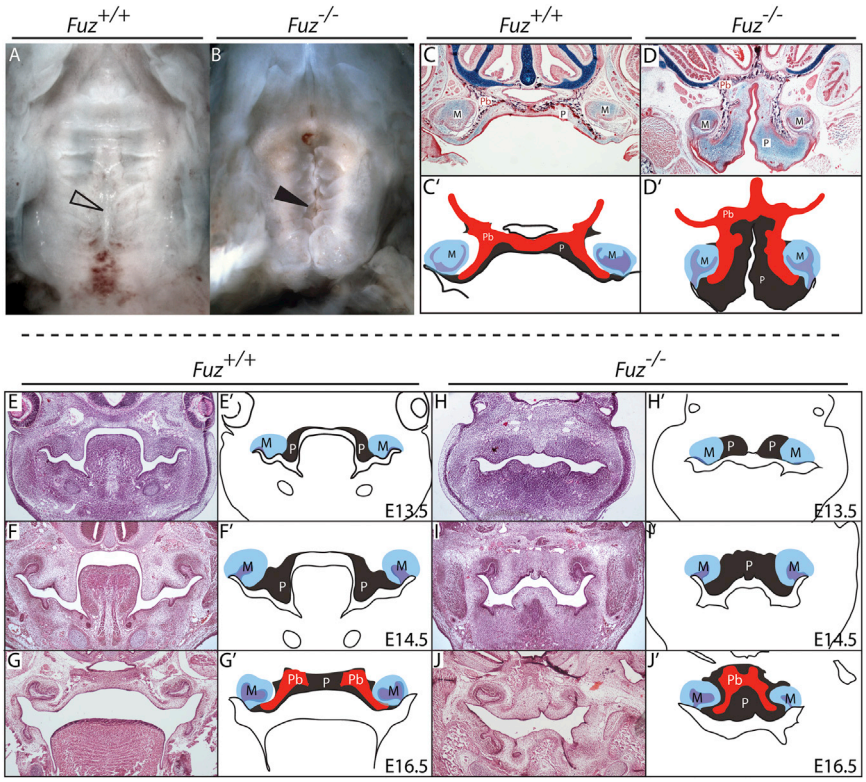

Figure 1. *Fuz* Mutant Mice Are a Model for High Arched Palate

(A and B) Ventral views of E17.5 palates. Mutants exhibit a narrow palate (arrowheads) and disrupted rugal organization compared to littermates.

(C and D) Sirius red/alcian blue staining of E17.5 coronal sections. Bilateral palatine bones are formed in both control and mutant, abutting at the midline (black). Mutant palatine bones (Pb) are mediolaterally shortened with an increase in the ventral extension. Note enlarged palatal mesenchyme (P). Molars (M) appear normal.

(C′ and D′) Schematics depicting skewed palatal anatomy.

(E–J) Hemotoxylin and eosin staining of coronal sections at indicated stages.

(E′–J′) Schematics of sections identifying palatal mesenchyme (gray, P), molars (blue and purple, M), and palatal bone condensations (red, Pb). In (H) through (J′), mutant palatal condensations are medially constrained and do not extend into the oral cavity. Palatine bone can be observed in both mutants and controls by E16.5.

See also Figure S1.

et al., 2012; Berkowitz, 1971; Hennekam et al., 2010; Kreiborg and Cohen, 1992; Letra et al., 2007; Rynearson, 2000; Vadiati Saberi and Shakoorpour, 2011). This finding is curious, because while FGF signals have been implicated in controlling cilium length (Hong and Dawid, 2009; Neugebauer et al., 2009), there has been no evidence to date suggesting a link between FGF dysregulation syndromes and the ciliopathies.

To characterize ciliopathic craniofacial defects, we examined mice with a mutation in the gene encoding *Fuzzy* (*Fuz*), which has recently emerged as a key regulator of ciliogenesis (Gray et al., 2009; Park et al., 2006). Initially described as a *Drosophila* planar cell polarity effector gene (Collier and Gubb, 1997), studies in both *Xenopus* and mice identified Fuz as a central regulator of vertebrate ciliogenesis (Brooks and Wallingford, 2012; Gray et al., 2009; Park et al., 2006). Consistent with the key role of cilia in Hedgehog (Hh) signaling, disruption of Fuz affects Hedgehog-dependent patterning events in both frogs and mice (Gray et al., 2009; Park et al., 2006), and in mice, loss of *Fuz* has been shown directly to disrupt the processing of Gli3 (Heydeck et al., 2009). Recently, live imaging analyses revealed that Fuz is essential for normal trafficking of the retrograde intraflagellar transport (IFT) machinery in vertebrate cilia; when Fuz is depleted, localization of IFT-A proteins, such as IFT43, is disrupted (Brooks and Wallingford, 2012). As a consequence, IFT trains become stalled, leading to shortened cilia and impaired signal transduction. Finally, *Fuz* is of particular interest because it is mutated in human patients with birth defects (Seo et al., 2011) and because *Fuz* mutant mice display a variety of craniofacial phenotypes (Zhang et al., 2011).

Here, we present the *Fuz* mutant mouse as a useful genetic model for the study of high arched palate. Although current hypotheses suggest that high arched palate arises from constriction of the upper jaw (Hennekam et al., 2010), our data demonstrate that the primary cause of ciliopathic high arched palate is instead excessive NC producing an enlarged first branchial arch (BA1) and maxillary hyperplasia early in embryogenesis. We have also discovered a surprising mechanistic basis for this phenotype, as we observed a dramatic increase in FGF signaling due to increased cranial *Fgf8* gene expression. Genetic reduction of *Fgf8* rescues the maxillary defects in *Fuz* mutant mice. Finally, we observed a similar maxillary expansion and upregulation of *Fgf8* expression in another ciliopathy mouse model, OFD-1 (Ferrante et al., 2006). Thus, we have identified dysregulation of FGF function as the cause of facial defects in ciliopathic mutant mice, demonstrating etiological commonalities between two broad categories of human congenital anomalies: the ciliopathies and the FGF-related syndromes.

RESULTS

Fuz Mutant Mice Are a Model of High Arched Palate

Fuz mutant mice appear to have a cleft secondary palate (Figures 1A and 1B); however, frontal sections revealed that the palatal shelves were, in fact, not clefted (Figures 1C–1D′). Instead, in all mutants analyzed, the palatine bones displayed the classic inverted-V shape typical of a high arched palate (Figures 1D–1D′). Palatal narrowing and palatine bone defects were observed throughout the anterior-posterior extent of the secondary palate in mutants (Figure S1 available online). We also observed expanded mesenchyme within the oral cavity in *Fuz* mutant mice (Figure 1D, "P" in light blue area; Figure 1D′, gray area). Thus, the maxillary phenotypes of *Fuz* mutant mice bear a striking similarity to the high arched palate reported for human ciliopathy patients (Beales et al., 1999; Hennekam et al., 2010; Tagliani et al., 2010).

The embryological events leading to high arched palate have not been previously described, so we compared maxillary development in a staged series of wild-type and *Fuz*$^{-/-}$ littermates. In controls, the palatal shelves developed bilaterally, growing and extending ventrally into the oral cavity at E13.5 (Figures 1E and 1E′). The palatal primordia were evident at the appropriate stage in *Fuz* mutants but were displaced medially compared to littermates and did not extend ventrally (Figures 1H and 1H′, outlined in gray). At E14.5, palatal condensations in controls remained bilateral and were fully extended, flanking the tongue (Figures 1F-1F′), with the palate fusing by E16.5 (Figures 1G and 1G′). In mutants, however, the palatal condensations did not extend and instead appeared as one contiguous domain (Figures 1I–1J′). This medial shift of the palatal shelves was also evident from *Patched1 (Ptc1)* expression, which spans the midline (Figure S1A and S1B). Likewise, ossification of palatine bones was apparent at E17.5 in controls, and in *Fuz* mutants the palatine bones were displaced medially (Figures 1D and 1D′). Furthermore, analysis by microcomputed tomography (μCT) revealed that the majority of midfacial bones are present and ossifying. Though small and constrained, the mutant palatine bones are roughly normal in shape (Figures S1M–S1M″). These data raised the intriguing possibility that a recognizable palate can form despite an initial failure of shelf outgrowth (Figures 1H and 1H′).

Fuz Mutant Mice Displayed Enlarged Maxillary Processes

When examined at earlier stages, we found that a larger maxillary process was evident in *Fuz* mutants as early as E9.0 (Figures 2A and 2B); by e9.5 the maxillary domain is substantially larger (compare Figures 2C and 2E to Figures 2D and 2F). Cell numbers were significantly increased in the maxilla, but there was no coincident increase in mitotic cells or change in apoptosis (Figures 2G and 2H; data not shown). Overall, this developmental progression is strikingly divergent from that underlying traditional cleft palates (Chai and Maxson, 2006), suggesting that the high arched palate, though commonly referred to as a "pseudocleft," is unrelated to cleft palate and arises by a distinct developmental mechanism.

Disruption of *Fuz* Leads to Excessive NC

We next sought to better understand the developmental origin of this defect. Because the maxillary process normally arises from NC cells emanating from the posterior mesencephalon, we lineage-traced the NC using a *Wnt1-cre* driver to follow cell migration into BA1 (Figures 2A and 2B′ blue/*lacZ*; Figures 2I–2L green/green fluorescent protein [GFP]) (Danielian et al., 1998; Muzumdar et al., 2007; Soriano, 1999). In *Fuz* mutants, we observed an early expansion of cranial NC cells (Figures 2A and 2B). In Figure 2B, the rostral extent of this expansion is marked by an asterisk. We also observed a general expansion of midhindbrain streams (Figures 2A–2B′; note brackets in Figures 2A and 2B). Most strikingly, dorsal views of these embryos revealed a substantial increase of labeled cells in BA1 and the second branchial arch (BA2) (arrowheads, Figures 2A′ and 2B′). To confirm the increase in the NC, we isolated E9.25 cranial tissues from a reporter line expressing membrane GFP (*mT/mG*) when crossed to the *Wnt1-cre* driver (schematic in Figure 2O) (Danielian et al., 1998; Muzumdar et al., 2007). Using flow cytometry, we analyzed *Wnt1-cre* induced GFP-positive cells and found a significant increase in the proportion of NC cells (summarized in Figure 2P; representative plot per genotype in Figure 2O). These experiments suggest that the observed maxillary hyperplasia may stem from an excess of NC cells.

Loss of *Fuz* Leads to Disorganized NC Migration

In addition to the significant increase in NC cell numbers, the migration of the NC was disrupted in *Fuz* mutant mice. For example, we frequently observed a large proportion of rostral crest cells collecting ectopically in the optic cup regions (Figure 2B, arrowhead). To examine this at a cellular level, we utilized membrane-bound GFP in *Wnt1-cre; R26*$^{mT/mG}$ embryos. Strikingly, three-dimensional confocal imaging revealed that the depth of the migratory streams was far greater in *Fuz* mutants (79 ± 16 μm deep in mutants versus 41 ± 20 μm deep in wild-type embryos; Figures 2K and 2L). This was surprising, as mesencephalic NC cells should remain adjacent to the epidermal ectoderm, avoiding the underlying mesenchyme (Noden, 1975). Furthermore, we noted cells rostral to the trigeminal ganglion in a region that should ordinarily be clear of NC cells (compare Figure 2I′ to Figure 2J′).

We had previously shown that morpholino oligonucleotides (MOs) were an effective means to block Fuz function in *Xenopus* (Park et al., 2006). When we examined expression of *Twist,* a migratory NC marker, following *Fuz* knockdown, we observed aberrant migration of the anterior cranial crest (Figures 2M and 2N, arrowheads), consistent with the observed craniofacial defects (Park et al., 2006). In many cases, we noted increased and ectopic migration of the anterior NC into the eye field (Figure 2N, black arrowhead and inset). Together, these data suggest that *Fuz* plays an evolutionarily conserved role in controlling NC cell contributions to BA1.

Disruption of Cranial Hedgehog Signaling at Early Stages in *Fuz* Mutant Mice

We next sought to understand the molecular basis of the maxillary hyperplasia in *Fuz* mutant mice. *Fuz* controls ciliogenesis, and cilia are central to proteolytic cleavage of Gli effector proteins that transduce Hedgehog signals (Goetz and Anderson, 2010; Liu et al., 2005; Singla and Reiter, 2006). Indeed, loss of *Fuz* leads to defective Hedgehog signaling in the spinal cord and limb (Gray et al., 2009; Heydeck et al., 2009; Park et al., 2006), and Heydeck et al. showed that, during patterning of the limb, *Fuz* mutation leads to aberrant proteolytic processing of Gli3 (Heydeck et al., 2009).

However, changes in palatal Hh signaling could not account for the observed craniofacial phenotypes, as the Hh target gene *Ptc1* continues to be expressed in *Fuz* mutant palatal primordia at E14.5 (Figures S1A–S1B′), and unlike the *Fuz* mutation, loss or gain of Hh activation in the palate leads to a true cleft rather than an arched palate (Cobourne et al., 2009; Gritli-Linde et al., 2007; Hu and Helms, 1999; Lan and Jiang, 2009; Mo et al., 1997; Rice et al., 2004). Furthermore, *Gli3* mutation also leads to sporadic cleft palate due to obstruction by the tongue (Huang et al., 2008). These data suggest that, if a Gli processing defect is involved, it must occur prior to palate formation.

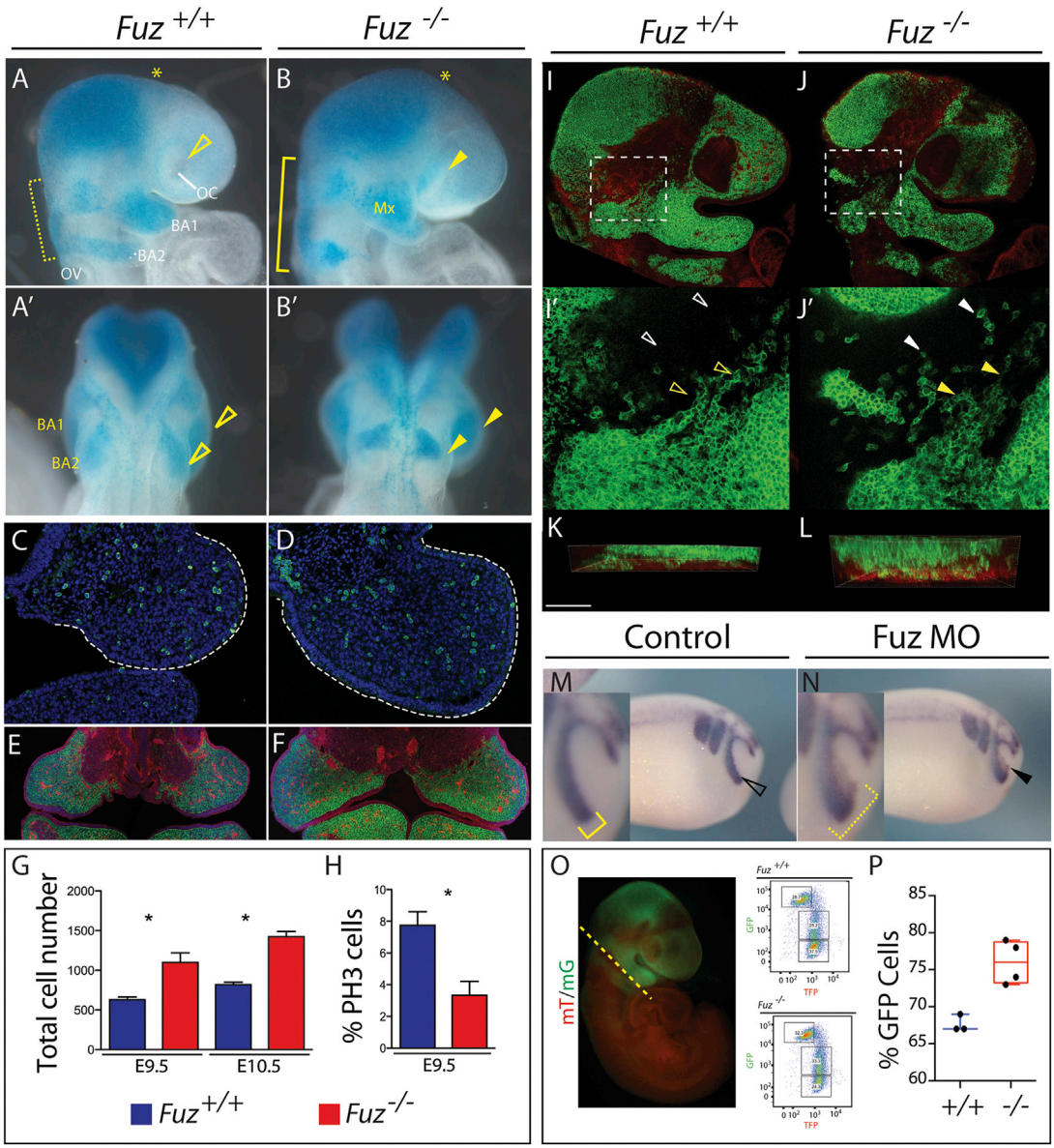

Figure 2. Increase in NC in Maxillary Compartment

Wnt1-cre-driven *LacZ* (blue) or *GFP* (green) marks NC contributions.

(A and B) Lateral views of E9.25 embryos. BA1 and BA2 NC streams are wider compared to controls (B compared to A, yellow bracket). Increased NC disrupts the optic cup (OC) in *Fuz* mutants compared to controls (B compared to A, arrowhead). BA2 NC stream is also increased in size and has failed to migrate as far as BA2 control NC. Mx, maxillary compartment of BA1. OV, optic vesicle.

(A′ and B′) Dorsal views. Maxillary BA1 is enlarged compared to controls (B compared to A, top arrowhead). BA2 has failed to migrate sufficiently compared to controls (bottom arrowhead).

(C and D) PH3 staining (green) and DAPI (blue) of E9.0, maxillary compartment. Mutant maxilla is enlarged (white dotted line).

(E and F) Coronal sections of E10.5 *Wnt1-cre; R26R*$^{mT/mG}$; *Fuz*$^{+/+}$, or *Wnt1-cre; R26R*$^{mT/mG}$;*Fuz*$^{-/-}$ maxillae. *Wnt1-cre*-driven membrane-GFP (green) marks NC contributions. Epithelial membrane-Tomato (red) highlights all other tissue derivatives. Mutant maxillae are larger compared to controls. Enlarged maxillae comprise NC-derived mesenchyme.

(G) Quantification of DAPI-positive cells from representative sections of E9.5 and 10.5 embryos. Note increase in cell number in mutant (red) maxilla compared to wild-type (blue) ($p < 0.004$). Error bars indicate SD.

(H) Quantification of E9.5 maxillary PH3-positive cells compared to total cell number. A significant decrease in the percentage of PH3-positive cells is observed in mutant maxillae (red) compared to controls (blue) ($p < 0.01$). Error bars indicate SD.

(I and J) Single confocal z-sections of *Wnt1-cre; R26R*$^{mT/mG}$;*Fuz*$^{+/+}$ or *Wnt1-cre; R26R*$^{mT/mG}$;*Fuz*$^{-/-}$ E9.5 embryos. *Wnt1-cre*-driven membrane-GFP (green) marks NC contributions.

(I′–J′) Magnified maximum projections of (I) and (J), indicated by a white dotted box. In controls, chains of *Wnt1-cre*-driven membrane-GFP-positive NC are observed (yellow arrowheads), with few isolated cells between brain and maxillary compartment (white arrowheads). Isolated NC cells are observed in mutant embryos, indicated by a white arrowhead in (J′), and NC chains are disorganized.

(legend continued on next page)

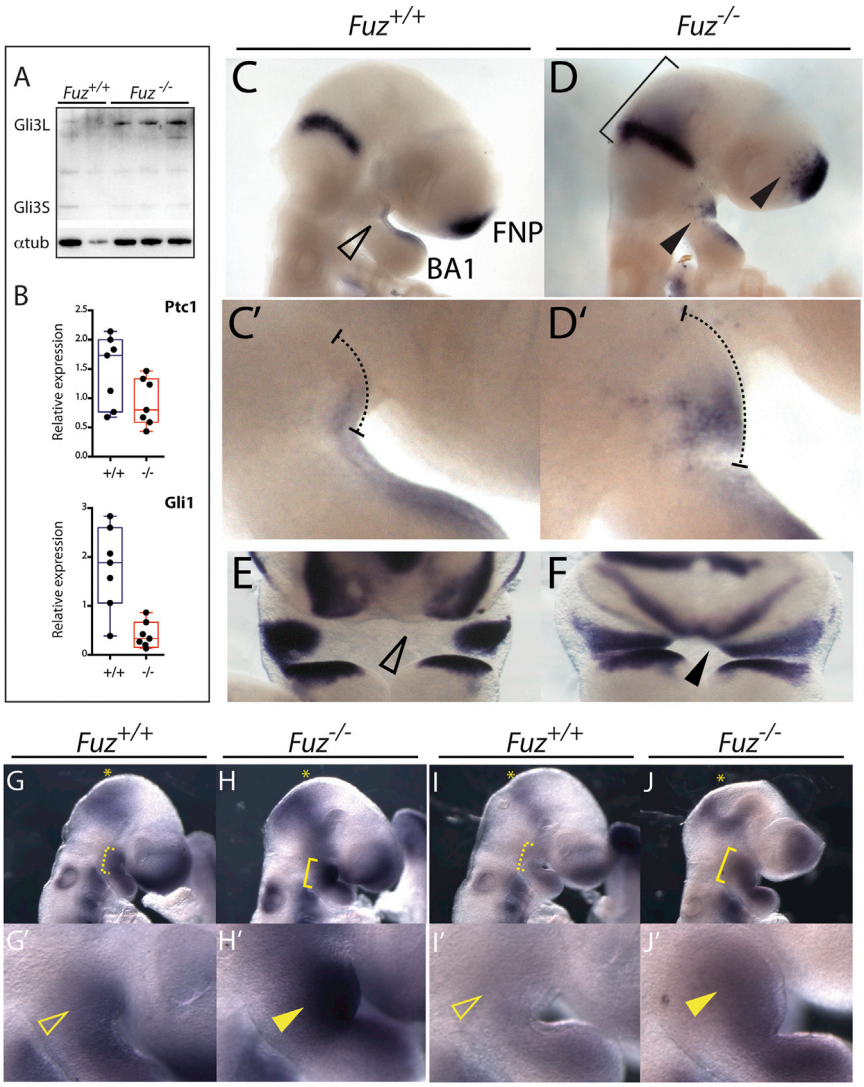

Figure 3. Gli3 Processing and Hh and FGF Signaling Are Altered in *Fuz* Mutants

(A) Western blot analysis of activator and repressor forms of Gli3 (Gli3-L and Gli3-S, respectively) in E9.0 embryos. Increased Gli3-L and reduced Gli3-S was detected in $Fuz^{-/-}$ embryos in (A), lanes 3–5, compared to controls in (A), lanes 1 and 2. Alpha-tubulin was analyzed as a loading control.

(B) qPCR of Hh target genes *Patched 1 (Ptc1)* and *Gli1* from E9.0 $Fuz^{+/+}$ and $Fuz^{-/-}$ heads. Relative mRNA levels are normalized to *β-actin*. *Ptc1* and *Gli1* are decreased in mutants (red) compared to controls (blue). Whiskers represent maximum/minimum data values with median and quartiles represented in the box.

(C and D) Lateral views of *Fgf8* expression in E9.0 embryos. *Fgf8* is expressed in the midhindbrain boundary (MHB), frontonasal prominence (FNP), and the BA1 epithelium. In mutants, *Fgf8* expression domains are expanded, indicated by bracket and arrowheads.

(C′ and D′) Magnified view of BA1 in control and mutant embryos. Dotted line indicates extent of maxillary compartment. Note enlarged maxillary prominence.

(E and F) Frontal view of *Fgf8* expression in E10.5 embryos. Note mediolateral expansion of maxillary *Fgf8* expression in the mutant, indicated by black arrowhead.

(G and H) Lateral views of *Erm1* mRNA expression in E9.5 embryos. *Erm1* is expressed in the MHB, FNP, and BA1. In mutants, expression of *Erm1* is expanded ventrally from the MHB (yellow asterisk) and in BA1 (yellow bracket).

(G′ and H′) Magnified view of BA1. *Erm1* expression is increased in mutant maxillae (yellow arrowheads).

(I and J) Lateral views of *Pea3* expression in E9.5 embryos. *Pea3* is expressed in the MHB, FNP, and BA1. In mutants, expression of *Pea3* is expanded in BA1 (yellow bracket).

(I′ and J′) Magnified view of BA1 in control and mutant embryos. *Pea3* expression is increased in mutant maxillae (yellow arrowhead).

See also Figure S2.

As it happens, Gli3 plays a crucial role in patterning the tissues that give rise to NC destined for BA1 (Blaess et al., 2006). Therefore, we assessed Hh signaling in the cranial regions of e9.0 embryos. We found a dramatic increase of full-length Gli3 in our mutants and a concurrent decrease in the short repressor form of Gli3 (Figure 3A). We also observed a reduction of Hh target gene expression in cranial tissues (Figure 3B), which may contribute to the observed NC defect.

Expanded FGF Expression in *Fuz* Mutants

We then considered molecular changes downstream of the early Gli processing defects in $Fuz^{-/-}$ mice. One possibility was that

(K and L) Z-projections of (I′) and (J′). The thickness of NC streams anterior to the prospective trigeminal ganglion is increased in mutants (WT = 41 ± 20 μm thick; mutant = 79 ± 16 μm deep). The immediately underlying membrane-Tomato-positive mesenchymal cells are shown in red, at the bottom of the image. The overlying epithelium is not included. Scale bar, 100 μm. This doubling in thickness is consistent with increased NC invasion into BA1.

(M and N) *Twist* in situ hybridization of stage 22 embryos injected unilaterally with *Fuz* MO. In controls, *Twist* is expressed in three streams, where the anterior NC stream surrounds the optic placode, indicated in (M) by open arrowhead and inset (bracket). Ectopic *Twist* expression is observed in the optic placode in Fuz morphants, indicated in (N) by arrowhead and inset (bracket).

(O) Representative epifluorescence image of an E9 *Wnt1-cre; R26*$^{mT/mG}$ embryo. Lineage-traced NC cells are labeled GFP (green), and nonrecombined cells are Tomato positive (red). Dashed line illustrates where embryos were bisected caudal to BA1. *Wnt1-cre; R26R*$^{mT/mG}$; $Fuz^{+/+}$, or *Wnt1-cre; R26R*$^{mT/mG}$;$Fuz^{-/-}$ embryo heads were dissociated and GFP positive, Tomato, or double-labeled cells were analyzed by flow cytometry. Representative flow cytometry plots from single E9 *Wnt1-cre; R26*$^{mT/mG}$; $Fuz^{+/+}$, or *Wnt1-cre; R26R*$^{mT/mG}$;$Fuz^{-/-}$ dissociated heads. mG, *Wnt1-cre*-driven membrane-GFP; mT, membrane-Tomato.

(P) The percentage of *Wnt1-Cre*-driven GFP-positive cells was significantly increased in mutants (79% ± 2%) compared to controls (68% ± 1%) ($p = 0.0103$). Whiskers represent maximum/minimum data values with median and quartiles represented in the box.

loss of *Fuz* leads to upregulation of Wnt target genes (e.g., Zhang et al., 2011); however, we found no changes in levels of activated β-catenin at early stages (e9.0) in $Fuz^{-/-}$ heads (data not shown). Next, as mentioned, high arched palate is common in FGF hyperactivation syndromes (Hajihosseini et al., 2001; Itoh and Ornitz, 2011; Wilkie et al., 1995). While there is no link between cilia and FGF signal transduction per se, loss of Gli3 can lead to increased *Fgf8* gene transcription, most obviously in the telencephalon (Aoto et al., 2002; Blaess et al., 2006; Cordero et al., 2004; Kuschel et al., 2003; Okada et al., 2008; Rash and Grove, 2007; Theil et al., 1999; Ueta et al., 2008). Indeed, a recent report suggests that loss of cilia-dependent signaling can similarly result in *Fgf8* expansion during development of the corpus callosum (Benadiba et al., 2012).

Therefore, we examined *Fgf8* levels in *Fuz* mutants. Strikingly, at E9.5, *Fgf8* expression was significantly expanded in *Fuz* mutants (Figures 3D and 3F), though there was minimal difference in mRNA levels prior to e9.0 (Figure S2). *Fgf8* is normally expressed in the midhindbrain boundary, the frontonasal process, and at low levels within the lateral epithelium of the maxillo-mandibular cleft (Figures 3C and 3C′). In *Fuz* mutants, *Fgf8* expression was expanded in all of these domains, with an anterior expansion from the midhindbrain domain (Figure 3D, bracket) and a mediolateral expansion within the mandibular and maxillary prominences (Figures 3D and 3D′). This expansion was maintained in mutant maxilla at E10.5 (Figure 3F). In addition, we found that *Fuz* knockdown in *Xenopus* also resulted in broader *Fgf8* gene expression, most strikingly in the domain abutting the migratory NC and in the frontal midline (Figure S3).

Key transcriptional targets of FGF signaling, *Erm1* and *Pea3* (Firnberg and Neubüser, 2002; Raible and Brand, 2001; Roehl and Nüsslein-Volhard, 2001), were strongly upregulated in *Fuz* mutants (Figures 3I–3J′) including a clear rostral expansion of both messenger RNAs (mRNAs) surrounding the mesencephalon (Figures 3G–3J, asterisk). Furthermore, both genes were robustly expressed throughout the expanded maxillary primordia, in contrast to the wild-type littermates (Figures 5H′ and 5J′, arrowhead). Together, these data identify a surprising role for *Fuz* in the regulation of *Fgf8* gene expression, and suggest that an aberrant increase in FGF signaling underlies the craniofacial anomalies in *Fuz* mutant mice.

Fgf8 Heterozygosity Rescues Maxillary Hyperplasia and Palate Defects in *Fuz* Mutant Mice

Our analysis of *Fuz* mutants suggested that excessive FGF signals drive the maxillary hyperplasia that underlies the observed palate defects. To test this model directly, we asked if decreasing the *Fgf8* gene dose might ameliorate the craniofacial defects in *Fuz* mutants. Using a null allele of *Fgf8*, in which the coding region is replaced with the *lacZ* gene (Ilagan et al., 2006), we halved the dose of *Fgf8* in $Fuz^{-/-}$ mice. We observed substantial rescue of maxillary hyperplasia in $Fuz^{-/-}$; $Fgf8^{lacZ/+}$ compound mutants (compare *Fuz* mutants in Figures 4B and 4B′ to rescued embryos in Figures 4C and 4C′). Heterozygosity of *Fgf8* also rescued the brain overgrowth and ocular phenotypes observed in *Fuz* mutants (compare Figure 4E to Figure 4F). Most strikingly, loss of one allele of *Fgf8* restored the e16.5 $Fuz^{-/-}$ palate to a normal width (Figures 4H–4K; Figure S3), confirming that the early maxillary phenotype is due in large part to an increase in FGF.

Because the *Fgf8* and NC phenotypes we observed seemed localized to the cranial structures, we hypothesized that phenotypic rescue after decreasing *Fgf8* dose should be specific to the head. Indeed, we found that *Fgf8* heterozygosity had little effect on digit development phenotypes in *Fuz* mutant mice (Figure S3). Together, these data suggest that the proximate cause for craniofacial defects in *Fuz* mutant mice is expanded *Fgf8* expression, while the polydactyly is independent of *Fgf8*, resulting directly from aberrant cilia-mediated Gli3 regulation (Heydeck et al., 2009).

Conditional Disruption of *Fuz* in the NC Does Not Result in High Arched Palate

Our data so far lead us to propose a model in which early dysregulation of cranial Gli processing in *Fuz* mutant mice leads to excessive expression of *Fgf8*, which in turn causes an excess of NC. We further propose that it is this early excess of NC, rather than attendant crest migration defects, that results in maxillary hyperplasia and high arched palate. To test this model, we used the NC-specific *Wnt1-cre* driver to conditionally delete the *Fuz* gene. Notably, specific deletion of *Fuz* in NC cells did not elicit early hyperplasia of the maxillary process or high arched palate (Figure 5; data not shown). Instead, these animals had a true cleft, indicating that, in the NC, *Fuz* is required only much later for palatal shelf elevation or depression of the tongue. These data suggest that the early maxillary phenotypes in *Fuz* mutant mice result from Fuz requirements in the neural tissue prior to NC induction (see also the model, Figure 7).

Maxillary Hyperplasia and FGF8 Upregulation in OFD-1 Mice

We next asked if *Fgf8* misregulation might be a general principle in ciliopathies. We examined the mouse model of OFD syndrome, *Ofd-1* (Ferrante et al., 2006). OFD patients frequently present with high arched palate (Figure 6F) (Hennekam et al., 2010; Prattichizzo et al., 2008; Tagliani et al., 2010), and OFD-1 is essential for ciliogenesis and centriole morphology (Ferrante et al., 2006; Singla et al., 2010). Importantly, *Ofd-1* mutant animals were strikingly similar to the $Fuz^{-/-}$ animals, with an enormously enlarged maxillary process and a clear expansion of cranial *Fgf8* expression (Figures 6A–6D).

Broad Similarity between *Fuz* Mutant Mice and FGF Hyperactivation Syndromes

Finally, the similarity of palatal phenotypes between OFD patients and patients with FGF hyperactivation syndromes such as Apert (Figures 6E–6G) suggest that ciliopathic cranial phenotypes stem from excessive FGF signaling. If this were the case, we hypothesized that $Fuz^{-/-}$ mice might also display craniosynostosis, another common feature of FGF hyperactivation syndromes. Therefore, we examined skull ossification using Alizarin red staining and found complete synostosis of the coronal sutures in *Fuz* mutant mice, akin to that seen in Apert syndrome (Figures 6I–6I′, arrowhead). Mutants also displayed other hallmarks of FGF syndromes, including fusion of the cervical vertebra and upper airway anomalies (data not

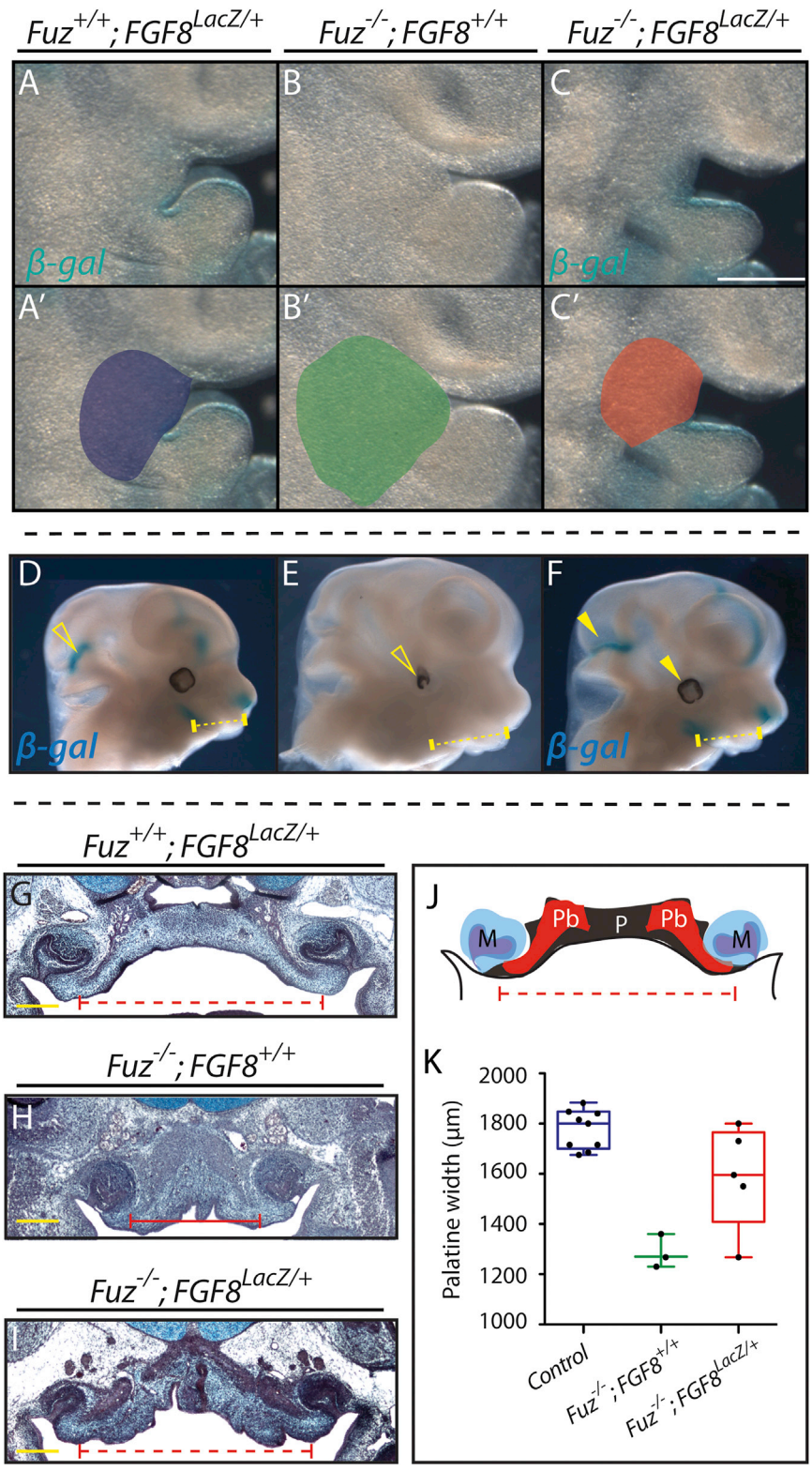

Figure 4. *Fgf8* Reduction Rescues Maxillary Hyperplasia and Palatal Width in Compound Mutants

(A–C) Lateral views of BA1. Maxillary size is expanded in $Fuz^{-/-}$ mutants in (B) compared to $Fgf8^{LacZ/+}$ in (A). Maxillary expansion is rescued in $Fuz^{-/-}$; $Fgf8^{LacZ/+}$ embryos in (C). *Fgf8* expression is also rescued in compound mutants as β-gal staining reveals similar BA1 epithelial expression in compound mutants and *Fgf8* heterozygotes.

(A′–C′) Maxillary size is schematized for each genotype.

(D–F) Lateral view, E12.5. Maxillary size is expanded in mutants in (E) compared to $Fgf8^{LacZ/+}$ in (D). Maxillary expansion is rescued in $Fuz^{-/-}$; $Fgf8^{LacZ/+}$ embryos in (F). Normal *Fgf8* expression (β-gal/blue) is also restored in compound mutants. Brain overgrowth and eye defects are rescued in compound mutants (arrowheads).

(G–I) Trichrome staining of coronal sections of E16.5 embryos. Palatal width and bone angle are decreased in mutant embryos in (H) compared to controls in (G). Palatal width in $Fuz^{-/-}$; $Fgf8^{LacZ/+}$ in (I) appears normal compared to controls in (H). Angle of palatine bone is partially rescued when compared to controls, as shown in (I) compared to (G) and (H).

(J) Schematic of palatal anatomy.

(K) Quantification of palatal width in E16.5 $Fuz^{+/+}$; $Fgf8^{LacZ/+}$(blue), $Fuz^{-/-}$; $Fgf8^{+/+}$ (green), and $Fuz^{-/-}$; $Fgf8^{LacZ/+}$(red) embryos. Palatal width is significantly decreased in $Fuz^{-/-}$; $Fgf8^{+/+}$ compared to controls, while *Fgf8* heterozygosity rescues palatal width in *Fuz* mutants ($p < 0.0005$, one-way analysis of variance). Whiskers represent maximum/minimum data values with median and quartiles represented in the box.

See also Figure S3.

shown) (Anderson et al., 1997; Kreiborg et al., 1992; Moore et al., 1995). Thus, our data suggest widespread commonalities between ciliopathic craniofacial defects and FGF hyperactivation syndromes.

DISCUSSION

Recent evidence reveals significant roles for cilia in human development and disease. First, mutations in genes known to promote cilia biogenesis and IFT have been implicated in a number of human syndromes (Ferkol and Leigh, 2012). Second, analysis of animal models suggests that a variety of developmental disorders, including craniofacial dysmorphology, result from defects in ciliary function (Huber and Cormier-Daire, 2012). Finally, advances in clinical genomics have improved annotation of disease alleles, subsequently identifying numerous, unclassified syndromes as ciliopathies (Brugmann et al., 2010). The challenge now is understanding how these seemingly heterogeneous disorders arise (Novarino et al., 2011), and our data suggest that commonalities in phenotype are likely to reflect shared signaling events, which converge into shared phenotypes. The results reveal an association between ciliopathies

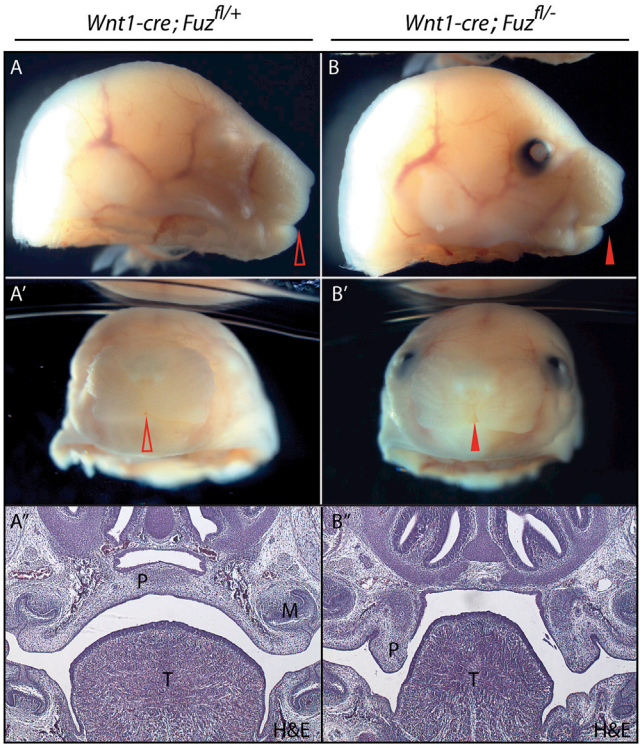

Figure 5. Maxillary Hyperplasia Is Not Due to *Fuz* Function in the NC

(A and B) Lateral views of E17.5 *Wnt1-cre; Fuz*$^{fl/+}$ and *Wnt1-cre; Fuz*$^{fl/-}$ embryos. The control embryo in (A) is an albino and lacks pigment in the eye. Arrowheads indicate rostral midline.

(A′ and B′) Frontal views of E17.5 *Wnt1-cre; Fuz*$^{fl/+}$ and *Wnt1-cre; Fuz*$^{fl/-}$ embryos. A cleft lip is observed in conditional null embryos [(B′) compared to (A′), indicated by arrowheads].

(A″ and B″) Hemotoxylin and eosin (H&E) staining of coronal sections of E17.5 *Wnt1-cre; Fuz*$^{fl/+}$ and *Wnt1-cre; Fuz*$^{fl/-}$ embryos. Sections show the anterior secondary palate (P), tongue (T), and molars (M). Palatal shelves are elevated and fused across the midline in control embryos; however, a failure in shelf elevation is observed in *Wnt1-cre; Fuz*$^{fl/-}$ embryos [(B″) compared to (A″), indicated by P]. The tongue also appears smaller and irregularly shaped in mutants [(B″) compared to (A″) indicated by T].

and FGF syndromes, in turn providing insights into the diversity of phenotypes seen in craniofacial anomalies.

We present the *Fuz* mutant as a genetic model of ciliopathic high arched palate and provide experimental evidence of the causes of this defect (Figure 7). Some aspects of skeletal development in *Fuz* mutants have been previously described; however, those reports focus on mandibular outgrowth (Zhang et al., 2011). We propose that the high arched palate arises due to perturbation of facial development in the *Fuz* mutant well before the stages examined previously and that the reported effects on Hh and Wnt signaling are secondary to an earlier developmental defect (Zhang et al., 2011).

Our data suggest that early expansion in *Fgf* gene expression drives maxillary phenotypes in the *Fuz* mutant model (Figure 7), but how does loss of a ciliopathy gene lead to an expansion of FGF signaling? In wild-type embryos, Gli3 repressor is expressed in the midbrain, where it acts as a transcriptional repressor, and indeed, Gli3R normally suppresses *Fgf8* expression in neural tissues, as loss of Gli3 leads to an increase in *Fgf8* (Aoto et al., 2002). Gli3 processing from Gli3-A (activator) to Gli3-R (repressor) is thought to occur at the distal tip of the cilium (Figure 7A) (Endoh-Yamagami et al., 2009; Lai et al., 2011; Tukachinsky et al., 2010; Wen et al., 2010). This distal tip of the ciliary axoneme is specifically lost in the absence of Fuz (Brooks and Wallingford, 2012) and likely leads to attenuated Gli3 processing (Figure 3). Subsequently, loss of Gli3R reduces transcriptional inhibition, permitting expansion of hindbrain fates, and *Fgf8* expression.

Previous studies in chicken embryos have implicated brain-specific *Fgf8* in the control of NC numbers (Creuzet et al., 2004). How does this occur? DiI labeling has shown that, in mouse, anterior NC destined for BA1 arises from the posterior mesencephalon and rhombomere 1 (Osumi-Yamashita et al., 1994). Loss of Hh activity leads to dorsalization or expansion of these structures (Fedtsova and Turner, 2001), concurrently increasing *Fgf8* expression and the NC domain. As a consequence, increased numbers of NC cells migrate toward BA1, overfilling it and forming enlarged maxillae (Figures 2 and 3). Subsequently, *Fgf8* is also upregulated in the BA1 epithelium, as well as in the frontonasal prominence (Figure 3). Following NC migration, the palatal condensation (Figure 7, red) arises medially, adjacent to *Fgf8* expression domains; in mutants, the grossly enlarged maxillary region causes a medial shift in palatal condensations (Figure 7).

These findings are significant for exposing an etiological link between the ciliopathies and FGF hyperactivation disorders. Furthermore, our data suggest that the long-held midface hypoplasia model for high arched palate should be revisited (Hayward et al., 2004; Hennekam et al., 2010). One source of confusion may be the disparity between observations in human patients versus phenotypes associated with mouse models. For example, Snyder-Warwick and colleagues examine palatal development in mice carrying a Crouzon mutation (FGFR2^{C342Y}), which causes increased FGF signaling associated with craniosynostosis (Snyder-Warwick et al., 2010). In these mice, heterozygotes, which should mirror the human genotype, have normal palates. Furthermore, homozygotes have a true cleft, mimicking a loss of FGFR2b (Hosokawa et al., 2009; Rice et al., 2004). This clearly does not model the oral aspects of the human syndrome, as it was noted nearly 40 years ago that true clefts in Crouzon patients were likely to be misdiagnoses (Peterson and Pruzansky, 1974).

Importantly, the relationship between ciliopathy and FGF hyperactivation syndromes is not limited to the palate, as *Fuz* mutant mice also display other manifestations of the FGFR-associated syndromes, such as craniosynostoses, fusions of the cervical vertebrae, and tracheal cartilaginous sleeve (Figure 6; data not shown). Finally, we note that this relationship is not restricted to animal models, as high arched palate and synostoses also co-occur in the human ciliopathy Sensenbrenner syndrome (Levin et al., 1977; Sensenbrenner et al., 1975). Notably, the cilia defects in Sensenbrenner syndrome are caused by mutations in proteins of the retrograde IFT particle, including IFT43 (Arts et al., 2011), and we recently showed that ciliogenesis defects following disruption of *Fuz* stem from a failure of IFT43 trafficking (Brooks and Wallingford, 2012).

Thus, in summary, our studies of a high arched palate model have revealed that excessive *FGF* transcription and increased

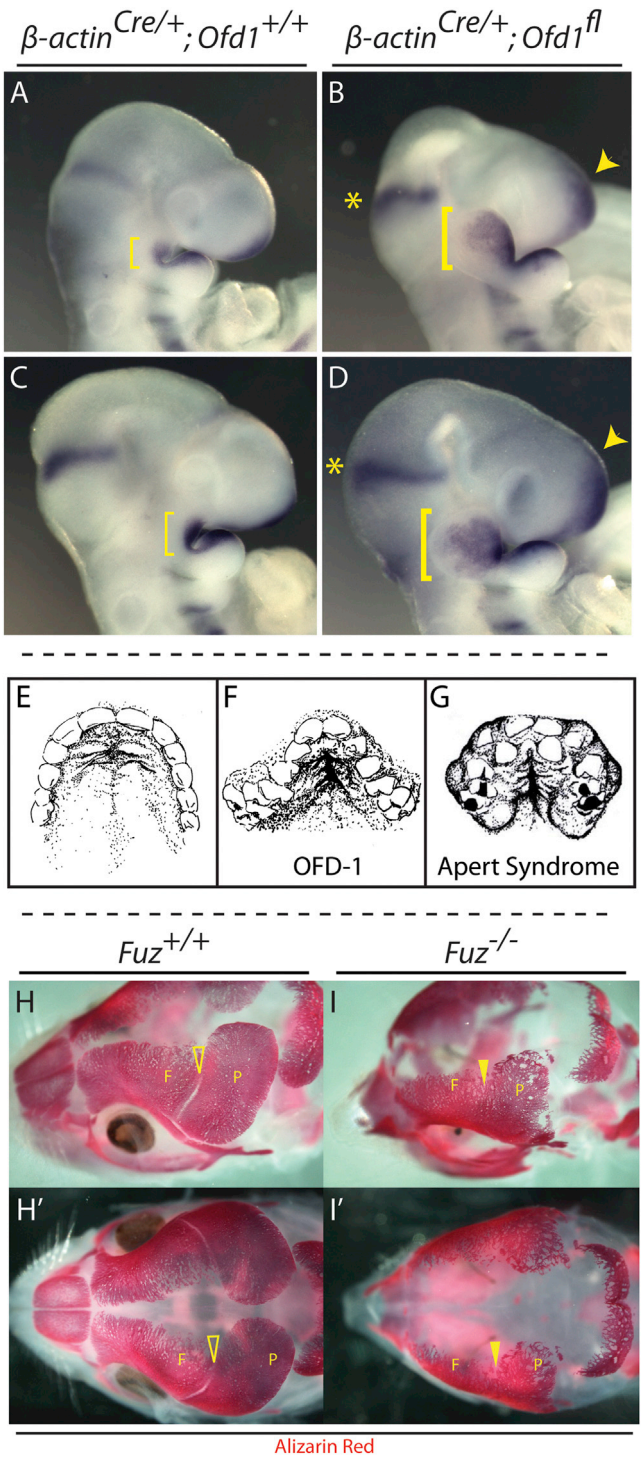

Figure 6. *Ofd-1* Mutants Also Show Expanded Maxillary Compartments and Cranial FGF8 Expression Domains

(A–D) Lateral views of E9.5 embryos showing cranial *Fgf8* mRNA expression domains. The 21 and 23 somite *ofd-1* mutants have enlarged maxillae compared to stage-matched control embryos, indicated by yellow brackets in (B) and (D) compared to (A) and (C), respectively. Maxillary *Fgf8* expression is expanded in mutants compared to controls [brackets in (B) and (D) compared to (A) and (C), as well as expression in the frontonasal process, indicated by arrowheads].

NC may be key factors in the poorly understood etiology of ciliopathic craniofacial defects. Furthermore, our report demonstrates that the pathological events underlying this phenotype are surprisingly different from those leading to a traditional cleft palate, raising the possibility that clinical diagnoses and management of high arched palate should also be reconsidered in this developmental and molecular context.

EXPERIMENTAL PROCEDURES

Mouse Lines

The following mouse lines were used: *Fuz* mutants: $Fuz^{gt(neo)}$ (Gray et al., 2009); conditional *Fuz* mutants: $Fuz^{fl/fl}$, which were generated according to standard methods and will be described elsewhere; conditional *Ofd-1* mutants: $Ofd1^{tm2.1Bfra}$ (Ferrante et al., 2006); *Fgf8* mutants: $Fgf8^{lacZ}$ (Ilagan et al., 2006); *Wnt1-cre* driver: *Tg(Wnt1-cre)11Rth* (Danielian et al., 1998); and reporter lines: $R26R^{mT/mG}$: $GT(Rosa)26Sor^{tm4(ACTB-tdTomato-EGFP)Luo}$ (Muzumdar et al., 2007) and $R26R^{lacZ}$: $Gt(ROSA)26Sor^{tm1Sor}$ (Soriano, 1999). Genotyping was performed as described in the original publications cited earlier. In all phenotypes depicted, at least four animals per genotype were examined. All animal work was performed in accordance with UK Home Office Regulations.

Western Blotting

Tissues rostral to and including BA1 were dissected from E9.0 embryos. Protein preparations and western blotting were carried out according to established protocols. Primary antibodies used were anti-Gli3 (clone H-280, 1:1,000, Santa Cruz Biotechnology no. sc-20688) and anti-alpha tubulin (clone DM1a, 1:5,000, Sigma T6199). Chemiluminescent signal was visualized using a BioRad ChemiDoc.

Real-Time PCR

Tissues rostral to and including BA1 were dissected from E9.0 embryos. Reverse transcription and cDNA synthesis were carried out according to standard protocols. Real-time PCR (RT-PCR) reactions were performed on a Rotorgene Q 2-series using the following gene-specific primer pairs.

β-actin (F: CTAAGGCCAACCGTGAAAG, R: ACCAGAGGCATACAGGGACA)
Gli1 (F: CAGGGAAGAGAGCAGACTGAC, R: CGCTGCTGCAAGAGACT)
Patched1 (F: AAGCCGACTACATGCCAGAG, R: AAGGGAACTGAGCGTACTCG)
Fgf8 (F: AGGTCTCTACATCTGCATGAAC, R: TGTTCTCCAGCACGATCTCT)
Erm (F: TGCCCACTTCATCGCCTGGAC, R: TAGCGGAGAGAGCGGCTCAG)

Staining and Histology

All mRNA in situ hybridization, immunohistochemistry, β-gal activity, and histological staining were performed according to standard protocols. Mouse

(E–G) OFD-1 and Apert syndrome patients exhibit high arched palate. In (E), a ventral view of a normal palate shows a hard palate with shallow, anterior bilateral rugae and smooth posterior palate (after photo by Millicent Odunze: http://plasticsurgery.about.com/od/Cleft-Lip-And-Palate/ss/What-Is-A-Cleft-Palate_3.htm). In (F), a ventral view is shown of the palate from OFD 1 (OFD-1) patient (after Tagliani et al., 2010; Figure 2F). (G) shows a ventral view of palate from the Apert syndrome patient (after Rynearson, 2000). Both (F) ciliopathic and (G) FGF-related high arched palates are narrow with a deep medial cleft extending from the anterior hard palate. Rugal-like swellings are more numerous and are extant with the medial cleft. Soft tissue swellings and dental crowding are observed in both groups.
(H–I′) Loss of Fuz causes coronal craniosynostosis. E17.5 heads stained with Alizarin red. (H) and (I) show dorsolateral views. (H′) and (I′) show dorsal views. Alizarin red negative coronal suture (open arrowheads) separates frontal (F) and parietal (P) bones in wild-type embryos. Coronal suture is absent in mutant embryos (closed arrowheads).

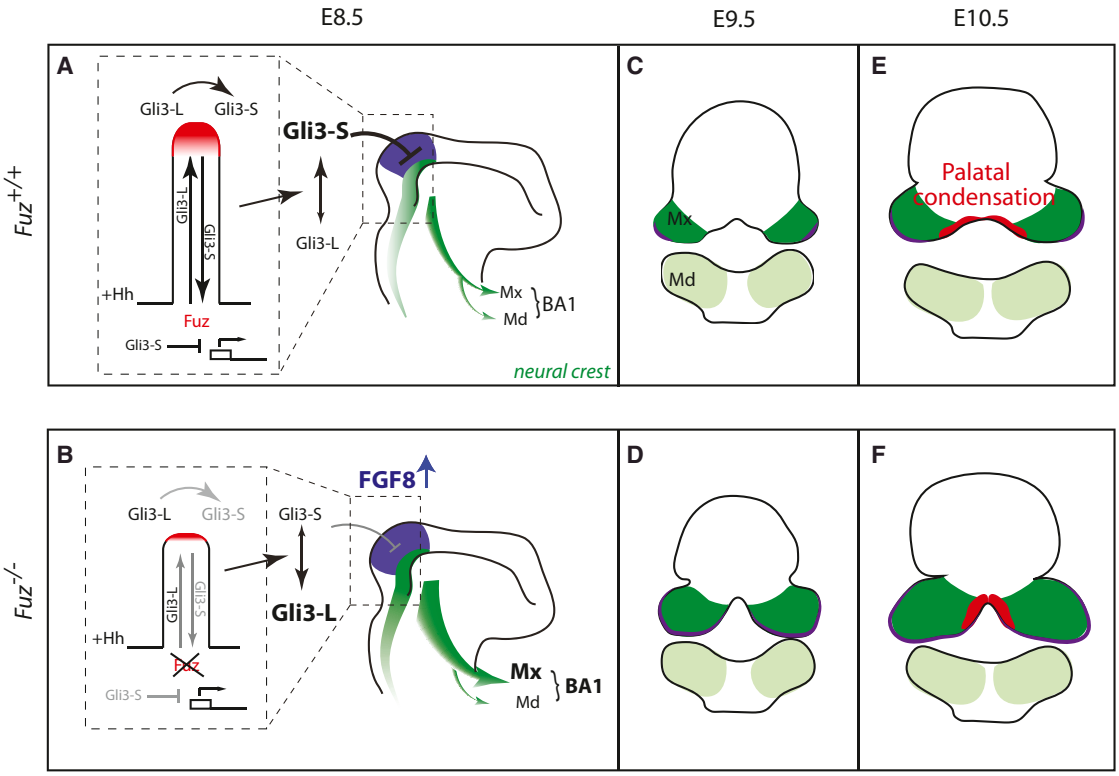

Figure 7. Proposed Model for Palatal Defects in *Fuz* Mutants

(A and B) Schematics depict E8.5 embryos. In Hedgehog signaling, anterograde transport delivers Gli3L (Gli3-activator) to the distal CLAMP-positive ciliary tip (red). Gli3-L is processed into Gli3-S (Gli3 repressor) which undergoes retrograde transport, repressing transcription of targets such as *FGF8*. Anterior NC (dark green) arises from the posterior mesencephalon and anterior hindbrain (purple), and is normally limited by a balance of Hh and FGF signals. NC then migrates into BA1, comprising maxillary and mandibular compartments (Mx and Md, respectively). When Fuz function is lost, ciliary transport and the distal compartment are severely disrupted leading to disruption of Gli processing and an expansion in cranial NC numbers, specifically maxillary NC.

(C–F) In (C) and (D), schematics depict coronal sections of E9.5 embryos. In coronal sections, the maxilla forms as two bilateral prominences and *Fgf8* is expressed in lateral maxillary epithelia, indicated by purple in (C) through (F). In mutants, the maxillary compartment is enlarged and epithelial *Fgf8* is expanded. In (E) and (F), schematics depict coronal sections of E10.5 embryos. Palatal condensations (red) are medial to *FGF8* expression domains. In wild-type animals, these flank midline mesenchyme but remain separated. In *Fuz* mutants, expansion of *FGF8* causes a medial shift of the palatal condensations. Subsequently, the normal bilateral palatal primordia join at the midline.

and *Xenopus* embryos were collected in cold PBS and fixed overnight in 4% paraformaldehyde or MEMFA, respectively. mRNA in situ hybridization was performed as previously described (Sive et al., 2000; Wilkinson et al., 1989). The following mRNA probes were used: mouse *Fgf8* (Mahmood et al., 1995), mouse *erm* (Hippenmeyer et al., 2002), mouse *Pea3* (Livet et al., 2002), *X. laevis Fgf8* (Monsoro-Burq et al., 2003), and *X. laevis twist* (Hopwood et al., 1989). Primary antibodies used for immunohistochemistry: anti-rabbit phospho-histone H3 (PH3) (BDH, 1:200) or anti-rabbit β-catenin (Sigma, 1:200). Sections were coverslipped with ProLong Gold antifade reagent with DAPI (Invitrogen, P36931).

Confocal Microscopy and Image Analysis

To analyze NC migration, whole-mount E9.0 embryos were cleared using 70% glycerol/PBS and mounted on slides. Sagittal confocal z-stacks were obtained using a Leica TCS SP5 DM16000. Image sequences were reconstructed using Imaris image analysis software. Thickness of NC streams were determined by measuring the depth of GFP positive NC cells at three points anterior to the trigeminal ganglion, posterior to the maxillary compartment (outlined in Figure 3).

μCT

Specimens were scanned using a GE Explore Locus SP μCT scanner. The specimens were immersed in 20% (w/v) Pluronic F-127 (Sigma) at 4°C and warmed to room temperature for immobilization. Specimens were scanned to produce 8 μm voxel size volumes, using an X-ray tube voltage of 80 kVp and a tube current of 80 μA. An aluminum filter (0.05 mm) was used to adjust the energy distribution of the X-ray source. The specimens were characterized further by making three-dimensional isosurfaces, generated and measured using Microview software (GE).

Flow Cytometry of Embryo Heads

Cell purification from embryonic tissues was performed as previously described (Schulz et al., 2012). Heads from *Wnt1-cre;* $R26^{mT/mG}$ embryos, as depicted in Figure 2E, were digested and passed through a 100 μm cell strainer. Flow cytometry was performed using a BD Biosciences FACSAria II cell sorter. Live cells were identified using side scatter and forward scatter (FSC-A), followed by doublet exclusion using forward scatter width against FSC-A. Populations were identified using endogenous expression of GFP and Tomato. All data were analyzed using FlowJo 9.53 (Celeza GmbH).

SUPPLEMENTAL INFORMATION

Supplemental Information includes three figures and can be found with this article online at http://dx.doi.org/10.1016/j.devcel.2013.05.021.

ACKNOWLEDGMENTS

We are grateful to Martyn Cobourne and Marc Dionne for critical reading of the manuscript, Angela Gates and Alasdair Edgar for assistance, the Basson laboratory for help with FGFs, the New Hunt's House Biological Services Unit for excellent animal care, and Albert Basson, Jeremy Green, Paul Sharpe, and Brunella Franco for contributing mouse lines. Work in the Geissmann laboratory (E.G.P. and C.S.) was supported by grants from the Medical Research Council (MRC; G0900867) and the European Research Council (ERC-2010-StG-261299). C.S. was supported by a fellowship from the German National Academy of Sciences Leopoldina (LPDS 2009-31). B.W. and R.H.F. were supported by National Institutes of Health (NIH) grants (ES020619, NS076465, and HD067244). J.B.W. is an Early Career Scientist of the Howard Hughes Medical Institute; work in his laboratory was funded by The March of Dimes and The Burroughs Wellcome Fund. Additional support to J.M.T. was provided by the National Institute of Dental and Craniofacial Research/NIH (F32DE023272). This work was funded by grants to K.J.L. from the Wellcome Trust (WT081880AIA, a Wellcome VIP award for J.M.T., a Wellcome Trust Vacation Studentship for Y.Y.), grants from the Biotechnology and Biological Sciences Research Council (BB/E013872, BB/I021922/1), an MRC studentship (B.Z.Y.), and the King's College London Dental Institute.

Received: August 22, 2012
Revised: March 29, 2013
Accepted: May 23, 2013
Published: June 24, 2013

REFERENCES

Agochukwu, N.B., Solomon, B.D., Doherty, E.S., and Muenke, M. (2012). Palatal and oral manifestations of Muenke syndrome (FGFR3-related craniosynostosis). J. Craniofac. Surg. *23*, 664–668.

Anderson, P.J., Hall, C., Evans, R.D., Harkness, W.J., Hayward, R.D., and Jones, B.M. (1997). The cervical spine in Crouzon syndrome. Spine (Phila Pa 1976) *22*, 402–405.

Aoto, K., Nishimura, T., Eto, K., and Motoyama, J. (2002). Mouse GLI3 regulates Fgf8 expression and apoptosis in the developing neural tube, face, and limb bud. Dev. Biol. *251*, 320–332.

Arts, H.H., Bongers, E.M., Mans, D.A., van Beersum, S.E., Oud, M.M., Bolat, E., Spruijt, L., Cornelissen, E.A., Schuurs-Hoeijmakers, J.H., de Leeuw, N., et al. (2011). C14ORF179 encoding IFT43 is mutated in Sensenbrenner syndrome. J. Med. Genet. *48*, 390–395.

Beales, P.L., Elcioglu, N., Woolf, A.S., Parker, D., and Flinter, F.A. (1999). New criteria for improved diagnosis of Bardet-Biedl syndrome: results of a population survey. J. Med. Genet. *36*, 437–446.

Benadiba, C., Magnani, D., Niquille, M., Morlé, L., Valloton, D., Nawabi, H., Ait-Lounis, A., Otsmane, B., Reith, W., Theil, T., et al. (2012). The ciliogenic transcription factor RFX3 regulates early midline distribution of guidepost neurons required for corpus callosum development. PLoS Genet. *8*, e1002606.

Berkowitz, S. (1971). Stereophotogrammetric analysis of casts of normal and abnormal palates. Am. J. Orthod. *60*, 1–18.

Blaess, S., Corrales, J.D., and Joyner, A.L. (2006). Sonic hedgehog regulates Gli activator and repressor functions with spatial and temporal precision in the mid/hindbrain region. Development *133*, 1799–1809.

Brooks, E.R., and Wallingford, J.B. (2012). Control of vertebrate intraflagellar transport by the planar cell polarity effector Fuz. J. Cell Biol. *198*, 37–45.

Brugmann, S.A., Cordero, D.R., and Helms, J.A. (2010). Craniofacial ciliopathies: A new classification for craniofacial disorders. Am. J. Med. Genet. A. *152A*, 2995–3006.

Chai, Y., and Maxson, R.E., Jr. (2006). Recent advances in craniofacial morphogenesis. Dev. Dyn. *235*, 2353–2375.

Cobourne, M.T., Xavier, G.M., Depew, M., Hagan, L., Sealby, J., Webster, Z., and Sharpe, P.T. (2009). Sonic hedgehog signalling inhibits palatogenesis and arrests tooth development in a mouse model of the nevoid basal cell carcinoma syndrome. Dev. Biol. *331*, 38–49.

Collier, S., and Gubb, D. (1997). Drosophila tissue polarity requires the cell-autonomous activity of the fuzzy gene, which encodes a novel transmembrane protein. Development *124*, 4029–4037.

Cordero, D., Marcucio, R., Hu, D., Gaffield, W., Tapadia, M., and Helms, J.A. (2004). Temporal perturbations in sonic hedgehog signaling elicit the spectrum of holoprosencephaly phenotypes. J. Clin. Invest. *114*, 485–494.

Creuzet, S., Schuler, B., Couly, G., and Le Douarin, N.M. (2004). Reciprocal relationships between Fgf8 and neural crest cells in facial and forebrain development. Proc. Natl. Acad. Sci. USA *101*, 4843–4847.

Danielian, P.S., Muccino, D., Rowitch, D.H., Michael, S.K., and McMahon, A.P. (1998). Modification of gene activity in mouse embryos in utero by a tamoxifen-inducible form of Cre recombinase. Curr. Biol. *8*, 1323–1326.

Endoh-Yamagami, S., Evangelista, M., Wilson, D., Wen, X., Theunissen, J.W., Phamluong, K., Davis, M., Scales, S.J., Solloway, M.J., de Sauvage, F.J., and Peterson, A.S. (2009). The mammalian Cos2 homolog Kif7 plays an essential role in modulating Hh signal transduction during development. Curr. Biol. *19*, 1320–1326.

Fedtsova, N., and Turner, E.E. (2001). Signals from the ventral midline and isthmus regulate the development of Brn3.0-expressing neurons in the midbrain. Mech. Dev. *105*, 129–144.

Ferkol, T.W., and Leigh, M.W. (2012). Ciliopathies: the central role of cilia in a spectrum of pediatric disorders. J. Pediatr. *160*, 366–371.

Ferrante, M.I., Zullo, A., Barra, A., Bimonte, S., Messaddeq, N., Studer, M., Dollé, P., and Franco, B. (2006). Oral-facial-digital type I protein is required for primary cilia formation and left-right axis specification. Nat. Genet. *38*, 112–117.

Firnberg, N., and Neubüser, A. (2002). FGF signaling regulates expression of Tbx2, Erm, Pea3, and Pax3 in the early nasal region. Dev. Biol. *247*, 237–250.

Goetz, S.C., and Anderson, K.V. (2010). The primary cilium: a signalling centre during vertebrate development. Nat. Rev. Genet. *11*, 331–344.

Goodwin, A., Oberoi, S., Landan, M., Charles, C., Groth, J., Martinez, A., Fairley, C., Weiss, L., Tidyman, W., Klein, O., et al. (2012). Craniofacial and dental development in cardio-facio-cutaneous syndrome: the importance of Ras signaling homeostasis. Clin. Genet.

Gray, R.S., Abitua, P.B., Wlodarczyk, B.J., Szabo-Rogers, H.L., Blanchard, O., Lee, I., Weiss, G.S., Liu, K.J., Marcotte, E.M., Wallingford, J.B., and Finnell, R.H. (2009). The planar cell polarity effector Fuz is essential for targeted membrane trafficking, ciliogenesis and mouse embryonic development. Nat. Cell Biol. *11*, 1225–1232.

Gritli-Linde, A., Hallberg, K., Harfe, B.D., Reyahi, A., Kannius-Janson, M., Nilsson, J., Cobourne, M.T., Sharpe, P.T., McMahon, A.P., and Linde, A. (2007). Abnormal hair development and apparent follicular transformation to mammary gland in the absence of hedgehog signaling. Dev. Cell *12*, 99–112.

Hajihosseini, M.K., Wilson, S., De Moerlooze, L., and Dickson, C. (2001). A splicing switch and gain-of-function mutation in FgfR2-IIIc hemizygotes causes Apert/Pfeiffer-syndrome-like phenotypes. Proc. Natl. Acad. Sci. USA *98*, 3855–3860.

Hayward, R., Jones, B., and Dunaway, D. (2004). The Clinical Management of Craniosynostosis (London: MacKeith Press).

Hennekam, R., Allanson, J., and Krantz, I. (2010). Gorlin's Syndromes of the Head and Neck (New York: Oxford University Press).

Heydeck, W., Zeng, H., and Liu, A. (2009). Planar cell polarity effector gene Fuzzy regulates cilia formation and Hedgehog signal transduction in mouse. Dev. Dyn. *238*, 3035–3042.

Hippenmeyer, S., Shneider, N.A., Birchmeier, C., Burden, S.J., Jessell, T.M., and Arber, S. (2002). A role for neuregulin1 signaling in muscle spindle differentiation. Neuron *36*, 1035–1049.

Hong, S.K., and Dawid, I.B. (2009). FGF-dependent left-right asymmetry patterning in zebrafish is mediated by Ier2 and Fibp1. Proc. Natl. Acad. Sci. USA *106*, 2230–2235.

Hopwood, N.D., Pluck, A., and Gurdon, J.B. (1989). A Xenopus mRNA related to Drosophila twist is expressed in response to induction in the mesoderm and the neural crest. Cell *59*, 893–903.

Hosokawa, R., Deng, X., Takamori, K., Xu, X., Urata, M., Bringas, P., Jr., and Chai, Y. (2009). Epithelial-specific requirement of FGFR2 signaling during tooth and palate development. J. Exp. Zoolog. B Mol. Dev. Evol. *312B*, 343–350.

Hu, D., and Helms, J.A. (1999). The role of sonic hedgehog in normal and abnormal craniofacial morphogenesis. Development *126*, 4873–4884.

Huang, X., Goudy, S.L., Ketova, T., Litingtung, Y., and Chiang, C. (2008). Gli3-deficient mice exhibit cleft palate associated with abnormal tongue development. Dev. Dyn. *237*, 3079–3087.

Huber, C., and Cormier-Daire, V. (2012). Ciliary disorder of the skeleton. Am. J. Med. Genet. C. Semin. Med. Genet. *160C*, 165–174.

Ilagan, R., Abu-Issa, R., Brown, D., Yang, Y.P., Jiao, K., Schwartz, R.J., Klingensmith, J., and Meyers, E.N. (2006). Fgf8 is required for anterior heart field development. Development *133*, 2435–2445.

Itoh, N., and Ornitz, D.M. (2011). Fibroblast growth factors: from molecular evolution to roles in development, metabolism and disease. J. Biochem. *149*, 121–130.

Kreiborg, S., and Cohen, M.M., Jr. (1992). The oral manifestations of Apert syndrome. J. Craniofac. Genet. Dev. Biol. *12*, 41–48.

Kreiborg, S., Barr, M., Jr., and Cohen, M.M., Jr. (1992). Cervical spine in the Apert syndrome. Am. J. Med. Genet. *43*, 704–708.

Kuschel, S., Rüther, U., and Theil, T. (2003). A disrupted balance between Bmp/Wnt and Fgf signaling underlies the ventralization of the Gli3 mutant telencephalon. Dev. Biol. *260*, 484–495.

Lai, C.K., Gupta, N., Wen, X., Rangell, L., Chih, B., Peterson, A.S., Bazan, J.F., Li, L., and Scales, S.J. (2011). Functional characterization of putative cilia genes by high-content analysis. Mol. Biol. Cell *22*, 1104–1119.

Lan, Y., and Jiang, R. (2009). Sonic hedgehog signaling regulates reciprocal epithelial-mesenchymal interactions controlling palatal outgrowth. Development *136*, 1387–1396.

Letra, A., de Almeida, A.L., Kaizer, R., Esper, L.A., Sgarbosa, S., and Granjeiro, J.M. (2007). Intraoral features of Apert's syndrome. Oral Surg. Oral Med. Oral Pathol. Oral Radiol. Endod. *103*, e38–e41.

Levin, L.S., Perrin, J.C., Ose, L., Dorst, J.P., Miller, J.D., and McKusick, V.A. (1977). A heritable syndrome of craniosynostosis, short thin hair, dental abnormalities, and short limbs: cranioectodermal dysplasia. J. Pediatr. *90*, 55–61.

Liu, A., Wang, B., and Niswander, L.A. (2005). Mouse intraflagellar transport proteins regulate both the activator and repressor functions of Gli transcription factors. Development *132*, 3103–3111.

Livet, J., Sigrist, M., Stroebel, S., De Paola, V., Price, S.R., Henderson, C.E., Jessell, T.M., and Arber, S. (2002). ETS gene Pea3 controls the central position and terminal arborization of specific motor neuron pools. Neuron *35*, 877–892.

Lorente, C.A., Tassinari, M.S., and Keith, D.A. (1981). The effects of phenytoin on rat development: an animal model system for fetal hydantoin syndrome. Teratology *24*, 169–180.

Mahmood, R., Bresnick, J., Hornbruch, A., Mahony, C., Morton, N., Colquhoun, K., Martin, P., Lumsden, A., Dickson, C., and Mason, I. (1995). A role for FGF-8 in the initiation and maintenance of vertebrate limb bud outgrowth. Curr. Biol. *5*, 797–806.

Martínez-Abadías, N., Percival, C., Aldridge, K., Hill, C.A., Ryan, T., Sirivunnabood, S., Wang, Y., Jabs, E.W., and Richtsmeier, J.T. (2010). Beyond the closed suture in apert syndrome mouse models: evidence of primary effects of FGFR2 signaling on facial shape at birth. Dev. Dyn. *239*, 3058–3071.

Mo, R., Freer, A.M., Zinyk, D.L., Crackower, M.A., Michaud, J., Heng, H.H., Chik, K.W., Shi, X.M., Tsui, L.C., Cheng, S.H., et al. (1997). Specific and redundant functions of Gli2 and Gli3 zinc finger genes in skeletal patterning and development. Development *124*, 113–123.

Monsoro-Burq, A.H., Fletcher, R.B., and Harland, R.M. (2003). Neural crest induction by paraxial mesoderm in Xenopus embryos requires FGF signals. Development *130*, 3111–3124.

Moore, M.H., Lodge, M.L., and Clark, B.E. (1995). Spinal anomalies in Pfeiffer syndrome. Cleft Palate Craniofac. J. *32*, 251–254.

Moore, S.J., Green, J.S., Fan, Y., Bhogal, A.K., Dicks, E., Fernandez, B.A., Stefanelli, M., Murphy, C., Cramer, B.C., Dean, J.C., et al. (2005). Clinical and genetic epidemiology of Bardet-Biedl syndrome in Newfoundland: a 22-year prospective, population-based, cohort study. Am. J. Med. Genet. A. *132*, 352–360.

Muzumdar, M.D., Tasic, B., Miyamichi, K., Li, L., and Luo, L. (2007). A global double-fluorescent Cre reporter mouse. Genesis *45*, 593–605.

Neugebauer, J.M., Amack, J.D., Peterson, A.G., Bisgrove, B.W., and Yost, H.J. (2009). FGF signalling during embryo development regulates cilia length in diverse epithelia. Nature *458*, 651–654.

Noden, D.M. (1975). An analysis of migratory behavior of avian cephalic neural crest cells. Dev. Biol. *42*, 106–130.

Novarino, G., Akizu, N., and Gleeson, J.G. (2011). Modeling human disease in humans: the ciliopathies. Cell *147*, 70–79.

Okada, T., Okumura, Y., Motoyama, J., and Ogawa, M. (2008). FGF8 signaling patterns the telencephalic midline by regulating putative key factors of midline development. Dev. Biol. *320*, 92–101.

Osumi-Yamashita, N., Ninomiya, Y., Doi, H., and Eto, K. (1994). The contribution of both forebrain and midbrain crest cells to the mesenchyme in the frontonasal mass of mouse embryos. Dev. Biol. *164*, 409–419.

Park, T.J., Haigo, S.L., and Wallingford, J.B. (2006). Ciliogenesis defects in embryos lacking inturned or fuzzy function are associated with failure of planar cell polarity and Hedgehog signaling. Nat. Genet. *38*, 303–311.

Peterson, S.J., and Pruzansky, S. (1974). Palatal anomalies in the syndromes of Apert and Crouzon. Cleft Palate J. *11*, 394–403.

Prattichizzo, C., Macca, M., Novelli, V., Giorgio, G., Barra, A., and Franco, B.; Oral-Facial-Digital Type I (OFDI) Collaborative Group. (2008). Mutational spectrum of the oral-facial-digital type I syndrome: a study on a large collection of patients. Hum. Mutat. *29*, 1237–1246.

Raible, F., and Brand, M. (2001). Tight transcriptional control of the ETS domain factors Erm and Pea3 by Fgf signaling during early zebrafish development. Mech. Dev. *107*, 105–117.

Rash, B.G., and Grove, E.A. (2007). Patterning the dorsal telencephalon: a role for sonic hedgehog? J. Neurosci. *27*, 11595–11603.

Rice, R., Spencer-Dene, B., Connor, E.C., Gritli-Linde, A., McMahon, A.P., Dickson, C., Thesleff, I., and Rice, D.P. (2004). Disruption of Fgf10/Fgfr2b-coordinated epithelial-mesenchymal interactions causes cleft palate. J. Clin. Invest. *113*, 1692–1700.

Roehl, H., and Nüsslein-Volhard, C. (2001). Zebrafish pea3 and erm are general targets of FGF8 signaling. Curr. Biol. *11*, 503–507.

Rynearson, R.D. (2000). Case report: orthodontic and dentofacial orthopedic considerations in Apert's syndrome. Angle Orthod. *70*, 247–252.

Schulz, C., Gomez Perdiguero, E., Chorro, L., Szabo-Rogers, H., Cagnard, N., Kierdorf, K., Prinz, M., Wu, B., Jacobsen, S.E., Pollard, J.W., et al. (2012). A lineage of myeloid cells independent of Myb and hematopoietic stem cells. Science *336*, 86–90.

Sensenbrenner, J.A., Dorst, J.P., and Owens, R.P. (1975). New syndrome of skeletal, dental and hair anomalies. Birth Defects Orig. Artic. Ser. *11*, 372–379.

Seo, J.H., Zilber, Y., Babayeva, S., Liu, J., Kyriakopoulos, P., De Marco, P., Merello, E., Capra, V., Gros, P., and Torban, E. (2011). Mutations in the planar cell polarity gene, Fuzzy, are associated with neural tube defects in humans. Hum. Mol. Genet. *20*, 4324–4333.

Singla, V., and Reiter, J.F. (2006). The primary cilium as the cell's antenna: signaling at a sensory organelle. Science *313*, 629–633.

Singla, V., Romaguera-Ros, M., Garcia-Verdugo, J.M., and Reiter, J.F. (2010). Ofd1, a human disease gene, regulates the length and distal structure of centrioles. Dev. Cell *18*, 410–424.

Sive, H.L., Grainger, R.M., and Harland, R.M. (2000). Early Development of *Xenopus laevis*: A Laboratory Manual (Cold Spring Harbor, NY: Cold Spring Harbor Laboratory Press).

Slaney, S.F., Oldridge, M., Hurst, J.A., Moriss-Kay, G.M., Hall, C.M., Poole, M.D., and Wilkie, A.O. (1996). Differential effects of FGFR2 mutations on syndactyly and cleft palate in Apert syndrome. Am. J. Hum. Genet. *58*, 923–932.

Snyder-Warwick, A.K., Perlyn, C.A., Pan, J., Yu, K., Zhang, L., and Ornitz, D.M. (2010). Analysis of a gain-of-function FGFR2 Crouzon mutation provides evidence of loss of function activity in the etiology of cleft palate. Proc. Natl. Acad. Sci. USA *107*, 2515–2520.

Somlo, S., Rutecki, G., Giuffra, L.A., Reeders, S.T., Cugino, A., and Whittier, F.C. (1993). A kindred exhibiting cosegregation of an overlap connective tissue disorder and the chromosome 16 linked form of autosomal dominant polycystic kidney disease. J. Am. Soc. Nephrol. *4*, 1371–1378.

Soriano, P. (1999). Generalized lacZ expression with the ROSA26 Cre reporter strain. Nat. Genet. *21*, 70–71.

Tagliani, M.M., Gomide, M.R., and Carrara, C.F. (2010). Oral-facial-digital syndrome type 1: oral features in 12 patients submitted to clinical and radiographic examination. Cleft Palate Craniofac. J. *47*, 162–166.

Theil, T., Alvarez-Bolado, G., Walter, A., and Rüther, U. (1999). Gli3 is required for Emx gene expression during dorsal telencephalon development. Development *126*, 3561–3571.

Tobin, J.L., Di Franco, M., Eichers, E., May-Simera, H., Garcia, M., Yan, J., Quinlan, R., Justice, M.J., Hennekam, R.C., Briscoe, J., et al. (2008). Inhibition of neural crest migration underlies craniofacial dysmorphology and Hirschsprung's disease in Bardet-Biedl syndrome. Proc. Natl. Acad. Sci. USA *105*, 6714–6719.

Tukachinsky, H., Lopez, L.V., and Salic, A. (2010). A mechanism for vertebrate Hedgehog signaling: recruitment to cilia and dissociation of SuFu-Gli protein complexes. J. Cell Biol. *191*, 415–428.

Ueta, E., Kurome, M., Teshima, Y., Kodama, M., Otsuka, Y., and Naruse, I. (2008). Altered signaling pathway in the dysmorphogenesis of telencephalon in the Gli3 depressed mouse embryo, Pdn/Pdn. Congenit. Anom. (Kyoto) *48*, 74–80.

Vadiati Saberi, B., and Shakoorpour, A. (2011). Apert syndrome: report of a case with emphasis on oral manifestations. J. Dent. (Tehran) *8*, 90–95.

Wen, X., Lai, C.K., Evangelista, M., Hongo, J.A., de Sauvage, F.J., and Scales, S.J. (2010). Kinetics of hedgehog-dependent full-length Gli3 accumulation in primary cilia and subsequent degradation. Mol. Cell. Biol. *30*, 1910–1922.

Wilkie, A.O., Slaney, S.F., Oldridge, M., Poole, M.D., Ashworth, G.J., Hockley, A.D., Hayward, R.D., David, D.J., Pulleyn, L.J., Rutland, P., et al. (1995). Apert syndrome results from localized mutations of FGFR2 and is allelic with Crouzon syndrome. Nat. Genet. *9*, 165–172.

Wilkinson, D.G., Bhatt, S., and McMahon, A.P. (1989). Expression pattern of the FGF-related proto-oncogene int-2 suggests multiple roles in fetal development. Development *105*, 131–136.

Zhang, Z., Wlodarczyk, B.J., Niederreither, K., Venugopalan, S., Florez, S., Finnell, R.H., and Amendt, B.A. (2011). Fuz regulates craniofacial development through tissue specific responses to signaling factors. PLoS ONE *6*, e24608.

Rare Diseases 1, e27109; 2013; © 2013 Landes Bioscience

Common skeletal features in rare diseases

New links between ciliopathies and FGF-related syndromes

Basil Z Yannakoudakis and Karen J Liu*

Department of Craniofacial Development and Stem Cell Biology; King's College London; London, UK

Congenital skeletal anomalies are rare disorders, with a subset affecting both the cranial and appendicular skeleton. Two categories, craniosynostosis syndromes and chondrodysplasias, frequently result from aberrant regulation of the fibroblast growth factor (FGF) signaling pathway. Our recent work has implicated FGF signaling in a third category: ciliopathic skeletal dysplasias. In this work, we have used mouse mutants in two ciliopathy genes, *Fuzzy (Fuz)* and *orofacial digital syndrome-1 (Ofd-1)*, to demonstrate increase in *Fgf8* gene expression during critical stages of embryogenesis. While the mechanisms underlying FGF dysregulation differ in the different syndromes, our data raise the possibility that convergence on FGF signal transduction may underlie a wide range of skeletal anomalies. Here, we provide additional evidence of the skeletal phenotypes from the *Fuz* mouse model and highlight similarities between human ciliopathies and FGF-related syndromes.

Keywords: ciliopathy, FGF, skeletal dysplasia

Abbreviations: C, cleft; CF, cervical fusion; CS, coronal synostosis; HA, high arch; PD, polydactyly; SD, syndactyly; SL, short limbs; SS, sagittal synostosis

*Correspondence to: Karen J Liu;
Email: karen.liu@kcl.ac.uk

Submitted: 08/18/2013; Revised: 10/24/2013;
Accepted: 11/06/2013;
Published Online: 12/03/2013

http://dx.doi.org/10.4161/rdis.27109

Citation: Yannakoudakis BZ, Liu KJ. Common skeletal features in rare diseases: New links between ciliopathies and FGF-related syndromes. Rare Diseases 2013; 1:e27109

Addendum to: Tabler JM, Barrell WB, Szabo-Rogers HL, Healy C, Yeung Y, Perdiguero EG, Schulz C, Yannakoudakis BZ, Mesbahi A, Wlodarczyk B, et al. Fuz mutant mice reveal shared mechanisms between ciliopathies and FGF-related syndromes. Dev Cell 2013; 25:623-35; PMID:23806618; http://dx.doi.org/10.1016/j.devcel.2013.05.021

Fibroblast growth factors are well-studied signaling molecules that are critical for embryonic development.[1,2] In humans, 22 structurally related FGF ligands have been identified; most of these are secreted proteins that bind with varying affinities to tyrosine kinase receptors (FGFR1–4). The majority of FGF ligands can bind promiscuously to multiple different FGFRs; further complexity is generated by alternative splicing of FGFR1, 2 and 3. Ligand binding induces receptor dimerization and cross-phosphorylation, which then initiates a broad range of intracellular signaling cascades such as PI3 kinase (PI3K), MAPK, phospholipase C (PLCγ) or JAK/STAT. Activation of the pathway elicits diverse cellular responses, including proliferation and differentiation of multiple cell types. In recent years, developmental studies, as well as identification of human alleles, has made it clear that precise temporal and spatial activation of FGF signaling is necessary for normal development.

The FGF signaling pathway is a key regulator of skeletal development. In humans, mutations in the FGF receptors (FGFRs) are a hallmark of two classes of skeletal anomalies: craniosynostoses and chondrodysplasias (reviewed by Ornitz et al.).[1] Craniosynostosis syndromes are characterized by premature fusion of the cranial sutures and are frequently accompanied by malformations of the axial skeleton. In contrast, chondrodysplasias feature truncation of the appendicular skeleton, due to an increase in FGF signaling during endochondral ossification. Both craniosynostosis and chondrodysplasia syndromes are associated with autosomal dominant mutations of the FGF receptors, which result in increased activation of the signaling pathway.[1] The array of phenotypes correlates with specific mutations in different receptors, but the net effect appears to be that sustained or increased FGF signaling tips the balance between critical steps in osteoblast differentiation.[1,2]

Ciliopathies are a heterogeneous group of disorders that arise from abnormal formation or function of the cilium.[3] Cilia are finger-like organelles at the cell surface

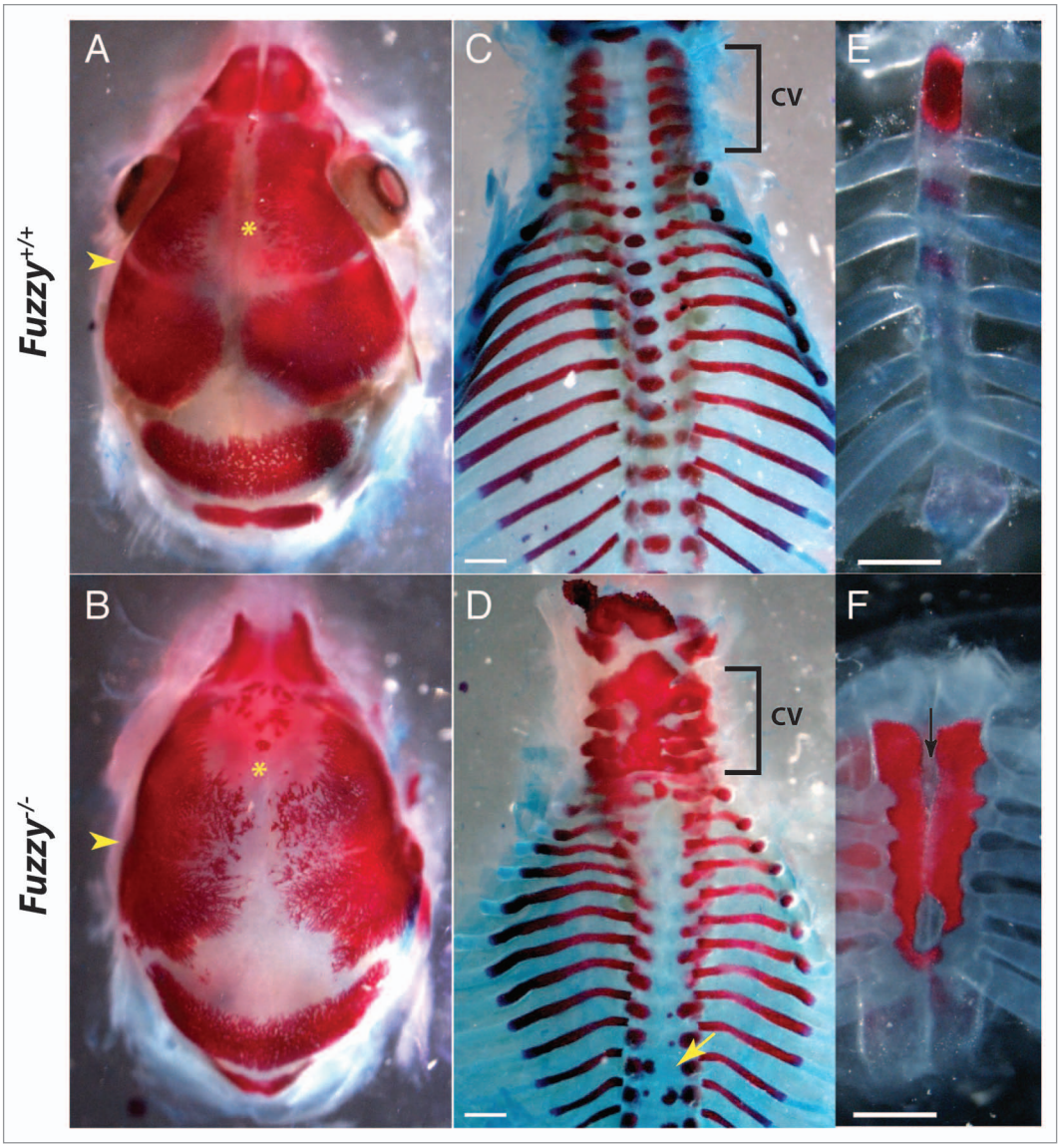

Figure 1. Skeletal preparations of wild-type and *Fuz*$^{-/-}$ embryos at E18.5. Alizarin red staining marks the bone. Alcian blue staining marks the cartilage. (**A and B**) Dorsal views of the skull. (**A**) Control. (**B**) Mutant mice display synostosis of the coronal suture (yellow arrowhead) as well as an open anterior fontanelle (yellow asterix). (**C and D**) Dorsal view of the axial skeleton. (**C**) Control. (**D**) In mutant animals, the cervical vertebra (cv, bracket) are fused. Ossification of the centrum in thoracic vertebra is lost or aberrant (yellow arrow). (**E and F**) Frontal views of the sternum. (**E**) Control. (**F**) In mutants, the sternum is shorter, hyperossified and cleft/bifid (black arrow).

comprised of a microtubule axoneme attached to a basal body. Depending on the microtubule arrangement, a cilium may be motile or immotile. Disorders of the motile cilia frequently involve fluid flow; for example, patients with primary ciliary dyskinesia have difficulty clearing mucus from their lungs due to defects in the multi-ciliated epithelium.[4] Immotile or primary cilia stand alone and are required for function of many signaling pathways.[5] To date, ciliopathic skeletal phenotypes have mainly been attributed to changes in primary cilia-dependent transduction of Hedgehog signals.[6] This has been best studied in the long bones; however, the phenotypic range of ciliopathies is extremely broad. As a consequence, it can be difficult to diagnose or treat ciliopathies, and the underlying etiology is often unclear.

Ciliopathies affecting the skeleton are rare syndromic anomalies. Some patients exhibit limb phenotypes such as syndactyly or polydactyly [in the case of Bardet-Biedl syndrome (MIM #209900)].[7,8] Dysplasia of the ribs, and occasional shortened limbs, are also seen, as in Jeune asphyxiating thoracic dystrophy (MIM #208500).[9] Frequently, ciliary defects also lead to changes in the craniofacial skeleton in humans and mice,[10-12] with craniosynostosis observed in Sensenbrenner syndrome or cranioectodermal dysplasia (MIM #614378).[13] The broad range of systems affected suggests varied molecular causes. Thus, grouping similar skeletal phenotypes across multiple disorders, and

Table 1. Skeletal phenotypes observed in ciliopathies and FGF syndromes. Included are selected human disorders and animal models. Unfortunately, due to space constraints, we regret that we are unable to cite all relevant papers.

	Affected structure						
	Skull/Face	**Palate**	**Limb/Hand**	**Vertebra**	**Rib/Thorax**	**Sternum**	**Refs.**
Ciliopathies							
Human							
Meckel	encephalocele	C	PD	?	-	-	20
Bardet-Biedl	Shape change	HA	PD, SD	scoliosis	-	-	37
Joubert	-	C?	-	Cervical fusion	-	-	28
OFD1	Shape change	HA	PD	-	-	-	20
Jeune	-	-	PD	Cervical stenosis	irregular	bulge	9, 38
Sensenbrenner	SS	HA	SL, PD	-	Short ribs	-	13, 39–41
Ellis-Van Creveld	-	-	SL, PD	-	Short ribs	-	42
Mouse Models							
Meckel: *MKS1*^{hlb614}/*MKS1*^{krc}	-	C	-	-	-	bifid, fused	35, 43
Ellis-van Creveld: *EVC*	-	-	SL	Fusions	Short ribs	-	44, 45
Orofacial Digital: *OFD1*	-	C	SL, PD	-	-	bifid, fused	46, 47
Sensenbrenner: *WDR35*	-	-	-	-	Short ribs	-	48
Ciliopathy: *Fuz*	CS	HA	SL, PD	Cervical fusion	Short ribs	Fused, bifid	14, 16–18
Craniosynostosis							
Human							
Apert	CS	HA	SD	Cervical fusion	-	-	19, 49
Crouzon	CS	HA	SL, SD	Cervical fusion	-	-	21, 50
Pfeiffer	CS	HA	SD	Cervical fusion	-	-	22, 23
Mouse Models							
Crouzon/Pfeiffer: *Fgfr2c*^{C342Y}	CS	C	-	-	-	Fused	51, 52
Pfeiffer: Tg(*Fgfr1*^{P252R})	CS	-	PD	Homeotic transformation	-	Fusions	27
Apert: *Fgfr2*$^{IIIc/\Delta}$	CS	-	-	-	-	Fused	29, 53
Apert: *Fgfr2*^{S252W}	CS	C	-	-	-	Fusions	30
Chondrodysplasia							
Human							
Chondrodysplasia punctata 2	variable	-	SL	Scoliosis fusions	calcified	calcified	20
Hypochondroplasia	variable	-	SL	stenosis	-	-	53
Thanatophoric dysplasia	-	-	SL	flattened	Short ribs	-	54
Achondroplasia	Small base	-	SL	stenosis	Small chest	-	55
Mouse Models							
Achondroplasia: *Fgfr3*^{G374R}	-	-	SL	Cervical fusion	-	-	56
Thanatophoric Dysplasia: FGFR3369	-	-	SL	-	Short ribs	-	57

Abbreviations: SS, sagittal synostosis; CS, coronal synostosis; C, cleft palate; HA, high arched palate; PD, polydactyly; SD, syndactyly; SL, short limbs

comparison with animal models, may provide useful insight into the underlying molecular events.

The *Fuzzy* gene is associated with neural tube defects and has previously been shown to be a ciliopathy gene.[14-17] In our current work, we examine the requirements for *Fuz* in development of the craniofacial structures.[18] Craniofacial defects include craniosynostosis and facial anomalies (**Fig. 1A and B**).[18] As documented in Tabler et al., *Fuz* mutant mice have a complete synostosis of the coronal suture, as well as an open anterior fontanelle, reminiscent of Apert syndrome synostoses (MIM #101200) (**Fig. 1A-B**).[19] Our analysis of the *Fuzzy* mutant also showed broader defects of the skeleton. Consistent

with ciliopathic Hedgehog phenotypes, *Fuz* mutants have polydactyly and shortened long bones.[17] Most interesting, we also found anomalous elements in the axial skeleton. The cervical vertebra (cv) were frequently fused (**Fig. 1C and D**, bracket), while ossification of the centrum in the thoracic vertebra is generally absent. Occasionally, small islands of ectopic ossification are seen (**Fig. 1C and D**, yellow arrow). As in ciliopathies such as Jeune Syndrome (MIM #208500), the ribs are shorter. Surprisingly, the sternum is hyperossified, shorter, and bifid (**Fig. 1E and F**, black arrow marks cleft). In earlier stages, cartilaginous joints are formed (data not shown); by embryonic day (E)18.5, the sternal joints have been obliterated (**Fig. 1E and F**).

This array of phenotypes suggested a similarity to several classes of FGFR-dependent skeletal anomalies, including craniosynostosis syndromes and chondrodysplasias.[20] All of these syndromes arise from dysregulation of FGF receptors;[1] however, the status of FGF signaling in ciliopathy mutants has not been well explored. **Table 1** catalogs the skeletal malformations ciliopathies and FGF related syndromes. We found significant overlap across the range of disorders.

Many craniosynostosis patients have a progressive fusion of the cervical spine, with two thirds of Apert patients exhibiting complex fusions in the C5-C6 segment.[21] C2-C3 fusions are also quite common in these syndromes, with additional reports from Saethre-Chotzen (MIM #101400) and Pfeiffer syndromes (MIM#101600).[22-24] To our knowledge, FGF-induced chondrodysplasias are not associated with spinal stenosis; however, cases have been reported in rhizomelic chondrodysplasia punctata patients.[25] Interestingly, congenital scoliosis due to vertebral defects has also been linked to aberrant *FGF* signaling during development.[26] In addition, in a mouse model of Pfeiffer syndrome, vertebral homeotic transformations have been noted.[27] Thus, phenotypes seen in the different mouse models, combined with some reported anomalies of the cervical vertebra in Joubert Syndrome (MIM #213300), suggest that ciliopathy patients could be assessed for spinal aberrations.[28]

Sternal abnormalities, a common feature of ciliopathies and FGF syndromes, are another striking phenotype seen in *Fuz* mutants. Premature or ectopic fusion of the sternum is seen in a number of mouse models, including Apert/Pfeiffer Syndrome and achondroplasia mice.[27,29-31] The current data suggest that hyperactivation of FGF receptors leads to an impairment in sternal joint formation and subsequent hyperossification. In humans, premature ossification of the sternum is a hallmark of Noonan syndrome.[32] The causative mutation in Noonan syndrome is *PTPN11*, which encodes SHP-2, a key regulator of the FGF-Ras-MAPK pathway.[33] Finally, sternal anomalies are also observed in ciliopathic animal models.[34,35]

Taken together, our data suggest that the skeletal anomalies described may all converge on deregulation of the FGF signaling pathway. Indeed, we found that a subset of phenotypes in our ciliopathic mouse mutants, *Fuz* and *OFD-1*, are attributable to increased *Fgf8* gene expression and genetic reduction of *FGF8* rescued these phenotypes.[18]

Our approach of cataloguing human phenotypes, and comparison to animal models, led us to a surprising role for FGFs in ciliopathies. However, clearly, FGFs alone, or in combination with Hedgehog signaling, cannot be the sole molecular players in skeletal dysplasias. FGF signaling plays roles at multiple steps in both endochondral and intramembranous ossification.[1] For example, during long bone formation, signaling via FGFR2 and FGFR3 promotes chondrocyte condensation and differentiation respectively. Later in this process, FGFR3 is needed to limit the amounts of proliferative pre-hypertrophic chondrocytes. In intramembranous ossification, as seen in the calvaria, FGFs are involved in every step of osteoblast differentiation and subsequent ossification. *FGFR1* and *2* are expressed at the osteogenic front, and are necessary for osteoblast differentiation. *FGF2* is expressed in the sutures, and signals to the adjacent osteogenic cells. Thus, specific phenotypes observed in the human syndromes described can be attributed to inappropriate temporal or spatial activation of the pathway. For example, hyperactivation of FGFR3 severely reduces regions of pre-hypertrophic chondrocyte proliferation resulting in short long bones. Conversely, FGFR1 and 2 dysregulation leads to premature osteoblast differentiation and craniosynostosis.

Dysregulation of Gli processing is also known to cause a variety of skeletal defects, notably in the long bones, vertebra and sternum. *Gli2* mouse mutants have shortened long bones and absence or malformation of vertebral bodies, while *Gli3* mutants have slightly shortened long bones accompanied by polydactyly, as well as fusions of the cervical vertebra and bifid, hyperossified sterna.[36] Thus, there is substantial phenotypic overlap between *Gli* mutants and other animal models of skeletal syndromes. As described above, it is likely that correct timing and location of a suite of signals is critical for shaping the skeleton. Because pathological mutations can lead to changes at multiple levels during development, we propose that further comparison of human phenotypes and animal models can provide important insights into the genetic networks governing overlapping disease phenotypes.

Disclosure of Potential Conflicts of Interest

No potential conflict of interest was disclosed.

Acknowledgments

We thank the Liu lab for discussions and Marc Dionne for critical reading of the manuscript. This work was funded by grants from the Wellcome Trust, BBSRC, and an MRC studentship.

References

1. Ornitz DM, Marie PJ. FGF signaling pathways in endochondral and intramembranous bone development and human genetic disease. Genes Dev 2002; 16:1446-65; PMID:12080084; http://dx.doi.org/10.1101/gad.990702
2. Mohammadi M, Olsen SK, Ibrahimi OA. Structural basis for fibroblast growth factor receptor activation. Cytokine Growth Factor Rev 2005; 16:107-37; PMID:15863029; http://dx.doi.org/10.1016/j.cytogfr.2005.01.008
3. Veland IR, Awan A, Pedersen LB, Yoder BK, Christensen ST. Primary cilia and signaling pathways in mammalian development, health and disease. Nephron Physiol 2009; 111:39-53; PMID:19276629; http://dx.doi.org/10.1159/000208212
4. Rossman CM, Forrest JB, Lee RM, Newhouse MT. The dyskinetic cilia syndrome. Ciliary motility in immotile cilia syndrome. Chest 1980; 78:580-2; PMID:6448132; http://dx.doi.org/10.1378/chest.78.4.580
5. Eggenschwiler JT, Anderson KV. Cilia and developmental signaling. Annu Rev Cell Dev Biol 2007; 23:345-73; PMID:17506691; http://dx.doi.org/10.1146/annurev.cellbio.23.090506.123249
6. Haycraft CJ, Serra R. Cilia involvement in patterning and maintenance of the skeleton. Curr Top Dev Biol 2008; 85:303-32; PMID:19147010; http://dx.doi.org/10.1016/S0070-2153(08)00811-9
7. David A, Bitoun P, Lacombe D, Lambert JC, Nivelon A, Vigneron J, Verloes A. Hydrometrocolpos and polydactyly: a common neonatal presentation of Bardet-Biedl and McKusick-Kaufman syndromes. J Med Genet 1999; 36:599-603; PMID:10465109
8. Beales PL, Elcioglu N, Woolf AS, Parker D, Flinter FA. New criteria for improved diagnosis of Bardet-Biedl syndrome: results of a population survey. J Med Genet 1999; 36:437-46; PMID:10874630
9. Baujat G, Huber C, El Hokayem J, Caumes R, Do Ngoc Thanh C, David A, Delezoide AL, Dieux-Coeslier A, Estournet B, Francannet C, et al. Asphyxiating thoracic dysplasia: clinical and molecular review of 39 families. J Med Genet 2013; 50:91-8; PMID:23339108; http://dx.doi.org/10.1136/jmedgenet-2012-101282
10. Brugmann SA, Cordero DR, Helms JA. Craniofacial ciliopathies: A new classification for craniofacial disorders. Am J Med Genet A 2010; 152A:2995-3006; PMID:21108387; http://dx.doi.org/10.1002/ajmg.a.33727
11. Macca M, Franco B. The molecular basis of oral-facial-digital syndrome, type 1. Am J Med Genet C Semin Med Genet 2009; 151C:318-25; PMID:19876934; http://dx.doi.org/10.1002/ajmg.c.30224
12. Walczak-Sztulpa J, Eggenschwiler J, Osborn D, Brown DA, Emma F, Klingenberg C, Hennekam RC, Torre G, Garshasbi M, Tzschach A, et al. Cranioectodermal Dysplasia, Sensenbrenner syndrome, is a ciliopathy caused by mutations in the IFT122 gene. Am J Hum Genet 2010; 86:949-56; PMID:20493458; http://dx.doi.org/10.1016/j.ajhg.2010.04.012
13. Levin LS, Perrin JC, Ose L, Dorst JP, Miller JD, McKusick VA. A heritable syndrome of craniosynostosis, short thin hair, dental abnormalities, and short limbs: cranioectodermal dysplasia. J Pediatr 1977; 90:55-61; PMID:830894; http://dx.doi.org/10.1016/S0022-3476(77)80764-6
14. Seo JH, Zilber Y, Babayeva S, Liu J, Kyriakopoulos P, De Marco P, Merello E, Capra V, Gros P, Torban E. Mutations in the planar cell polarity gene, Fuzzy, are associated with neural tube defects in humans. Hum Mol Genet 2011; 20:4324-33; PMID:21840926; http://dx.doi.org/10.1093/hmg/ddr359
15. Park TJ, Haigo SL, Wallingford JB. Ciliogenesis defects in embryos lacking inturned or fuzzy function are associated with failure of planar cell polarity and Hedgehog signaling. Nat Genet 2006; 38:303-11; PMID:16493421; http://dx.doi.org/10.1038/ng1753
16. Heydeck W, Zeng H, Liu A. Planar cell polarity effector gene Fuzzy regulates cilia formation and Hedgehog signal transduction in mouse. Dev Dyn 2009; 238:3035-42; PMID:19877275; http://dx.doi.org/10.1002/dvdy.22130
17. Gray RS, Abitua PB, Wlodarczyk BJ, Szabo-Rogers HL, Blanchard O, Lee I, Weiss GS, Liu KJ, Marcotte EM, Wallingford JB, et al. The planar cell polarity effector Fuz is essential for targeted membrane trafficking, ciliogenesis and mouse embryonic development. Nat Cell Biol 2009; 11:1225-32; PMID:19767740; http://dx.doi.org/10.1038/ncb1966
18. Tabler JM, Barrell WB, Szabo-Rogers HL, Healy C, Yeung Y, Perdiguero EG, Schulz C, Yannakoudakis BZ, Mesbahi A, Wlodarczyk B, et al. Fuz mutant mice reveal shared mechanisms between ciliopathies and FGF-related syndromes. Dev Cell 2013; 25:623-35; PMID:23806618; http://dx.doi.org/10.1016/j.devcel.2013.05.021
19. Cohen MM Jr., Kreiborg S. Skeletal abnormalities in the Apert syndrome. Am J Med Genet 1993; 47:624-32; PMID:8266987; http://dx.doi.org/10.1002/ajmg.1320470509
20. Hennekam R, et al. Gorlin's Syndromes of the Head and Neck Oxford University Press, USA, 2010.
21. Hemmer KM, McAlister WH, Marsh JL. Cervical spine anomalies in the craniosynostosis syndromes. Cleft Palate J 1987; 24:328-33; PMID:3479279
22. Moore MH, Cantrell SB, Trott JA, David DJ. Pfeiffer syndrome: a clinical review. Cleft Palate Craniofac J 1995; 32:62-70; PMID:7727489; http://dx.doi.org/10.1597/1545-1569(1995)032<0062:PSACR>2.3.CO;2
23. Moore MH, Lodge ML, Clark BE. Spinal anomalies in Pfeiffer syndrome. Cleft Palate Craniofac J 1995; 32:251-4; PMID:7605793; http://dx.doi.org/10.1597/1545-1569(1995)032<0251:SAIPS>2.3.CO;2
24. Anderson PJ, Hall CM, Evans RD, Hayward RD, Harkness WJ, Jones BM. The cervical spine in Saethre-Chotzen syndrome. Cleft Palate Craniofac J 1997; 34:79-82; PMID:9003917; http://dx.doi.org/10.1597/1545-1569(1997)034<0079:TCSISC>2.3.CO;2
25. Khanna AJ, Braverman NE, Valle D, Sponseller PD. Cervical stenosis secondary to rhizomelic chondrodysplasia punctata. Am J Med Genet 2001; 99:63-6; PMID:11170096; http://dx.doi.org/10.1002/1096-8628(20010215)99:1<63::AID-AJMG1117>3.0.CO;2-9
26. Sparrow DB, Chapman G, Smith AJ, Mattar MZ, Major JA, O'Reilly VC, Saga Y, Zackai EH, Dormans JP, Alman BA, et al. A mechanism for gene-environment interaction in the etiology of congenital scoliosis. Cell 2012; 149:295-306; PMID:22484060; http://dx.doi.org/10.1016/j.cell.2012.02.054
27. Hajihosseini MK, Lalioti MD, Arthaud S, Burgar HR, Brown JM, Twigg SR, Wilkie AO, Heath JK. Skeletal development is regulated by fibroblast growth factor receptor 1 signalling dynamics. Development 2004; 131:325-35; PMID:14668415; http://dx.doi.org/10.1242/dev.00940
28. Juric-Sekhar G, Adkins J, Doherty D, Hevner RF. Joubert syndrome: brain and spinal cord malformations in genotyped cases and implications for neurodevelopmental functions of primary cilia. Acta Neuropathol 2012; 123:695-709; PMID:22331178; http://dx.doi.org/10.1007/s00401-012-0951-2
29. Hajihosseini MK, Wilson S, De Moerlooze L, Dickson C. A splicing switch and gain-of-function mutation in FgfR2-IIIc hemizygotes causes Apert/Pfeiffer-syndrome-like phenotypes. Proc Natl Acad Sci U S A 2001; 98:3855-60; PMID:11274405; http://dx.doi.org/10.1073/pnas.071586898
30. Wang Y, Xiao R, Yang F, Karim BO, Iacovelli AJ, Cai J, Lerner CP, Richtsmeier JT, Leszl JM, Hill CA, et al. Abnormalities in cartilage and bone development in the Apert syndrome FGFR2(+/S252W) mouse. Development 2005; 132:3537-48; PMID:15975938; http://dx.doi.org/10.1242/dev.01914
31. Wang Q, Green RP, Zhao G, Ornitz DM. Differential regulation of endochondral bone growth and joint development by FGFR1 and FGFR3 tyrosine kinase domains. Development 2001; 128:3867-76; PMID:11585811
32. Hoeffel JC, Pernot C, Juncker P. Radiologic patterns of the sternum in Noonan's syndrome with congenital heart defect. Am J Dis Child 1981; 135:1044-6; PMID:6794358
33. Tartaglia M, Kalidas K, Shaw A, Song X, Musat DL, van der Burgt I, Brunner HG, Bertola DR, Crosby A, Ion A, et al. PTPN11 mutations in Noonan syndrome: molecular spectrum, genotype-phenotype correlation, and phenotypic heterogeneity. Am J Hum Genet 2002; 70:1555-63; PMID:11992261; http://dx.doi.org/10.1086/340847
34. Zhang Q, Murcia NS, Chittenden LR, Richards WG, Michaud EJ, Woychik RP, Yoder BK. Loss of the Tg737 protein results in skeletal patterning defects. Dev Dyn 2003; 227:78-90; PMID:12701101; http://dx.doi.org/10.1002/dvdy.10289
35. Cui C, Chatterjee B, Francis D, Yu Q, SanAgustin JT, Francis R, Tansey T, Henry C, Wang B, Lemley B, et al. Disruption of Mks1 localization to the mother centriole causes cilia defects and developmental malformations in Meckel-Gruber syndrome. Dis Model Mech 2011; 4:43-56; PMID:21045211; http://dx.doi.org/10.1242/dmm.006262
36. Mo R, Freer AM, Zinyk DL, Crackower MA, Michaud J, Heng HH, Chik KW, Shi XM, Tsui LC, Cheng SH, et al. Specific and redundant functions of Gli2 and Gli3 zinc finger genes in skeletal patterning and development. Development 1997; 124:113-23; PMID:9006072
37. Waters A, et al. Bardet-Biedl Syndrome. In: RA P, et al., eds. GeneReviews. Seattle (WA): University of Washington, Seattle, 2011.
38. Ho NC, Francomano CA, van Allen M. Jeune asphyxiating thoracic dystrophy and short-rib polydactyly type III (Verma-Naumoff) are variants of the same disorder. Am J Med Genet 2000; 90:310-4; PMID:10710229; http://dx.doi.org/10.1002/(SICI)1096-8628(20000214)90:4<310::AID-AJMG9>3.0.CO;2-N
39. Bredrup C, Saunier S, Oud MM, Fiskerstrand T, Hoischen A, Brackman D, Leh SM, Midtbø M, Filhol E, Bole-Feysot C, et al. Ciliopathies with skeletal anomalies and renal insufficiency due to mutations in the IFT-A gene WDR19. Am J Hum Genet 2011; 89:634-43; PMID:22019273; http://dx.doi.org/10.1016/j.ajhg.2011.10.001
40. Sensenbrenner JA, Dorst JP, Owens RP. New syndrome of skeletal, dental and hair anomalies. Birth Defects Orig Artic Ser 1975; 11:372-9; PMID:1227553
41. Young ID. Cranioectodermal dysplasia (Sensenbrenner's syndrome). J Med Genet 1989; 26:393-6; PMID:2661822; http://dx.doi.org/10.1136/jmg.26.6.393
42. Smith HL, Hand AM. Chondroectodermal dysplasia (Ellis-van Creveld syndrome); report of two cases. Pediatrics 1958; 21:298-307; PMID:13505024

43. Weatherbee SD, Niswander LA, Anderson KV. A mouse model for Meckel syndrome reveals Mks1 is required for ciliogenesis and Hedgehog signaling. Hum Mol Genet 2009; 18:4565-75; PMID:19776033; http://dx.doi.org/10.1093/hmg/ddp422
44. Pacheco M, Valencia M, Caparrós-Martín JA, Mulero F, Goodship JA, Ruiz-Perez VL. Evc works in chondrocytes and osteoblasts to regulate multiple aspects of growth plate development in the appendicular skeleton and cranial base. Bone 2012; 50:28-41; PMID:21911092; http://dx.doi.org/10.1016/j.bone.2011.08.025
45. Ruiz-Perez VL, Blair HJ, Rodriguez-Andres ME, Blanco MJ, Wilson A, Liu YN, Miles C, Peters H, Goodship JA. Evc is a positive mediator of Ihh-regulated bone growth that localises at the base of chondrocyte cilia. Development 2007; 134:2903-12; PMID:17660199; http://dx.doi.org/10.1242/dev.007542
46. Ferrante MI, Zullo A, Barra A, Bimonte S, Messaddeq N, Studer M, Dollé P, Franco B. Oral-facial-digital type I protein is required for primary cilia formation and left-right axis specification. Nat Genet 2006; 38:112-7; PMID:16311594; http://dx.doi.org/10.1038/ng1684
47. Bimonte S, De Angelis A, Quagliata L, Giusti F, Tammaro R, Dallai R, Ascenzi MG, Diez-Roux G, Franco B. Ofd1 is required in limb bud patterning and endochondral bone development. Dev Biol 2011; 349:179-91; PMID:20920500; http://dx.doi.org/10.1016/j.ydbio.2010.09.020
48. Mill P, Lockhart PJ, Fitzpatrick E, Mountford HS, Hall EA, Reijns MA, Keighren M, Bahlo M, Bromhead CJ, Budd P, et al. Human and mouse mutations in WDR35 cause short-rib polydactyly syndromes due to abnormal ciliogenesis. Am J Hum Genet 2011; 88:508-15; PMID:21473986; http://dx.doi.org/10.1016/j.ajhg.2011.03.015
49. Rynearson RD. Case report: orthodontic and dentofacial orthopedic considerations in Apert's syndrome. Angle Orthod 2000; 70:247-52; PMID:10926435
50. Anderson PJ, Hall C, Evans RD, Harkness WJ, Hayward RD, Jones BM. The cervical spine in Crouzon syndrome. Spine (Phila Pa 1976) 1997; 22:402-5; PMID:9055367; http://dx.doi.org/10.1097/00007632-199702150-00009
51. Eswarakumar VP, Ozcan F, Lew ED, Bae JH, Tomé F, Booth CJ, Adams DJ, Lax I, Schlessinger J. Attenuation of signaling pathways stimulated by pathologically activated FGF-receptor 2 mutants prevents craniosynostosis. Proc Natl Acad Sci U S A 2006; 103:18603-8; PMID:17132737; http://dx.doi.org/10.1073/pnas.0609157103
52. Perlyn CA, DeLeon VB, Babbs C, Govier D, Burell L, Darvann T, Kreiborg S, Morriss-Kay G. The craniofacial phenotype of the Crouzon mouse: analysis of a model for syndromic craniosynostosis using three-dimensional MicroCT. Cleft Palate Craniofac J 2006; 43:740-8; PMID:17105336; http://dx.doi.org/10.1597/05-212
53. Bellus GA, McIntosh I, Smith EA, Aylsworth AS, Kaitila I, Horton WA, Greenhaw GA, Hecht JT, Francomano CA. A recurrent mutation in the tyrosine kinase domain of fibroblast growth factor receptor 3 causes hypochondroplasia. Nat Genet 1995; 10:357-9; PMID:7670477; http://dx.doi.org/10.1038/ng0795-357
54. Elejalde BR, de Elejalde MM. Thanatophoric dysplasia: fetal manifestations and prenatal diagnosis. Am J Med Genet 1985; 22:669-83; PMID:4073120; http://dx.doi.org/10.1002/ajmg.1320220404
55. Georgoulis G, Alexiou G, Prodromou N. Achondroplasia with synostosis of multiple sutures. Am J Med Genet A 2011; 155A:1969-71; PMID:21739570; http://dx.doi.org/10.1002/ajmg.a.33744
56. Murakami S, Balmes G, McKinney S, Zhang Z, Givol D, de Crombrugghe B. Constitutive activation of MEK1 in chondrocytes causes Stat1-independent achondroplasia-like dwarfism and rescues the Fgfr3-deficient mouse phenotype. Genes Dev 2004; 18:290-305; PMID:14871928; http://dx.doi.org/10.1101/gad.1179104
57. Chen L, Adar R, Yang X, Monsonego EO, Li C, Hauschka PV, Yayon A, Deng CX. Gly369Cys mutation in mouse FGFR3 causes achondroplasia by affecting both chondrogenesis and osteogenesis. J Clin Invest 1999; 104:1517-25; PMID:10587515; http://dx.doi.org/10.1172/JCI6690